National Library of Canada
Bibliothèque nationale du Canada

Acquisitions and Bibliographic Services Branch
Direction des acquisitions et des services bibliographiques

395 Wellington Street
Ottawa, Ontario
K1A 0N4

395, rue Wellington
Ottawa (Ontario)
K1A 0N4

Your file Votre référence

Our file Notre référence

NOTICE

The quality of this microform is heavily dependent upon the quality of the original thesis submitted for microfilming. Every effort has been made to ensure the highest quality of reproduction possible.

If pages are missing, contact the university which granted the degree.

Some pages may have indistinct print especially if the original pages were typed with a poor typewriter ribbon or if the university sent us an inferior photocopy.

Reproduction in full or in part of this microform is governed by the Canadian Copyright Act, R.S.C. 1970, c. C-30, and subsequent amendments.

AVIS

La qualité de cette microforme dépend grandement de la qualité de la thèse soumise au microfilmage. Nous avons tout fait pour assurer une qualité supérieure de reproduction.

S'il manque des pages, veuillez communiquer avec l'université qui a conféré le grade.

La qualité d'impression de certaines pages peut laisser à désirer, surtout si les pages originales ont été dactylographiées à l'aide d'un ruban usé ou si l'université nous a fait parvenir une photocopie de qualité inférieure.

La reproduction, même partielle, de cette microforme est soumise à la Loi canadienne sur le droit d'auteur, SRC 1970, c. C-30, et ses amendements subséquents.

Canada

Chromatographic-Mass Spectrometric Analysis of Polycyclic Aromatic Compounds

By

Joseph F. Anacleto

Submitted in partial fulfilment of the
requirements for the degree of
Doctor of Philosophy

at

Dalhousie University
Halifax, Nova Scotia
September 1993

© Copyright by Joseph F. Anacleto, 1993

National Library of Canada
Bibliothèque nationale du Canada

Acquisitions and Bibliographic Services Branch
Direction des acquisitions et des services bibliographiques

395 Wellington Street
Ottawa, Ontario
K1A 0N4

395, rue Wellington
Ottawa (Ontario)
K1A 0N4

Your file Votre référence

Our file Notre référence

The author has granted an irrevocable non-exclusive licence allowing the National Library of Canada to reproduce, loan, distribute or sell copies of his/her thesis by any means and in any form or format, making this thesis available to interested persons.

L'auteur a accordé une licence irrévocable et non exclusive permettant à la Bibliothèque nationale du Canada de reproduire, prêter, distribuer ou vendre des copies de sa thèse de quelque manière et sous quelque forme que ce soit pour mettre des exemplaires de cette thèse à la disposition des personnes intéressées.

The author retains ownership of the copyright in his/her thesis. Neither the thesis nor substantial extracts from it may be printed or otherwise reproduced without his/her permission.

L'auteur conserve la propriété du droit d'auteur qui protège sa thèse. Ni la thèse ni des extraits substantiels de celle-ci ne doivent être imprimés ou autrement reproduits sans son autorisation.

ISBN 0-315-93622-3

Canada

Name Joseph F. Anacleto

Dissertation Abstracts International is arranged by broad, general subject categories. Please select the one subject which most nearly describes the content of your dissertation. Enter the corresponding four digit code in the spaces provided.

Analytical Chemistry — SUBJECT TERM

0486 — SUBJECT CODE

U·M·I

Subject Categories

THE HUMANITIES AND SOCIAL SCIENCES

COMMUNICATIONS AND THE ARTS
Architecture 0729
Art History 0377
Cinema 0900
Dance 0378
Fine Arts 0357
Information Science 0723
Journalism 0391
Library Science 0399
Mass Communications 0708
Music 0413
Speech Communication 0459
Theater 0465

EDUCATION
General 0515
Administration 0514
Adult and Continuing 0516
Agricultural 0517
Art 0273
Bilingual and Multicultural 0282
Business 0688
Community College 0275
Curriculum and Instruction 0727
Early Childhood 0518
Elementary 0524
Finance 0277
Guidance and Counseling 0519
Health 0680
Higher 0745
History of 0520
Home Economics 0278
Industrial 0521
Language and Literature 0279
Mathematics 0280
Music 0522
Philosophy of 0998
Physical 0523
Psychology 0525
Reading 0535
Religious 0527
Science 0714
Secondary 0533
Social Sciences 0534
Sociology of 0340
Special 0529
Teacher Training 0530
Technology 0710
Tests and Measurements 0288
Vocational 0747

LANGUAGE, LITERATURE AND LINGUISTICS
Language
- General 0679
- Ancient 0289
- Linguistics 0290
- Modern 0291

Literature
- General 0401
- Classical 0294
- Comparative 0295
- Medieval 0297
- Modern 0298
- African 0316
- American 0591
- Asian 0305
- Canadian (English) 0352
- Canadian (French) 0355
- English 0593
- Germanic 0311
- Latin American 0312
- Middle Eastern 0315
- Romance 0313
- Slavic and East European 0314

PHILOSOPHY, RELIGION AND THEOLOGY
Philosophy 0422
Religion
- General 0318
- Biblical Studies 0321
- Clergy 0319
- History of 0320
- Philosophy of 0322

Theology 0469

SOCIAL SCIENCES
American Studies 0323
Anthropology
- Archaeology 0324
- Cultural 0326
- Physical 0327

Business Administration
- General 0310
- Accounting 0272
- Banking 0770
- Management 0454
- Marketing 0338

Canadian Studies 0385
Economics
- General 0501
- Agricultural 0503
- Commerce Business 0505
- Finance 0508
- History 0509
- Labor 0510
- Theory 0511

Folklore 0358
Geography 0366
Gerontology 0351
History
- General 0578
- Ancient 0579
- Medieval 0581
- Modern 0582
- Black 0328
- African 0331
- Asia, Australia and Oceania 0332
- Canadian 0334
- European 0335
- Latin American 0336
- Middle Eastern 0333
- United States 0337

History of Science 0585
Law 0398
Political Science
- General 0615
- International Law and Relations 0616
- Public Administration 0617

Recreation 0814
Social Work 0452
Sociology
- General 0626
- Criminology and Penology 0627
- Demography 0938
- Ethnic and Racial Studies 0631
- Individual and Family Studies 0628
- Industrial and Labor Relations 0629
- Public and Social Welfare 0630
- Social Structure and Development 0700
- Theory and Methods 0344

Transportation 0709
Urban and Regional Planning 0999
Women's Studies 0453

THE SCIENCES AND ENGINEERING

BIOLOGICAL SCIENCES
Agriculture
- General 0473
- Agronomy 0285
- Animal Culture and Nutrition 0475
- Animal Pathology 0476
- Food Science and Technology 0359
- Forestry and Wildlife 0478
- Plant Culture 0479
- Plant Pathology 0480
- Plant Physiology 0817
- Range Management 0777
- Wood Technology 0746

Biology
- General 0306
- Anatomy 0287
- Biostatistics 0308
- Botany 0309
- Cell 0379
- Ecology 0329
- Entomology 0353
- Genetics 0369
- Limnology 0793
- Microbiology 0410
- Molecular 0307
- Neuroscience 0317
- Oceanography 0416
- Physiology 0433
- Radiation 0821
- Veterinary Science 0778
- Zoology 0472

Biophysics
- General 0786
- Medical 0760

EARTH SCIENCES
Biogeochemistry 0425
Geochemistry 0996
Geodesy 0370
Geology 0372
Geophysics 0373
Hydrology 0388
Mineralogy 0411
Paleobotany 0345
Paleoecology 0426
Paleontology 0418
Paleozoology 0985
Palynology 0427
Physical Geography 0368
Physical Oceanography 0415

HEALTH AND ENVIRONMENTAL SCIENCES
Environmental Sciences 0768
Health Sciences
- General 0566
- Audiology 0300
- Chemotherapy 0992
- Dentistry 0567
- Education 0350
- Hospital Management 0769
- Human Development 0758
- Immunology 0982
- Medicine and Surgery 0564
- Mental Health 0347
- Nursing 0569
- Nutrition 0570
- Obstetrics and Gynecology 0380
- Occupational Health and Therapy 0354
- Ophthalmology 0381
- Pathology 0571
- Pharmacology 0419
- Pharmacy 0572
- Physical Therapy 0382
- Public Health 0573
- Radiology 0574
- Recreation 0575
- Speech Pathology 0460
- Toxicology 0383

Home Economics 0386

PHYSICAL SCIENCES

Pure Sciences

Chemistry
- General 0485
- Agricultural 0749
- Analytical 0486
- Biochemistry 0487
- Inorganic 0488
- Nuclear 0738
- Organic 0490
- Pharmaceutical 0491
- Physical 0494
- Polymer 0495
- Radiation 0754

Mathematics 0405
Physics
- General 0605
- Acoustics 0986
- Astronomy and Astrophysics 0606
- Atmospheric Science 0608
- Atomic 0748
- Electronics and Electricity 0607
- Elementary Particles and High Energy 0798
- Fluid and Plasma 0759
- Molecular 0609
- Nuclear 0610
- Optics 0752
- Radiation 0756
- Solid State 0611

Statistics 0463

Applied Sciences

Applied Mechanics 0346
Computer Science 0984
Engineering
- General 0537
- Aerospace 0538
- Agricultural 0539
- Automotive 0540
- Biomedical 0541
- Chemical 0542
- Civil 0543
- Electronics and Electrical 0544
- Heat and Thermodynamics 0348
- Hydraulic 0545
- Industrial 0546
- Marine 0547
- Materials Science 0794
- Mechanical 0548
- Metallurgy 0743
- Mining 0551
- Nuclear 0552
- Packaging 0549
- Petroleum 0765
- Sanitary and Municipal 0554
- System Science 0790

Geotechnology 0428
Operations Research 0796
Plastics Technology 0795
Textile Technology 0994

PSYCHOLOGY
General 0621
Behavioral 0384
Clinical 0622
Developmental 0620
Experimental 0623
Industrial 0624
Personality 0625
Physiological 0989
Psychobiology 0349
Psychometrics 0632
Social 0451

TABLE OF CONTENTS

Table of Contents iv

List of Tables vii

List of Figures viii

Abstract xviii

Abbreviations and Symbols Used xix

Acknowledgments xxi

I. INTRODUCTION

I.1 Polycyclic Aromatic Compounds (PAC) 1

I.2 Formation of PAC 3

I.3 Distribution of PAC in the Environment 4

I.4 Importance of PAC 7

I.5 Analytical Methods 8

I.6 Research Objectives 14

II. EXPERIMENTAL

II.1 Materials 16

II.2 Open Column Chromatography 19

II.3 Normal-Phase Liquid Chromatography-Diode Array Detection 21

II.4 Normal-Phase Liquid Chromatography-Mass Spectrometry 22

II.5 Reversed-Phase Liquid Chromatography-Diode Array Detection 22

II.6 Reversed-Phase Liquid Chromatography-Mass Spectrometry 23

II.6.1 The Moving Belt Interface 23

II.6.2 The Particle Beam Interface 23

II.6.3 The Heated Pneumatic Nebulizer Interface 24

II.6.4 The Ionspray Interface 25

II.7 Supercritical Fluid Chromatography-Photoionization Detection 26

II.8 Supercritical Fluid Chromatography-Mass Spectrometry 27

RESULTS AND DISCUSSION

III. CHROMATOGRAPHIC METHODS 28

III.1 Reversed-Phase Liquid Chromatography 28

III.2 Normal-Phase Liquid Chromatography 35

III.3 Supercritical Fluid Chromatography 43

IV. THE MOVING BELT INTERFACE 52

IV.1 Reversed-Phase LC Coupled to the Moving Belt Interface 54

IV.2 Normal-Phase LC Coupled to the Moving Belt Interface 63

V. THE PARTICLE BEAM INTERFACE 75

V.1 Reversed-Phase LC Coupled to the Particle Beam Interface 80

V.2 Quantitative Analysis 94

VI. THE HEATED PNEUMATIC NEBULIZER INTERFACE 107

VI.1 Reversed-Phase LC Coupled to the Heated Nebulizer Interface 113

VI.1.1 Benzene Charge-Transfer Ionization 122

VI.1.2 Negative Ion 130

VI.1.3 Qualitative Analysis 139

VI.1.4 Quantitative Analysis 160

VI.2 SFC Coupled to the Heated Nebulizer Interface 171

VII. THE IONSPRAY INTERFACE 196

VII.1 Charge-Transfer and Electrochemical Ionization 202

VIII. CONCLUSIONS 210

IX. APPENDIX A 224

X. REFERENCES 226

LIST OF TABLES

I-1 Separation methods for polycyclic aromatic compounds. 9

I-2 Analytical methods for polycyclic aromatic compounds. 11

III-1: Physical parameters of selected supercritical fluids. 45

V-1: Particle beam quantitation results for the NIST coal tar SRM 1597 using external calibration. 102

V-2: Particle beam quantitation results for the NIST coal tar SRM 1597 using internal standardization with perdeutero-PAH. 105

VI-1: APCI/MS quantitation results for the NIST coal tar SRM 1597 using external calibration and normal source conditions. 165

VI-2: APCI/MS quantitation results for the NIST coal tar SRM 1597 using internal standardization with perdeutero-PAH under normal source conditions. 168

VI-3: APCI/MS quantitation results for the NIST coal tar SRM 1597 using internal standardization with perdeutero-PAH under benzene charge-transfer conditions. 170

VIII-1: A comparison of four LC-MS interfaces based primarily on their ability to analyze PAC. 213

LIST OF FIGURES

I-1 Polycyclic aromatic compounds. 2

I-2 The structural range of petroleum hydrocarbons. 6

II-1: The hydrotreated tar sand oil samples. 18

II-2: The neutral alumina fractionation scheme. 20

III-1: Reversed-phase LC-UV chromatograms of the NIST SRM 1597 coal tar mixture using (a) an aqueous acetonitrile gradient, and (b) an aqueous acetonitrile/dichloromethane gradient. 32

III-2: Reversed-phase LC-UV chromatograms of the carbon black extract using (a) an aqueous acetonitrile/dichloromethane gradient, and (b) an acetonitrile/dichloromethane gradient. 34

III-3: Normal-phase LC-UV chromatograms of the NIST SRM 1597 coal tar mixture using four commercially available columns with a hexane/dichloromethane gradient. 38

III-4: Normal-phase LC-UV chromatograms of the tar sand oil neutral fraction using three commercially available columns with a hexane/dichloromethane gradient. 40

III-5: Normal-phase LC-UV chromatograms of the tar sand oil nitrogen-containing PAC fraction using three commercially available columns with a hexane/dichloromethane gradient. 41

III-6: Carbon dioxide phase diagram. 44

III-7: SFC-PID chromatograms of (a) a mixture of PAH standards, and (b) the NIST SRM 1597 coal tar mixture using a silica column. 49

III-8: SFC-PID chromatograms of (a) a mixture of PAH standards, and (b) the NIST SRM 1597 coal tar mixture using a C_{18} column. 51

IV-1: A schematic diagram of the moving belt LC-MS interface. 53

IV-2: (a) Full scan EI mass spectrum of coronene, and (b) the calibration curve obtained for coronene using the belt interface. The inset shows the single ion monitoring chromatogram for the injection of 25 pg of coronene. 56

IV-3: (a) Full scan EI mass spectrum of carbazole, and (b) the calibration curve obtained for carbazole using the belt interface. The inset shows the single ion monitoring chromatogram for the injection of 1.9 ng of carbazole. 58

IV-4: (a) LC-UV and (b) LC-MS total ion chromatograms from the analysis of the carbon black extract using a C_{18} column with an acetonitrile/dichloromethane gradient. 59

IV-5: LC-MS selected ion chromatograms generated from the analysis of Figure IV-4b. 61

IV-6: EI mass spectra obtained during the LC-MS analysis of the carbon black extract (Figure IV-4b). Spectra were obtained at the tops of the peaks marked with asterisks in Figure IV-5. 62

IV-7: Selected ion chromatograms from the LC-MS analysis of the NIST SRM 1597 coal tar mixture using a Whatman PAC column. 65

IV-8: Selected ion chromatograms from the LC-MS analysis of the NIST SRM 1597 coal tar mixture using a Techsil NO_2 column. 66

IV-9: LC-MS total ion chromatograms of the tar sand oil neutral fraction using (a) a Waters NH_2, (b) a Whatman PAC, and (c) a Techsil NO_2 column. 68

IV-10: LC-MS total ion chromatograms of the tar sand oil nitrogen-containing PAC fraction using (a) a Waters NH_2, (b) a Whatman PAC, and (c) a Techsil NO_2 column. 69

IV-11: LC-MS selected ion chromatograms of alkylated mass 228 PAH generated from the analysis of Figure IV-9b. 70

IV-12: LC-MS selected ion chromatograms of alkylated carbazole generated from the analysis of Figure IV-10a. 72

IV-13: Background subtracted EI mass spectra obtained from the top of the peaks in (a) Figure IV-12 (m/z 182, second trace), and (b) Figure IV-11 (m/z 228, top trace). 73

V-1: Schematic diagram of a particle beam LC-MS interface. 76

V-2: Background subtracted EI mass spectra of three PAH standards obtained with the particle beam interface. 81

V-3: LC-MS total ion chromatogram (TIC, top trace) and selected ion chromatograms from six replicate injections of a solution containing benz[*a*]anthracene (m/z 228), benzo[*a*]pyrene (m/z 252) and dibenz[*a,h*]anthracene (m/z 278). 82

V-4: Particle beam LC-MS calibration curves obtained for (a) benz[*a*]anthracene, (b) benzo[*a*]pyrene, and (c) dibenz[*a,h*]anthracene. Left insets show an expansion of the low ng region of the curves. Right insets show the low level LC-MS responses obtained for each standard. 84

V-5: (a) LC-UV and (b) particle beam LC-MS total ion chromatograms from the analysis of the NIST SRM 1597 coal tar mixture using a C_{18} column with an aqueous acetonitrile gradient. 87

V-6: LC-MS selected ion chromatograms generated from the analysis of Figure V-5b. 88

V-7: (a) LC-UV and (b) particle beam LC-MS total ion chromatograms from the analysis of the carbon black extract using a C_{18} column with an aqueous acetonitrile/dichloromethane gradient. 90

V-8: LC-MS selected ion chromatograms generated from the analysis of Figure V-7b. 91

V-9: (a) LC-UV and (b) particle beam LC-MS total ion chromatograms from the analysis of the tar sand oil neutral fraction using a C_{18} column with an aqueous acetonitrile/dichloromethane gradient. Selected ion chromatograms generated from the analysis of Figure V-9b. 93

V-10: Analysis of a SRM 1647/DPAC-1 solution (10:1 volume ratio) using particle beam LC-MS. A total of 24 ions monitored in three acquisition periods. 97

V-11: External calibration curves obtained from the analyses of the SRM 1647/DPAC-1 solutions using particle beam LC-MS. 100

V-12: Plots of the proteo-/deutero-PAH peak areas vs the SRM 1647/DPAC-1 volume ratios using particle beam LC-MS. 104

VI-1: A schematic diagram of the heated nebulizer interface. 108

VI-2: Atmospheric pressure chemical ionization reagent ion formation in ambient air. 111

VI-3: Background subtracted positive-ion APCI mass spectra of PAH standards. 115

VI-4: Background subtracted positive-ion APCI mass spectra of PAC standards. 117

VI-5: Heated nebulizer LC-MS calibration curves obtained for (a) benz[*a*]anthracene, (b) benzo[*a*]pyrene, and (c) dibenz[*a*,*h*]anthracene monitoring molecular cations. Left insets show an expansion of the low ng region of the curves. Right insets show the low level LC-MS responses. 119

VI-6: Heated nebulizer LC-MS calibration curves obtained for (a) benz[*a*]anthracene, (b) benzo[*a*]pyrene, and (c) dibenz[*a*,*h*]anthracene monitoring protonated molecules. Left insets show an expansion of the low ng region of the curves. Right insets show the low level LC-MS responses. 120

VI-7: Background subtracted benzene charge-transfer APCI mass spectra of benz[*a*]anthracene using the heated nebulizer interface with increasing amounts of benzene added to the source. 124

VI-8: Background subtracted benzene charge-transfer APCI mass spectra of benzo[*a*]pyrene using the heated nebulizer interface with increasing amounts of benzene added to the source. 125

VI-9: Background subtracted benzene charge-transfer APCI mass spectra of dibenz[*a*,*h*]anthracene using the heated nebulizer interface with increasing amounts of benzene added to the source. 126

VI-10: Heated nebulizer LC-MS calibration curves obtained for (a) benz[*a*]anthracene, (b) benzo[*a*]pyrene, and (c) dibenz[*a*,*h*]anthracene monitoring molecular cations while adding 20 μL/min of benzene to the source. Left insets show an

expansion of the low ng region of the curves. Right insets show the low level LC-MS responses. 128

VI-11: Heated nebulizer LC-MS calibration curves obtained for (a) benz[*a*]anthracene, (b) benzo[*a*]pyrene, and (c) dibenz[*a,h*]anthracene monitoring protonated molecules while adding 20 μL/min of benzene to the source. Left insets show an expansion of the low ng region of the curves. Right insets show the low level LC-MS responses. 129

VI-12: Negative ion atmospheric pressure chemical ionization reagent ion formation in ambient air. 132

VI-13: Background subtracted negative ion APCI mass spectra of PAH standards. 134

VI-14: Background subtracted negative ion APCI mass spectra of perdeutero-PAH standards. 137

VI-15: Background subtracted negative ion APCI mass spectra of mass 252 PAH isomers. 138

VI-16: (a) LC-UV and (b) heated nebulizer LC-MS total ion chromatograms from the analysis of the NIST SRM 1597 coal tar mixture using a C_{18} column with an aqueous acetonitrile/dichloromethane gradient. 142

VI-17: LC-MS selected ion chromatograms generated from the analysis of Figure VI-16b. 143

VI-18: LC-MS selected ion chromatograms generated from the analysis of Figure VI-16b. 144

VI-19: LC-MS selected ion chromatograms generated from the analysis of Figure VI-16b. 145

VI-20: (a) LC-UV and (b) heated nebulizer LC-MS total ion chromatograms from the analysis of the carbon black extract using a C_{18} column with an aqueous acetonitrile/dichloromethane gradient. 147

VI-21: LC-MS selected ion chromatograms generated from the analysis of Figure VI-20b. 148

VI-22: LC-MS selected ion chromatograms generated from the analysis of Figure VI-20b. 149

VI-23: LC-MS selected ion chromatograms generated from the analysis of Figure VI-20b. 150

VI-24: (a) LC-UV and (b) heated nebulizer LC-MS total ion chromatograms from the analysis of the tar sand oil neutral fraction using a C_{18} column with an aqueous acetonitrile/dichloromethane gradient. 153

VI-25: LC-MS selected ion chromatograms of mass 202 PAH and their alkylated homologues generated from the analysis of Figure VI-24b. 154

VI-26: LC-MS selected ion chromatograms of mass 228 PAH and their alkylated homologues generated from the analysis of Figure VI-24b. 155

VI-27: (a) LC-UV and (b) heated nebulizer LC-MS total ion chromatograms from the analysis of the tar sand oil nitrogen-containing PAC fraction using a C_{18} column with an aqueous acetonitrile/dichloromethane gradient. 157

VI-28: LC-MS selected ion chromatograms of carbazole and its alkylated homologues generated from the analysis of Figure VI-27b. 158

VI-29: LC-MS selected ion chromatograms of alkylated hydroaromatic benzocarbazole generated from the analysis of Figure VI-27b. 159

VI-30: Analysis of a SRM 1647/DPAC-1 solution (10:1 volume ratio) using heated nebulizer LC-MS. A total of 48 ions monitored in six acquisition periods. 161

VI-31: Heated nebulizer LC-MS external calibration curves obtained from the analysis of the SRM 1647/DPAC-1 solutions. 164

VI-32: Plots of the proteo-/deutero-PAH peak areas vs the SRM 1647/DPAC-1 volume ratios using heated nebulizer LC-MS. 167

VI-33: Schematic diagram of the SFC-APCI/MS interface. 173

VI-34: (a) SFC-PID and (b) SFC-APCI/MS reconstructed ion chromatograms (sum of $M^{+\cdot}$ and MH^+ ions) from the analysis of PAH standards using a C_{18} column. 175

VI-35: Background subtracted positive-ion SFC-APCI mass spectra of PAH standards. 177

VI-36: Background subtracted positive-ion SFC-APCI mass spectra of benz[*a*]anthracene using (a) water and (b) benzene vapour in the source. Insets show the respective single ion monitoring responses of the (a) protonated molecule and (b) molecular ion for 250 pg of benz[*a*]anthracene. 178

VI-37: Background subtracted positive-ion SFC-APCI mass spectra of benz[*a*]anthracene using (a) normal source conditions and (b) D_2O vapour in the source. 181

VI-38: Fragment ion APCI mass spectra of (a) the m/z 278 adduct ion in Figure VI-37a, and (b) the m/z 280 adduct ion in Figure VI-37b. 183

VI-39: The m/z 278 adduct ion fragmentation pathway as deduced from MS/MS experiments. 185

VI-40: Background subtracted positive-ion SFC-APCI mass spectra of five mass 228 PAH isomers. 186

VI-41: (a) SFC-PID and (b) SFC-APCI/MS total ion chromatograms from the analysis of the NIST SRM 1597 coal tar mixture using a C_{18} column. 188

VI-42: SFC-APCI/MS selected ion chromatograms (sum of $M^{+\cdot}$ and MH^+ ions) generated from the analysis of Figure VI-41b. 189

VI-43: SFC-APCI/MS selected ion chromatograms (MH^+ ions) of mass 228 PAH and their alkylated homologues generated from the analysis of the tar sand oil neutral fraction using a silica column. 192

VI-44: SFC-APCI/MS selected ion chromatograms (MH^+ ions) of carbazole and its alkylated homologues generated from the analysis of the tar sand oil nitrogen-containing PAC fraction using a silica column. 194

VI-45: Background subtracted positive-ion SFC-APCI mass spectra from the analyses shown in (a) Figure VI-44 and (b) Figure VI-43. 195

VII-1: A schematic diagram of the ionspray LC-MS interface. 197

VII-2: The ion evaporation process as proposed by Iribarne and Thomson. 199

VII-3: Background subtracted ionspray mass spectra of aminopyrene in a flow of (a) 1:1 aqueous acetonitrile (50 ng injection), and (b) 1:1 aqueous acetonitrile with 0.1% TFA (5 ng injection). 201

VII-4: Background subtracted ionspray mass spectra of (a) carbazole, (b) 9-cyanoanthracene, and (c) nitropyrene in a flow of 1:1 aqueous acetonitrile with 0.1% TFA. 203

VII-5: Background subtracted charge-transfer ionspray mass spectra of (a) tetracene and (b) perylene using DDQ as an electron acceptor. 206

VII-6: Background subtracted electrochemical oxidation ionspray mass spectra of (a) tetracene and (b) perylene. 209

ABSTRACT

Four liquid chromatography-mass spectrometry (LC-MS) interfaces were evaluated for their ability to analyze complex mixtures of high molecular weight polycyclic aromatic compounds (PAC). The moving belt interface permits the use of electron ionization (EI) since the mobile phase is removed before the analyte reaches the high vacuum ion source. This was particularly useful for the analysis of a carbon black extract since polycyclic aromatic hydrocarbons (PAH) produce intense molecular ions which are ideal for compound identification and enhanced sensitivity.

The particle beam interface also allows the acquisition of EI mass spectra. The detection limits obtained with this interface were very poor in comparison to the other interfaces studied. Non-linear external calibration curves, which are characteristic of this interface, were also obtained for the analysis of PAH standards.

The heated nebulizer interface, which uses atmospheric pressure chemical ionization (APCI), produces both molecular ions ($M^{+\cdot}$) and protonated molecules (MH^+) of PAC. This ionization technique was particularly suited to the analysis of tar sand oil fractions since the highly alkylated PAC present in these samples produced simple spectra without the fragmentation observed with EI. The heated nebulizer interface was modified to also act as a supercritical fluid chromatography (SFC)-MS interface utilizing the same restrictor used in off-line experiments with a photoionization detector.

The ionspray LC-MS interface was only capable of analyzing mixtures of nitrogen-containing PAC (or basic PAC) in acidic mobile phases because the ionization process (i.e., ion evaporation) requires the analyte to pre-form ions in solution. Alternative ionization techniques using this interface (e.g., charge-transfer complexation and electrochemical oxidation) were also investigated.

Of the LC-MS interfaces studied, the heated nebulizer was clearly the best choice for PAC analyses, especially for the high molecular weight compounds that are not amenable to common gas chromatographic techniques.

ABBREVIATIONS AND SYMBOLS USED

APCI: Atmospheric pressure chemical ionization

API: Atmospheric pressure ionization

CI: Chemical ionization

CID: Collisionally induced dissociation

Da: Dalton

DAD: Diode array detector

DDQ: 2,3-Dichloro-5,6-dicyano-*p*-benzoquinone

EI: Electron ionization

eV: Electron volts

FAB: Fast atom bombardment

FID: Flame ionization detector

FPD: Flame photometric detector

GC: Gas chromatography

GC-MS: Gas chromatography-mass spectrometry

HPLC: High performance liquid chromatography

ID: Inner diameter

IE: Ionization energy

IR: Infrared

kV: Kilovolts

LC: Liquid chromatography

LC-MS: Liquid chromatography-mass spectrometry

MeOH: Methanol

min: Minutes

MS: Mass spectrometry

msec: Milliseconds

NICI: Negative ion chemical ionization

NIST: National Institute of Standards and Technology

NMR: Nuclear magnetic resonance spectroscopy

NPLC: Normal-phase liquid chromatography

NRC: National Research Council of Canada

ODS: Octadecylsilica (C_{18})

PAC: Polycyclic aromatic compound(s)

PAH: Polycyclic aromatic hydrocarbon(s)

PANH: Polycyclic aromatic nitrogen heterocycle

PAOH: Polycyclic aromatic oxygen heterocycle

PASH: Polycyclic aromatic sulphur heterocycle

PID: Photoionization detector

psi: Pounds per square inch

RPLC: Reversed-phase liquid chromatography

RSD: Relative standard deviation

SFC: Supercritical fluid chromatography

SFC-MS: Supercritical fluid chromatography-mass spectrometry

SIC: Selected ion chromatograms

SRM: Standard reference material

TIC: Total ion chromatogram

TID: Thermionic detector

UV: Ultra-violet

ACKNOWLEDGMENTS

I wish to express my sincere gratitude to my supervisors Dr. Mike Quilliam and Dr. Louis Ramaley for their support and guidance. Special thanks go to Dr. Bob Boyd, Dr. Stephen Pleasance and Pearl Blay. I would also like to thank everyone in the analytical section at NRC, especially Dr. Pierre Thibault, Dr. Greig Sim, Bill Hardstaff, Ed Dyer, Glenn McCully and Don Embree. I am grateful for the assistance provided by Ruth Bailey and David North from Health and Welfare Canada.

The funding from the Chemistry Department, NSERC and Dr. Frank Benoit of Health and Welfare Canada is gratefully appreciated.

Finally, I am eternally grateful for the love and support provided by my wife Patty. You were right all along, this thesis stuff does come to an end sooner or later (and I'm still as sane as I was before I started).

I. INTRODUCTION

I.1 Polycyclic Aromatic Compounds

Polycyclic aromatic compounds (PAC) have captured the attention of a very large number of research groups for several decades.[1] This interest is a result of the ubiquitous nature of these compounds and their potentially hazardous effects on nature and man. The formation, distribution and importance of these compounds have been studied in detail and the following paragraphs will provide a brief introduction to these topics. The analytical methods that have been developed over the years for the determination of PAC are quite extensive. A brief survey of these methods, with particular emphasis on chromatographic techniques, will also be presented.

When discussing PAC, it is often convenient to divide this large class of compounds into smaller groups. The divisions are based on the functionality of the compounds. Figure I-1 illustrates several sub-groups that can be obtained from PAC. Each PAC sub-group can be considered to be derived from the polycyclic aromatic hydrocarbons (PAH). PAH are simply condensed benzenoid hydrocarbons containing five- or six-membered rings, or two ring systems connected by a single bond (biaryls). Substitution of one or more hydrogens on the rings with a functional group produces a new sub-group classification. Some functional groups commonly associated with PAC include alkyl, amino, nitro, cyano, keto, and hydroxy groups (see Figure I-1).

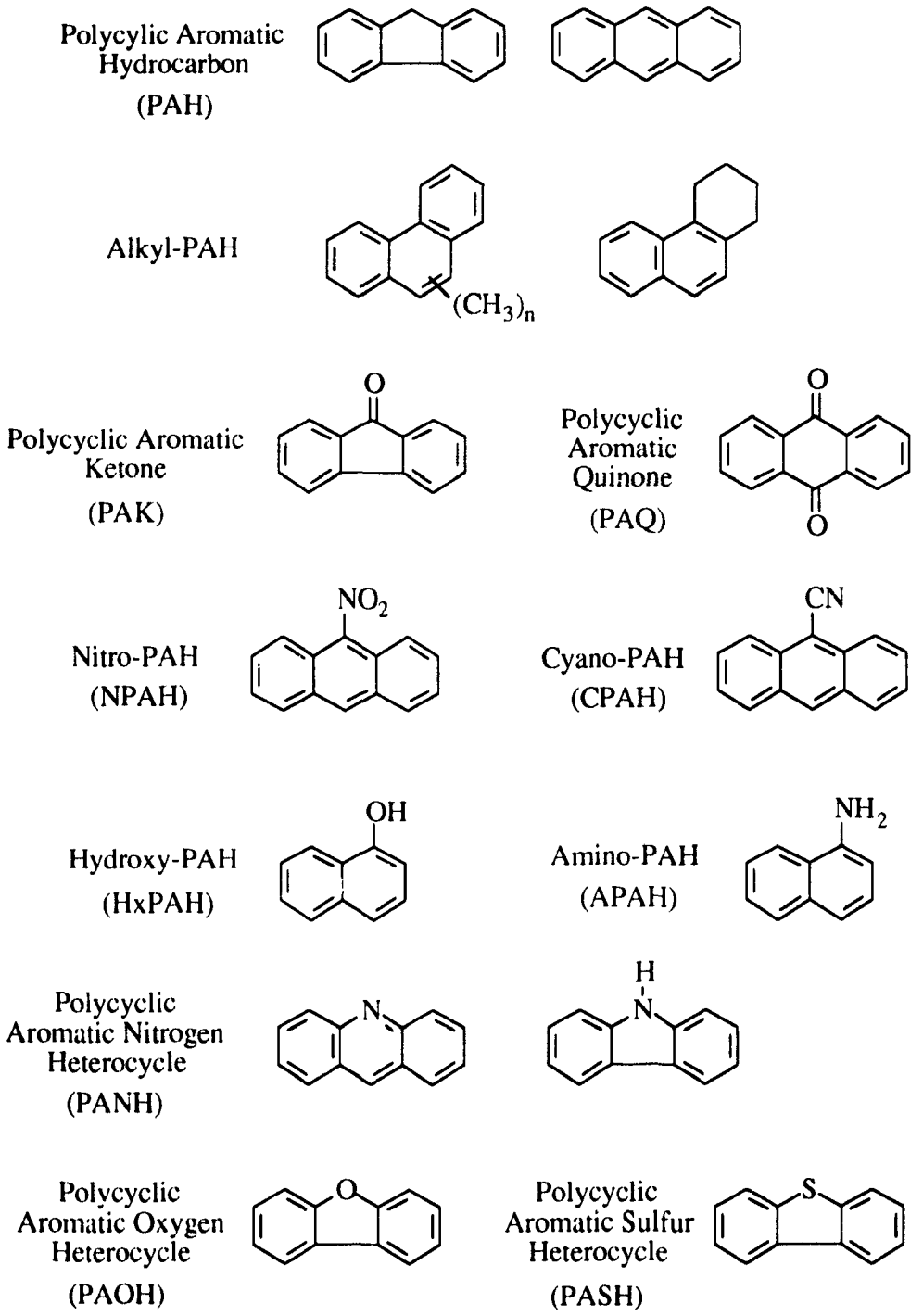

Figure I-1: Polycyclic aromatic compounds.

Heterocyclic PAC are formed by the substitution of one or more ring carbons with oxygen, sulphur or nitrogen in either a five or six membered ring. Benzofurans and benzothiophenes are examples of O and S substitution (in a five membered ring) and quinolines and carbazoles are examples of N substitution (in a six and five membered ring, respectively).

For many of the PAC described above, there may be a large number of isomeric structures. In general, the number of possible isomers increases with molecular weight and with the degree of substitution on the ring system.

I.2 Formation of PAC

PAC can be formed from both natural (e.g., biosynthesis and natural combustion) and anthropogenic (e.g., high temperature combustion) sources, although the latter are by far the major contributors of environmentally hazardous compounds of this class.[1] The mechanisms of formation of PAC during incomplete combustion of organic material is far from being completely understood. It is believed that two distinct reaction steps are involved: pyrolysis and pyrosynthesis. At high temperatures, organic compounds are partially cracked into smaller, unstable molecules (pyrolysis). These fragments, mostly radicals, recombine to yield larger, relatively stable aromatic hydrocarbons (pyrosynthesis). Once formed, simple PAC might undergo further pyrosynthetic reactions to yield higher condensed ring structures (i.e., high molecular weight PAC).

In general, all organic compounds containing carbon and hydrogen may serve as precursors of PAH. Pyrolysis of a substance displaying chain branching or unsaturation usually results in an overall increase in the production of PAH. When oxygen, sulphur, or nitrogen is present in the starting materials, heterocyclic PAC analogs of the PAH can be produced. Substituted PAC (e.g., nitro-PAC) may result from atmospheric reactions with reactive gases.[2,3]

I.3 Distribution of PAC in the Environment

The sources of environmental PAC include a variety of processes, both natural and anthropic. PAC have been found in air, water, marine sediments, food, tobacco smoke, and fossil fuels. The amount of research conducted on the distribution of PAC in these matrices has been so extensive that it is almost impossible to cite all the papers that have been published on these subjects.[1]

Airborne PAC are always associated with various types of aerosols, both natural (such as forest fires, volcanic dust, and dust-rise by wind) and man-made (combustion and industry). The distribution of PAC in the atmosphere is governed by aerosol transport from place to place primarily by wind currents, fall-out by precipitation, and chemical degradation. During the last 40 years, many studies throughout the world have been undertaken to characterize the PAC content in airborne particulate matter.[1] The results

have produced very detailed and comprehensive identifications of PAC primarily by combined gas chromatography-mass spectrometry (GC-MS).

The presence of PAC in the water environment has received much less attention than the polluted air problem. The distribution of PAC in different bodies of water depends on their point sources: crude oil spills from tankers, oil drilling or storage areas; terrestrial run-off of rain water that scrubs PAC from the air, soil, pavements, slag dumps, and coal storage piles; atmospheric deposition of particulates directly into streams and lakes; and effluents from industrial plants.[1] The low polarity of PAH render them fairly water insoluble, and therefore, a large proportion of the PAC content of polluted water is adsorbed on suspended solids that are eventually incorporated in the sediment. Extracts of PAC contaminated sediments are usually quite complex and contain a variety of alkyl and cycloalkyl derivatives as well as sulphur and oxygen heterocycles.[4,5]

PAC fractions from fossil fuels are generally much more complex than fractions obtained from combustion sources. They are extremely rich in alkylated and hydroaromatic species. Figure I-2 illustrates the structural range of petroleum hydrocarbons as a three-dimensional, continuous array.[1] Generally, each compound type occurs as a continuous homologous series in petroleum. Similar diagrams could be constructed to represent the oxygen, sulphur, and nitrogen heterocyclic fractions.

Coal, shale, and tar sand derived oils tend to contain larger quantities of alkylated PAC, heterocyclic constituents, and hydroaromatics than does petroleum.[1] High boiling (or heavy) distillates, such as those from tar sands, have been rarely examined for two main reasons: first, the

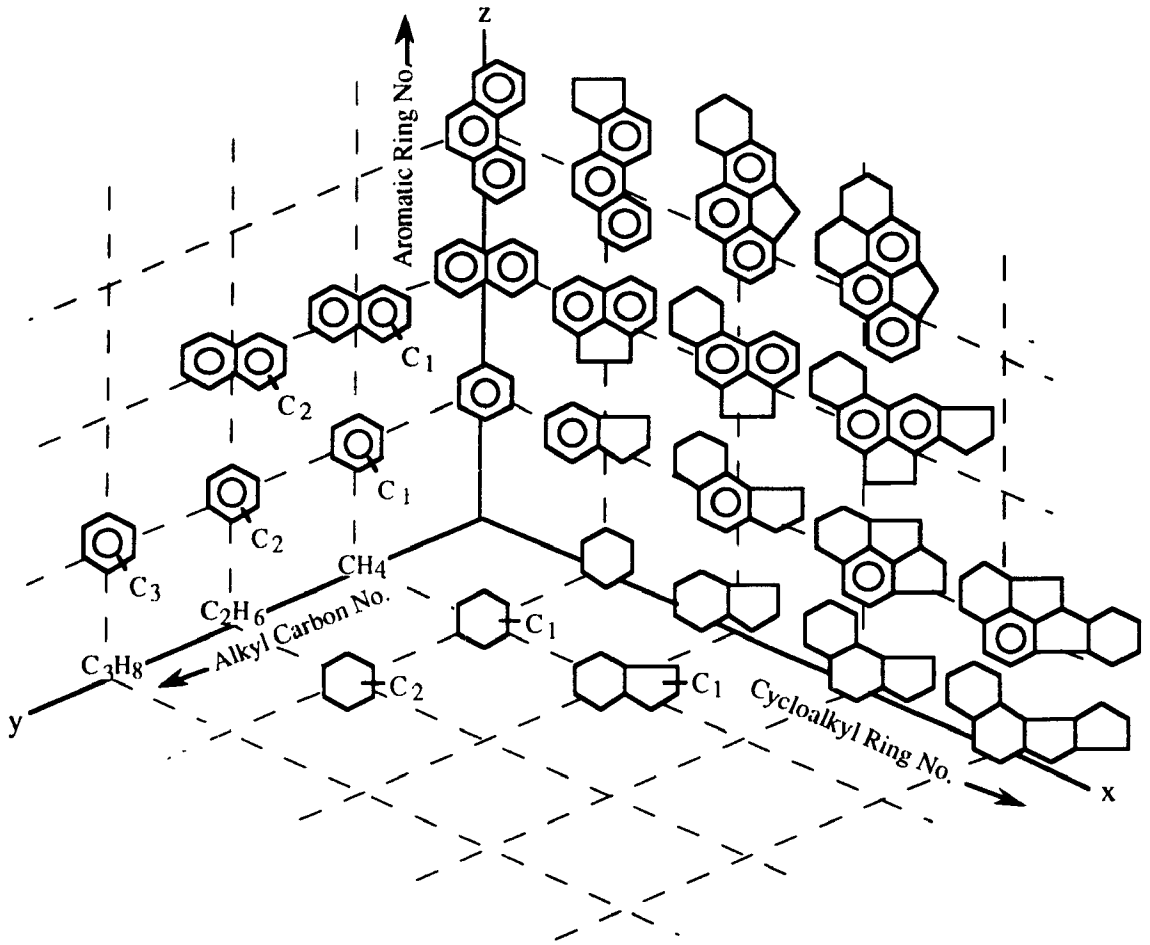

Figure I-2: The structural range of petroleum hydrocarbons (adapted from reference 1).

components of these heavy distillates were so complex that standard analytical techniques such as gas chromatography were unable to give any conclusive information about the composition of these oils; and second, heavy oil distillates that have a wider and higher boiling range were not interesting to the petroleum industry previously because they are much more difficult and more costly to refine than the light oils. Recently, however, more interest has been shown in heavy distillates, particularly in Canada, as an alternate fuel source of the future.[6,7]

I.4 Importance of PAC

The medical profession recognizes a variety of diseases with different symptoms and origins under the expression "cancer". In each case, the common characteristic is uncontrolled cell growth. It has been estimated that 70-90% of human and animal cancer is caused by environmental factors.[1] Among the environmental chemicals concerned, PAC comprise the largest group of carcinogens. Air pollutants (and PAC adsorbed on airborne particulates) are believed to be major contributors to the higher death rate from lung cancer in urban areas compared to rural areas. Occupational skin cancer resulting from prolonged exposure of workers' skin to soot, petroleum fractions, coal products, etc., is also assumed to be PAC-related.

The health hazards discussed above are not the only concerns in the petroleum and synthetic crude oil industry; PAC also interfere in various upgrading processes required in the production of usable products. In

particular, nitrogen-containing PAC are suspected of deactivating and poisoning catalysts during cracking and reforming processes. Plugging problems and reduced heat exchange also arise from the formation of high molecular weight PAH deposits in exchangers, transfer lines, and valves.[8]

I.5 Analytical Methods

As a result of the complex nature of most real world PAC-containing samples, fractionation according to chemical class is usually required before identification of individual components can be achieved. Table I-1 lists some of the methods that have been described in the literature. Most these methods have been shown to provide an adequate fractionation for the sample of interest. Open column liquid chromatographic methods, with alumina and silica being the popular normal phase supports, have become the most common method for chemical class separations. Other packings such as aminopropyl- and cyanopropyl- derivatized silica gels, Sephadex LH-20, and ion exchange resins have also been used (see Table I-1). In most cases, comprehensive isolation procedures usually employ the sequential combination of two or more separation steps.

Some samples, synthetic fuel fractions in particular, require even higher chromatographic resolution than can be achieved with open column methods. High performance liquid chromatography (HPLC) and preparative-HPLC have been shown to provide rapid and highly efficient separations that

TABLE I-1: Separation methods for polycyclic aromatic compounds.

Methods	Selected References
Soxhlet Extraction	9, 10
Distillation	11, 12
Liquid - Liquid Extraction	13, 14, 15, 16, 17, 18, 19, 20
Alumina Column	21, 22, 23, 24, 25, 26, 27, 28, 29
Silica Column	19, 26, 28, 25, 30, 31, 32, 33, 34
Gel Permeation	12, 35
Sephadex LH-20 Column	9, 16, 18, 36, 37, 38
$FeCl_3$ Clay Column	39
Ion Exchange	12, 14, 40, 41
Thin Layer Chromatography	12, 42
Normal Phase Liquid Chromatography	8, 33, 37, 43, 44, 45, 46, 47
Reverse Phase Liquid Chromatography	27, 48
Supercritical Fluid Extraction	49, 50
Derivative Formation	31, 32, 51, 52, 53

are very reproducible.[54] Considerable emphasis in the literature has been placed on the use of commercially-available chemically bonded normal-phase supports (e.g., aminopropyl-, cyanopropyl- and nitrophenyl-silane packing materials). Normal-phase HPLC separations have been used to provide chemical class separations (similar to those provided by open column methods), as well as to further fractionate a single PAC sub-class according to the number of condensed rings.[55]

Methods of analysis that offer good resolving power and both selective and sensitive detection are required for the final analysis of complex PAC fractions. Table I-2 lists some of the common analytical techniques described in the literature. The most popular method has been gas chromatography (GC), with almost all the work done in the last decade using wall-coated fused silica capillary columns. The two commonly used all-purpose detectors for GC analyses are the flame ionization detector (FID) and the mass spectrometer (MS). The latter detection method provides high sensitivity together with a wealth of structural information. The coupling of GC to MS is relatively easy since the pumping speeds of conventional mass spectrometers can easily accommodate the low capillary column GC gas flow rates.

HPLC has several advantages over GC, namely: less sample clean-up is required, thermally-labile compounds are more easily analyzed since they are not exposed to excessive heat, derivatization is usually not necessary and PAC with high molecular weights may be analyzed because volatility is not a requirement. HPLC is also an inherently better quantitative method because of the injection volume precision available with fixed loop injectors (as opposed to syringe injections with GC). The high chromatographic efficiency

TABLE I-2: Analytical methods for polycyclic aromatic compounds.

Methods	Selected References
Gas Chromatography	
Detectors:	
Mass Spectrometry	56, 57, 58, 59
FID	45, 60, 61, 63, 62
Other	64, 65, 66, 67, 68
High Performance Liquid Chromatography	
Reversed-Phase Columns	69, 70, 71, 72, 73, 74
Normal-Phase Columns	43, 44, 69, 75, 76, 77
Detectors:	
UV/vis	5, 70, 78, 79, 80, 81, 82
Fluorescence	83, 84, 85, 86, 87
Mass Spectrometry	88, 89, 90, 91, 92, 93
Other	30, 94, 95, 96
Supercritical Fluid Chromatography	
Packed Column	97, 98, 99, 100, 101, 102
Capillary Column	103, 104, 105, 106, 107, 108
Detectors:	
FID	101, 105, 109, 107, 110, 50
UV	98, 99, 100, 101, 111, 110
MS	97, 112, 113, 114, 115, 116
Other	18, 102, 105, 106, 117
Mass Spectrometry	
EI	2, 9, 86, 118, 119, 120
CI	121, 122, 123, 124, 125, 126
FAB	127, 128, 129, 130, 131, 132
Other	119, 133, 134, 135, 136, 137

available from capillary GC, however, is not currently available from conventional HPLC. Thus, HPLC chromatographic peaks are more likely to contain unresolved components. The availability of both sensitive general-purpose and selective detectors remains among the most serious limitation of modern LC. The ultraviolet (UV) absorption detector, the most widely used detector for LC, can provide sensitive detection of UV-absorbing compounds, and the use of UV/visible diode array detectors (DAD) allows for the acquisition of UV/vis spectra of eluting compounds during an LC separation. Fortunately, aromatic compounds are strong absorbers of UV light and the UV/vis detector can be considered a "universal detector" for this class of compounds. Since various PAC have different absorptivities at a given wavelength, the selectivity (as well as the sensitivity) of this detector can be enhanced by monitoring at the wavelengths that give the greatest absorption for each target compound The multi-signal detection capability of the DAD allows several wavelengths to be monitored simultaneously. In addition, the acquisition of several spectra during a compound's elution can be used to examine the peak's purity (if the impurity and analyte have slightly different spectra and retention times). One limitation of the UV detector is the wide variations in relative molar responses resulting from the different UV spectra and extinction coefficients of PAC.

The need for a more sensitive, selective and yet universal detector for LC resulted in considerable interest in the development of routine LC-MS methodologies. The combination of LC and MS has been a more challenging task than it was for GC-MS, but LC-MS offers the analytical chemist one of the most powerful analytical techniques at the present time. The problems

associated with interfacing these two fundamentally different techniques have been considerable; for example, the typical pumping speed for a MS is 5 mL /min of gas, whereas an LC operating at 1 mL/min (water) will produce 1200 mL/min of gas. Significant progress has been made in this area since the first successful LC-MS attempts were made in the early seventies.[138,139] Three general strategies have been used in the development of LC-MS interfaces: a) flow rate reduction by splitting or by using micro-LC (e.g., direct liquid introduction and continuous flow FAB interfaces); b) mobile phase removal (e.g., the moving belt and particle beam interfaces); and c) special ionization/interface methods (e.g., thermospray, the heated pneumatic nebulizer and ionspray).

Supercritical fluid chromatography (SFC) using either capillary or packed columns is a rapidly developing method for the separation and identification of organic compounds that lack sufficient volatility or thermal stability to be separated by GC.[140,141] The use of SFC to separate higher molecular weight PAH and analyze heavy oils has been reported by several research groups (see Table I-2).

The most common detector for capillary SFC has been the FID, whereas, the UV detector has been favoured for packed-column SFC. Each of these detection methods provide relatively good sensitivity, wide dynamic ranges, analytical ruggedness and ease of use. A number of approaches in combining SFC with MS have been reported, some of which are listed in Table I-2. The difficulties involved in developing an effective SFC-MS interface, especially for packed-column SFC that operates at higher flow rates, have been due to the pressure requirements of conventional MS ion sources.

The majority of the previous attempts have used modified LC-MS interfaces such as the moving belt system or thermospray sources.[114]

Mass spectrometry alone has also been another very useful technique for characterization of complex mixtures of PAC. For example, LC fractions can be collected, evaporated and then analyzed by electron ionization (EI) MS using a direct insertion probe.[142] The choice of other ionization modes, such as chemical ionization (CI) and fast atom bombardment (FAB), is also available when this approach is used in the analysis of PAC.[121,128]

Other spectroscopic techniques such as UV/vis or infrared spectroscopy are also important for the characterization of PAC fractions. Nuclear magnetic resonance (NMR) spectroscopy has been used to deduce structural parameters for heavy oil distillates.[7,143] The NMR spectral data are normally used in conjunction with other analytical data, such as elemental combustion analysis and molecular weight measurements, to obtain a number of important average molecular parameters. However, average compositional parameters do not provide information on the distributions of molecular sizes and chemical types among the extremely large number of individual constituents in heavy oils.

I.6 Research Objectives

The principal objectives of this research effort were to develop, implement and critically evaluate high performance liquid chromatography -

mass spectrometry (LC-MS) interfaces for the analysis of PAC. Four markedly different interfaces were included in this study, *viz*: moving belt, particle beam, heated pneumatic nebulizer, and ionspray. The use of supercritical fluid chromatography as an alternative to LC was considered for those interfaces that show particular promise in the analysis of PAC. This generally involves a slight modification of the interface to accommodate the different operating conditions necessary to maintain the supercritical fluid.

Standard chromatographic detectors, such as the ultraviolet (UVD) and photoionization (PID) detectors, were used to ensure adequate chromatographic separations were achieved prior to mass spectrometric experiments. Mixtures of PAC standards as well as a few "real world" samples containing complex mixtures and high molecular weight PAC, were used to compare chromatographic and LC-MS performance. These comparisons were based on the ability of each technique to provide tentative compound identifications, isomer discrimination, and detection of high molecular weight PAC.

Finally, the optimized chromatographic-MS methods that provide the best qualitative information, based on the criteria mentioned above, were evaluated for their ability to quantify PAC in complex mixtures. Detection limits and linear dynamic ranges were determined using PAC standards, while the concentrations of PAC in a certified coal tar standard reference material were measured using both external and internal standard methods.

II. EXPERIMENTAL

II.1 Materials

HPLC grade hexane, acetonitrile, dichloromethane, chloroform, methanol and benzene were obtained from BDH Chemicals (BDH Inc., Toronto, Ont.) and were used without further purification. Distilled water was passed through a Milli-Q water purification system (Millipore Corp., Bedford, MA) before use. All solvent mixtures are specified as volume/volume ratios.

PAC standards from Aldrich (Milwaukee, WS, USA), Supelco (Oakville, Ont., Canada) and Anachemia (Montreal, Quebec, Canada) were used without further purification. A dried carbon black extract, prepared by extracting an experimental carbon black with methylene chloride in a Soxhlet apparatus, was obtained from J. Fetzer of Chevron Oil. The sample was dissolved in dichloromethane and filtered before use in LC analyses.

A complex mixture of PAC from coal tar, Standard Reference Material (SRM) 1597, and 16 priority pollutant PAH (in acetonitrile), SRM 1647, were purchased from the National Institute of Standards and Technology (NIST, Gaithersburg, MD, USA). A solution containing 21 perdeutero PAH (DPAC-1), being developed by the Marine Analytical Chemistry Standards Program (MASCP) of the National Research Council (NRC) of Canada, was used as an internal standard solution for quantitation experiments.

The DPAC-1 internal standard solution was spiked at four different levels into the NIST SRM 1647 PAH mixture in ratios of 1:1, 1:5, 1:10 and 1:15 (v/v). The perdeutero solution was designed to have analyte concentrations

that are similar to those found in natural samples but the SRM 1647 solution has all analytes at roughly the same concentration. The four spike ratios were thus chosen to ensure that the concentrations of the native and perdeutero PAH were in a ratio of approximately 1:1 in at least one of the solutions. The DPAC-1 internal standard solution was also spiked into the NIST SRM 1597 coal tar mixture in a ratio of 3:1 (v/v). This spike ratio ensured that most of the analyte concentration ratios fell with the ranges covered by the DPAC-1/SRM 1647 solutions. Since the volumes of all the solutions dispensed were measured accurately, the final mixtures were also used for external calibration experiments.

A series of ten tar sand oil samples were kindly supplied by Emerson C. Sanford of Syncrude Canada Ltd. (Figure II-1). Sample 1A is a feed bitumen that goes into the upgrading processes. The next three samples (1B, 1C, 1D) are from a laboratory hydrotreating study in which conditions were controlled to avoid thermal cracking. The three samples are from distiling the total liquid product: sample 1B - IBP-343°C, 1C - 343-524°C, and 1D -524°C+ or pitch. Similarly the next three samples (1E, 1F, 1G) are distillate cuts with the same ranges. However, in this experiment, conditions were such that considerable thermal cracking took place. The final three samples (1H, 1I, 1J) were from a run in which the conditions were the same as the first except that no catalyst was used. These samples were chosen to cover a broad range of conditions in the laboratory reactor. The ultimate goal of this collaboration between our lab and Syncrude Canada is to determine the effects of the various hydrotreating processes on the PAC content of the oils using the analytical techniques being developed.

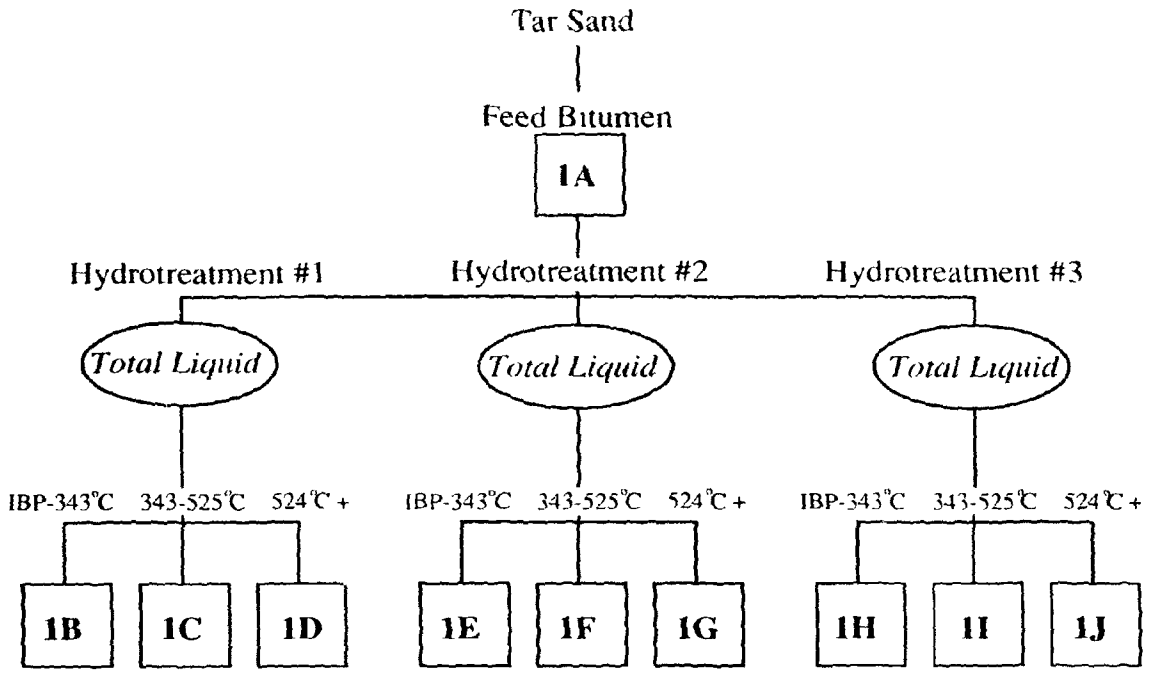

Figure II-1: The hydrotreated tar sand oil samples (1A - 1J).

II.2 Open Column Chromatography

After reviewing a variety of separation methods in the literature, the fractionation procedure described by Later *et al.*[25] was selected as the basis for separating the tar sand oils into compound classes. The method was modified slightly to accommodate the expected complexity of the samples. A schematic diagram of the modified separation method is shown in Figure II-2. Neutral alumina (Brockmann grade I, BDH Chemicals) was dried in an oven at 150-170°C for at least 5 hours before use. Approximately 4 grams of the neutral alumina were coated with 0.3 grams of the oil and placed at the top of an 11 mm ID glass chromatography column that was dry-packed with 12 grams of neutral alumina. The sample was then eluted from the column with the following solvents to produce a series of fractions: 50 mL hexane, the aliphatic hydrocarbon fraction; 50 mL of benzene, the neutral PAH fraction; 100 mL of chloroform:ethanol (99:1), the nitrogen-containing PAC fraction; and 50 mL of methanol and 50 mL of methanol:water (4:1), the remaining polar compounds.

A further modification of this method was required because of some overlap between the aliphatic and neutral PAH fractions, and the neutral PAH and nitrogen-containing PAC fractions. The volume of hexane and benzene was therefore increased to 100 mL each to help minimize this overlap. All the results shown in this thesis were obtained from the analysis of the oil labelled 1F (Figure II-1), which was hydrotreated under conditions such that considerable thermal cracking took place.

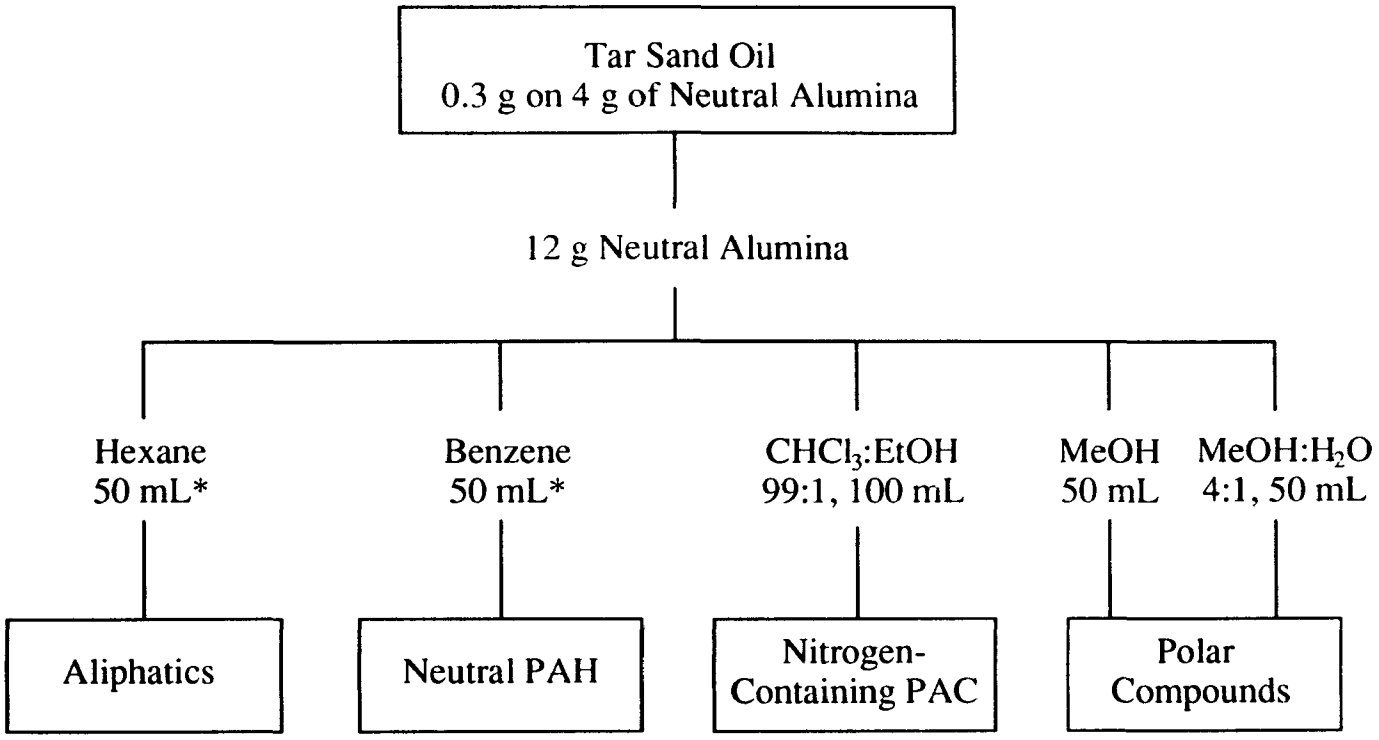

* Changed to 100 mL in later experiments.

Figure II-2: The neutral alumina fractionation scheme.

II.3 Normal-Phase Liquid Chromatography-Diode Array Detection

All LC-UV/Vis analyses were performed with an HP1090M chromatograph (Hewlett-Packard Palo Alto, CA, USA) equipped with a ternary DR5 solvent delivery system, a built-in HP1040A diode array detector (DAD), and an HP7994A data system. The detector was configured for acquisition of absorbance at 368 ± 132 nm and/or 254 ± 2 nm.

The following commercially available normal-phase LC columns were used: (a) Whatman 5 μm Partisil-5 PAC RAC II, 10 cm x 4.6 mm ID (Whatman Inc., Clifton, NJ, USA); (b) Waters 10 μm Energy Analysis NH_2, 30 cm x 3.9 mm ID (Waters Chromatography Division, Mississauga, Ont.); (c) Waters 10 μm μBondapak CN, 30 cm x 3.9 mm ID; and (d) Techsil 10 μm NO_2, 25 cm x 4.0 mm ID (hplc Technology Inc., Wilmslow, UK).

The mobile phase gradient used with all the columns was as follows (with linear programs between each time point):

Time (min)	% Hexane	% Dichloromethane
0	100	0
20	100	0
25	99.5	0.5
30	98	2
35	95	5
40	85	15
45	60	40
50	0	100
65	0	100
70	100	0

A mobile phase flow rate of 1.0 mL/minute and injection volumes of 5 μL were used on all columns.

II.4 Normal-Phase Liquid Chromatography-Mass Spectrometry

The LC-MS experiments employing an electron ionization (EI) mass spectrometer (VG 20-250 quadrupole mass filter, VG Analytical, Altrincham, UK) were conducted using a VG belt-transport LC-MS interface. A VG spray deposition probe was used to partially evaporate and deposit the LC effluent onto the moving polyimide belt. The nominal electron energy was 70 eV, with a trap current of 100 μA. The source temperature was 250°C, and the belt heater at the tip of the belt interface, located within the body of the ion source, was operated at 0.8 V (belt surface temperature unknown). The belt speed was maintained at 1.6 cm/second and the source pressure was typically 1.5×10^{-5} Torr. In addition, an iso-propyl alcohol belt wash was employed in order to avoid memory effects. Full scan mass spectra were acquired over a range of m/z 100 to 500 with a scan cycle time of 3 seconds. A VG 11-250 data system was used for instrument control and for data acquisition and processing. Normal-phase LC conditions were identical with those used in the LC-UV/Vis experiments (described above).

II.5 Reversed-Phase Liquid Chromatography-Diode Array Detection

All analyses were performed on Vydac 201TP52 columns (25 cm x 2.1 mm ID, 5 μm, Separations Group, Hesperia, CA, USA) using the same experimental set-up described earlier for normal-phase LC-UV/Vis. A 0.2

mL/min mobile phase linearly programmed from 60% aqueous acetonitrile to 100% acetonitrile over 30 minutes and holding for an additional 30 minutes before being programmed back to the initial conditions in 5 minutes was used for most experiments. Additional mobile phase gradients used in this study include: 60% aqueous acetonitrile linearly programmed to 100% acetonitrile over 30 minutes, holding for 5 minutes before being linearly programmed to 100% dichloromethane over 40 minutes and holding for 20 minutes, then programmed back to the initial conditions in 10 minutes; and, starting at 100% acetonitrile for 15 minutes and increasing linearly to 100% dichloromethane over 40 minutes, holding for 40 minutes and then programmed back to the initial conditions in 5 minutes.

II.6 Reversed-Phase Liquid Chromatography-Mass Spectrometry

II.6.1 The Moving Belt Interface

The mass spectral and moving belt interface conditions used in reversed-phase LC-MS experiments were identical with those used for normal-phase LC-MS (described earlier). Full scan mass spectra were acquired over a range of m/z 150 to 600 with a scan cycle time of 3 seconds. Selected ion recording experiments were performed using a dwell time of 200 msec per ion. Reversed-phase LC conditions were identical with those used in the LC-UV/Vis experiments (described above).

II.6.2 The Particle Beam Interface

Analyses were performed on a Hewlett-Packard instrument consisting of a model 1090 Series II liquid chromatograph with a ternary PV5 solvent

delivery system, a model 59980A particle beam interface, and a model 5988A quadrupole mass spectrometer. Ultrahigh purity helium (Liquid Carbonic, Scarborough, Ont., Canada) was used as the nebulizing gas at a flow rate of approximately 1.5 L/min. The temperature of the desolvation chamber was maintained at 45°C. Positive ion EI spectra were obtained at 70 eV with a source temperature of 250°C. Full scan mass spectra were acquired over a range of m/z 100 to 500 with a scan cycle time of 3 seconds. LC conditions were identical with those used in the reversed-phase LC-UV/Vis experiments.

Selected ion recording experiments on the NIST-SRM/DPAC-1 quantitation solutions monitored a total of 24 ions in three acquisition periods (8 ions per period, 1 second total scan time): first period, 0-9.8 minutes; second period, 9.8-33.5 minutes; and the last period, 33.5-60 minutes.

II.6.3 The Heated Pneumatic Nebulizer Interface

Analyses were performed on a SCIEX (Thornhill, Ont.) API III triple quadrupole mass spectrometer equipped with an atmospheric pressure ionization (API) source and a heated nebulizer LC-MS interface. The corona discharge electrode was maintained at 2 kV and high purity air was used as the nebulizing gas at a flow rate of 1.2 L/min. Full scan mass spectra were acquired over a range of m/z 50 to 450 or m/z 100 to 500 with total scan cycle times between 2 and 3 seconds. A Macintosh IIx computer was used for instrument control, data acquisition and processing. LC conditions and equipment were identical with those used in the reversed-phase LC-UV/Vis

experiments.

Benzene charge-transfer experiments were performed by modifying the heated nebulizer interface to allow the post-column addition of benzene to the APCI source. A capillary tube was fed through the make-up gas inlet line directly to the heated quartz tube of the interface (Figure VI-1). As the benzene is pumped through this capillary tube into the interface it is instantly vaporized and carried by the coaxial make-up gas flow into the corona discharge plasma.

Selected ion recording experiments on the NIST-SRM/DPAC-1 quantitation solutions monitored a total of 48 ions ($M^{+\cdot}$ and MH^+) in six acquisition periods (8 ions per period, 1 second total scan time): first period, 0-8.8 minutes; second period, 8.8-10.5 minutes; third period, 10.5-18 minutes; fourth period, 18-33.4 minutes; fifth period, 33.4-46 minutes; and the last period, 46-60 minutes.

II.6.4 The Ionspray Interface

Analyses were performed on a SCIEX API III triple quadrupole mass spectrometer equipped with an atmospheric pressure ionization (API) source and an ionspray LC-MS interface. The ionspray needle was maintained at 5.6 kV and high purity air was used as the nebulizing gas at a flow rate of 0.6 L/min. Full scan mass spectra were acquired over a range of m/z 50 to 450 with a total scan cycle time of 2 seconds. A Macintosh IIx computer was used for instrument control, data acquisition and processing. LC conditions were identical with those used in the reversed-phase LC-UV/Vis experiments, except that 0.1% TFA was added to the mobile phases for some experiments.

Flow injection analysis was accomplished by removing the LC column from the liquid chromatograph and allowing the mobile phase and injected samples to pass directly to the interface.

Charge-transfer complexation and electrochemical oxidation ionspray mass spectra were acquired by the flow injection analysis of PAC standards dissolved in dichloromethane containing an excess of 2,3-dichloro-5,6-dicyano-*p*-benzoquinone (DDQ) and in 100% dichloromethane, respectively.

II.7 Supercritical Fluid Chromatography-Photoionization Detection

Analyses were performed on a microbore packed-column SFC system that was comprised of a Brownlee Microgradient syringe pump (Brownlee Labs, Chromatography Division of Applied Biosystems, Santa Clara, CA, USA), a Rheodyne Model 7520 injector (Supelco) fitted with a 1.0 or 0.5 μL loop, and a column heater and controller (FIA-tron Systems Inc., Oconomowoc, WI, USA). Supercritical conditions were maintained with the use of commercially available integral restrictors (Suprex Corporation, Pittsburg, PA, USA) rated with flow rates in the range 50-100 mL/min. SFC grade CO_2 (over-pressured with helium at 1500 psi) was purchased from Matheson Gas Products Canada. Separations were achieved on 200 x 1 mm ID column packed with 5 μm Deltabond C_{18} phases (Suprex) or on a 250 x 1 mm ID column packed with Brownlee SS251 5 μm Spheri-5 silica. Linear pressure programs from 2000 psi to 5000 psi over 20 minutes then holding for 20 minutes, and 2000 psi to 6500 psi over 20 minutes then holding for 20 minutes were used on the silica and C_{18} phases, respectively. Column temperatures were maintained at 80°C. A HNU Model P1-52-02

photoionization detector (HNU Systems, Newton, MA, USA) with a 10.2 eV lamp was maintained at 300°C. An IBM AT compatible computer was used for data acquisition and processing.

II.8 Supercritical Fluid Chromatography-Mass Spectrometry

All SFC-MS experiments were performed on a SCIEX API III triple quadrupole mass spectrometer. The SFC-MS interface was constructed from a commercially available heated nebulizer interface (SCIEX) and is shown schematically in Figure VI-33. Connection of the SFC column to the restrictor was made via a zero-dead-volume union mounted in the probe handle. The stainless steel probe tip was heated by a coil of resistance wire and its temperature (typically 300-350°C) was monitored with a thermocouple. The corona discharge electrode was maintained at 2 kV and high purity air was used as the nebulizing gas. Full scan mass spectra were acquired over a range of m/z 50 to 450 or m/z 100 to 500 with total scan cycle times between 2 and 3 seconds. Dwell times of 200 msec per ion were used for selected ion monitoring experiments. A collision energy of 30 eV was used for tandem mass spectrometric experiments, with argon as the target gas at an indicated thickness of 3.5×10^{14} molecules cm^{-2} and a step size of 0.5 Da. A Macintosh IIx computer was used for instrument control and data acquisition. SFC conditions were identical with those used in the SFC-PID experiments.

III. CHROMATOGRAPHIC METHODS

Chromatographic methods that provide high resolution separations are required for the analysis of real world PAC mixtures because of their high degree of complexity. GC is the most popular method for PAC analysis because of the high chromatographic efficiencies available from modern wall-coated fused silica capillary columns. However, the inability to analyze less volatile compounds (e.g., high molecular weight PAC) is the most important and severe limitation associated with GC techniques. Therefore, this study will deal entirely with alternate chromatographic methods, namely: LC and SFC.

This chapter is intended to provide a brief introduction to and discussion of the chromatographic techniques used in this study for the analysis PAC mixtures. The first two sections will deal with the two modes of modern LC, reversed-phase and normal-phase, while the last section will discuss the use of packed-column SFC. A brief description of the important aspects of the separation mechanisms and examples of PAC separations will be provided in all three sections.

III.1 Reversed-Phase Liquid Chromatography

High performance liquid chromatography (HPLC) is the most commonly used analytical separation technique due to its applicability to a wide range of analytes ranging from volatile to non-volatile, low to high

molecular weight and polar to non-polar. It is an excellent quantitative technique and in many cases provides high sensitivity. Reversed-phase high performance liquid chromatography (RPLC) is now the most commonly used LC method for the analysis of PAC. The ability to separate PAC classes and substituted analogs, as well as the selective separation it provides for most PAC isomers, are the main reasons for its widespread use. In RPLC, a polar mobile phase (e.g., aqueous methanol or acetonitrile) is eluted over a hydrophobic stationary phase, usually an octadecyl (C_{18}) or octyl (C_8) functional group bonded to silica packing material. Polar substances prefer the mobile phase and elute first and as the hydrophobic character of the solute increases, retention increases. Generally, the lower the polarity of the mobile phase, the higher its eluent strength. Gradient elution techniques (i.e., increasing the organic composition of the mobile phase with time) are usually required for the analysis of mixtures that contain PAC with a wide range of solubilities (i.e., low and high molecular weight PAC).

Several studies[144,145,146,147] have shown that reversed-phase columns, with C_{18} packing materials in particular, from various manufacturers provide different retention and selectivity characteristics for PAC. These studies have shown that several factors affect the separations, including phase type (monomeric or polymeric), pore diameter and surface area of the silica substrate, and surface coverage of the C_{18} ligand. In general, "polymeric" C_{18} phases (which are prepared using trichlorosilane reagents with the addition of a small amount of water) were found to provide greater selectivity for the separation of PAC, especially isomeric PAH, than the more common and widely used monomeric phases (which are prepared using monochlorosilane

reagents with the exclusion of water).

Initially, it was suggested[145] that the more uniform or "ordered" polymeric phases could discriminate isomeric PAH through the adsorptive interactions between the solute and stationary phase as the relatively planar molecules line up along the surface. The lower retention times observed for non-planar PAH isomers further supported this idea of an adsorption contribution to the retention mechanism. However, a subsequent retention model has been introduced[144] that provides a more thorough explanation of this observed behaviour. The "slot model" envisages the bonded phase as consisting of a number of narrow slots into which the solute molecules can penetrate. Planar molecules may be able to fit more easily into such narrow slots and interact more strongly with the C_{18} phase, whereas nonplanar molecules cannot penetrate as far into the slots, and thus interact less strongly with the stationary phase.[146] Long narrow molecules would be expected to fit into more of the available slots than would "square" molecules, and so are retained longer.

The remainder of this section will demonstrate the use of RPLC for the separation of two complex mixtures of PAC used subsequently in this thesis for the comparison of the LC-MS interfaces. Only polymeric C_{18} phases will be used in this study because of the highly selective separations that can provide for PAC (as mentioned above). The first complex sample is a National Institute of Standards and Technology (NIST) coal tar standard reference material (SRM 1597) that contains primarily low molecular weight PAC. This material has been extensively characterized in the past[63] and most of its components (including PAH, alkyl-PAH, PAOH, PASH, and PANH)

have been identified. The other sample is an extract of carbon black that contains a large proportion of high molecular weight PAH. Very few of the components present in this material have been positively identified since high molecular weight PAH standards are not readily available. However, this sample has been widely used as a test mixture in the development or comparison of analytical techniques designed specifically for the analysis of high molecular weight PAH.[142]

Figure III-1a shows the chromatogram generated from the analysis of the NIST coal tar using a water/acetonitrile gradient on a Vydac polymeric C_{18} column with the DAD set to acquire absorbance at 254 ± 2 nm The mobile phase was linearly programmed from 40:60 water/acetonitrile to 100% acetonitrile over 30 minutes, and held at 100% acetonitrile for another 30 minutes. This gradient produces a high resolution separation of the low molecular weight PAC components of this sample, but the higher molecular weight species (e.g., mass 300 to 376) eluting at the end of the chromatogram had much broader peak shapes. The low abundance of these species combined with these broad peaks shapes can make it very difficult to detect these components. In addition, it is likely that all the higher molecular weight PAC will not be eluted from the column within one run, but will continue to elute during subsequent runs and appear as "ghost" peaks.

To improve the peak shapes of the late eluting compounds and increase the likelihood that all the components are eluted from the column, the mobile phase gradient can be modified to include a second gradient step. Figure III-1b shows the chromatogram obtained from the analysis of the same coal tar sample in Figure III-1a, but with an aqueous

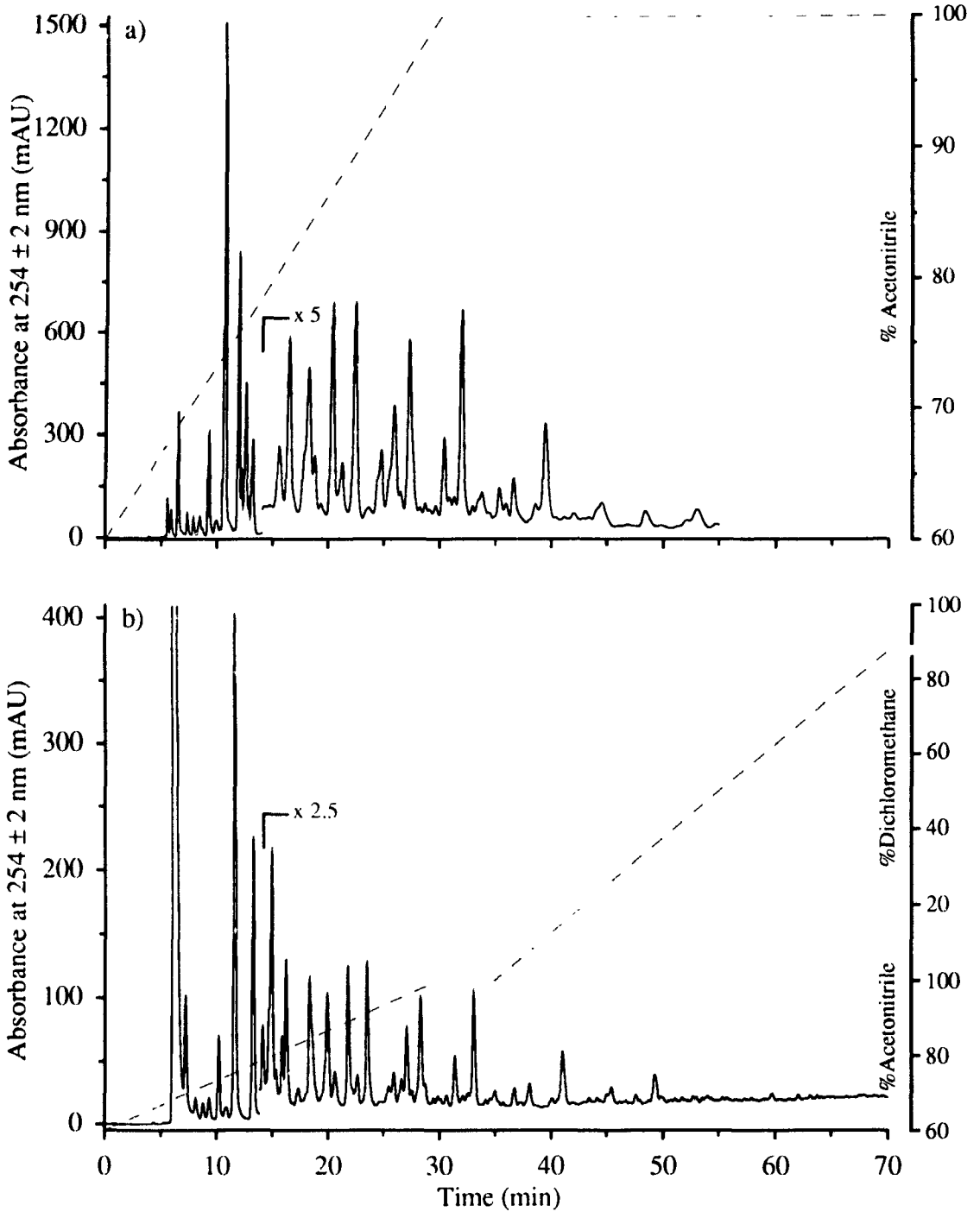

Figure III-1: Reversed-phase LC-UV chromatograms of the NIST SRM 1597 coal tar mixture using (a) an aqueous acetronitrile gradient, and (b) an aqueous acetonitrile/dichloromethane gradient.

acetonitrile/dichloromethane gradient. The new gradient starts off the same as before (40:60 water/acetonitrile to 100% acetonitrile in 30 minutes), but after holding at 100% acetonitrile for 5 minutes, the mobile phase is linearly programmed to 100% dichloromethane in 40 minutes. Dichloromethane is less polar than acetonitrile, and therefore a stronger solvent in RPLC. The additional gradient step results in lower retention times and improved peak shapes for the higher molecular weight PAC, while increasing the likelihood that all the sample components have eluted from the column.

Figure III-2a shows the chromatogram generated from the analysis of the carbon black extract using the aqueous acetonitrile/dichloromethane gradient outlined above. In contrast to the chromatogram obtained for the NIST coal tar (Figure III-1b), the trace of Figure III-2a has a large number of peaks eluting after 40 minutes, which correspond to the high molecular weight PAH, and very few peaks below 25 minutes (low molecular weight PAH). The use of dichloromethane in the final gradient step is essential in the separation and elution of the high molecular weight PAH in the carbon black extract. However, since this sample contains very few low molecular weight compounds, the initial water/acetonitrile gradient step can be shortened or even removed without a significant loss of chromatographic resolution. Figure III-2b shows the chromatogram obtained for the carbon black extract using a gradient starting, and held for 15 minutes at 100% acetonitrile, then programmed to 100% dichloromethane over 40 minutes, and held for another 15 minutes. The analysis time using this gradient is slightly shorter than that of Figure III-2a while still providing a good separation of the abundant high molecular PAH. The chromatographic

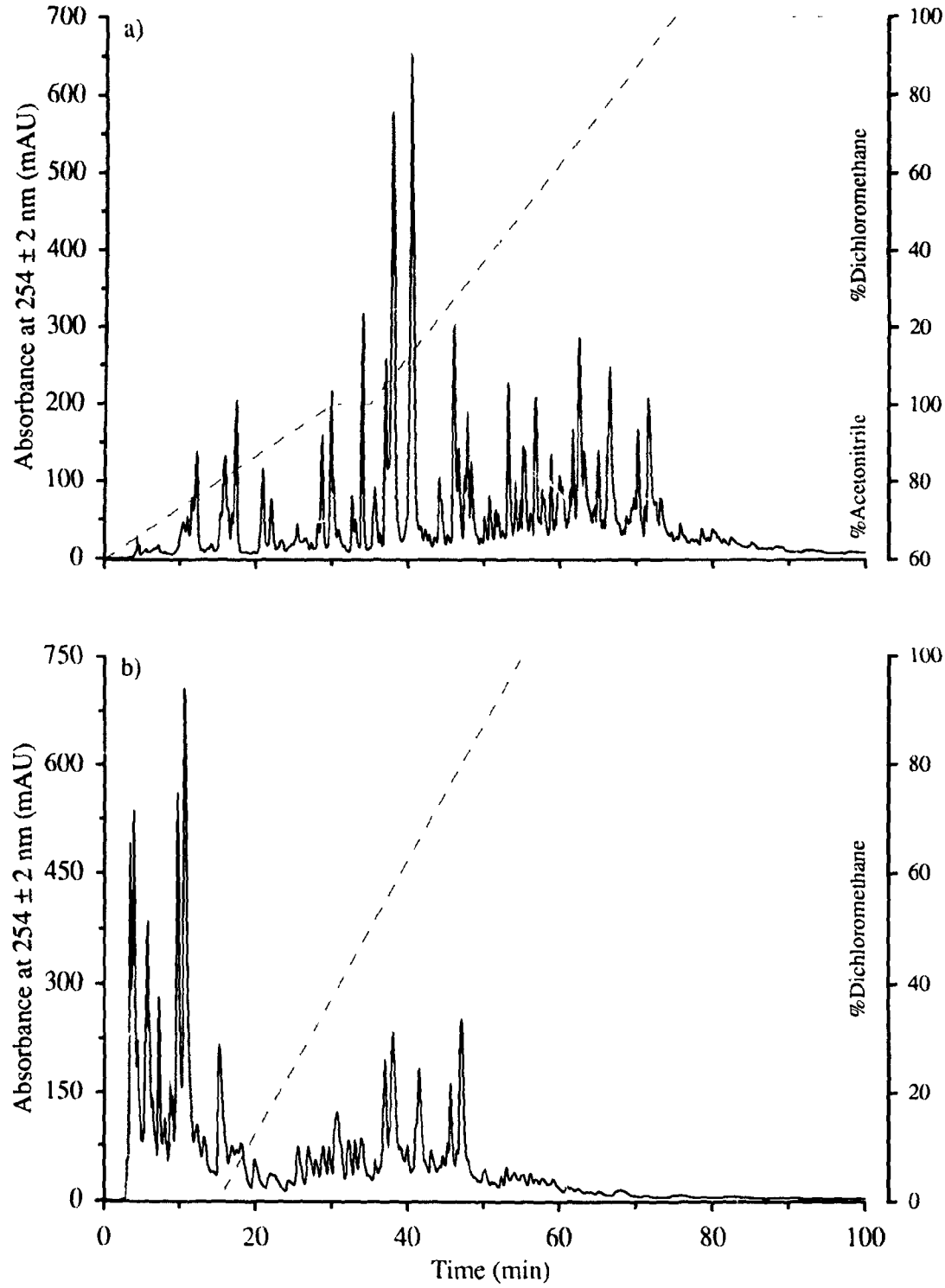

Figure III-2: Reversed-phase LC-UV chromatograms of the carbon black extract using (a) an aqueous acetonitrile/dichloromethane gradient, and (b) an acetonitrile/dichloromethane gradient.

resolution of the low molecular weight PAH has been sacrificed, but this loss is not important if the analyst is concerned only with the characterization of high mass PAC (without excessively long analysis times). In subsequent chapters, these separations will be tested on the LC-MS interfaces and much more information on these samples will be revealed.

III.2 Normal-Phase Liquid Chromatography

Normal-phase chromatography uses a polar stationary phase and a less polar mobile phase. Typical stationary phases include silica, alumina and chemically bonded phases containing aminoalkyl, cyanoethyl, phenylsilane and nitrophenyl functional groups. Mobile phase mixtures usually consist of a hydrocarbon solvent such as hexane, plus varying amounts of a more polar solvent, such as dichloromethane. PAC separations on the polar bonded phases are similar to those obtained on the classical adsorbents such as alumina and silica, i.e., saturated hydrocarbons elute prior to olefinic and aromatic hydrocarbons and the retention of PAC increases with the number of condensed aromatic rings (or the number of aromatic carbon atoms).[44,148] The exact retention mechanism is probably quite complex and will depend on the polar functional group of the stationary phase, but the interactions between the π-electron system of PAC solutes and the polar surface structures are believed to be quite significant.[1]

The presence of an alkyl group on a PAC ring system has only a slight effect on the π-electron system, and therefore only a slight effect on retention. As a result, normal-phase LC can provide very distinct class separations (e.g., all PAH with three rings, including alkyl-substituted members, have similar retention).[149] In addition, the class separation of PAH, PAOH and PANH can be readily achieved with these materials due to the more polar nature of the oxygen- and nitrogen-containing compounds.[55] All of these characteristics are often advantageous in the preparative separation of complex PAC mixtures into classes for subsequent analyses by GC and RPLC.[45,46,150] Analytical scale NPLC has also proven valuable as a tool for characterizing complex samples since overall changes in the composition of the saturated, aromatic and polar fractions can easily be determined. For example, this technique has been applied to the study of the molecular transformations of petroleum products that are upgraded in various hydrotreating processes.[151] The use of polar bonded phases also eliminates one of the major difficulties encountered with classical adsorbents such as silica, i.e., non-reproducible retention due to small changes in the moisture content of the eluent.[149]

Several polar phases have been used for the chromatographic separation of PAC, including amine (NH_2), diamine ($R(NH_2)_2$), nitrile (CN), diol ($R(OH)_2$), nitrophenyl (NO_2), and mixed functional group phases. In a comparison of nitrophenyl and aminosilane columns, Lankmayr and Müller[152] reported that the nitrophenyl phase provided the best separation of commonly found PAC. However, the application of aminosilane phases to the separation of PAC has been recommended by several groups.[149,150,153] Chmielowiec and George[44] also stated that a diamine phase was superior to

other polar bonded phases for PAC chromatography. A (2,4-dinitroanilopropyl)silica was also considered superior to alumina and a diamine phase by Grizzle and Thomson,[76] while other groups have preferred the use of cyano[45] or mixed cyano/aminosilica phases.[46,77]

The choice of a polar bonded stationary phase best suited for the separation of PAC is clearly quite confusing. However, it has been commonly accepted that the selection of an appropriate phase will depend on several factors: the type of PAC being studied, the mobile phases that are available, the manufacturer of the phase, and the column dimensions. Four different normal-phase columns were available for this study, *viz*: (a) Waters Energy Analysis NH_2, an amino phase bonded to 10μm spherical silica (3.9 mm ID x 30 cm); (b) Whatman Partisil-5 PAC RAC II, a mixed amino/cyano phase bonded to 5μm spherical silica (4.6 mm ID x 10 cm); (c) Techsil 10 NO_2, a nitrophenyl phase bonded to 10μm spherical silica (4.0 mm ID x 25 cm); and (d) Waters μBondapak CN, a cyano phase bonded to 10μm spherical silica (3.9 mm ID x 30 cm). Ideally, one of these columns will be suitable for the separation of the complex PAC mixtures used in this study (i.e., the NIST coal tar and the carbon black extract) that contain both low and high molecular weight PAC. In addition, it would be very useful if the stationary phase could also be used to characterize a set of tar sand oil fractions by separating them according to compound class (e.g., PAH, PANH, etc.).

The chromatograms for the NIST coal tar, using a hexane/dichloromethane gradient and detection at 254 ± 2 nm, for each of the four columns are shown in Figures III-3. The same mobile phase gradient was used on all four columns (see Experimental) to minimize the number of

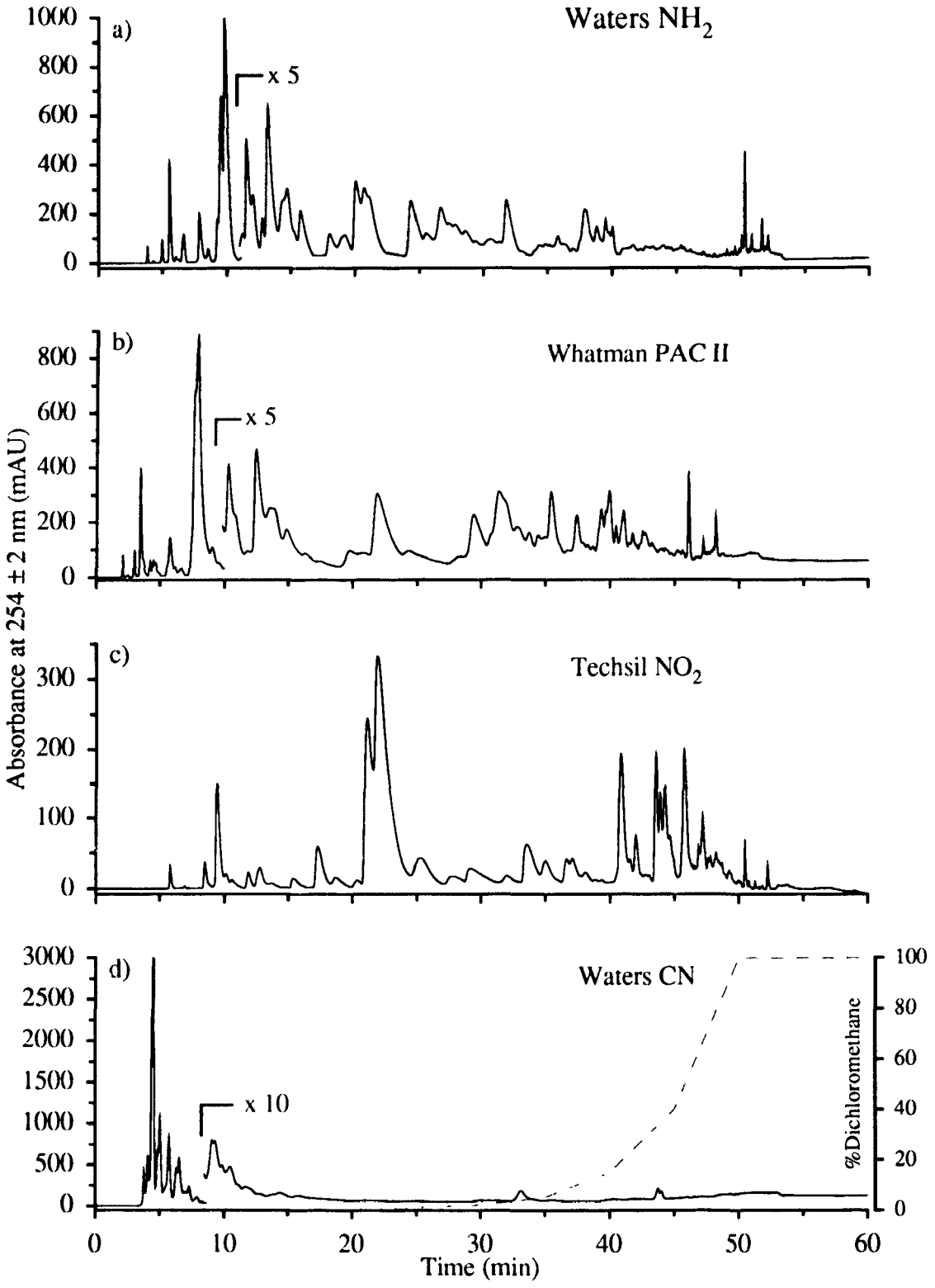

Figure III-3: Normal-phase LC-UV chromatograms of the NIST SRM 1597 coal tar mixture using four commercially available columns with a hexane/ dichloromethane gradient.

experiments. For best results, each column should have its own unique gradient that is optimized for that stationary phase. However, this would only increase the number of required experiments and complicate the comparison without a significant improvement in the outcome. Therefore, based solely on the chromatograms shown in Figure III-3, the Waters amino column would appear to provide a slightly better separation (i.e., an even distribution of partially resolved peaks over the entire chromatogram) than the other columns. The Whatman PAC column (mixed amino/cyano phase) produced a similar separation to the amino column, while the Techsil nitrophenyl stationary phase had a much higher retention for the PAC resulting in broad peaks at the beginning of the chromatogram and a large cluster of peaks at the end. Finally, the Waters cyano column produced a very poor separation; nearly all the components eluted within the first ten minutes of the chromatogram.

Figures III-4 and III-5 show the chromatograms generated from the analyses of neutral and basic fractions of a hydrotreated tar sand oil with the Waters amino, Whatman amino/cyano, and Techsil nitrophenyl normal phase columns. The Waters cyano column was not used for the analysis of the tar sand oil fractions since it performed so poorly in the separation of the coal tar. As mentioned above, normal phase columns are well suited for producing separations according to PAC compound class. The analysis of similar fractions of tar sand oils in the past have shown that the neutral fraction usually contains small PAH that are highly alkylated.[154,155] The Waters NH_2 chromatogram for the neutral fraction (Figure III-4a) shows a large envelope of unresolved peaks (labelled A) that elutes under about 15

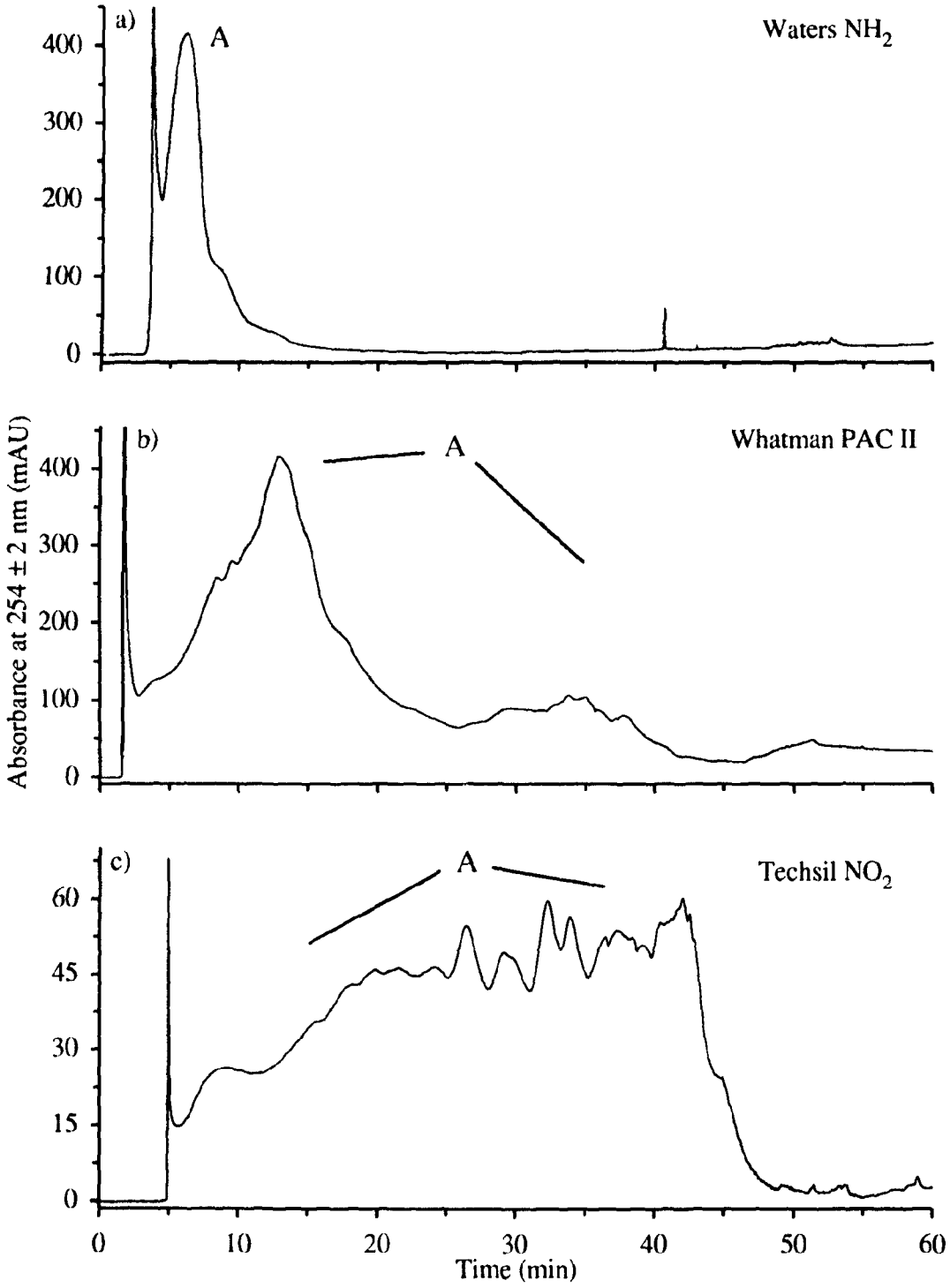

Figure III-4: Normal-phase LC-UV chromatograms of the tar sand oil neutral fraction using three commercially available columns with a hexane/dichloromethane gradient.

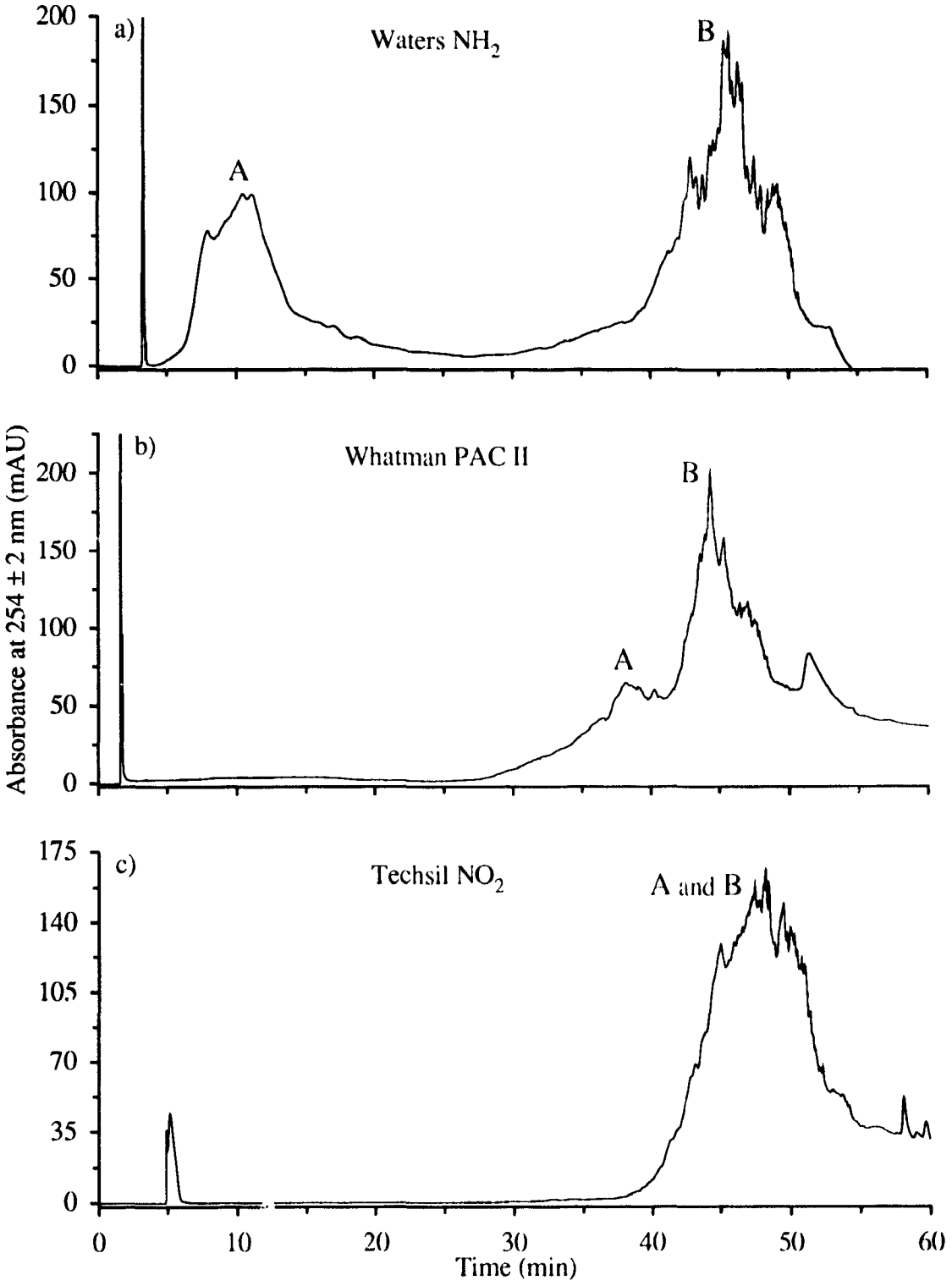

Figure III-5: Normal-phase LC-UV chromatograms of the tar sand oil nitrogen-containing PAC fraction using three commercially available columns with a hexane/ dichloromethane gradient.

minutes. This retention behaviour is consistent with the assumption that this fraction is comprised of a very large number of alkylated PAH. The fraction does not appear to contain any polar PAC since there are no peaks at much higher retention times. Both the Whatman PAC and Techsil NO_2 columns provided a better separation of the neutral fraction (Figures III-4b and 4c) since they appear to be more retentive for low molecular weight PAC.

The Waters NH_2 chromatogram of the basic PAC fraction (Figure III-5a) shows two very distinct envelopes of unresolved peaks labelled A and B. The second peak (B) corresponds to polar PAC, or more specifically, PANH and their highly alkylated analogs. Previous analyses of similar basic fractions have revealed that the PANH in these samples are comprised of carbazole and its alkylated homologues.[154] The first peak (A) in Figure III-5a corresponds to some of the PAH and alkyl-PAH from the neutral fraction (see Figure III-4a). Therefore, this chromatogram clearly illustrates that although the fractionation method used to preparatively separate the tar sand oil was intended to separate the neutral PAC from the more basic PANH, there was a significant overlap of the compound classes in the basic fraction. The chromatograms produced by the Whatman PAC and Techsil NO_2 columns (Figures III-5b and 5c) were not as informative since the separation between neutral PAH and the polar PANH was not as obvious. Subsequent chapters dealing with LC-MS will reveal much more about these samples and the separation characteristics of the columns.

III.3 Supercritical Fluid Chromatography

Supercritical fluid chromatography (SFC) employs a mobile phase consisting of a highly compressed gas near or above its critical temperature and pressure points. At the critical temperature of a substance, the vapour and liquid phases have the same densities. A gas cannot be liquefied when it is above its critical temperature, irrespective of the applied pressure. Above the critical temperature and pressure, the substance exists as a supercritical fluid. Figure III-6 is a phase diagram of carbon dioxide showing the solid, liquid, gas and supercritical states. Supercritical fluids are widely used in chromatography since their physical and chemical properties allow for high resolution separations of less volatile and thermally labile compounds in relatively short analysis times.

Some suitable mobile phases for SFC are listed in Table III-1. In addition to their critical temperatures and pressures, the chromatographically important properties of supercritical fluids include the density and viscosity of the fluid, and diffusion coefficients of solutes in the fluid. Above its critical point, a substance has density and solvating power approaching that of a liquid, but viscosity similar to that of a gas, and diffusivity intermediate between those of a gas and liquid. The supercritical fluids in Table III-1 have properties which make them very favourable as chromatographic phases. As long as intermolecular interactions are sufficiently strong, supercritical fluids are able to dissolve a variety of solutes, even those with high molecular weights. The density of a supercritical fluid, which influences the solubility and retention of solutes, can be easily changed by adjusting the applied

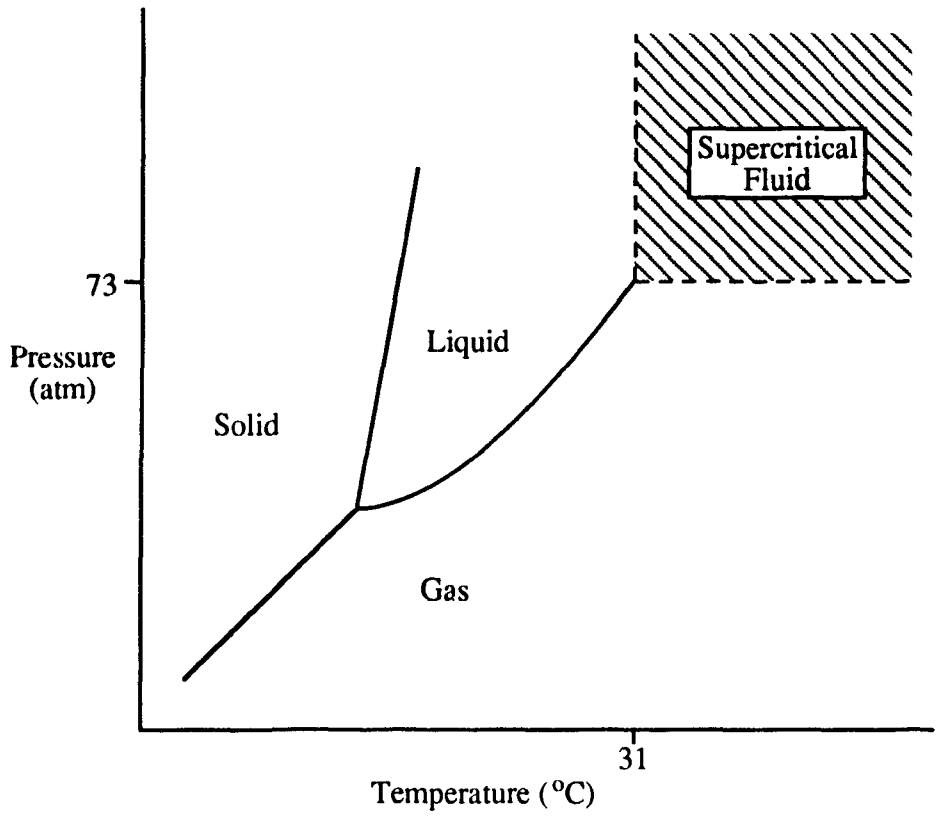

Figure III-6: Carbon dioxide phase diagram.

Table III-1: Physical parameters of selected supercritical fluids.

Fluid	Critical Temperature T_c(°C)	Critical Pressure P_c(atm)	Critical Density r_c(g/mL)
CO_2	31.3	72.9	0.47
N_2O	36.5	72.5	0.45
NH_3	132.5	112.5	0.24
n-C_5	196.6	33.3	0.23
n-C_4	152.0	37.5	0.23
SF_6	45.5	37.1	0.74
Xe	16.6	58.4	1.10
CCl_2F_2	111.8	40.7	0.56
CHF_3	25.9	46.9	0.52

pressure. The ability to slowly increase the mobile phase density as a function of time to decrease solute retention (pressure or density programming) is similar to temperature programming in GC and gradient elution in HPLC.

Conventional detectors from both GC and HPLC have been successfully adapted to SFC. The ultraviolet (UV) spectrophotometric detector has been the most widely used in SFC followed by the flame ionization detector (FID). Other detectors used include the fluorescence, flame photometric (FPD), thermionic (TID), and photoionization detector (PID).[102,105,110] The optical type detectors (UV, IR and fluorescence) must have very small volumes and be able to withstand high pressures. Fluid decompression and expansion must be accommodated in flame or ionization detection (FID, FPD, TID, PID, and MS). A pressure restrictor must be located either after the detector (for optical detectors) or at the end of the column (for ionization detectors) to maintain supercritical conditions in the column.

As with any other chromatographic technique, SFC offers a choice between open-tubular (or capillary) and packed columns. Each technique has its own merits and limitations, which are discussed below. Although there has been some controversy in the literature over whether capillary or packed columns are preferred, the present consensus is that both have a place in the analytical laboratory.[156]

The main advantage capillary column SFC has over packed column SFC is that longer capillary columns can be used. Thus, separations using capillary columns can be performed with much higher separation efficiencies. Common GC columns usually cannot be used in SFC because the stationary phases do not withstand the high solvating power of supercritical fluids. The

stationary phases for SFC have to be cross-linked by radical reactions to increase their lifetime. The small column diameters necessary in capillary SFC (typically 50 or 100 μm ID) make the method of sample introduction very important; small volumes and rapid injections are necessary.

Packed columns in SFC are very similar to those used in HPLC. Column diameters vary from 4.6 mm ID down to packed capillaries of 320 μm ID Packing materials used in the past include bare and modified silica, alumina, and some special materials. Many recent studies now employ packing materials designed for use in LC. Chemically bonded stationary phases which feature a monolayer of organic ligands on a silica surface have been used extensively. The advantages of using packed columns include: an increased sample capacity that permits larger amounts of analytes to be loaded onto the column resulting in wider dynamic ranges compared to capillary columns; much simpler and more accurate injection techniques; shorter analysis times; and, a wider variety of stationary phases. However, the main advantage of packed-column SFC over HPLC is the reduction in analysis time (increased resolution per unit time).

Two different packed columns were used in this study; a Brownlee SS251 5μm Spheri-5 silica (250 x 1mm ID), and an ODS (C_{18}) stationary phase. A photoionization detector (PID) was used as an off-line detector to optimize the separation prior to coupling to MS detection. A previous study has demonstrated that the PID provides improved selectivity and sensitivity over the flame ionization detector for PAC as well as increased detector stability when subjected to the high gas flow rates encountered in this type of SFC.[102] Mixtures of PAH standards and the NIST coal tar material were used to

develop suitable pressure programs that would provide optimal separations on both columns. Capillary column SFC techniques were not included in this thesis although they have been studied by other members of our research group.[155]

Figure III-7a shows the separation of a set of PAH standards on the silica column using a linear pressure program from 2000 psi to 5000 psi over 20 minutes and held at 5000 psi for an additional 10 minutes. Photoionization will occur when the ionization energy of the analyte is less than the UV lamp energy (10.2 eV). This is true for the earliest eluting component, phenanthrene (IE = 8.02 eV) and all the subsequent PAH, since ionization energies decrease with increasing size.[157] The standards are well resolved from each other, although the large solvent peak (hexane/dichloromethane) may present a problem for low molecular weight PAC. The chromatographic peak widths varied between 0.23 and 0.68 minutes at half height; approximately twice the widths normally produced by reversed-phase LC separations. Figure III-7b shows the chromatogram obtained from the NIST coal tar using the same column and pressure gradient. In comparison to the separation produced by reversed-phase LC (Figure III-1), the analysis time was shorter, but the overall separation does not appear to be as good (i.e., there are many more resolved peaks in the LC trace). This is probably due to the broad SFC peaks and silica stationary phase used in the separation; as mentioned earlier, reversed-phased packings provide different separation selectivities for PAC than polar normal-phase materials.

The separation of a similar set of PAH standards (in

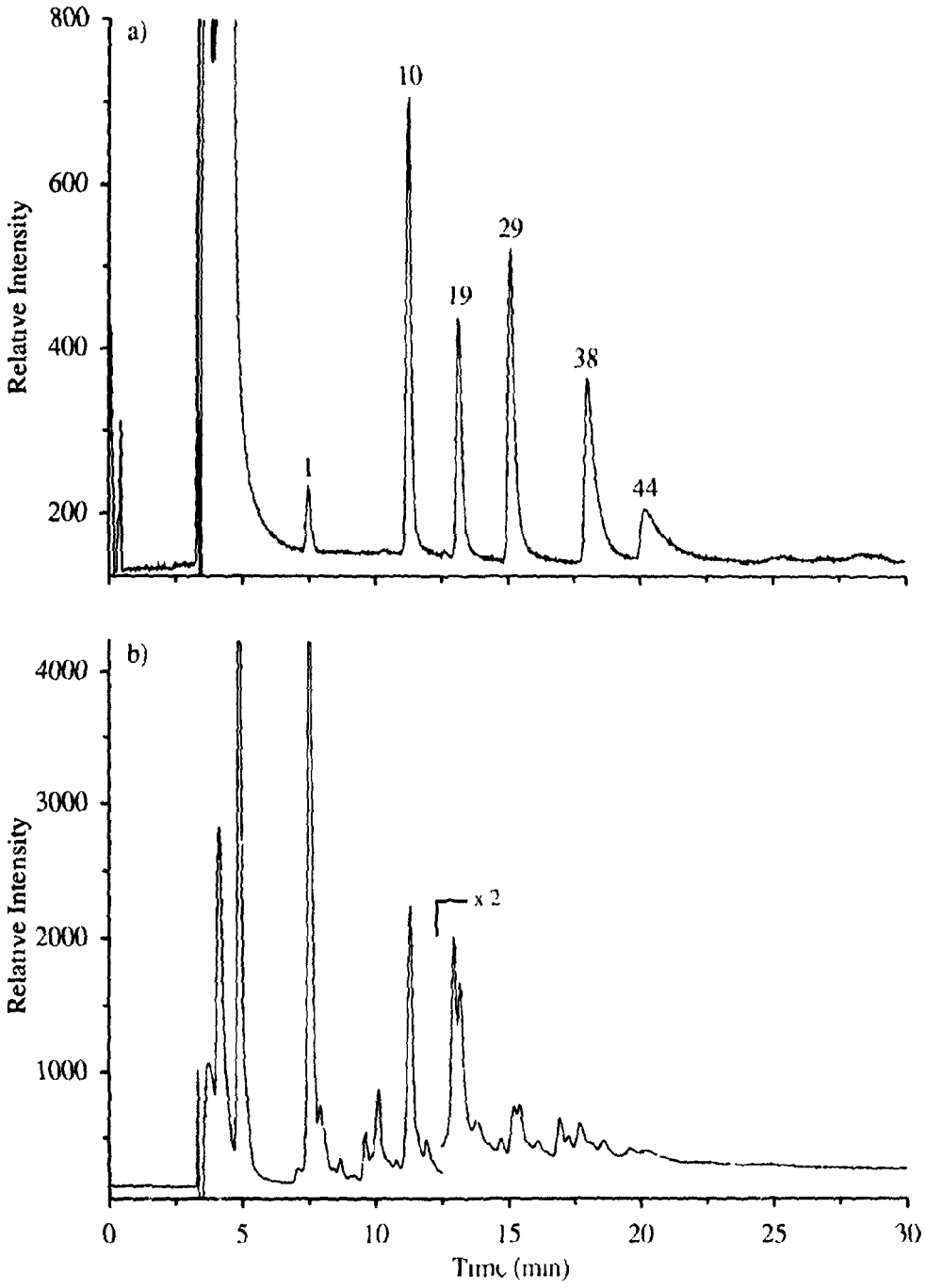

Figure III-7: SFC-PID chromatograms of (a) a mixture of PAH standards, and (b) the NIST SRM 1597 coal tar mixture using a silica column. See Appendix A for compound identities.

acetonitrile/dichloromethane) on the ODS column is shown in Figure III-8a. A linear pressure gradient from 2000 to 6500 psi in 20 minutes was used for this analysis. Once again, the standards are all well resolved from each other, although the sample solvent now produces a negative peak that may also interfere with the analysis of low molecular weight PAC. The chromatographic peaks remained broad; between 0.24 and 0.55 minutes at half height. Figure III-8b shows the chromatogram obtained from the NIST coal tar using the ODS column and the same pressure gradient as in Figure III-8a. There does appear to be a slight improvement over the previous analysis with the silica phase, but the separation provided by reversed-phase LC still appears better. Attempts to couple SFC to MS and further characterize these samples will be discussed in subsequent chapters.

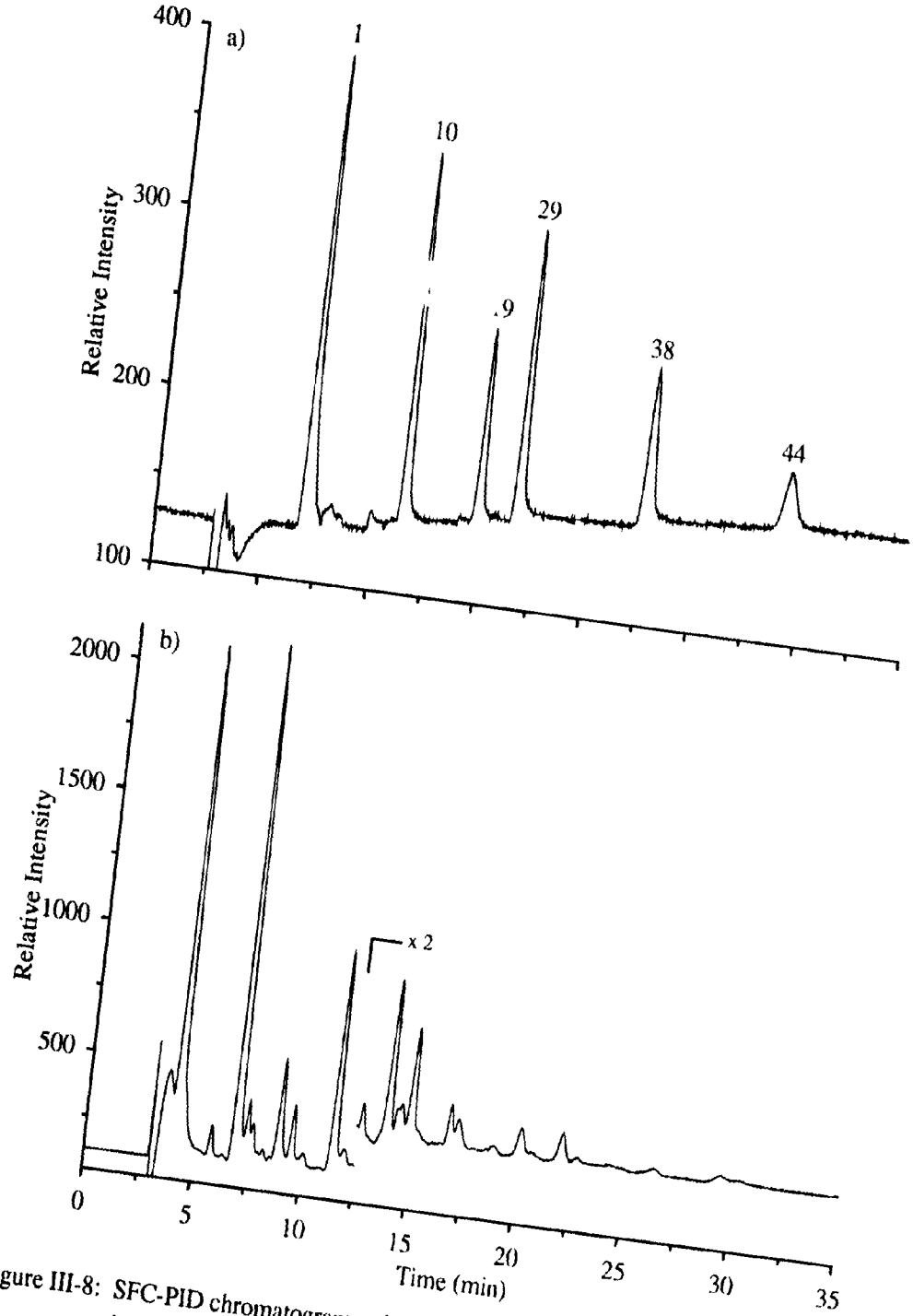

Figure III-8: SFC-PID chromatograms of (a) a mixture of PAH standards, and (b) the NIST SRM 1597 coal tar mixture using a C_{18} column. See Appendix A for compound identities.

IV. THE MOVING BELT INTERFACE

The first successful commercially available LC-MS interface was the transport, or moving belt, system. The VG Analytical version of this interface, which was available for this study, is shown in Figure IV-1. The belts used in this interface are usually made from polyimide and are disposed of once they are no longer usable (i.e., from breakage, stretching, or are too dirty). The effluent from an LC column is evenly deposited onto the belt surface that is supported on a pulley and driven by a variable speed motor. A probe heater and a nebulizing gas (such as N_2) can be used to assist in the deposition of the effluent. This is usually necessary when high flow rates and high water contents are used in a chromatographic separation. Solvent removal occurs as the belt passes through a series of tunnel vacuum seals and into the ion source. An infrared heater placed before the first vacuum chamber can also be used to assist in the evaporation of the mobile phase; this is also useful when high flow rates and high water contents are used in the LC separation. Once the belt enters the high vacuum ion source, it passes over a heater that vaporizes the sample directly into the ion source. The belt then passes over an additional heater, which cleans the belt by evaporating any residue left behind, and then out through the tunnel seals to be recycled.

A major advantage of the moving belt interface is its compatibility with more than one ionization mode (e.g., EI, CI, and FAB) since the solvents are almost completely removed before the sample is transferred into the ion source. The acquisition of conventional EI spectra facilitates the use of large spectral libraries for compound matching, which is particularly useful for the identification of unknown compounds. Disadvantages include the loss of

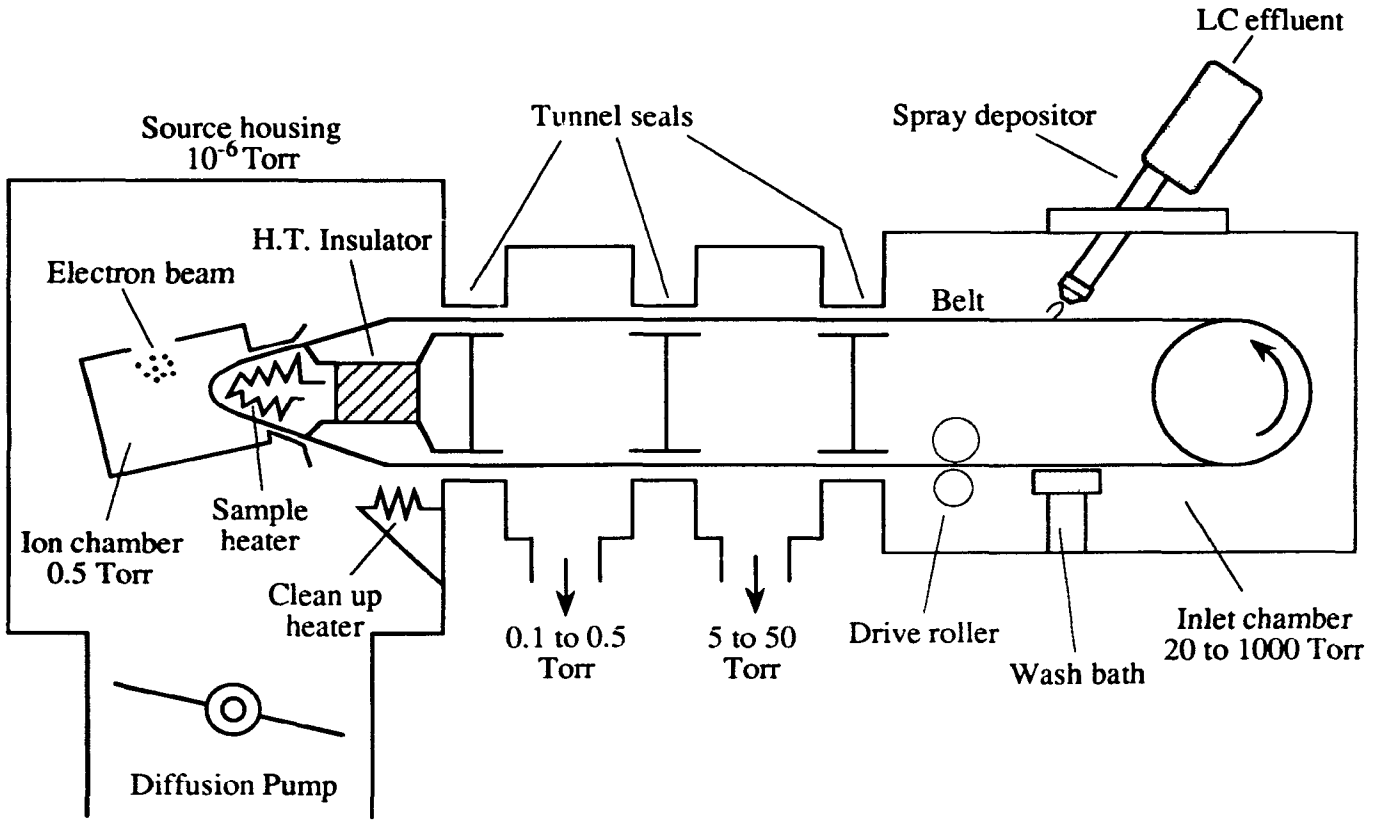

Figure IV-1: Schematic diagram of the moving belt interface.

volatile compounds before ionization can occur, and insufficient desorption of low volatility compounds from the belt. The latter can result in "ghost" signals as the belt recycles and a small amount of analyte desorbs each time it passes over the sample evaporator. This problem can be minimized by incorporating a wash bath on the belt (see Figure IV-1). The key to obtaining good overall performance from this interface is the optimization of the interface parameters (e.g., liquid flow rate, sample deposition, belt speed, sample evaporator temperature, and belt cleaners) for each LC separation.

IV.1 Reversed-Phase Liquid Chromatography Coupled to the Belt Interface

The use of RPLC combined with the moving belt interface for the analysis of PAC has been reported previously.[90,92,158] For example, the PAC content of a marine sediment extract[4,5] and coal tar liquids[90] have been characterized by LC-MS with the belt interface in conjunction with conventional LC detectors, such as the UV detector. Detection limits as low as 40 pg (using single ion monitoring LC-MS experiments) have been reported for benz[*a*]anthracene, naphtho[1,2,3,4-*def*]chrysene and dibenz[*a*,*h*]anthracene,[92] but these limits may not be reached with very volatile (e.g., naphthalene) or very involatile PAC (e.g., high molecular weight PAH). A linear dynamic range of at least 4 orders of magnitude has also been reported for naphtho[1,2,3,4-*def*]chrysene.[92]

In a comparison of chromatographic/MS techniques for the

determination of PAH in marine sediments,[4] the precision obtained from the belt interface using both external and internal standardization were between 1.9 to 19%, and 0.8 to 11% relative standard deviations (%RSD), respectively. These values compare well with the precisions obtained for the same sample using GC-MS: 14 to 40% for external standardization, and 0.8 to 6.2% for internal standardization.[4] However, the precision for naphthalene using the belt interface, which is not included in the ranges mentioned above, was approximately 50% RSD,[4] thus clearly illustrating the difficulty in analyzing volatile compounds with the belt interface. In addition, severe limitations placed on the mobile phase composition and flow rates were encountered in this previous study. In general, solvent gradients were restricted to a low aqueous content and/or low flow rate to ensure that nearly all the mobile phase was evaporated before the belt entered the ion source.[159]

The inclusion of this interface in this study was not intended to repeat any of the extensive studies performed in the past, but to provide a starting point for the comparison of the other interfaces that will be evaluated. The following experiments provided both a quick confirmation of the previous work and experience in chromatographic/MS analyses.

Figure IV-2a shows an EI mass spectrum acquired from the belt interface of a PAH standard (coronene, mass 300) that was eluted from a polymeric reversed-phase C_{18} column. The spectrum is relatively simple, consisting of an intense molecular ion ($M^{+\cdot}$) and small ions resulting from the loss of one to four hydrogen atoms. The $[M+1]^{+\cdot}$ ion is always present and is attributed to the ^{13}C isotope abundance. Doubly charged ions (M^{2+}) are also common in the EI mass spectra of PAH (see Figure IV-2a). A background

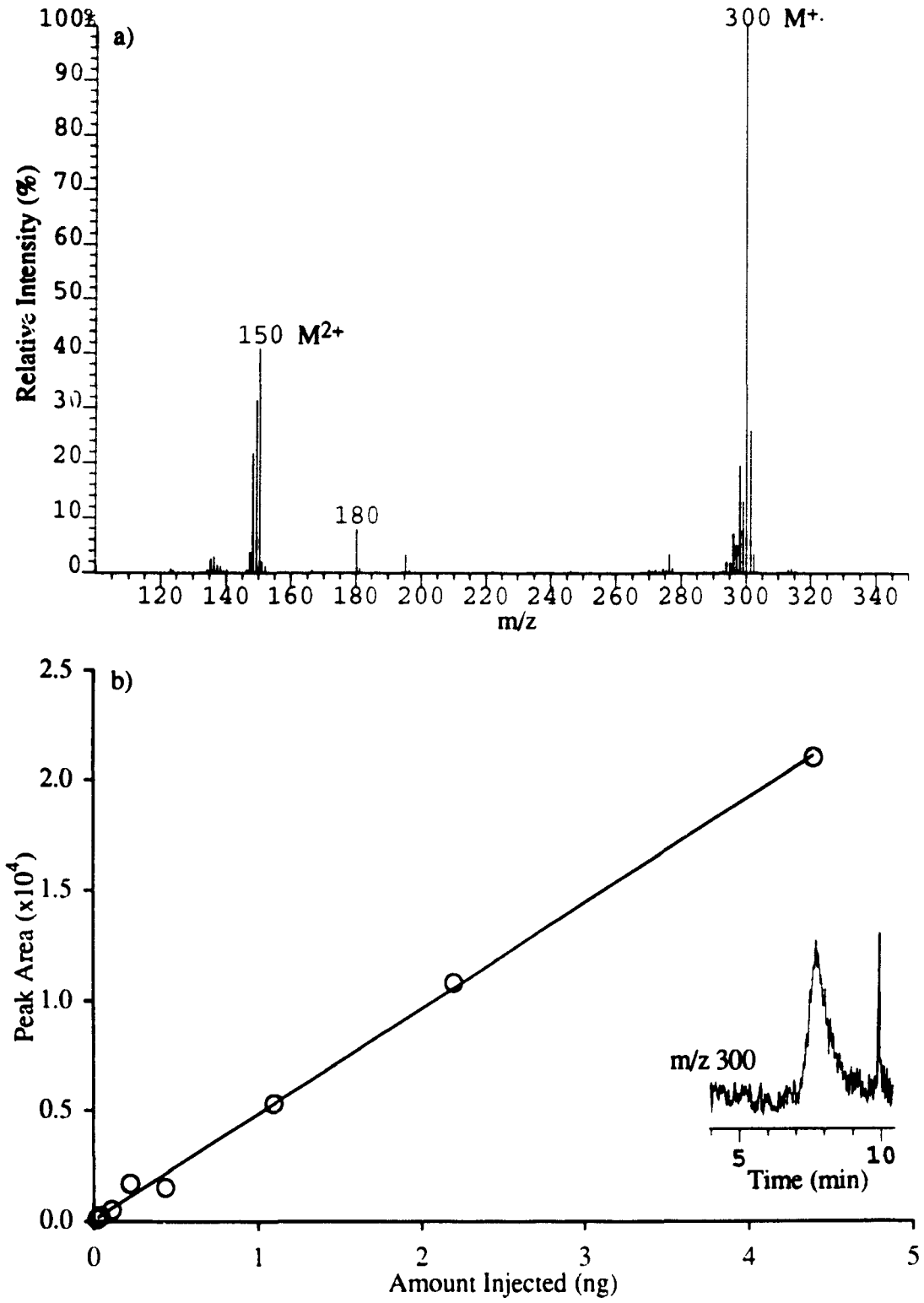

Figure IV-2: (a) Full scan EI mass spectrum of coronene and (b) the calibration curve for coronene using the belt interface. Inset shows the single ion monitoring chromatogram for the injection of 25 pg.

subtraction routine was used to remove the intense background ions arising from the polyimide belt from the spectra.[155]

The intense molecular ions produced under EI ionization are ideal for compound identification and for producing enhanced analyte signals when using single ion monitoring experiments. For example, the inset in Figure IV-2b shows the single ion monitoring chromatogram for 25 pg of coronene injected on-column. The calibration curve obtained for coronene shown in Figure IV-2b, from on-column injections between 0.025 and 5 ng, demonstrates a linear dynamic range of approximately 2.5 orders of magnitude (the actual linear range is probably greater than this).

There is very little difference in the appearance of the EI mass spectrum when a heteroatom is substituted in a PAH ring system; Figure IV-3a shows the mass spectrum for the nitrogen-containing PAC, carbazole. The odd molecular mass of carbazole, or any PAC with an odd number of nitrogen atoms, assists in its identification as a nitrogen-containing PAC. The detection limit for carbazole using the belt interface is approximately 2 ng (Figure IV-3b inset). A linear calibration curve was obtained between 2 and approximately 300 ng injected on-column (Figure IV-3b). The non-linearity above 300 ng probably arises from the inefficient desorption of the large amount of analyte off the belt surface and into the ion source.

An example of a RPLC-MS analysis of a complex mixture of PAC (i.e., the carbon black extract) with the belt interface is presented in Figure IV-4b. The corresponding chromatogram obtained with off-line UV detection is shown in Figure IV-4a. A short acetonitrile/dichloromethane gradient (described in Chapter III) was used in this analysis to eliminate the problems

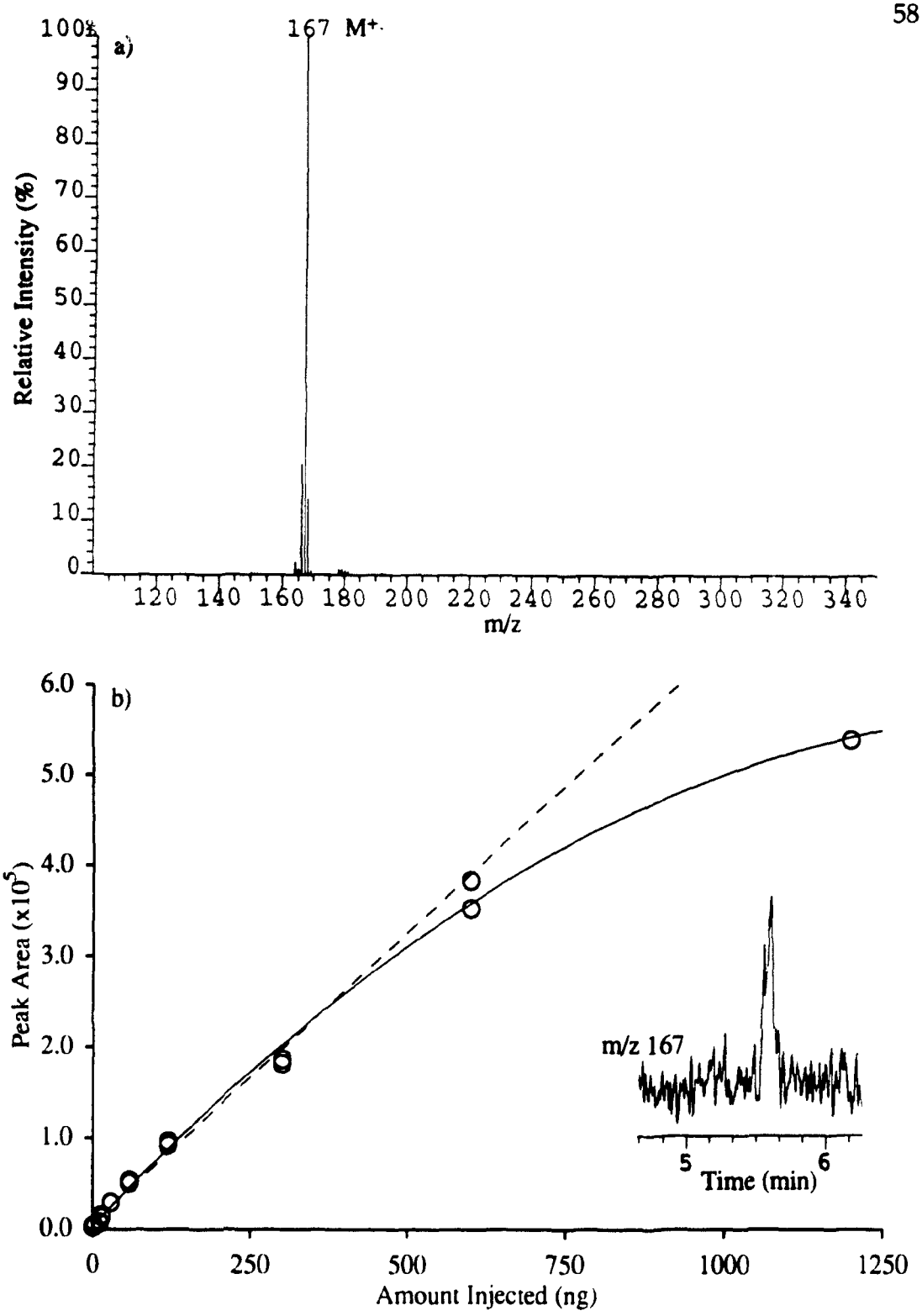

Figure IV-3: (a) Full scan mass spectrum of carbazole and (b) the calibration curve for for carbazole using the belt interface. Inset shows the single ion monitoring chromatogram for the injection of 1.9 ng of carbazole.

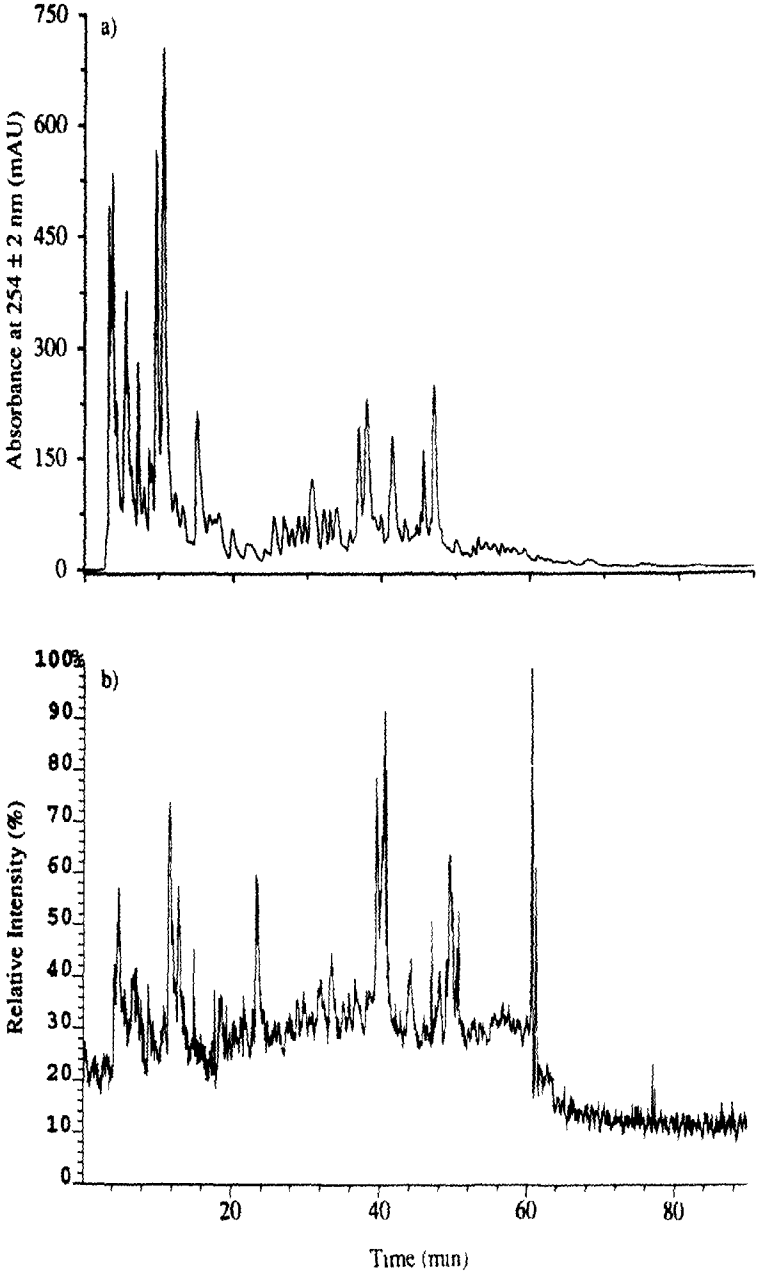

Figure IV-4: (a) LC-UV and (b) LC-MS total ion chromatograms from the analysis of the carbon black extract using a C_{18} column with an acetonitrile/ dichloromethane gradient.

associated with the evaporation of an aqueous mobile phases. The incomplete resolution of low molecular weight PAC is not significant in this instance since this sample contains predominantly high molecular weight PAH.

The traces in Figure IV-5 are single ion chromatograms (SIC's) that have been generated from the full scan mass spectral data set in order to detect the principal PAC present in the sample. These traces represent intensities of ions of specified m/z ratios detected by the MS as a function of time. Since EI is being used, fragment ions of higher molecular weight compounds can be confused with the molecular ions of lower mass compounds As a result, the mass spectrum at each peak maximum must be examined to determine which chromatographic peaks represent molecular species. Some representative mass spectra taken from the peaks marked with an asterisk are shown in Figure IV-6. Fortunately, since PAC generally produce abundant molecular ions and few fragment ions, most of the peaks in the SIC traces represent signals from molecular species.

The last few chromatograms in Figure IV-5 (m/z 398 and 424) show some significant and impressive results for this interface. It has been generally accepted that the belt interface cannot be used in the analysis of compounds with very low volatilities, yet these high molecular weight and relatively minor components (e.g., m/z 424) were detected in this study with no observable signs of ghost peaks.

The production of the SIC's shown in Figure IV-5 from the mass spectral data set provides much greater selectivity than can be achieved with UV detection (Figure IV-4a). However, since PAC isomers produce virtually

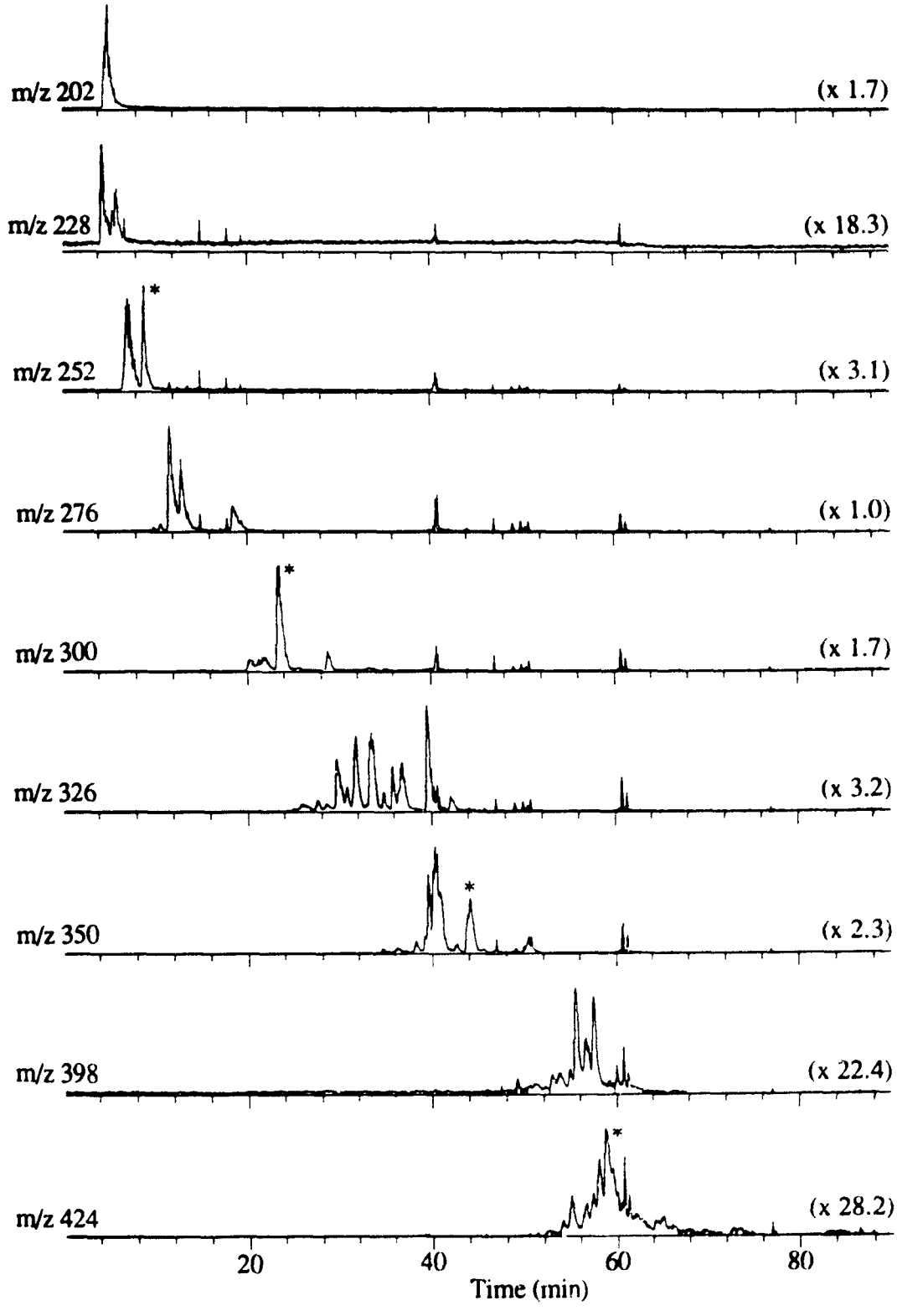

Figure IV-5: LC-MS selected ion chromatograms generated from the analysis of Figure IV-4b.

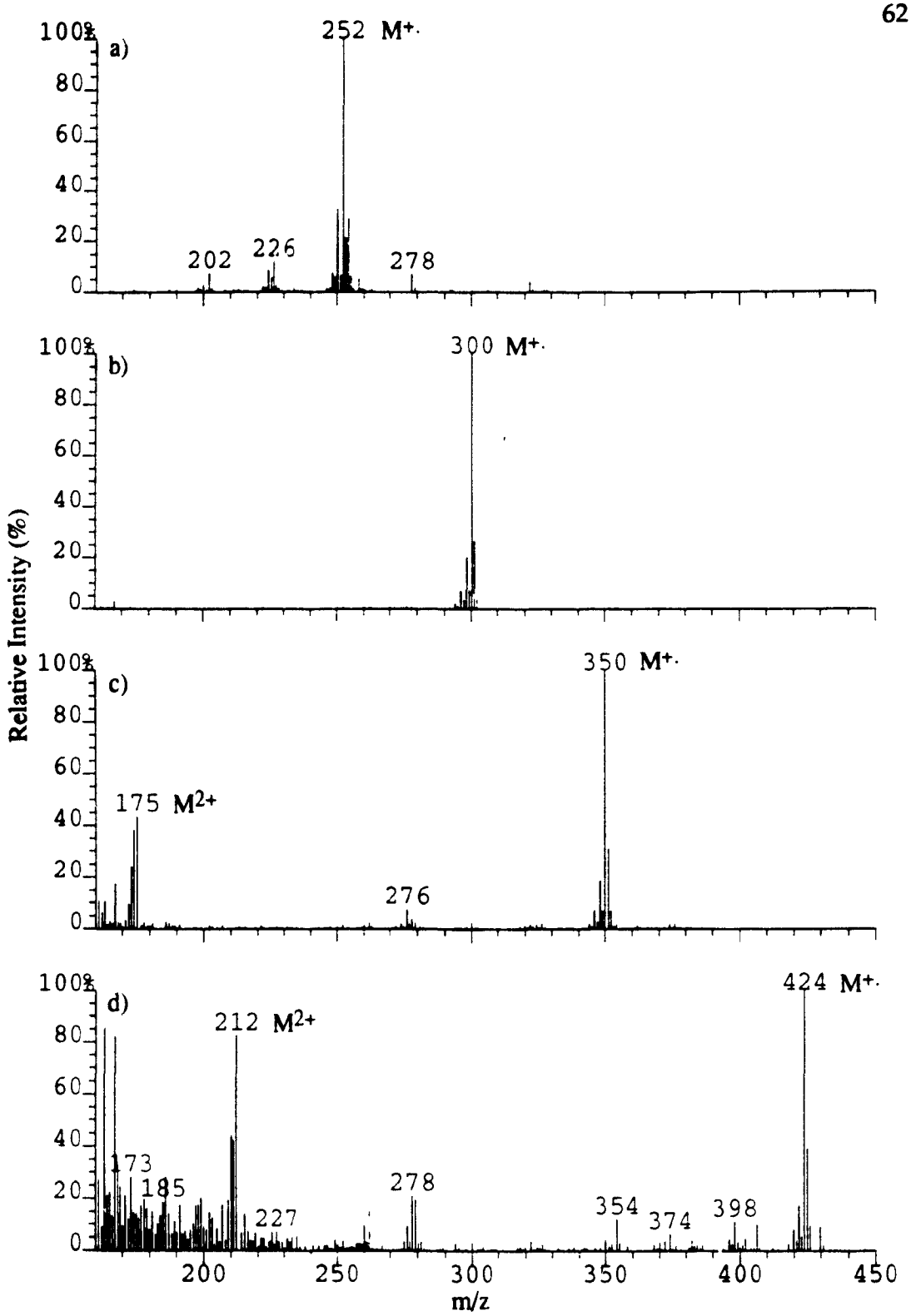

Figure IV-6: Background subtracted EI mass spectra obtained from the LC-MS analysis of the carbon black extract (Figure IV-4b). Spectra were taken at the top of the peaks marked with an asterisk in Figure IV-5.

identical EI mass spectra (although there are a few exceptions),[1] it is very difficult to differentiate between isomers or determine if two or more isomers are coeluting. Retention times can help only if all possible isomers are available for individual measurement; otherwise, there is always some uncertainty. In contrast, the UV spectra for PAC isomers are usually dramatically different and can be compared with those stored in spectral libraries. Therefore, a combination of EI and UV spectral data is usually the most practical solution to complex mixture analysis.[5]

IV.2 Normal-phase Liquid Chromatography Coupled to the Belt Interface

Some of the problems associated with coupling reversed-phase LC to the moving belt interface can be avoided by using normal-phase LC (NPLC). The volatile organic mobile phases commonly used for NPLC (e.g., hexane and dichloromethane) are easily vaporized from the belt surface thus allowing use of conventional flow rates (e.g., 1mL/min). The coupling of normal-phase LC to the belt interface for the analysis of PAC mixtures has therefore, become very common.[90,91,92,93,151,158,160]

The following experiments illustrate two applications of NPLC-MS using the belt interface. First, the separation of a complex mixture of PAC will be compared on three different NPLC columns. A previous examination of these columns was performed with UV detection (Figure III-3) and the conclusions regarding the separations were based solely on the appearance of

the chromatograms since individual compounds could not be readily identified. Almost all of the previously published reports studying the separation characteristics of NPLC columns have used simple sets of PAC standards in conjunction with conventional detectors.[44,46,76,77,149,150,152,153] This approach generally requires several analyses to produce a complete retention time "map" of the PAC for each column. The NPLC-MS method that will be discussed below produces a complete map of the columns with only one PAC sample and one analysis. This is possible because with MS detection the retention times of any number of the PAC components can be determined by generating SIC's at the appropriate m/z value.

Figures IV-7 and IV-8 show the normal-phase LC-MS SIC traces obtained from the analysis of the coal tar mixture using the Whatman mixed amino/cyano and Techsil nitrophenyl columns. The Waters amino column produced a separation (data not shown) that was similar to that of the Whatman column (Figure IV-7). All three columns separated the selected PAH in order of increasing mass, although individual PAH isomers were not well resolved (especially in comparison to RPLC separations). The more polar nitrogen-containing PAC (i.e., carbazole, m/z 167) elute near the end of the run and are well separated from PAH of similar mass. The Techsil nitrophenyl column produced very broad peaks at the beginning of the analysis and very sharp, poorly resolved peaks at the end. It may be possible to improve this separation with a modified gradient containing dichloromethane in the initial gradient step to sharpen the early eluting peaks, and a more gradual increase to 100% dichloromethane to improve the resolution at the end of the chromatogram. This was beyond the scope of this

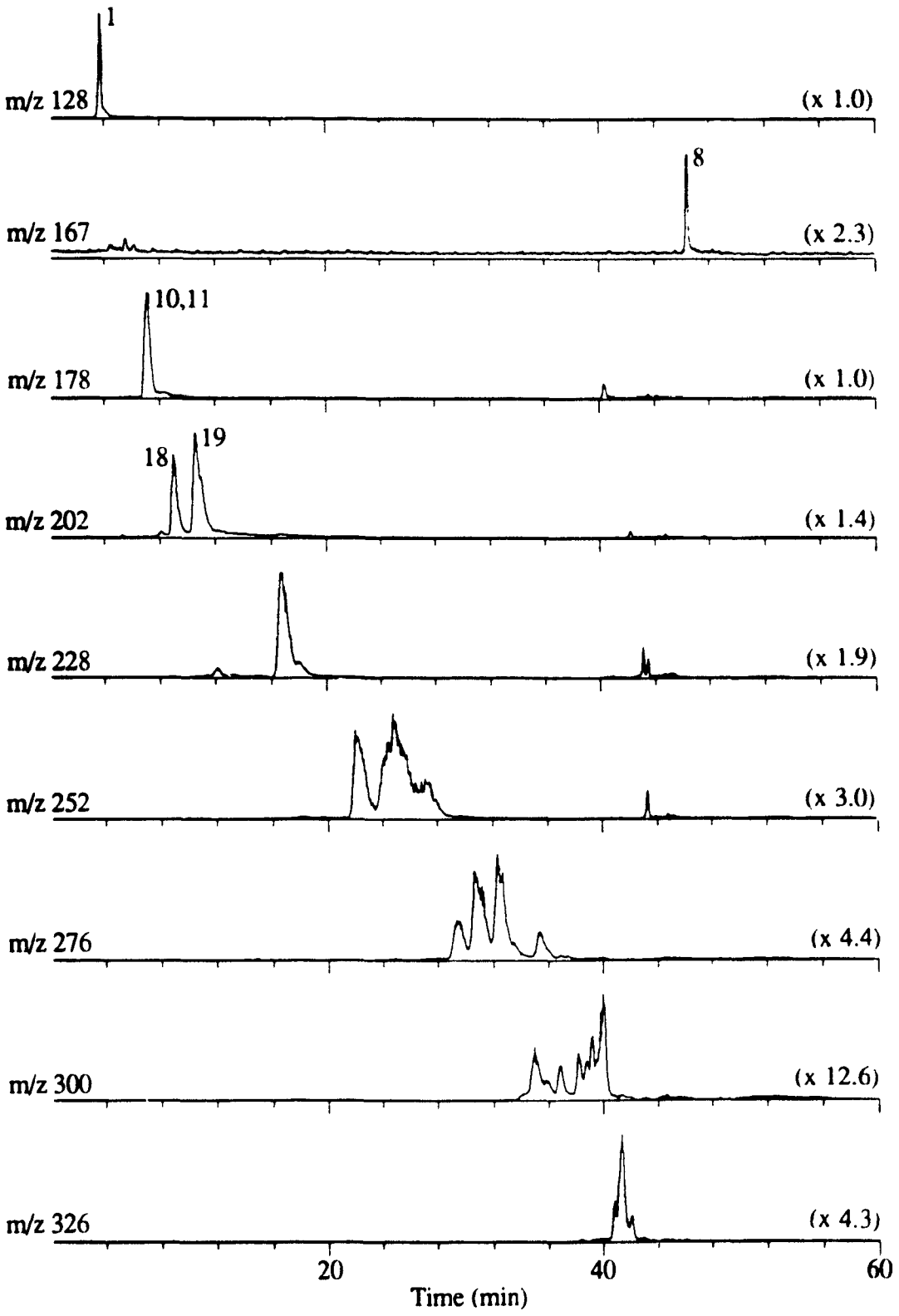

Figure IV-7: Selected ion chromatograms from the LC-MS analysis of the NIST SRM 1597 coal tar mixture using a Whatman PAC column. See Appendix A for compound identities.

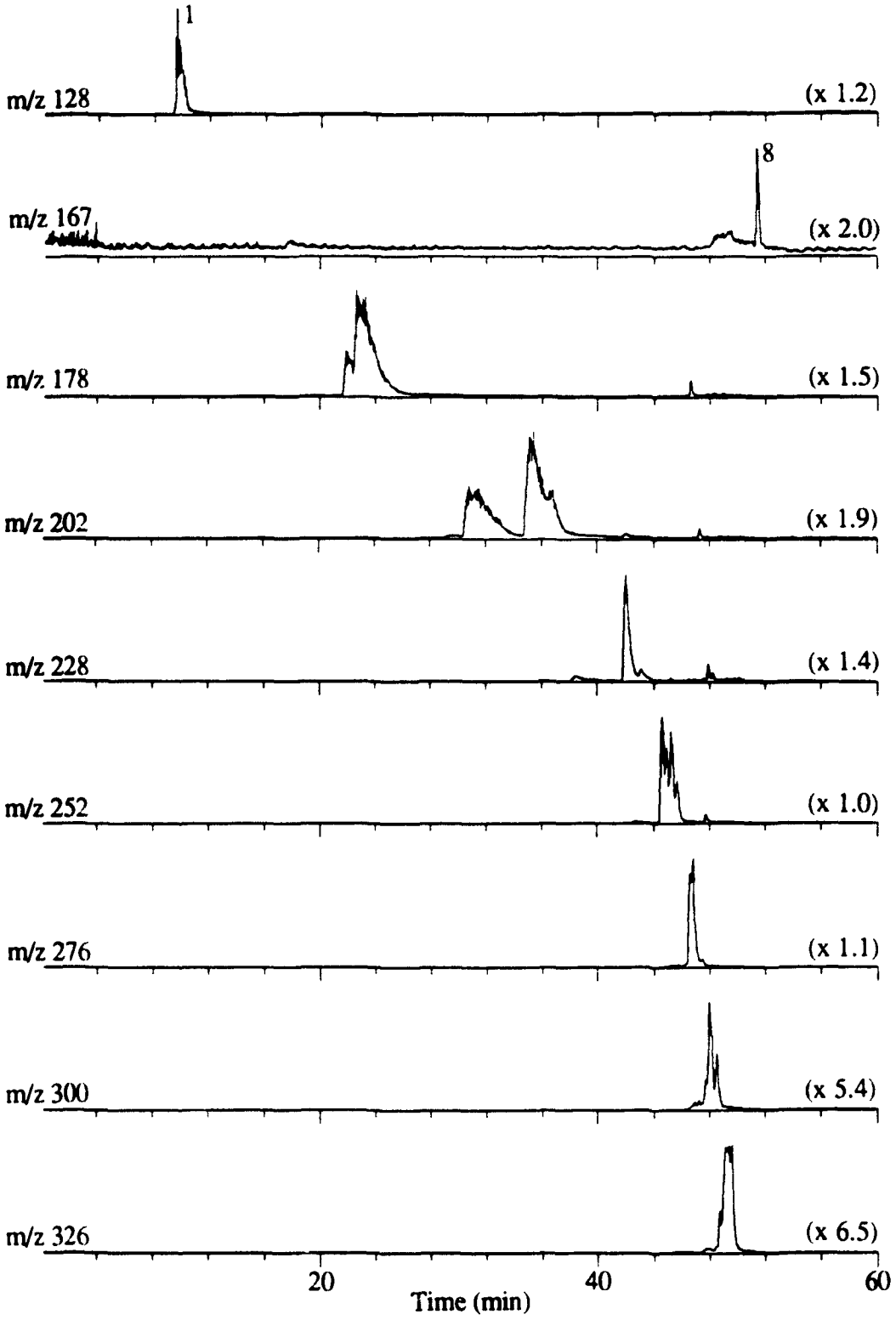

Figure IV-8: Selected ion chromatograms from the LC-MS analysis of the NIST SRM 1597 coal tar mixture using a Techsil NO_2 column. See Appendix A for compound identities.

study, however, since the objective was to obtain a quick comparison of the separation characteristics of the three columns. Under the present conditions, both the Waters NH_2 and Whatman PAC columns were well suited to the separation of PAH according to molecular weight.

For the second application of the NPLC-MS/belt method, two tar sand oil fractions were analyzed with the three columns mentioned above. Previous analyses of the two tar sand oil fractions using UV detection (Figure III-4 and III-5) produced chromatograms that were consistent with the fractionation of the original samples according to compound class (i.e., PAH and PANH). The following experiments have confirmed those results.

The NPLC-belt/MS TIC chromatograms obtained from the analysis of the neutral and basic PAC fractions on the Waters NH_2, Whatman PAC, and Techsil NO_2 columns are shown as Figures IV-9 and IV-10. The conclusions made earlier about the composition of these fractions based on the UV chromatograms (e.g., the presence of neutral PAC in the basic fraction, Chapter III, Figures III-4 and III-5) can also be made in this instance because of the excellent correspondence between the TIC and UV chromatograms. The ability to produce SIC from the mass spectral data sets, however, can provide much more detailed information about the sample. For example, the selected ion chromatograms for mass 228 PAH and its homologous series of alkylated compounds present in the neutral fraction are shown as Figure IV-11. The increasingly broad and unresolved chromatographic peaks are a result of the greater number of possible isomers with increasing alkylation. Similar series of alkylated PAH of different mass (up to mass 252) have also been extracted from the mass spectral data sets (data not shown).

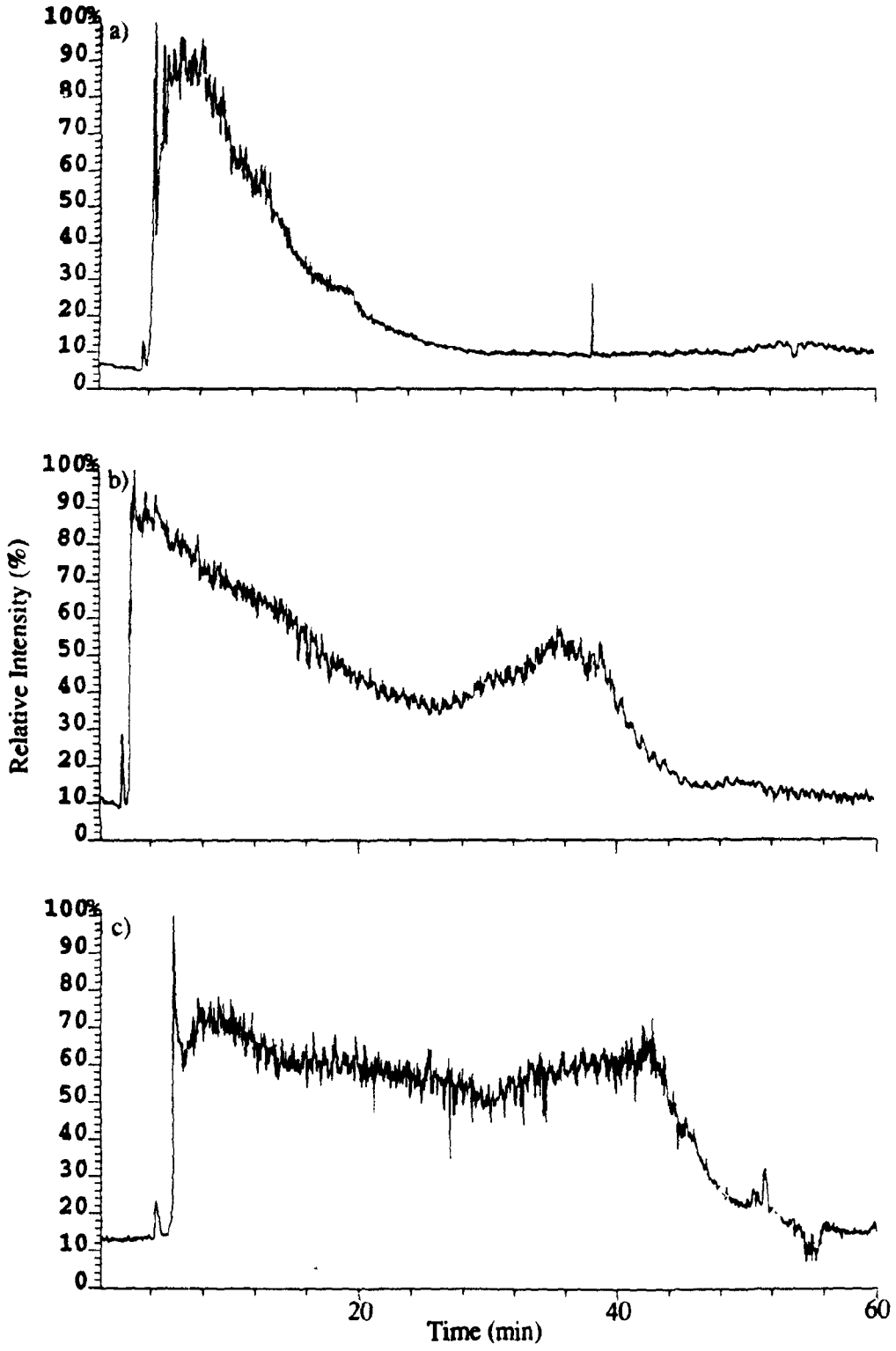

Figure IV-9: LC-MS total ion chromatograms of the tar sand oil neutral fraction using (a) a Waters NH_2, (b) a Whatman PAC and (c) a Techsil NO_2 column.

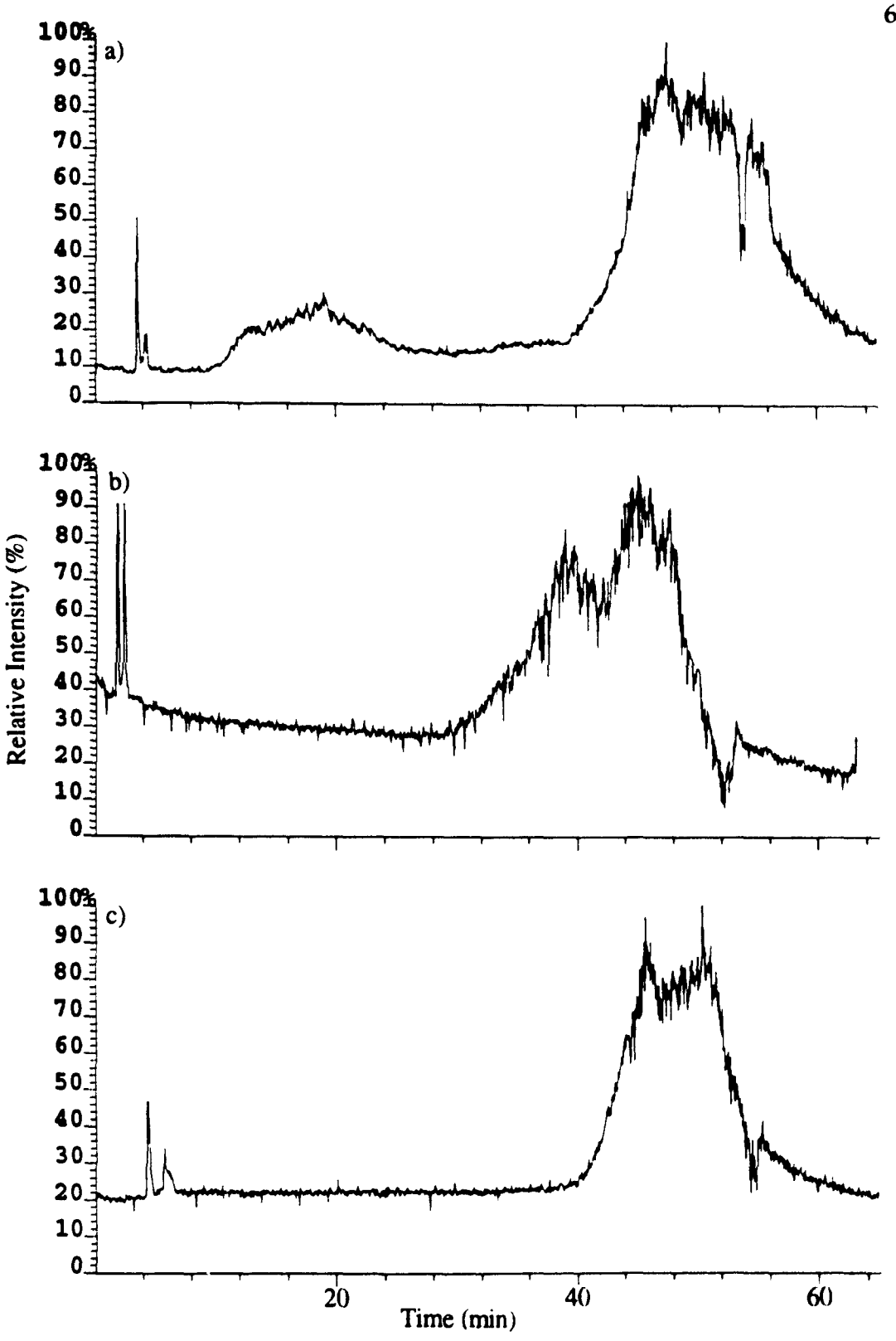

Figure IV-10: LC-MS total ion chromatograms of the tar sand oil nitrogen-containing PAC fraction using (a) a Waters NH_2 , (b) a Whatman PAC and (c) a Techsil NO_2 column.

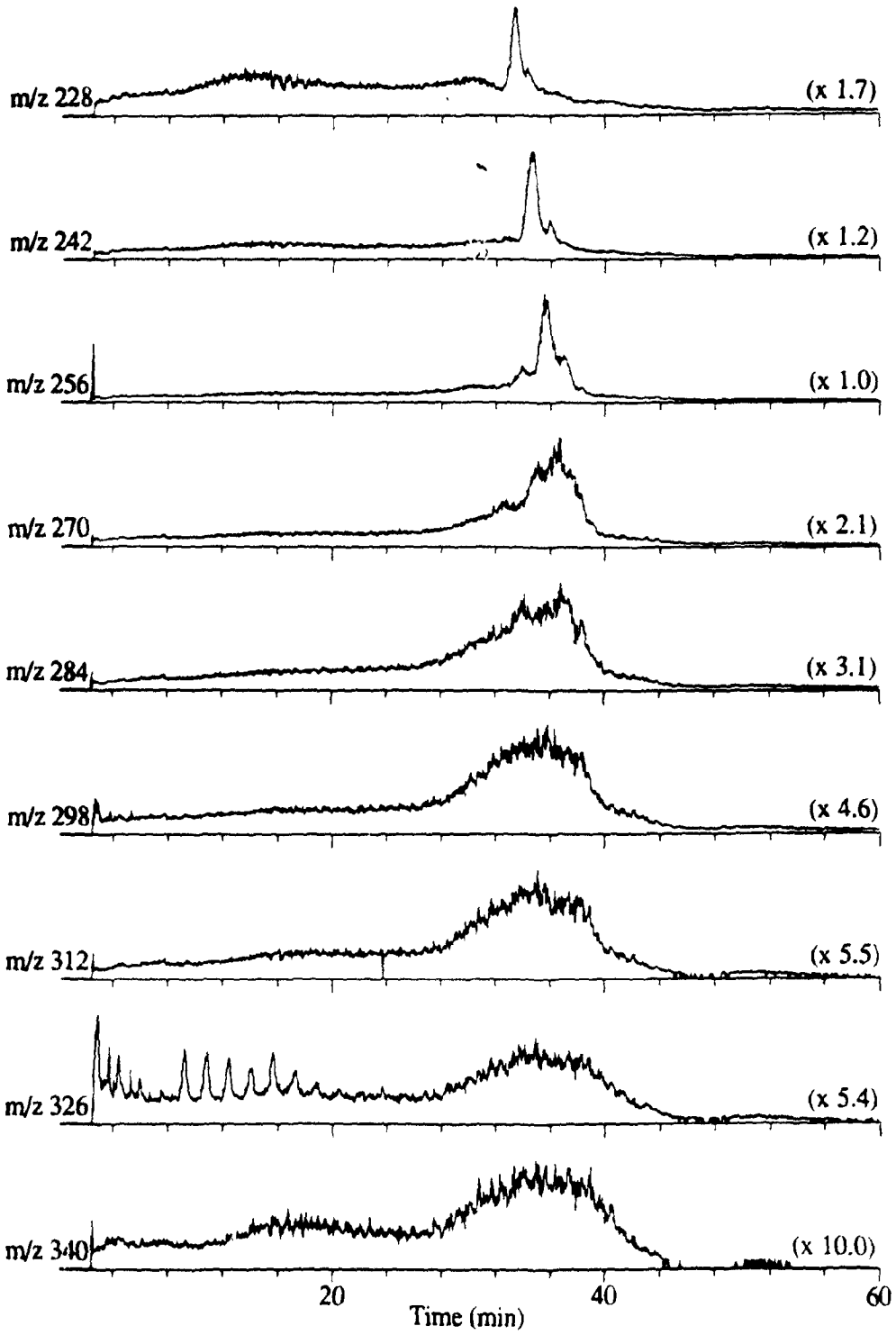

Figure IV-11: LC-MS selected ion chromatograms of alkylated mass 228 PAH generated from the analysis of Figure IV-9b.

Figure IV-12 shows the selected ion chromatograms that can be generated for carbazole and its alkylated homologues using the Waters NH_2 column. There is an abundance of alkylated carbazole compounds in this fraction, but undetectable amounts of carbazole itself. This may have been a result of the hydrotreating conditions (i.e., using thermal cracking) or the alumina fractionation scheme used to separate the oil into compound classes.

The peak areas that can be obtained from the chromatograms shown in Figures IV-11 and IV-12 could provide valuable information regarding the overall composition of the tar sand oil. The characterization of synthetic crude or high-boiling petroleum fractions is one area in which the combination of normal-phase LC and the moving belt interface has been used.[91,93,151,161] One of the limitations associated with the interpretation of this data, apart from the complexity of the samples, is a result of the extensive fragmentation of alkylated PAC when using EI. Figure IV-13 contains some representative background subtracted mass spectra obtained from the analysis of the neutral and basic tar sand oil fractions. The spectra are very complex resulting from the numerous fragment ions of the alkylated species. Molecular ions of individual PAC are therefore very difficult to identify. The peak areas from the selected ion chromatograms of the alkylated PAC shown as Figures IV-11 and IV-12 do not account for the fragmentation of these compounds, and should not be considered an accurate representation of the relative amounts of the individual species.

One solution to the fragmentation problem of conventional EI is the use of a softer ionization mode (e.g., low voltage EI or chemical ionization). When the bombarding electron energy of an EI source is reduced such that it

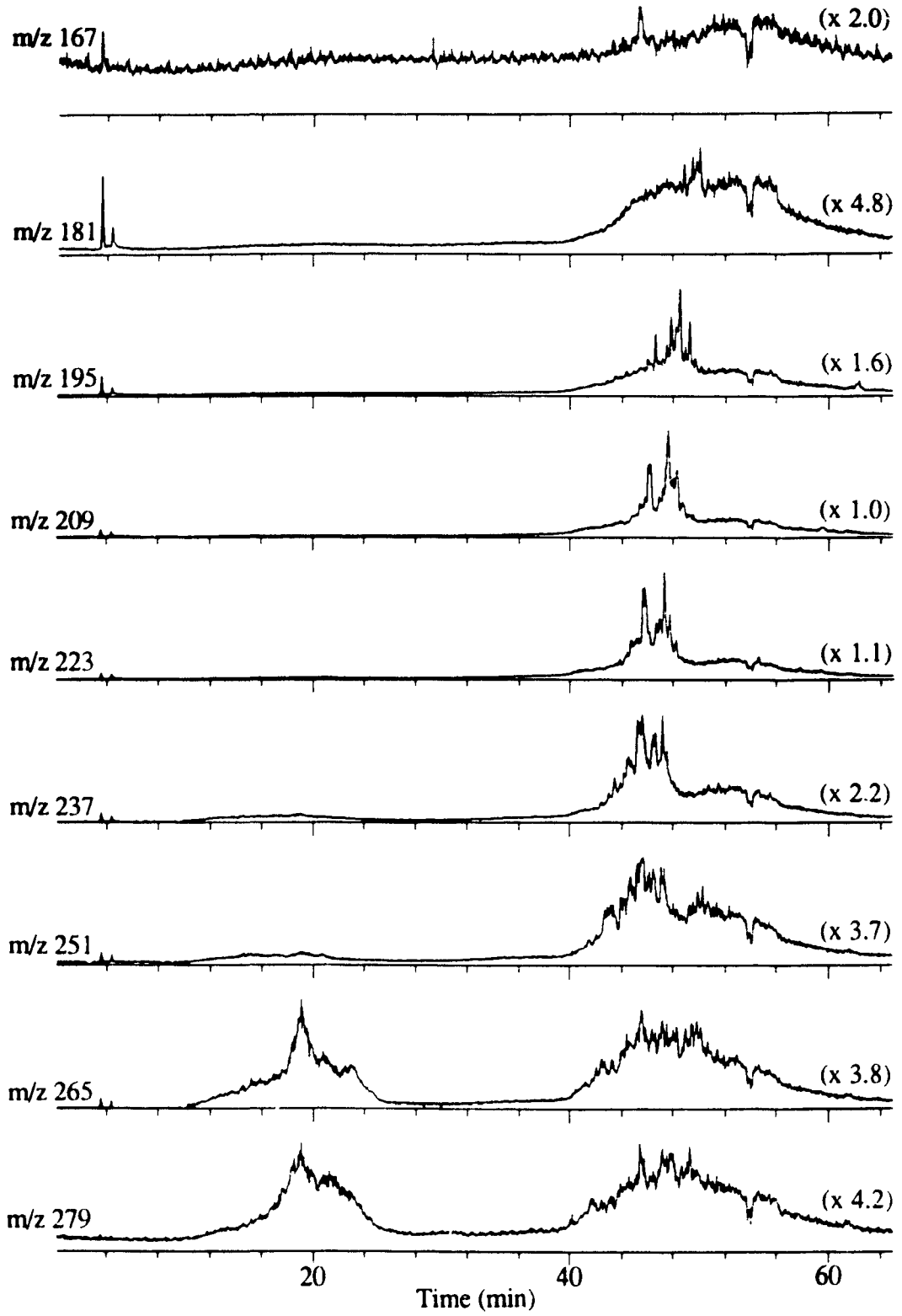

Figure IV-12: LC-MS selected ion chromatograms of alkylated carbazole generated from the analysis of Figure IV-10a.

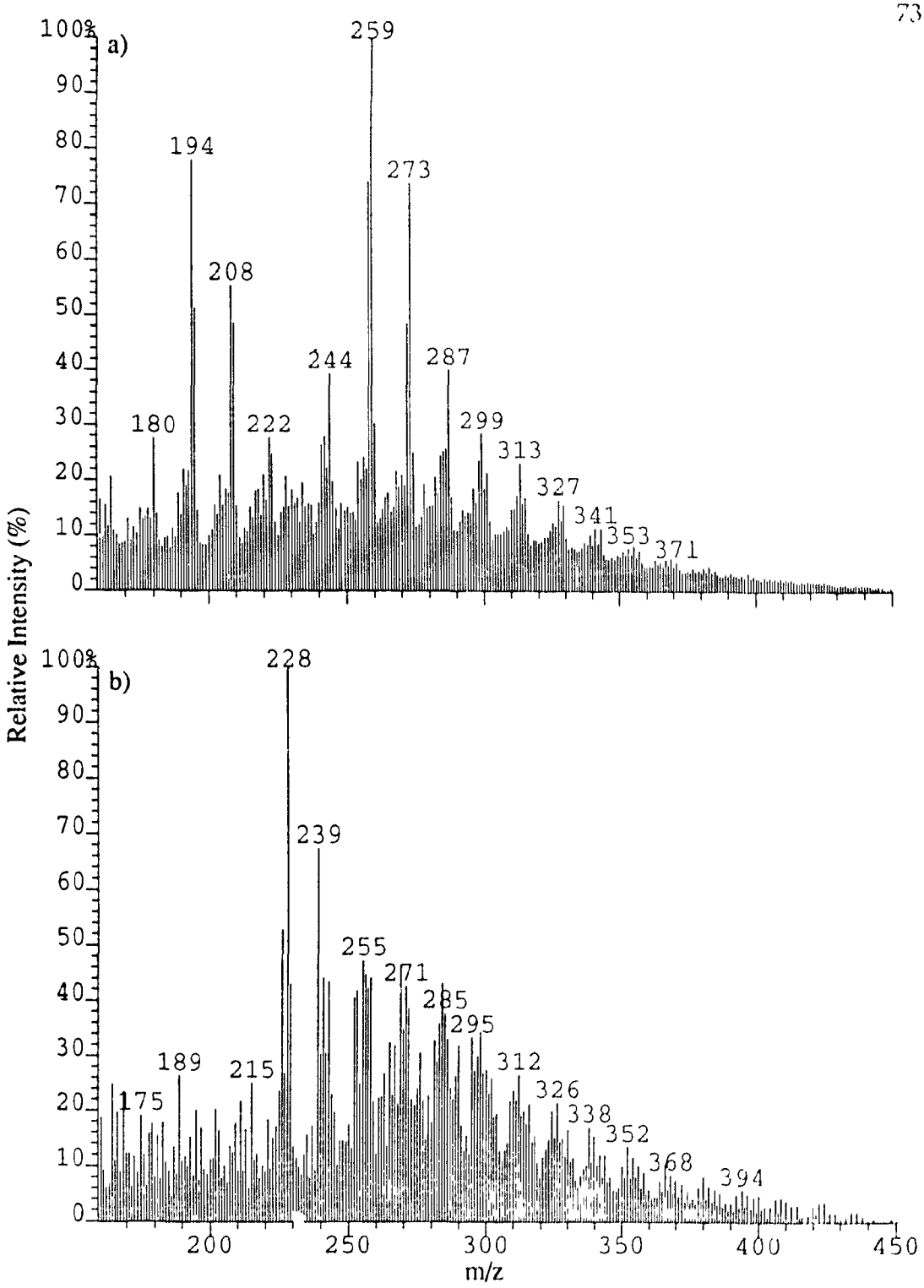

Figure IV-13: Background subtracted EI mass spectra obtained from the top of the peaks in (a) Figure IV-12 (m/z 182, second trace) and (b) Figure IV-11 (m/z 228, top trace).

is insufficiently energetic to cause carbon-hydrogen or carbon-carbon bond cleavage, only parent ions are observed in the spectra Relatively low sensitivity and reproducibility are, however, major disadvantages of low voltage EI.[1] Nonetheless, NPLC coupled to the moving belt interface while using low voltage EI has been demonstrated to be a valuable tool for the qualitative analysis of complex PAC fractions.[151,161] Chemical ionization using methane or ammonia, another soft ionization technique, has also been shown to be suitable for the analysis of heavy oil fractions [154]

V. THE PARTICLE BEAM INTERFACE

The particle beam interface is one of the recently developed approaches for coupling liquid chromatography to mass spectrometry.[162,163] A schematic diagram of a current version of this interface is shown as Figure V-1. In this device, the LC effluent is nebulized with a high velocity jet of helium that generates a stream of highly uniform sized droplets. The high velocity gas stream also assists in dispersing the droplets and preventing coagulation. The aerosol is then directed through a desolvation chamber maintained at a pressure slightly below ambient and a temperature above ambient, where the solvent rapidly evaporates from the droplets. Ideally, as the solvent evaporates, any analyte or other mobile phase components (e.g., buffers) present in the drops forms a solid residue, thus becoming a high velocity particle beam directed at the momentum separator portion of the interface. If the analyte present in the droplets is a liquid rather than a solid at room temperature, then the desolvated beam will consist of less volatile liquid drops.

A momentum separator is used to connect the aerosol generator and desolvation chamber to the high vacuum region of the mass spectrometer. The helium gas, solvent vapour and analyte particles exit the desolvation chamber through a nozzle, and then undergoes a supersonic expansion into the first low-pressure region (approximately 10 Torr) of the momentum separator. The high mass of the particles relative to the gas stream provides them with much greater momentum than the solvent vapour and helium gas. Consequently, the particles do not expand from the core of the expansion jet as rapidly as do the gases, and skimming the core of the gas jet results in a

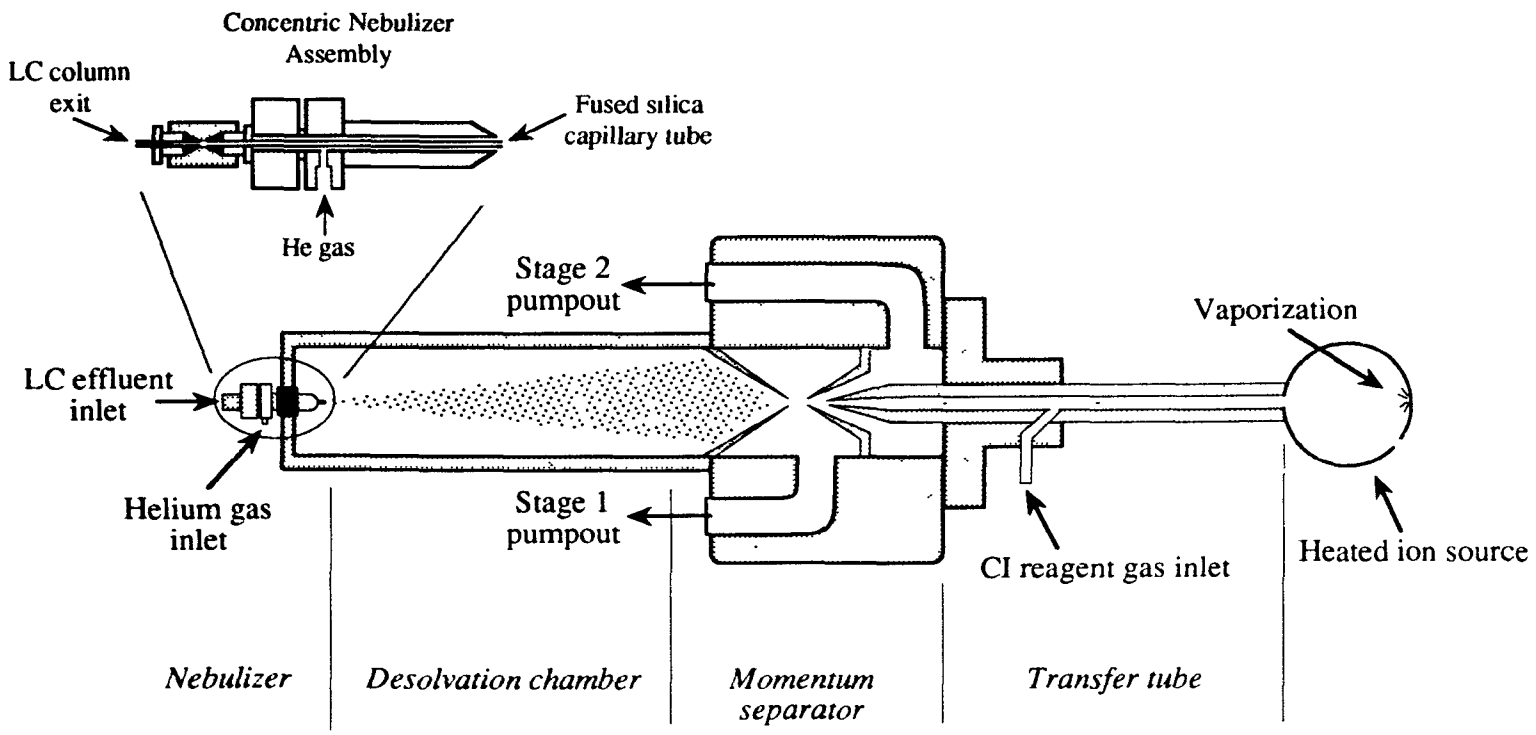

Figure V-1: Schematic diagram of a particle beam interface.

substantial enrichment of the analyte relative to the gases. The solvent vapour that has been skimmed off is pumped away mechanically. This process is then repeated in the second stage of the momentum separator, dropping the chamber pressure to approximately 1 Torr.

The analyte particles continue on a linear trajectory into the ion source region of the mass spectrometer after leaving the momentum separator. The narrow particle beam undergoes a rapid process of flash vaporization as it collides with the heated ion source wall. The vaporized analyte molecules are then ionized, using either EI or CI and the mass spectra are acquired on either magnetic sector or quadrupole mass spectrometers.

Achieving optimal performance from this type of interface usually requires the adjustment of several interface settings to accommodate the LC conditions required for the analysis. For example, the position of the fused-silica capillary tube that is connected to the LC column exit (Figure V-1), can be adjusted such that the tip protrudes or is withdrawn inside the concentric nebulizer assembly. The position of the capillary is critical for the production of a suitable aerosol and achieving good sensitivity. A protrusion of approximately 0.5 mm was found to provide optimal results.

Other important interface parameters include the temperatures of the desolvation chamber and the ion source. The former is usually not critical providing that condensation in the chamber is avoided. Temperatures between 35-45°C are recommended, although higher temperatures may be necessary for mobile phases that contain a high water content. Some compounds may be sensitive to ion source temperature, in particular, thermally labile analytes. Source temperatures of 250°C are suitable for most

compounds, although analytes with low volatilities (e.g., high molecular weight PAC) may require even higher temperatures.

The working principle of the particle beam interface is the same as that of the moving belt interface, i.e., removal of the mobile phase from the analyte before ionization. In each case, mobile phases with a high content of organic solvent and flow rates of 0.4 mL/min or less are recommended for best performance. Standard analytical columns (4.6 mm i.d. at 1 mL/min) will therefore require a post-column effluent split, while 2 mm i.d. column (0.2 mL/min) are ideal.

Particle beam LC-MS has become popular because of its ease of operation, compatibility with most LC mobile phases (including reversed-phase systems), and the ability to operate in both EI and CI modes of ionization. The generation of library-searchable EI spectra is probably its most important advantage over other LC-MS techniques, since this capability is critical in regulatory monitoring and identification of unknowns. In much of the related literature,[164,165] particle beam MS is used as only a confirmatory tool.

The use of the particle beam interface for quantitative analyses has been seriously hampered because of the non-linear calibration curves it often produces. Several groups have reported quadratic or second-order responses for a large number of analytes.[166,167,168] It has been suggested[167] that this non-linear behaviour is related to the amount of analyte in a particle and its transmission through the interface. Analyte transport efficiencies are generally less than 10% for most compounds in the particle beam interface.[169] Losses occur primarily in the momentum separator because of particle

sedimentation, turbulence and misalignment of nozzles and skimmer cones.[163] Sedimentation and turbulence are directly related to the size of analyte particles, which in turn is a function of analyte concentration[163] and the diameter of the nebulizer tip.[169] Thus, the non-linear curves are a result of small particles being produced at low analyte concentrations, which are more prone to turbulent losses and have reduced transport efficiencies. More efficient mass transport occurs at higher concentrations as the particle size increases.

This mass transport hypothesis is consistent with the observation that enhancements in ion abundances and even linearization of calibration curves occurs during coelution of the analyte with other components of the sample or when certain substances (e.g., ammonium acetate) are present in the mobile phase.[167,170] This effect has been attributed to the formation of larger particles containing both additive and analyte, which are transported more efficiently through the interface (the so-called "carrier" effect).

A subsequent theory, put forth by Doerge *et al.*,[168] suggests that detector non-linearity is the basis of the quadratic or even exponential calibration curves. They claim that the lower ion intensity levels produced by particle beam MS fall in the non-linear toe region of the detector response curve. The observed linearization of calibration plots with mobile phase additives occurs because the "enhanced" amounts of analyte push the detector response into its linear range.[168] A comparison of these two theories and their relevance to the results obtained in this study will be discussed in subsequent paragraphs.

The purpose of the following experiments was to determine how well the particle beam interface is suited for the analysis of PAC. In particular, the

detection limits, dynamic range, and calibration curve linearity of typical PAH standards were examined. The qualitative analysis of three complex real-world samples was then performed.

V.1 Reversed-Phase LC Coupled to the Particle Beam Interface

The EI mass spectra acquired for three PAH standards that were separated on a reversed-phase C_{18} column are shown as Figure V-2 The relatively simple spectra are similar to those obtained using the moving belt interface; intense molecular ions ($M^{+\cdot}$), small ions due to the loss of one to four hydrogen atoms, and doubly charged ions (M^{2+}) are all present. The background noise produced by this interface was very low in intensity and was generally only present at low mass (i.e., below m/z 150). The belt interface, in contrast, produced very intense background ions, at specific m/z ratios, from the polyimide belt.

During the acquisition of the spectra shown in Figure V-2 and the optimization of the interface, a very peculiar observation was made. Figure V-3 shows the chromatograms obtained from six replicate injections of a solution containing three PAH standards (benz[*a*]anthracene, benzo[*a*]pyrene, and dibenz[*a*,*h*]anthracene). The TIC clearly shows a dramatic decrease in the peak heights of all three standards with respect to time. The peak areas (relative to the first injection) obtained from the single ion chromatograms (monitoring molecular ions) for the individual PAH are shown next to the

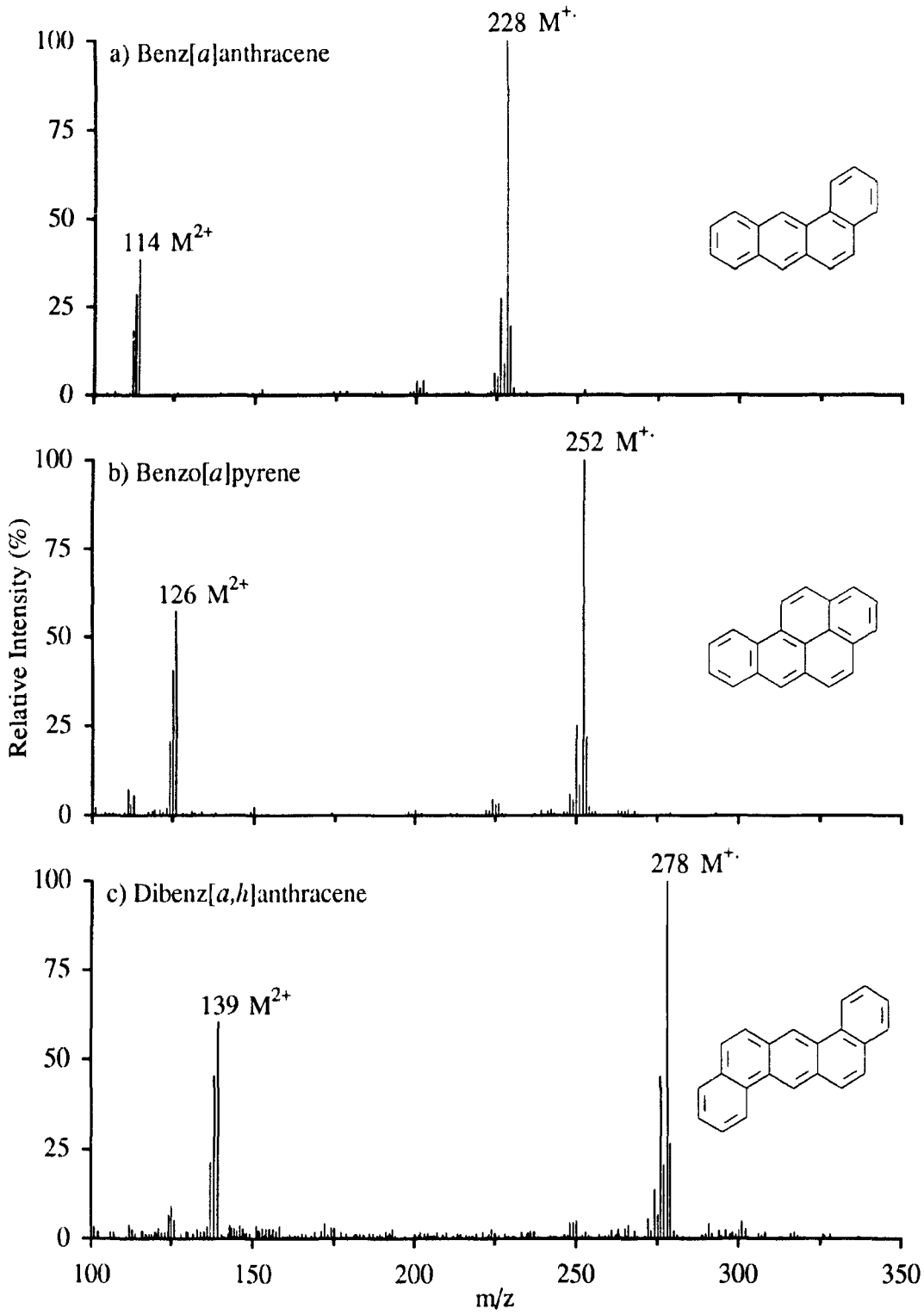

Figure V-2: Background subtracted EI mass spectra of three PAH standards obtained with the particle beam interface.

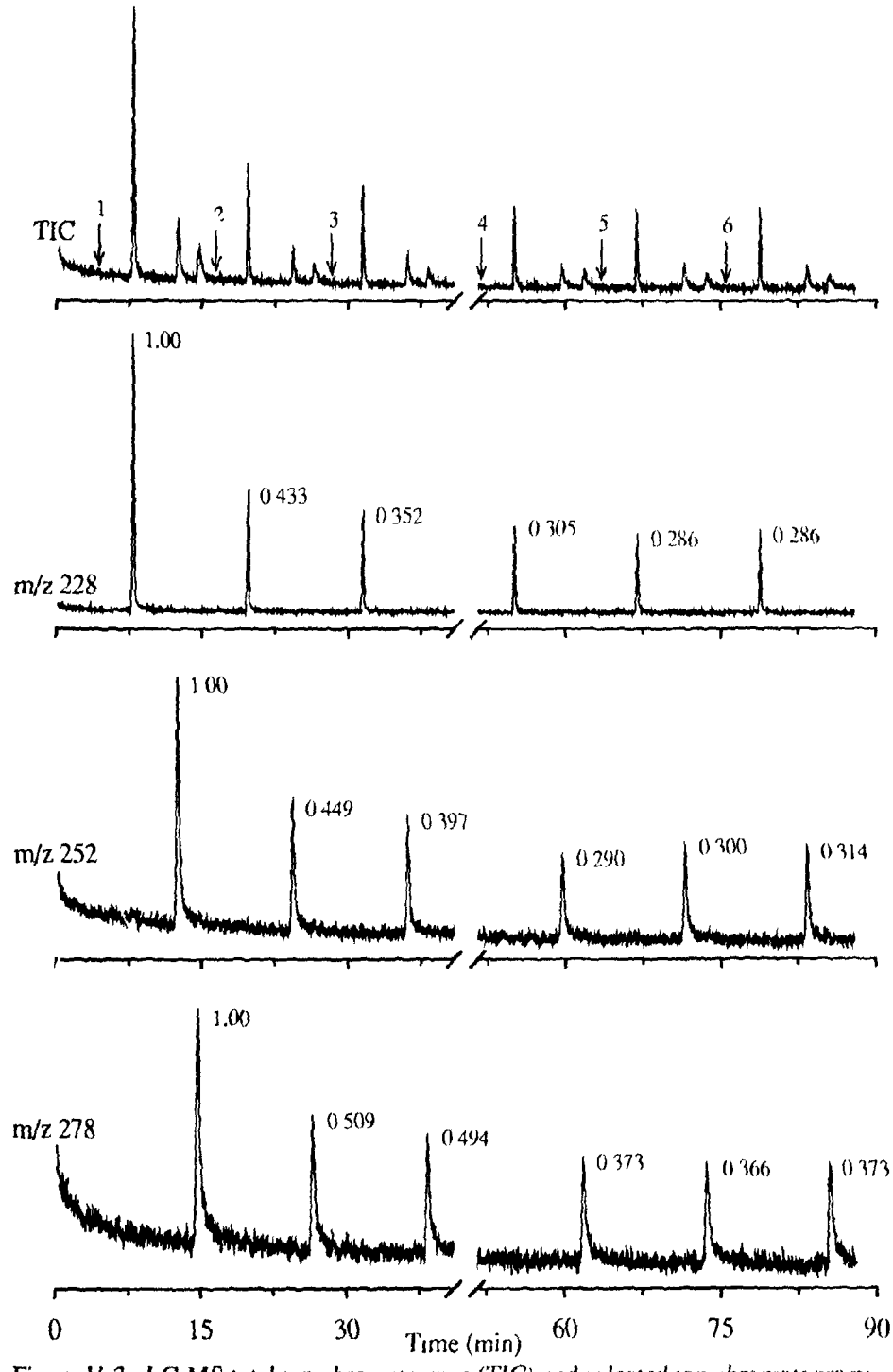

Figure V-3: LC-MS total ion chromatogram (TIC) and selected ion chromatograms from six replicate injections of a solution containing benz[*a*]anthracene (m/z 228), benzo[*a*]pyrene (m/z 252) and dibenz[*a,h*]anthracene (m/z 278)

peaks. The relative standard deviations (%RSD) for the six injections were as follows: benz[*a*]anthracene, 63%; benzo[*a*]pyrene, 59%; and dibenz[*a*,*h*]anthracene, 47%. These RSD's are extremely large and certainly not practical for quantitative or even semi-quantitative analyses. However, the peak areas appear to level-off after the fourth injection (about 40 minutes into the analysis). The %RSD's calculated for the last three injections are actually very good (and comparable to the belt interface): benz[*a*]anthracene, 3.8%, benzo[*a*]pyrene, 3.9%, and dibenz[*a*,*h*]anthracene, 1.0%.

This unusual behaviour probably results from changing source conditions (e.g., temperature) at the outset of an analysis. For example, the current to the filament is always switched on at the start of an acquisition and then turned back off when the acquisition is terminated. The filament can produce a significant amount of heat in a very localized area within the ion source and thus produce pronounced variations in ionization efficiency and ion transmission. Subsequent experiments performed on this instrument were designed to minimize the effects of this phenomenon. In general, the instrument was turned on approximately 20 to 30 minutes before the start of an analysis to allow, for example, the temperature of the filament and the entire source to equilibrate.

The calibration curves obtained for three PAH standards separated on a reversed-phase C_{18} column are shown as Figure V-4. All of the calibration solutions were analyzed in a single MS acquisition period after instrument conditions were allowed to stabilize (total analysis time of about 120 minutes). All three graphs have been fitted to quadratic equations, represented in each case by a solid line. A recent report has claimed that with the exception of

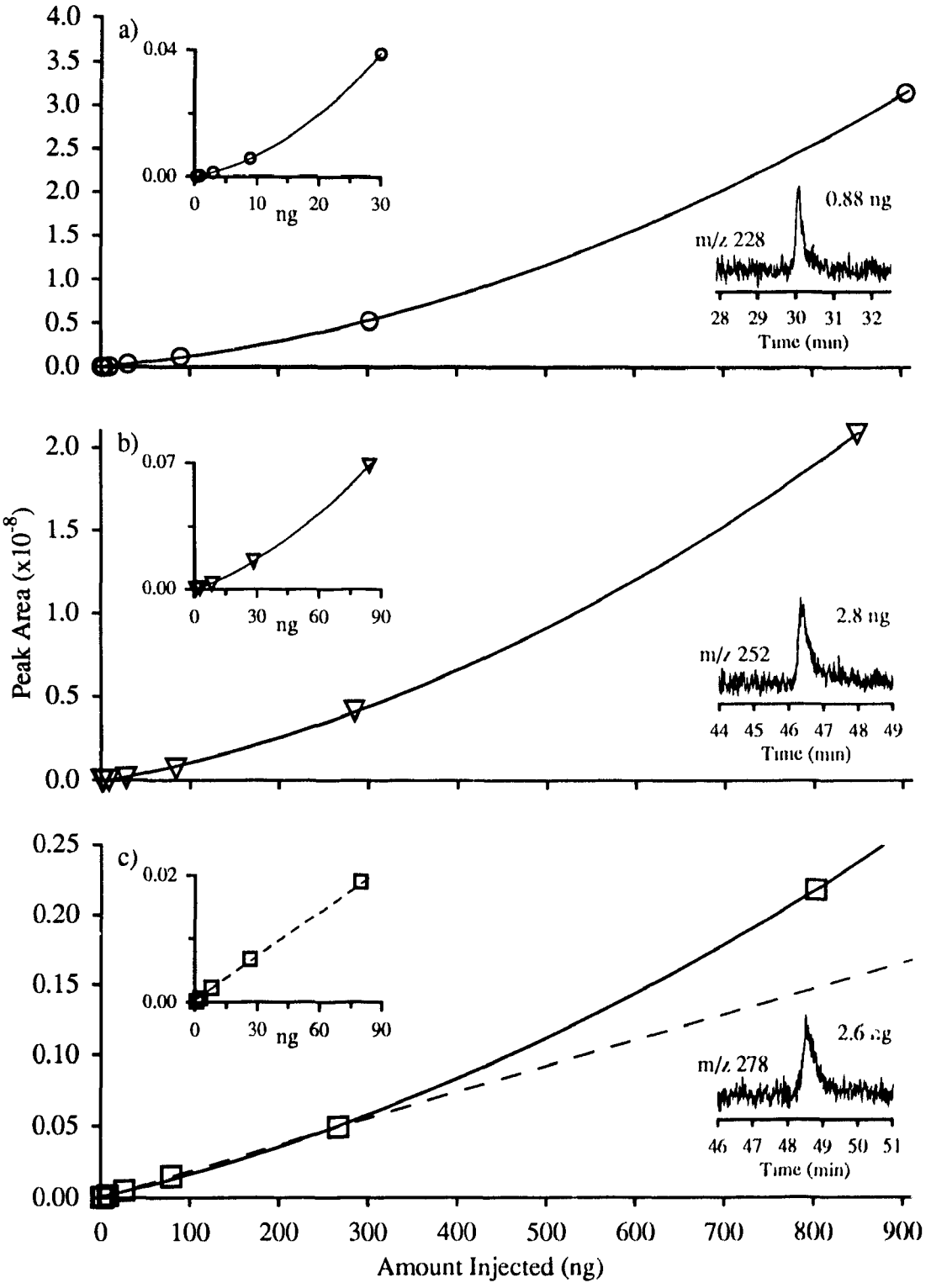

Figure V-4: Particle beam LC-MS calibration curves obtained for (a) benz[*a*]anthracene, (b) benzo[*a*]pyrene and (c) dibenz[*a,h*]anthracene. Left insets show an expansion of the low ng region. Right insets show the low level LC-MS responses obtained for each standard.

benz[*a*]anthracene and chrysene, several PAH standards exhibited linear response behaviour over the range of 20 ng to 1000 ng.[171] The expansion of the low mass region of the graphs (left insets) clearly shows that the curves for both benz[*a*]anthracene and benzo[*a*]pyrene are non-linear throughout the entire concentration range. The expansion of the dibenz[*a,h*]anthracene graph, however, reveals that the data do exhibit linear behaviour (dashed line), but only below 300 ng injected on-column. The belt interface produced curves that were the opposite to those shown in Figure V-4; linear responses below 300 ng was the norm, while the curves became non-linear in a downward direction at higher concentrations (as opposed to the upward curves of Figure V-4).

According to the particle beam "detector non-linearity" theory described earlier,[168] the calibration curves shown in Figure V-4 would imply that the absolute ion intensities produced by dibenz[*a,h*]anthracene were not in the non-linear toe region of the detector response curve, and therefore higher than those of the other standards. However, the ion intensities observed for dibenz[*a,h*]anthracene during these calibration experiments were actually lower than those obtained from the other two compounds (as evidenced by the peak area scales of Figure V-4), thus providing convincing evidence against this "detector non-linearity" theory.

The second insets of Figure V-4 show the low level LC-MS responses (between 0.88 ng and 2.8 ng injected on-column) for the three PAH standards. The signal-to-noise ratios for these chromatograms were approximately 2:1; a slight extrapolation to signal-to-noise ratios of 3:1 produces detection limits of 1.0, 3.4 and 3.9 ng for benz[*a*]anthracene, benzo[*a*]pyrene and

dibenz[*a,h*]anthracene, respectively. A previous study of 12 PAH standards also reported detection limits in the low ng range.[171] These limits are by no means universal for all PAC; the volatility of the compounds will ultimately determine the detection limit. This was also true for the belt interface; the more volatile low molecular weight PAH are more susceptible to losses in the interface thus producing much higher detection limits. This point will be further illustrated in the following paragraphs that discuss the qualitative analyses of three complex PAC mixtures as well as in the next section that describes the quantitative analyses of PAC present in a coal tar material.

Figure V-5 compares the chromatograms obtained from the LC-UV (top trace) and LC-particle beam MS (bottom trace) analysis of the NIST coal tar mixture. The chromatograms appear to be similar except for the absence of the early eluting compounds (under 15 minutes) in the particle beam trace. Several selected ion chromatograms obtained from this analysis are shown as Figure V-6; the peak numbers are listed in Appendix A with the corresponding compound identities established by matching retention times and mass spectra with those of standards. The early eluting compounds that were not detected by particle beam MS (Figure V-5b and V-6) correspond to PAH with molecular weights lower than 170 Da (e.g., acenaphthylene, acenaphthene, biphenyl, fluorene, etc.). A signal was obtained for naphthalene (Figure V-6, first trace) because it is present at a much higher concentration (1160 μg/g) than all the other components (460 μg/g and lower). Two previous reports have also stated that particle beam MS shows good sensitivity for only later eluting PAH with molecular weights greater than 170[165] or 220[171] Da. Presumably, the lower molecular weight PAH are

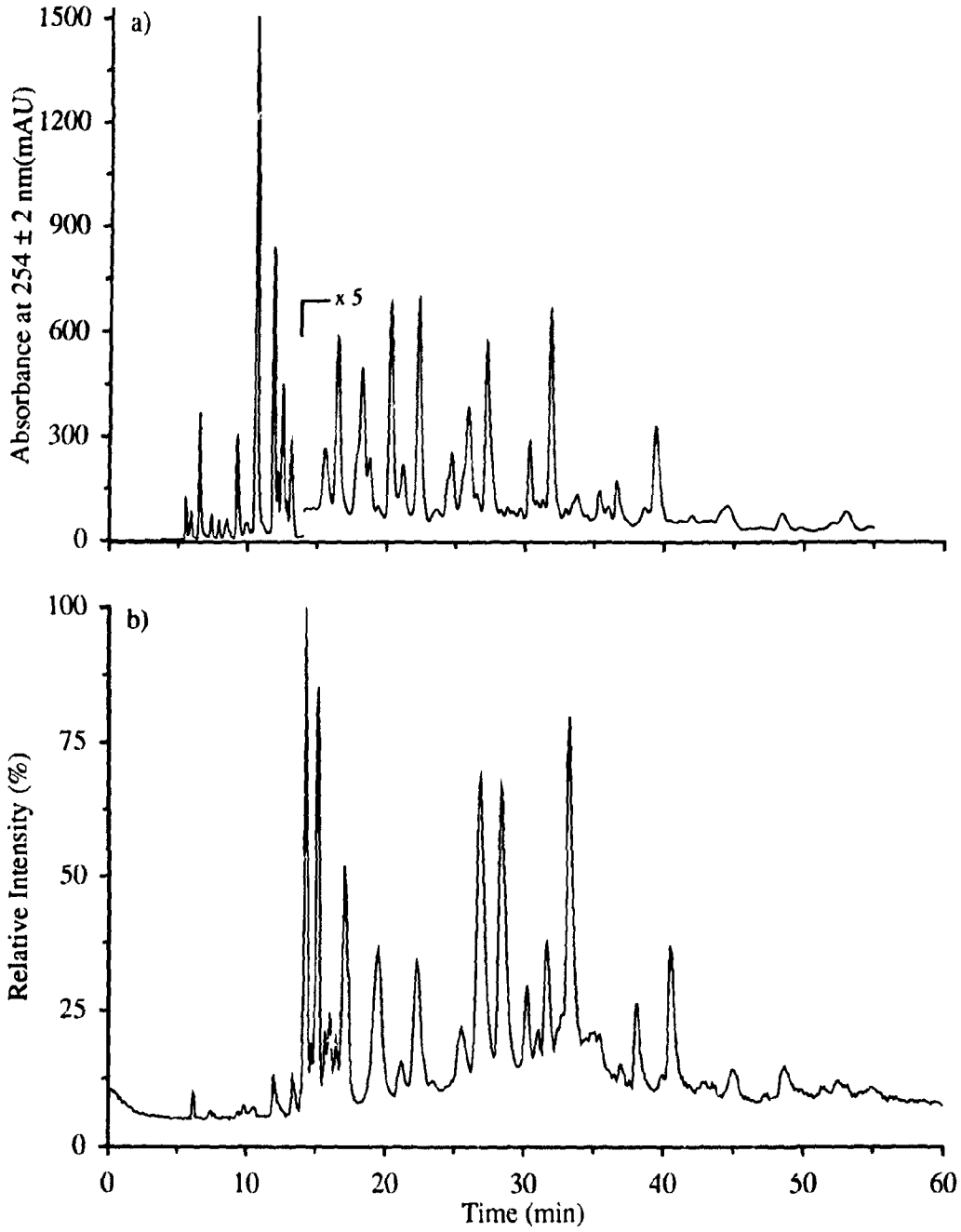

Figure V-5: (a) LC-UV and (b) particle beam LC-MS total ion chromatograms from the analysis of the NIST SRM 1597 coal tar mixture using a C_{18} column with an aqueous acetonitrile gradient.

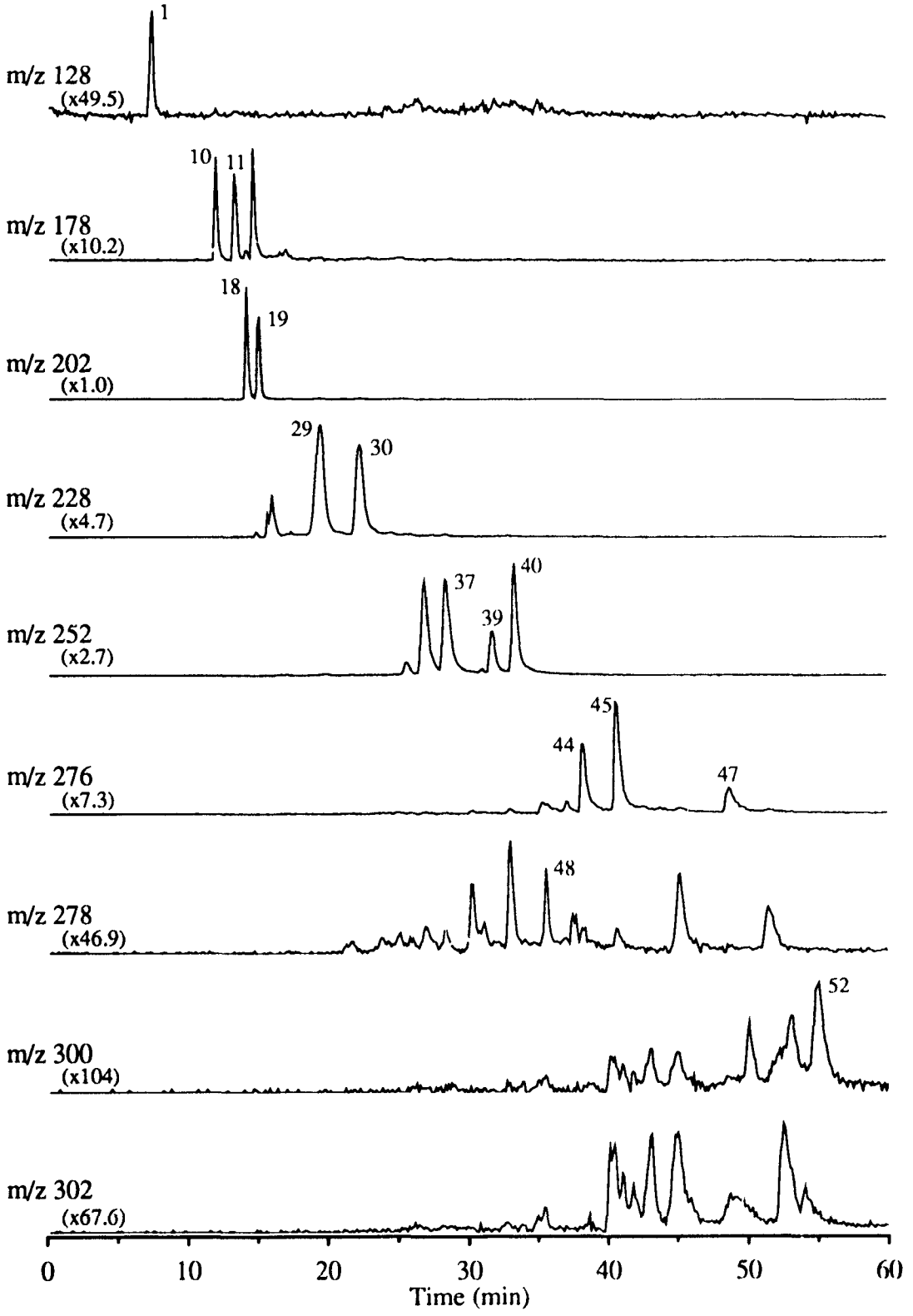

Figure V-6: LC-MS selected ion chromatograms generated from the analysis of Figure V-5b. See Appendix A for compound identities.

sufficiently volatile that they are lost to the vacuum in the interface. The larger and less volatile PAH present in this sample (up to mass 302) were not as susceptible to interface losses and were thus easily detected (Figure V-6).

The ability to detect high molecular weight PAH is significant since LC is capable of separating such compounds that are not amenable to GC analyses. The chromatograms obtained from the LC-UV and LC-particle beam MS analysis of a carbon black extract, containing primarily high molecular weight PAH,[142] are compared in Figure V-7. Surprisingly, the overall sensitivity of the particle beam instrument had dropped significantly from the previous analysis of the coal tar (Figure V-5b). The carbon black TIC (Figure V-7b) shows only a few of the many chromatographic peaks evident in the LC-UV trace (Figure V-7a). The selected ion chromatograms that could be generated from the MS data set are shown as Figure V-8. The concentrations of individual PAH in this sample were similar to those in the coal tar mixture (based on LC-UV responses), and one would have expected the detection of more components.

There are two probable reasons for the poor sensitivity observed in Figures V-7 and V-8. First, particle beam MS has been shown to be susceptible to tremendous fluctuations in absolute response during intra- and interday runs.[165] For example, instrument response factors for chlorinated phenoxy acid standards varied as much as 2 fold over a 24 hour period.[164] A subsequent reanalysis of the coal tar sample shown in Figure V-5, revealed that there was indeed a significant drop in instrument response (by at least a factor of two). Attempts to regain this loss in sensitivity by adjusting the interface settings were unsuccessful. The reasons for this unusual behaviour

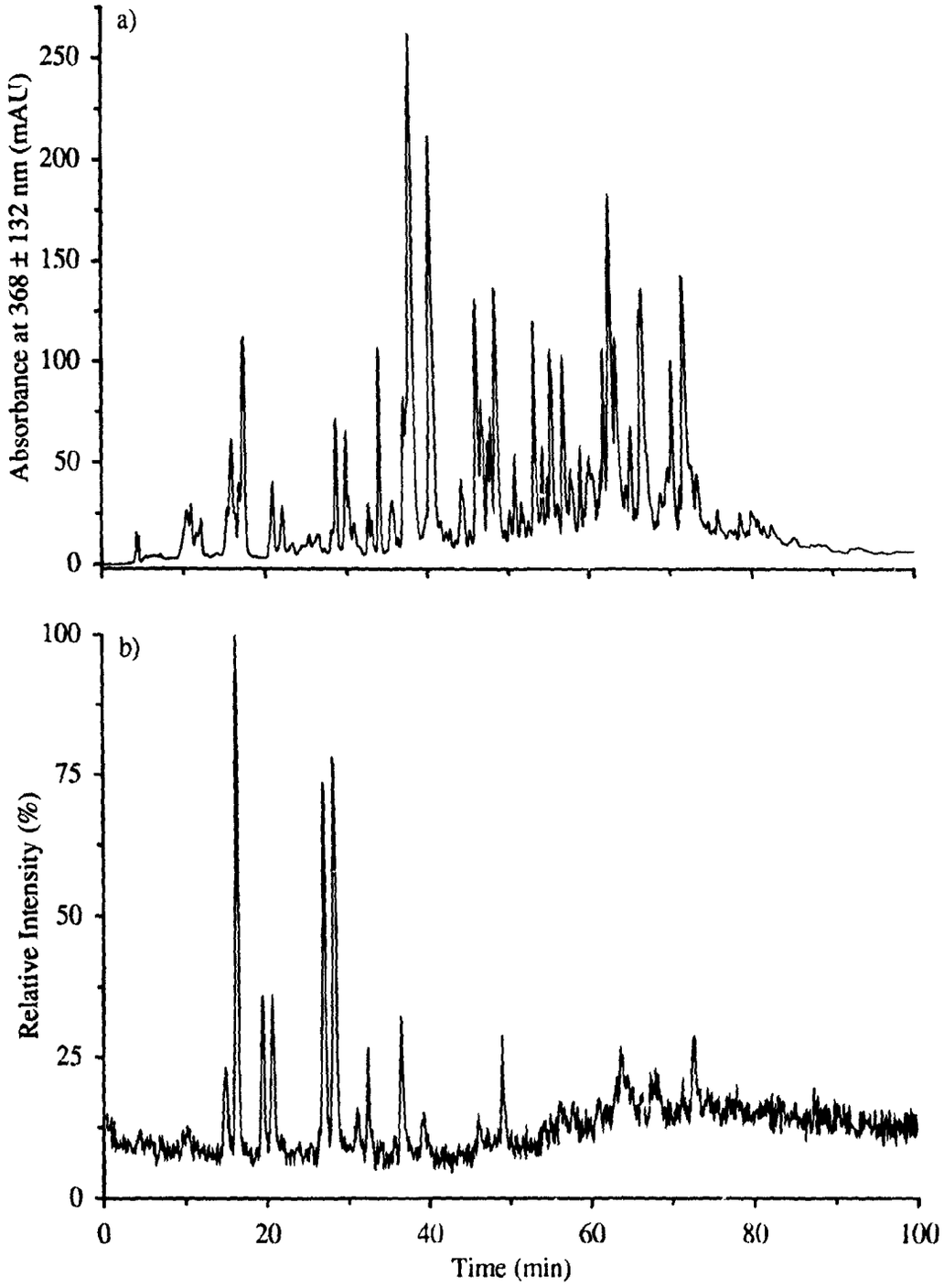

Figure V-7: (a) LC-UV and (b) particle beam LC-MS total ion chromatograms from the analysis of the carbon black extract using a C_{18} column with an aqueous acetonitrile/dichloromethane gradient.

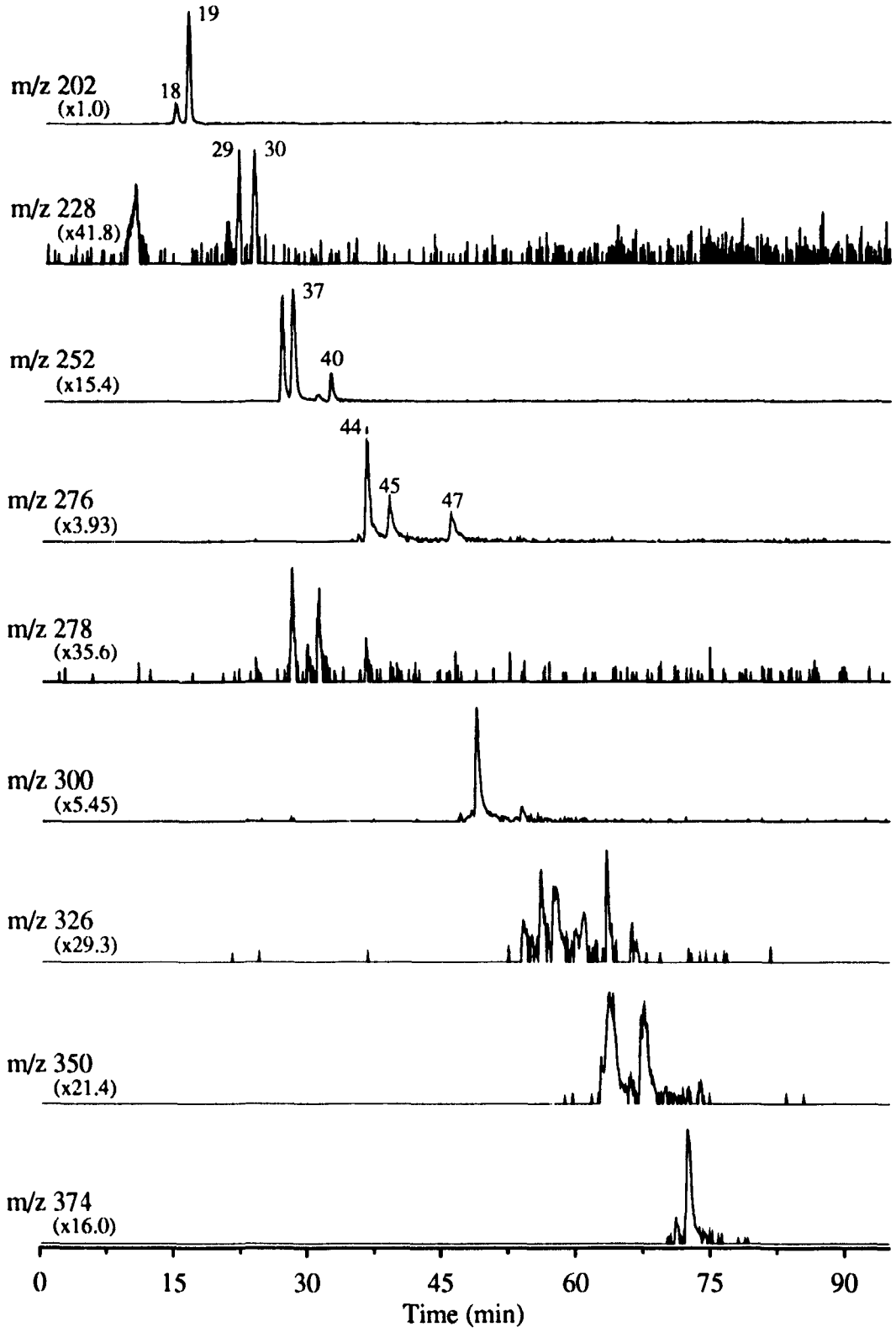

Figure V-8: LC-MS selected ion chromatograms generated from the analysis of Figure V-7b. See Appendix A for compound identities.

have not been addressed, although we believe that it may be related to degradation of the nozzles and skimmers within the momentum separator.

The low volatility of the high molecular weight PAH in the carbon black extract is the second reason for the poor sensitivity observed in Figures V-7 and V-8. The particle beam generated by the interface must strike the heated ion source and vaporize in order to be ionized. The high molecular weight PAH probably have volatilities that are sufficiently low enough that they are not efficiently vaporized in the source. PAH as high as mass 374 were detected (Figure V-8, bottom trace), although the isomers with the highest volatility were probably selectively detected. Attempts at increasing the source temperature to its highest recommended setting (from 250 to 300°C) resulted in only modest gains in sensitivity. This is in sharp contrast with the belt interface which was capable of thermally desorbing and detecting PAH as high as mass 448 from the belt surface (Figure IV-5).

The analysis of the tar sand oil neutral fraction, the final qualitative application of the particle beam interface, also produced rather disappointing results. Figure V-9 compares the LC-UV chromatogram with the particle beam TIC. The poor sensitivity that is evident from the TIC is partly a result of the drop in instrument response observed above for the carbon black extract. In addition, the constituents of this fraction, primarily small PAH and their highly alkylated homologues, are sufficiently volatile that they are being lost in the interface vacuum. The representative SIC shown as the bottom three chromatograms of Figure V-9 illustrate the inability of this type of interface to analyze complex mixtures of volatile compounds. This same fraction was analyzed with much greater success with the belt interface in

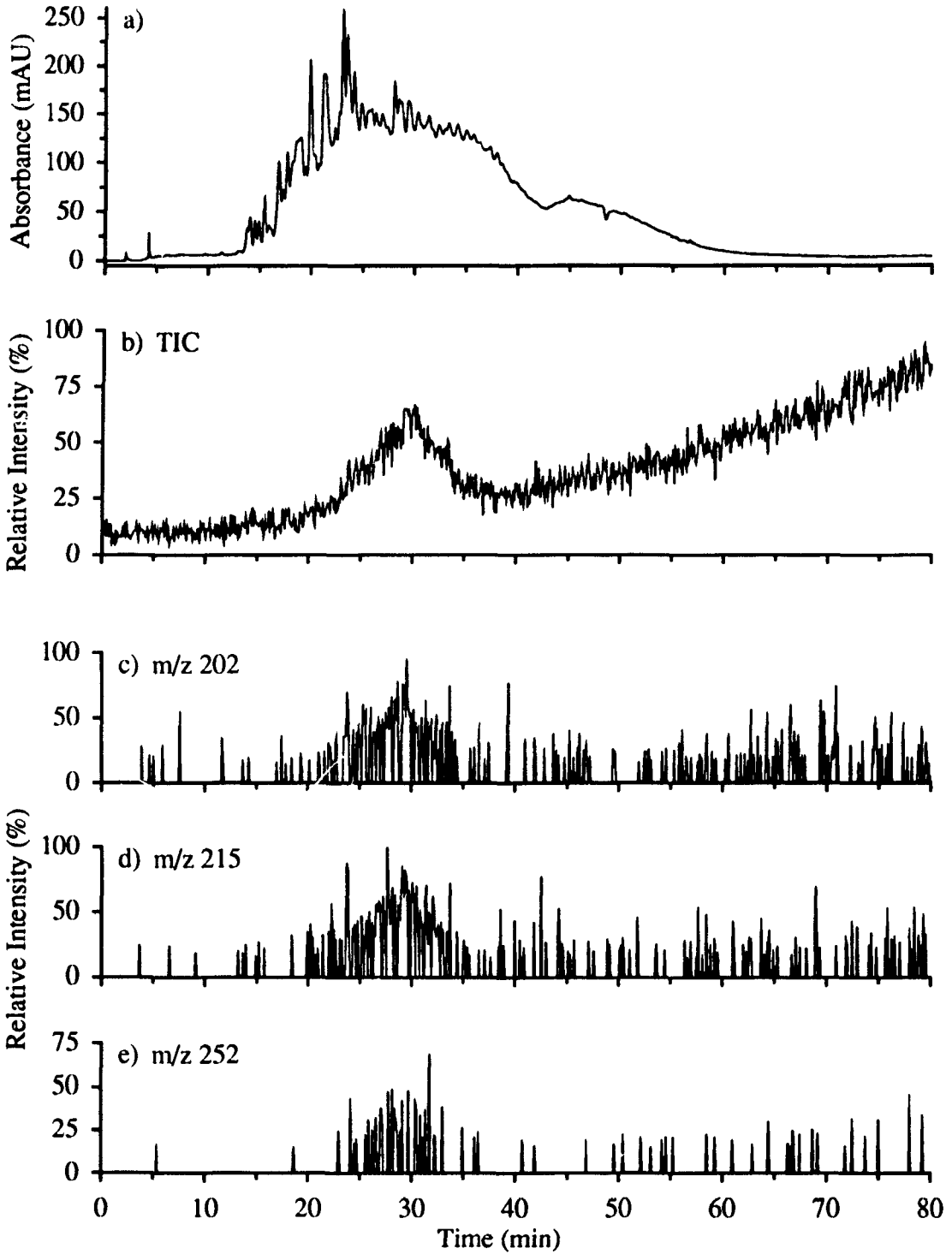

Figure V-9: (a) LC-UV (254 ± 2 nm) and (b) particle beam LC-MS total ion chromatograms from the analysis of the tar sand oil neutral fraction using a C_{18} column with an aqueous acetonitrile/dichloromethane gradient. Selected ion chromatograms (c - d) generated from the analysis of Figure V-9b.

conjunction with normal-phase columns (Figures IV-9, 11 and 13); the vaporization of the more volatile mobile phases required less extreme conditions and therefore, much less sample was lost to the interface vacuum.

V.2 Quantitative Analysis

While particle beam MS is generally accepted as being useful for the confirmation of analytes, it has been much less useful for quantitation. The results shown earlier in Figure V-4 have already demonstrated that the calibration curves for PAH can be either linear (e.g., dibenz[*a*,*h*]anthracene below 300 ng) or non-linear (e.g., benz[*a*]anthracene and benzo[*a*]pyrene). While non-linearity of detectors and instruments does not preclude their use in quantitative analysis, it does increase the requirements for calibration and necessitates interpolation from multipoint calibration curves. As an alternative, the linearization of calibration curves through the use of the carrier effect (i.e., using mobile phase additives) has been suggested.[170] Subsequent, more precise measurements, however, have indicated that this technique is limited to very few compounds and that non-linear behaviour was still prevalent.[167]

The presence of unexpected coeluting substances in real-world samples can also cause calibration errors and analytical bias. The detector signal given by target analytes has been shown to increase with coeluting matrix constituents.[166] Presumably, particle size discrimination in the momentum

separator with its influence on transport efficiency is also the basis of this phenomenon. This matrix effect could be minimized by ensuring that the coeluting substances that produce the signal enhancements are also present in the external calibration standards and that there are no unexpected coeluting substances. However, these restrictions are not easily satisfied when extremely complex samples containing many unknown compounds are analyzed.

The fluctuations in absolute response observed in intra- and interday runs mentioned earlier is also a significant obstacle when using an external calibration. The obvious way to overcome this type of problem is through the use of internal standards. In particular, isotopically labelled internal standards exhibit almost identical chemical behaviour to the native substances, but are readily differentiated by their mass spectra. If the internal standards are chromatographically resolved from the target compounds (which is true for perdeuterated PAH internal standards), the matrix effect can still cause calibration errors. The coelution of a matrix constituent with either the internal standard or the target compound will result in a corresponding increase in detector signal for that compound.

The only reliable means of preventing the selective enhancement of either the internal standard or the analyte is through the use of coeluting isotopically labelled internal standards. Unexpected coeluting substances in real world samples would then affect the transport of both the native and labelled species to the same extent. In addition, coeluting internal standards, if present in high enough quantities, could dramatically increase the particle size such that the ratio of the signals obtained from the native and labelled

species should be less sensitive to slight changes in particle mass and/or transmission efficiency. This type of isotope dilution calibration, however, is limited by the availability and cost of the labelled species and the requirement of coelution.

The following experiments were conducted to determine whether external calibration and/or isotopically labelled internal standards (that are chromatographically resolved from their native components) can be used to quantify the PAH present in a complex "real world" sample. A mixture of perdeutero-PAH standards (DPAC-1, described in Experimental) was spiked at four different levels into a certified NIST PAH standard mixture (SRM 1647) and a NIST complex mixture of PAH from coal tar (SRM 1597). These solutions were prepared primarily for internal standardization experiments, but since the volumes of both standard and internal standards were measured accurately, they were also used for external calibration experiments.

A total of 24 masses (i.e., m/z) were monitored (16 PAH and 16 perdeutero-PAH including isomers) in three acquisition periods (8 ions per period, 1 second total scan time, described in Experimental). An example of a typical analysis of a SRM 1647/DPAC-1 solution (in a 10:1 spike ratio) is shown as Figure V-10. Only seven of the 16 PAH that were monitored were detected (Figure V-10, second acquisition period, 9.8-33.5 minutes) and subsequently quantified. The lower molecular weight PAH (e.g., mass 178 and lower), which were present in much higher concentrations than the other components (see Table V-1), were among the PAH that were not detected (Figure V-10, first acquisition period, 0-9.8 minutes). These compounds were too volatile to be efficiently transported through the

Figure V-10: Analysis of a SRM 1647/DPAC-1 solution (10:1 volume ratio) using particle beam LC-MS. A total of 24 ions monitored in three acquisition periods: (a) TIC (sum of all molecular ions); Period 1, (b) m/z 128, (c) m/z 136, (d) m/z 152, (e) m/z 160, (f) m/z 154, (g) m/z 164, (h) m/z 166, (i) m/z 176; Period 2, (j) m/z 178, (k) m/z 188, (l) m/z 202, (m) m/z 212, (n) m/z 228, (o) m/z 240, (p) m/z 252, (q) m/z 264; Period 3, (r) m/z 276, (s) m/z 288, (t) m/z 278, (u) m/z 292, (v) m/z 300, (w) m/z 312, (x) m/z 302, (y) m/z 316. See Appendix A for compound identities. Peak numbers with an asterisk represent the perdeutero-PAH internal standards.

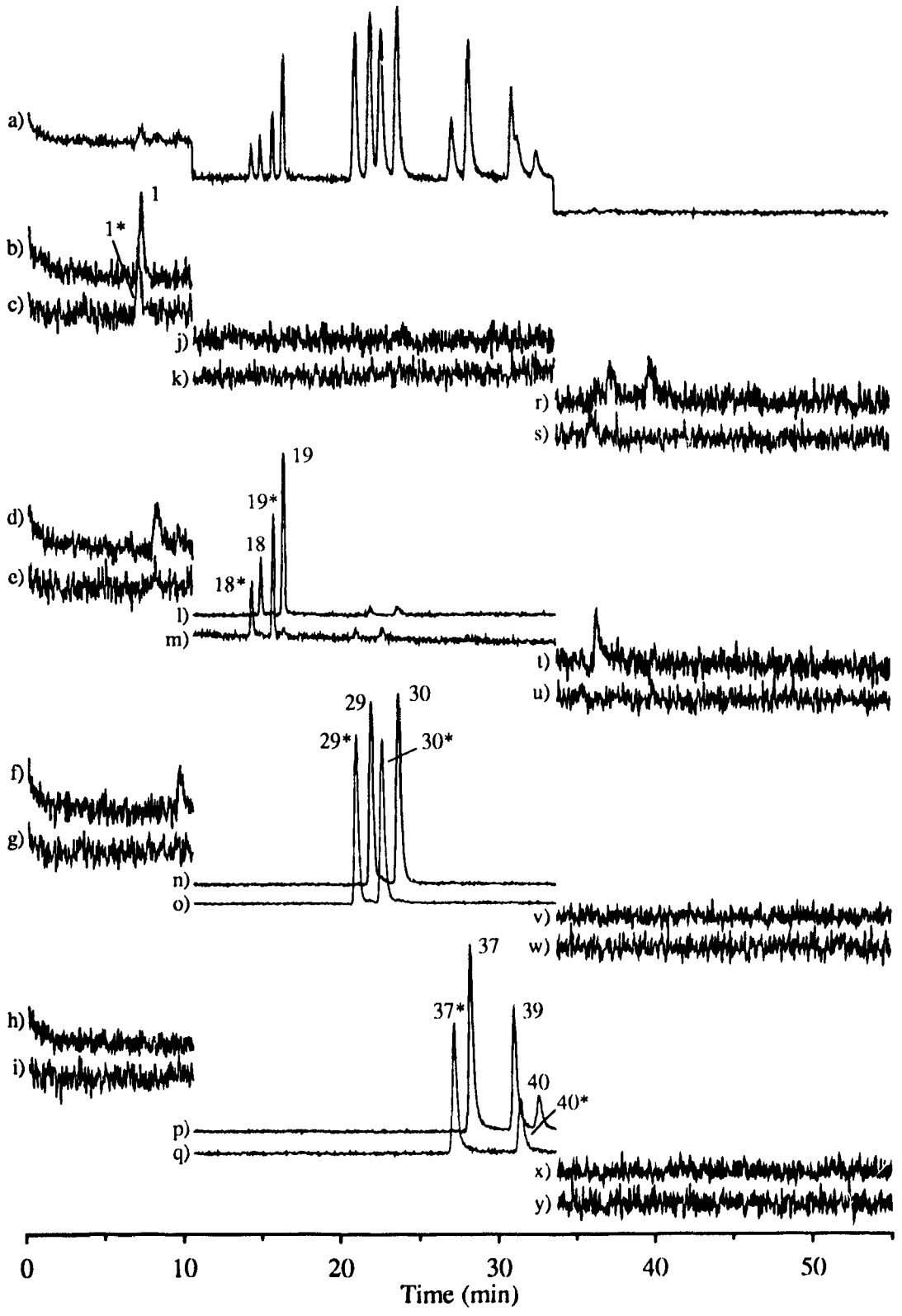

Figure V-10: Figure caption on preceding page.

interface, and therefore, have very high detection limits. The high molecular weight PAH (e.g., mass 276 and higher), which were present in similar concentrations to the PAH that were quantified (see Table V-1 below), were also not detected (Figure V-10, third acquisition period, 33.5-60 minutes). These compounds did not appear to be volatile enough to vaporize once they entered the hot ion source. The quantitation of these undetected PAH will require additional analyses with more concentrated solutions. This is a significant limitation associated with analytical techniques that have a large variation in response factors, such as the particle beam.

Three examples of the external calibration curves that were obtained from the analyses of the NIST 1647/DPAC-1 solutions are shown as Figure V-11. In each case, the linear regression curve did not pass through the origin (within experimental error) and the resulting regression coefficients varied between 0.44 and 0.62. Attempts to fit the data to a quadratic curve were unsuccessful because of an inadequate distribution of data points. The fluctuations in absolute response observed earlier during the qualitative analyses of complex mixtures of PAC, were also occurring during the calibration experiments and are largely responsible for the poor calibration results. For example, the relative standard deviation (%RSD) of the peak areas obtained from the triplicate injection of the third solution, Figure V-11, varied between 27 and 54%. The previously acquired calibration curves (Figure V-4) were not as susceptible to these fluctuations because all of the calibration solutions were analyzed continuously in one acquisition period under isocratic conditions. The fluctuations in absolute response are most pronounced when using gradient elution and multiple acquisitions, as in the

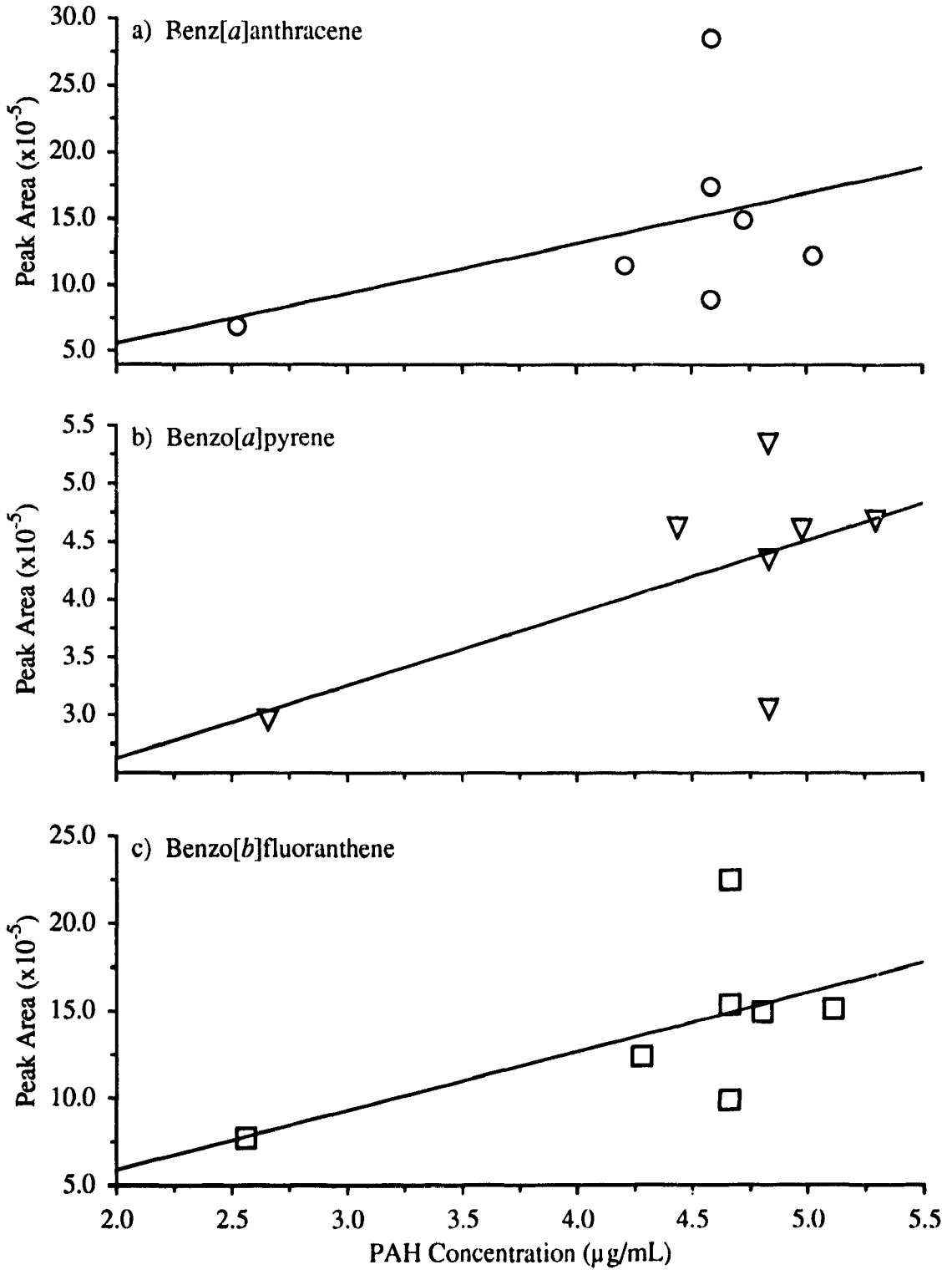

Figure V-11: External calibration curves obtained from the analysis of the SRM 1647/ DPAC-1 solutions using particle beam LC-MS.

present experiment.

PAH concentrations in the NIST coal tar, calculated from the linear regression data, are listed in Table V-1 and compared to those values reported by NIST. The precision in the determinations (triplicate injections of the DPAC-1 spiked coal tar solution) are similar to those reported above for the third standard solution: %RSD between 22 and 92%. The accuracy of the results (expressed as a percent error from the NIST value) range from -30 to -55%, and are clearly unacceptable in all cases. The extremely poor precision obtained during these analyses is the main reason for the low accuracy, although the complexity of the coal tar mixture makes it highly probable that errors due to the matrix effect may also be occurring.

To obtain the most accurate results from mass spectrometric measurements, it is often necessary to employ some form of internal standardization. This may be obtained through the use of some closely related compound of behaviour similar to that of the analyte of interest. However, in the chromatographic-mass spectrometric analysis of PAC in complex mixtures, it is useful to employ internal standards compounds that meet the following criteria: they are closely related chemically to a range of the analytes of interest, readily distinguishable from those analytes, completely absent in the sample and may be added to the sample in approximately the same concentrations as those of the target analytes. These conditions can be met, in mass spectrometric analysis, only by using isotopically labelled analogues of the compounds of interest.

A significant improvement in the precision of analysis was achieved by

Table V-1: Particle beam quantitation results for the NIST coal tar SRM 1597 using external calibration.

Compound	Certified Results* (μg/g)	Calculated Results (μg/g)	Stand. Dev. (n=3)	%RSD (n=3)	Relative Error (%)
Naphthalene	1160				
Acenaphthylene	250				
Acenaphthene					
Fluorene	140				
Phenanthrene	462				
Anthracene	101				
Fluoranthene	322	148	136	92	-54
Pyrene	235	117	37	32	-50
Benz[*a*]anthracene	98.6	53.0	12	22	-46
Chrysene	71.7	34.9	8.0	24	-51
Benzo[*b*]fluoranthene	66	43	12	29	-35
Benzo[*k*]fluoranthene	43	20	7.5	38	-55
Benzo[*a*]pyrene	95.8	67.4	23	35	-30
Benzo[*ghi*]perylene	53.7				
Dibenz[*a,h*]anthracene					
Indeno[123-*cd*]pyrene	60.2				

* Reference 172.

using the ratio of the analyte to internal standard peak areas. A plot of these ratios versus the measured SRM 1647/DPAC-1 volume ratio for three PAH are shown as Figure V-12. All seven PAH that were detected in these analyses produced linear curves similar to those of Figure V-12. The precision of the peak area ratios measured for the third standard (% RSD, triplicate injections) varied between 0.57 and 23%, a significant improvement over the external calibration precision. Negative y-intercepts, such as those observed in Figure V-12, are usually interpreted in terms of irreversible losses of analyte on the column or other components along the chromatographic train, or in the mass spectrometer ion source.[173] In this instance, analyte losses are known to occur in the particle beam interface.

PAH concentrations in the NIST coal tar, calculated using the internal standards, are listed in Table V-2. Except for fluoranthene and chrysene, the accuracy of the calculated concentrations are within acceptable limits. The matrix effect (i.e., the unexpected coelution of matrix constituents with either the internal standard or the native compound) is the most probable reason for the large error obtained for fluoranthene and chrysene. This was confirmed after a close examination of a full scan analysis of the coal tar solution. Another mass 202 isomer appeared to be coeluting with fluoranthene since the front base of its chromatographic peak was slightly broadened. The coal tar certificate of analysis does indicate the presence of a third isomer, acephenanthrylene, at a concentration of approximately 60 μg/g. The inclusion of the signal from this isomer into the measured peak area of fluoranthene as well as the probable transmission enhancement from the matrix effect would then account for the high calculated concentration.

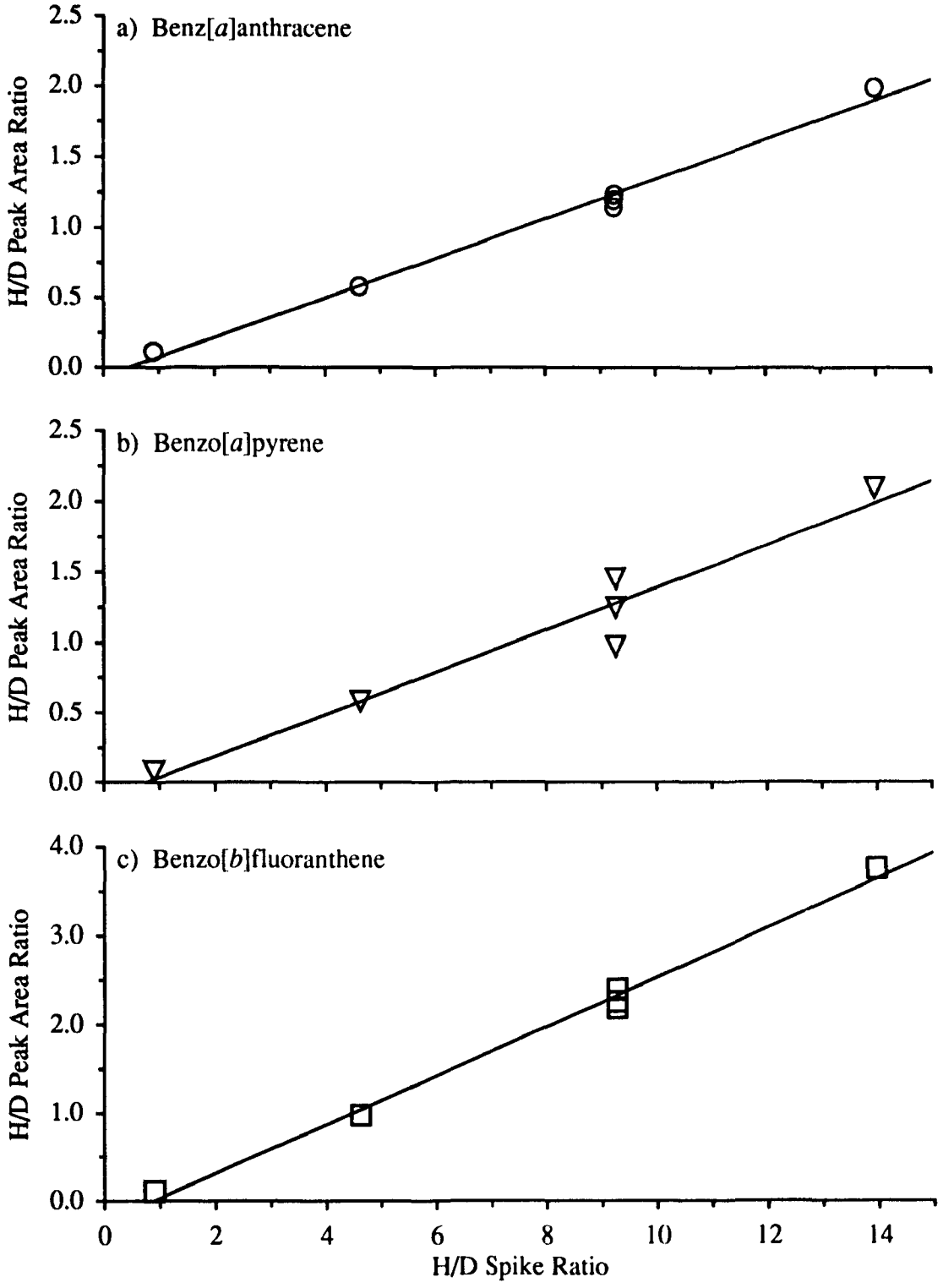

Figure V-12: Plots of the proteo-/deutero-PAH peak areas vs the SRM 1647/DPAC-1 volume ratios using particle beam LC-MS.

Table V-2: Particle beam quantitation results for the NIST coal tar SRM 1597 using internal standardization with perdeutero-PAH.

Compound	Certified Results* (μg/g)	Calculated Results (μg/g)	Stand. Dev. (n=3)	%RSD (n=3)	Relative Error (%)
Naphthalene	1160				
Acenaphthylene	250				
Acenaphthene					
Fluorene	140				
Phenanthrene	462				
Anthracene	101				
Fluoranthene	322	338	45	13	4.9
Pyrene	235	238	25	11	1.2
Benz[*a*]anthracene	98.6	97.2	2.3	2.4	-1.4
Chrysene	71.7	59.6	0.91	1.5	-17
Benzo[*b*]fluoranthene	66	64	1.3	2.1	-2.5
Benzo[*k*]fluoranthene†	43	41	2.3	5	-3.9
Benzo[*a*]pyrene	95.8	94.7	4.4	4.7	-1.2
Benzo[*ghi*]perylene	53.7				
Dibenz[*a,h*]anthracene					
Indeno[123-*cd*]pyrene	60.2				

* Reference 172.

† Perdeutero-benzo[*b*]fluoranthene used as internal standard.

The low concentration calculated for chrysene appears to be a result of coeluting matrix components with its perdeuterated internal standard. A full scan analysis revealed the presence of a coeluting mass 216 PAH (either a benzofluorene or a methylpyrene isomer) and a partially coeluting mass 226 PAH (probably cyclopenta[*cd*]pyrene). The chromatographic peaks of the remaining quantified PAH were also thoroughly examined, and except for perdeutero-benzo[*b*]fluoranthene, they all appeared free from unexpected coeluting substances. The perdeutero-benzo[*b*]fluoranthene peak was not completely resolved from another mass 252 PAH isomer (probably perylene), but this does not appear to affect the calculated result in Table V-2.

VI. THE HEATED PNEUMATIC NEBULIZER INTERFACE

The fundamental problem of coupling LC to MS is the inability of a regular mass spectrometer vacuum system to pump the full solvent vapour of the evaporated effluent. The moving belt and the particle beam interfaces have cleared this hurdle (to varying degrees) by removing the mobile phase from the analyte prior to entering the high vacuum ion source. The use of an atmospheric pressure ion (API) source (i.e., no vacuum at all in the source) avoids this problem altogether. At first it may appear impractical to couple ionization conducted at atmospheric pressure with mass analysis and detection carried out under high vacuum. In certain circumstances, however, there are distinct advantages to decoupling the sample inlet from the high vacuum that is necessary for reliable mass analysis. For example, this situation readily allows the coupling of numerous separation techniques, including LC, SFC, capillary electrophoresis , and ion chromatography, to MS.[174]

Figure VI-1 shows the basic components of the SCIEX heated nebulizer LC-MS interface and atmospheric pressure chemical ionization (APCI) source. The LC effluent flows through narrow bore stainless steel tubing where it is subsequently nebulized into a fine mist by a concentric jet of air or nitrogen. The micron sized droplets are swept by a make-up gas through a quartz tube heater where the mobile phase is rapidly evaporated via interactions with the heated gas (usually between 125 and 200°C), leaving extremely small particles each containing only a few analyte molecules. The vapour pressure of such small particles can be many times larger than that of the bulk material, permitting vaporization of analytes that have low volatilities or are

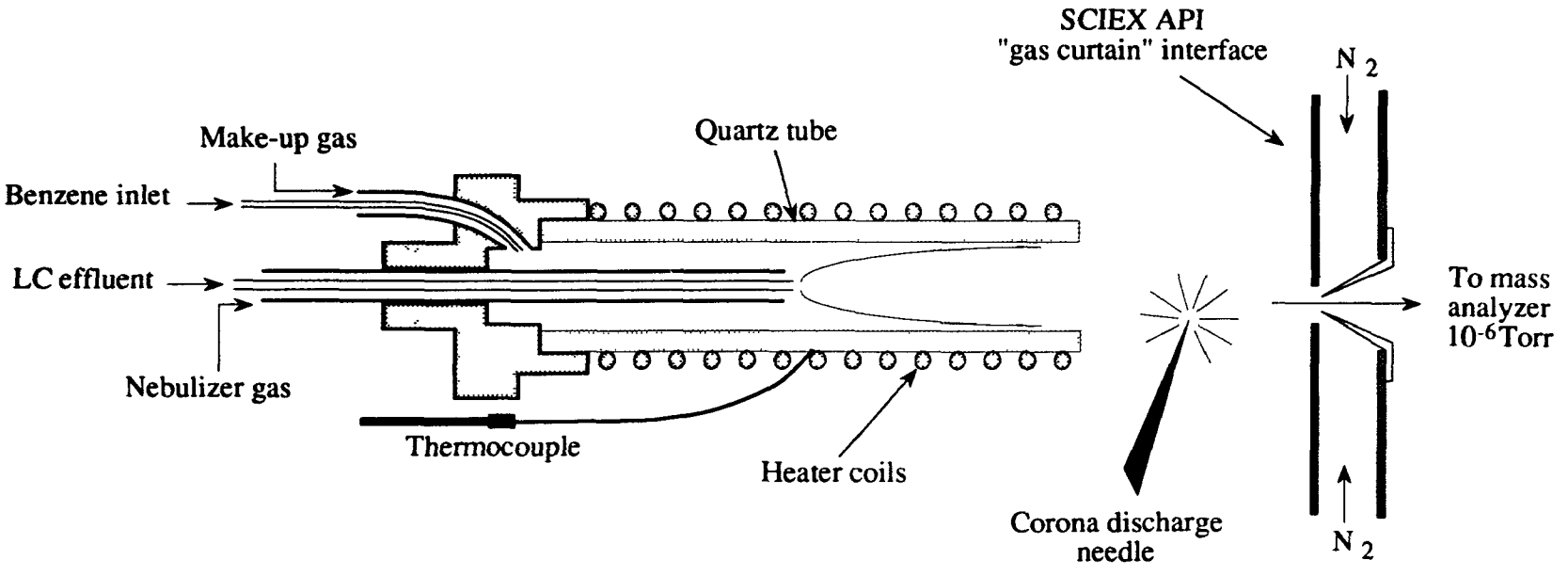

Figure VI-1: A schematic diagram of the heated nebulizer interface.

thermally labile. The heated gas and analyte mixture flows from the quartz tube into the reaction region of the API source, where the sample undergoes atmospheric pressure chemical ionization initiated by a corona discharge needle. The details of this ionization process will be discussed in subsequent paragraphs, but in general, the vaporized mobile phase used in the LC separation acts as a reagent gas, usually producing MH^+ product ions in the positive mode. These ions are focused and accelerated through a dry nitrogen curtain gas and a 100 μm orifice into the high vacuum analyzer region of the mass spectrometer, where they are mass analyzed. The gas curtain prevents any solvent, non-ionized sample or buffer from entering the analyzer region and thus maintains the vacuum system, lenses and quadrupole rods free from contamination. Clustered solvent molecules are also stripped from the ions as they pass through the gas curtain and the atmosphere-to-vacuum sampling orifice.

The pneumatic spray of the interface produces a steady pattern that is not prone to fluctuations, so that performance is stable and reproducible. Control of the nebulizer temperature is not critical because a wide variety of analytes can be vaporized under the same conditions. This interface takes full advantage of the large gas and solvent vapour throughput tolerated by the API source and provides routine operation using LC flow rates up to 2 mL/min with reversed-phase effluents. It can also tolerate volatile salts, acids, bases, and other additives that may be necessary for the chromatographic separation. The large amounts of solvent and sample that are constantly sprayed into the source are drawn out of the chamber to either a condenser or a fume hood by an air pump.

Atmospheric pressure chemical ionization relies on a source of ionizing electrons (in this case, a corona discharge) that produces ions from nearby gases. These ions readily undergo ion-molecule reactions with air and other gaseous molecules because of the short mean-free path between molecules at atmospheric pressure. In positive ion APCI, major primary ions (e.g., N_2^+, O_2^+, H_2O^+ and NO^+) are formed by the electron impact of corona-created electrons on the major neutral components in air. These highly reactive species trigger a complex reaction sequence, illustrated in Figure VI-2, that culminates in the formation of an equilibrium set of hydrated protons. Trace compounds can interact with these reactant ions in at least two different ways: charge-transfer, where the positive charge on the reactant ion is transferred to the analyte; and proton-transfer, where a proton is transferred from the reactant ion to the analyte. The latter process involves the proton hydrates as reactant ions:

$$H_3O^+(H_2O)_n + M \rightarrow MH^+(H_2O)_m + (n\text{-}m\text{+}1)H_2O$$

The water molecules clustered to the analyte are stripped off in the declustering region of the API source described above, prior to mass analysis. The governing factor for this ionization process is that the proton affinity of the analyte be greater than that of water, which is true for most organic compounds containing oxygen, sulphur or nitrogen.[175]

The proton hydrates have recombination energies (a measure of the ability to transfer positive charge) that are lower than most organic compounds and, as a result, they will not charge-transfer to these compounds.

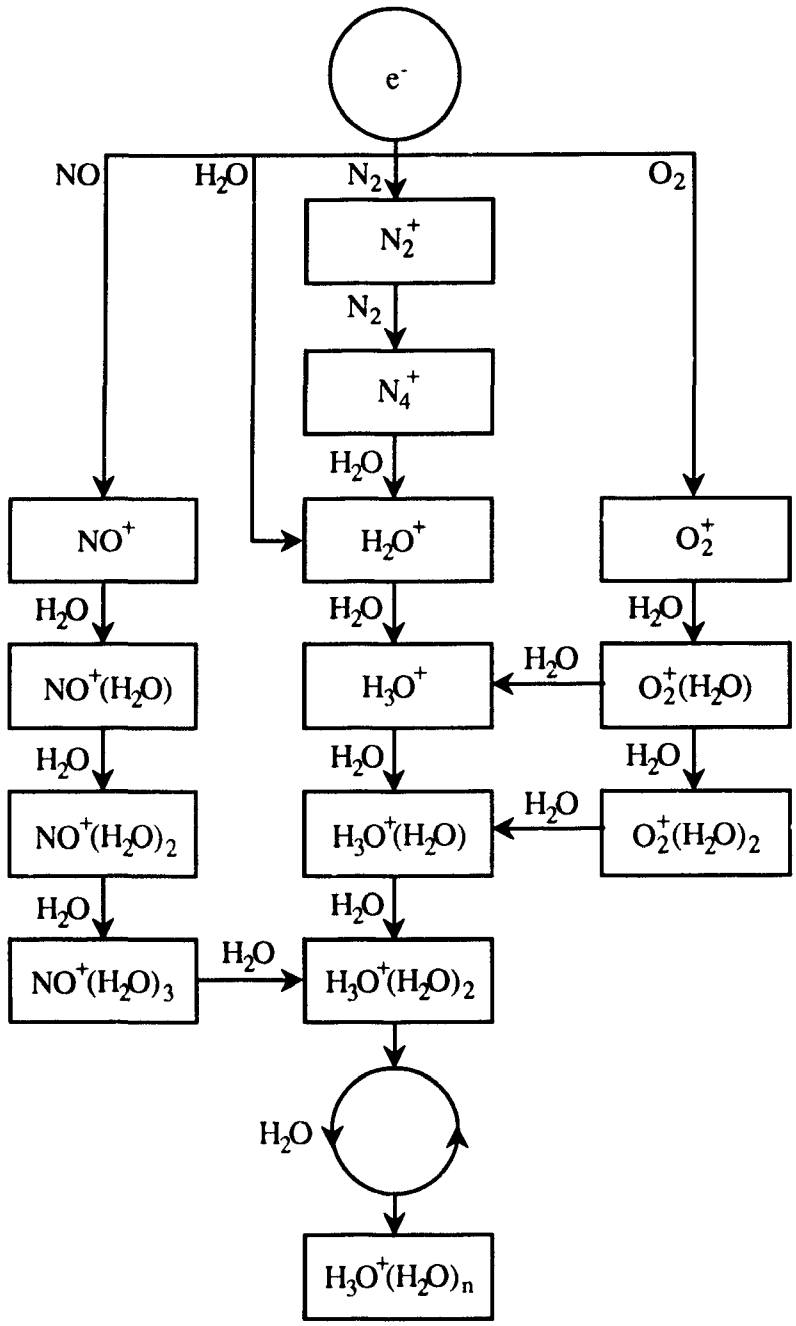

Figure VI-2: Atmospheric pressure chemical ionization reagent ion formation in ambient air.

The reactant ions for charge-transfer are mainly O_2^+, its hydrates and N_2^+, H_2O^+, and NO^+ to a lesser degree. Since these ions react rapidly with water vapour to form the proton hydrates, the sensitivity of APCI under ambient conditions will be much less for charge-transfer than proton-transfer.

Some of the earliest reports on the development of on-line LC-MS techniques, published by Horning *et al.* in 1974,[89,176,177] were based on the use of APCI. In 1975, they applied this new technique to the detection of several PAH standards separated with an isooctane mobile phase.[89] They observed that the PAH were bases in the gas phase and that proton-transfer reactions from the isooctane solvent produced predominant MH^+ ions. The LC performance was, however, very poor and the LC-MS detection limits were therefore not very impressive (0.5 ng for S/N of 2:1). Increases in signal-to-noise ratios were proposed through the use of improved chromatographic separations which would produce much narrower LC peaks.

Following the early introduction of this technique, general interest in API was limited because the traditional manufacturers of analytical mass spectrometers did not offer an API source. In the late 1970's and early 80's, one manufacturer (Sciex, Thornhill, Ontario) produced an API source attached to a quadrupole mass spectrometer. Air quality monitoring was one of the first applications and the original purpose of this instrument, which could be mounted in a van and used for on-site, real-time analyses of combustion related materials including gaseous PAH.[119,135,137,175,178] Instead of relying on only proton-transfer reactions from hydrated protons (produced from the moisture in the air), the source ion-molecule chemistry was altered by adding additional reagents to the inlet air stream. For example, when

benzene was added, the source chemistry was dominated by charge-transfer reactions, and proton-transfer was greatly suppressed simply because the added benzene ions replaced the protonated water species.[175] Under these conditions, trace compounds that have ionization energies lower than that of benzene (e.g., PAH) will pick up a charge from benzene and will be seen as the ionized molecular ion ($M^{+\cdot}$). Although all the PAH standards produced dominant molecular ions,[175] the tendency to abstract a proton was not totally suppressed because of the rather high proton affinities of the PAH. Consequently, two ions were usually seen: M^+ and MH^+.

It wasn't until 1983, nine years after the original report of on-line LC-MS using APCI,[89,176,177] that the heated nebulizer probe was developed by Sciex. Many published applications, and the subsequent introduction of the Sciex API III triple-quadrupole LC-MS/MS instrument, have propelled APCI from its early and humble beginnings into a rapidly growing LC-MS technique (it is now offered by all the major MS instrument manufacturers). The remainder of this chapter is devoted to the evaluation of this "new" LC-MS technology for the analysis of complex mixtures of PAC with an emphasis on the detection of high molecular weight components that are not amenable to common GC techniques.

VI.1 Reversed-Phase LC Coupled to the Heated Nebulizer Interface

The background noise produced in positive ion APCI is usually very

high, especially at low mass (e.g., below 250), because of a large proportion of ionized solvent and their clusters that can enter the MS; background subtraction is usually necessary to obtain clean mass spectra. Figure VI-3 illustrates the background subtracted positive-ion APCI mass spectra acquired from a mixture of PAH standards separated on a reversed-phase column using a water/acetonitrile gradient. Except for naphthalene, all the standards produced both $M^{+\cdot}$ and MH^+ ions. Though the proton affinity of naphthalene (196.3 kcal/mol) is greater than that of water (approximately 167 kcal/mol), it does not undergo proton-transfer ionization. The relative intensities of the MH^+ ions for the remaining PAH increase with molecular weight; this reflects the increase in proton affinity with increasing PAH size (or mass).[157] For example, the proton affinities for pyrene and perylene are 208.5 and 213.0 kcal/mol, respectively.

The ionization energies of PAH, which will directly influence the intensity of the $M^{+\cdot}$ ions produced by charge-transfer reactions, decrease with increasing PAH size.[157] The mass spectra of Figure VI-3, however, demonstrate that the proton affinity becomes the predominant factor in determining the M^+ to MH^+ ratio as the PAH increase in size. Correlations between the physical properties of PAH and $M^{+\cdot}/MH^+$ ion ratios have been reported as a means of distinguishing isomers using both chemical ionization[126] and fast-atom bombardment.[128] The rationale for this technique is that proton affinity and ionization energy are functions of molecular structure. Isomer discrimination by EI-MS (e.g., with the moving belt or particle beam interface) has been limited because the mass spectra of PAH isomers are almost identical. The $M^{+\cdot}/MH^+$ ion ratios produced by

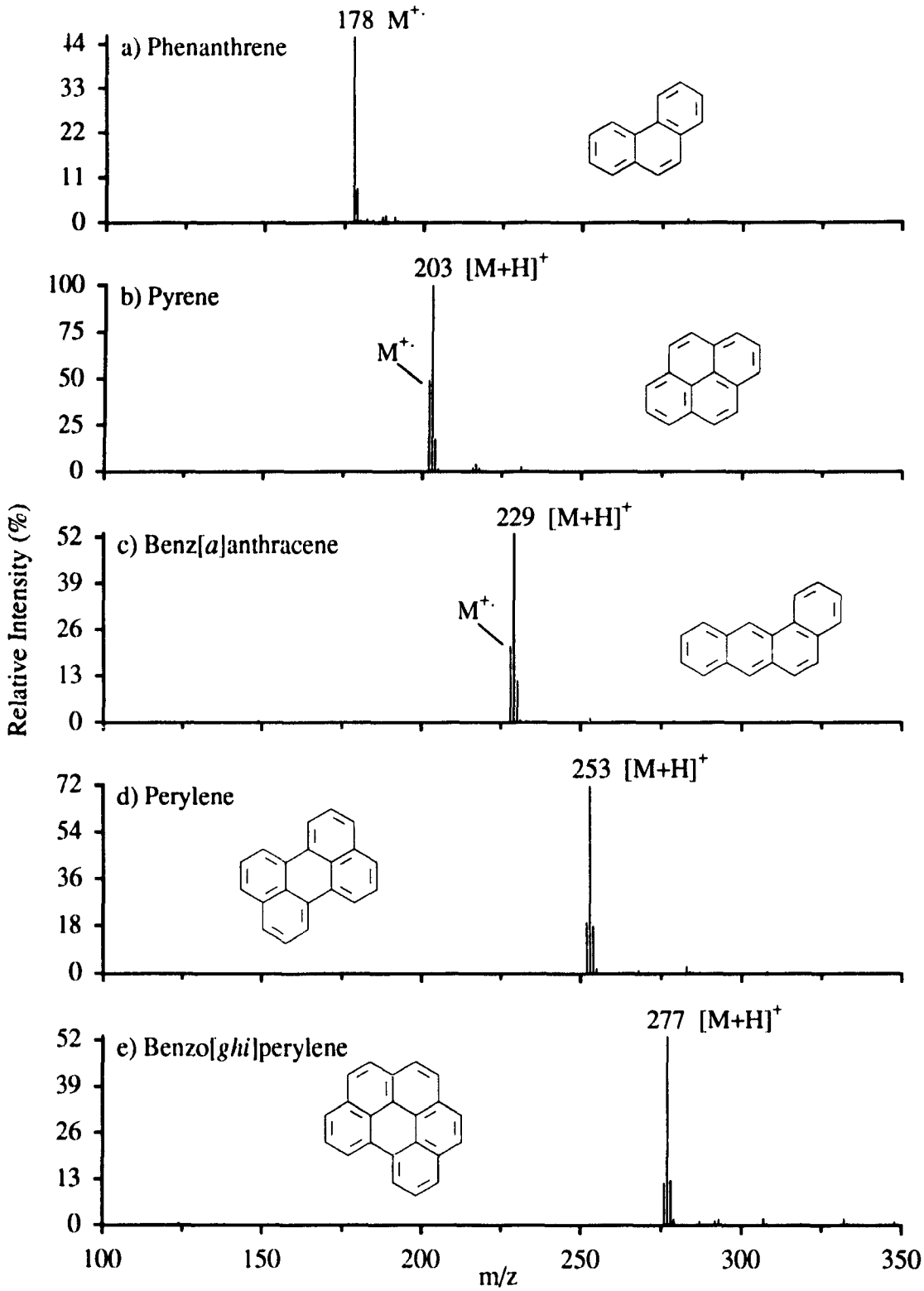

Figure VI-3: Background subtracted positive ion APCI mass spectra of PAH standards.

APCI may be used to discriminate between PAH isomers provided they have sufficiently different proton affinities or ionization energies (which is true for most PAH). However, the application of this technique may be limited since the $M^{+\cdot}/MH^+$ ratios are also dependant on the experimental conditions. For example, the mobile phase composition (which affects the APCI reagent ion composition), source temperature, and the intensity of declustering reactions occurring in the orifice region will all affect the $M^{+\cdot}/MH^+$ ratios. Further discussion and examples of this isomer discrimination technique will be provided in subsequent sections of this chapter.

The background subtracted APCI mass spectra of several heterocyclic and substituted PAC are shown as Figure VI-4. Most organic compounds containing oxygen, sulphur or nitrogen have proton affinities greater than that of water, but the oxygen and sulphur heterocyclic PAC produced ions from charge-transfer reactions only. This situation is similar to that encountered previously with naphthalene (Figure VI-3a). The effective proton affinities of these compounds must not be high enough for proton-transfer to be thermodynamically favourable. Unfortunately, the alternative charge-transfer ionization mechanism is inherently less sensitive and this is reflected in the poor signal-to-noise ratios obtained for these compounds.

The nitrogen heterocyclic PAC, carbazole and quinoline, both produced predominant MH^+ ions (Figures VI-4b and c), although carbazole also produced a much less intense $M^{+\cdot}$ peak at m/z 167. Again, these differences are related to proton affinities; carbazole, which is not very basic ($pK_b \approx 14$), has a much lower proton affinity ($\approx$ 215 kcal/mol) than the slightly basic quinoline (227.6 kcal/mol, $pK_b = 9.1$). All of the remaining substituted PAC

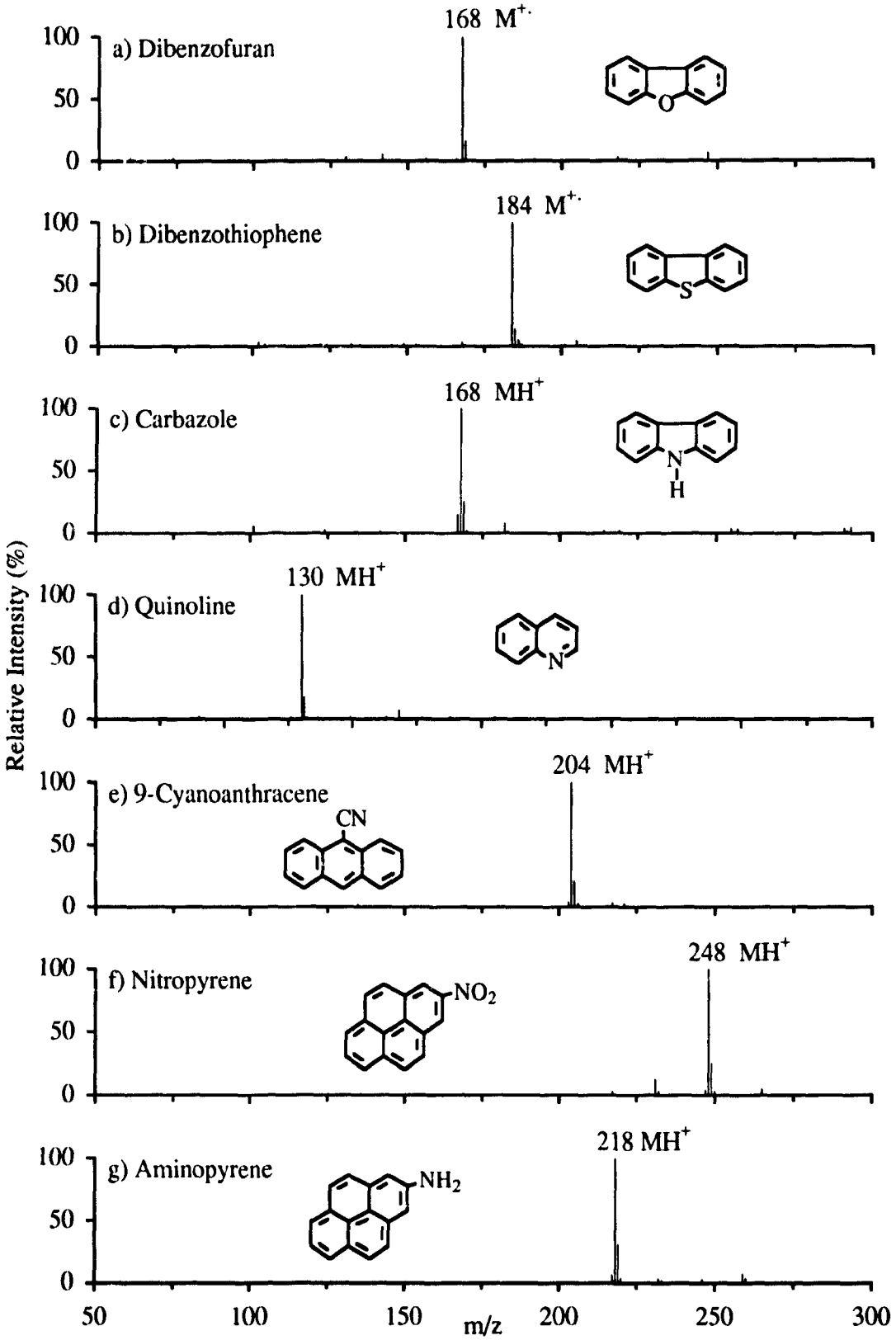

Figure VI-4: Background subtracted positive ion APCI mass spectra of PAC standards.

also produced predominant MH^+ ions (Figures VI-4d to f). Changes in the source conditions (i.e., using a 100% acetonitrile mobile phase in a dry source) could, however, force the cyano and nitro derivatives to produce intense $M^{+\cdot}$ ions. The proton affinities of these two compounds are not much different from their underivatized parent PAH, although the polar substituent does increase it slightly (unlike the amino group that greatly increases the basicity of the compound). Therefore, these compounds are subject to the same requirement of having higher effective proton affinities than the source reagent ions. In general, the $M^{+\cdot}/MH^+$ ratio of substituted PAC will be related to both the proton affinity and ionization energy of the unsubstituted parent PAH and the influence of the substituent on these quantities. This could lead to difficulties in the identification of unknown compounds since it might not be known whether the compound has produced an $M^{+\cdot}$ or an MH^+ ion.

The calibration curves obtained for three PAH standards, monitoring both the $M^{+\cdot}$ and MH^+ ions, are shown in Figures VI-5 and 6, respectively. Deviations from non-linearity, at high concentrations only, were observed for both of the benz[*a*]anthracene ions monitored (Figures VI-5a and 6a). The insets (on the left) of Figures VI-5 and 6 illustrate that the curves were linear extending down to the low-level concentrations. The demonstrated dynamic range and the ranges commonly reported in the literature[179,180] are at most three decades (10^3). This is much narrower than those that can be commonly achieved with the moving belt or particle beam interfaces. There are several possible explanations for these narrow ranges including the reduction of the working range of the detector by the high background noise associated with APCI. It is also conceivable that a rapid depletion of reagent ions occurs when

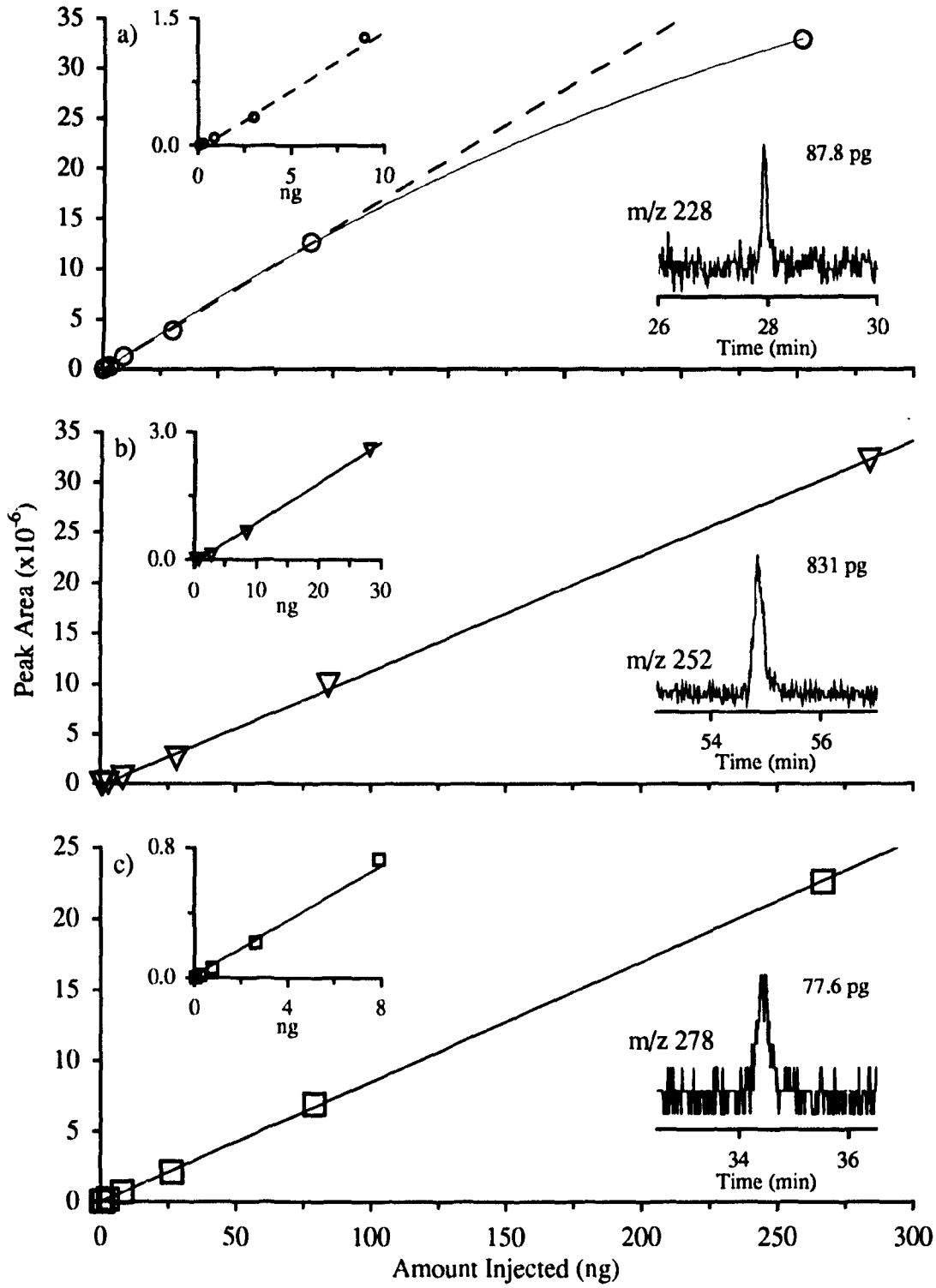

Figure VI-5: Heated nebulizer LC-MS calibration curves obtained for (a) benz[*a*]-anthracene, (b) benzo[*a*]pyrene and (c) dibenz[*a,h*]anthracene monitoring molecular ions. Left insets show an expansion of the low ng region. Right insets show the low level LC-MS responses obtained for each standard.

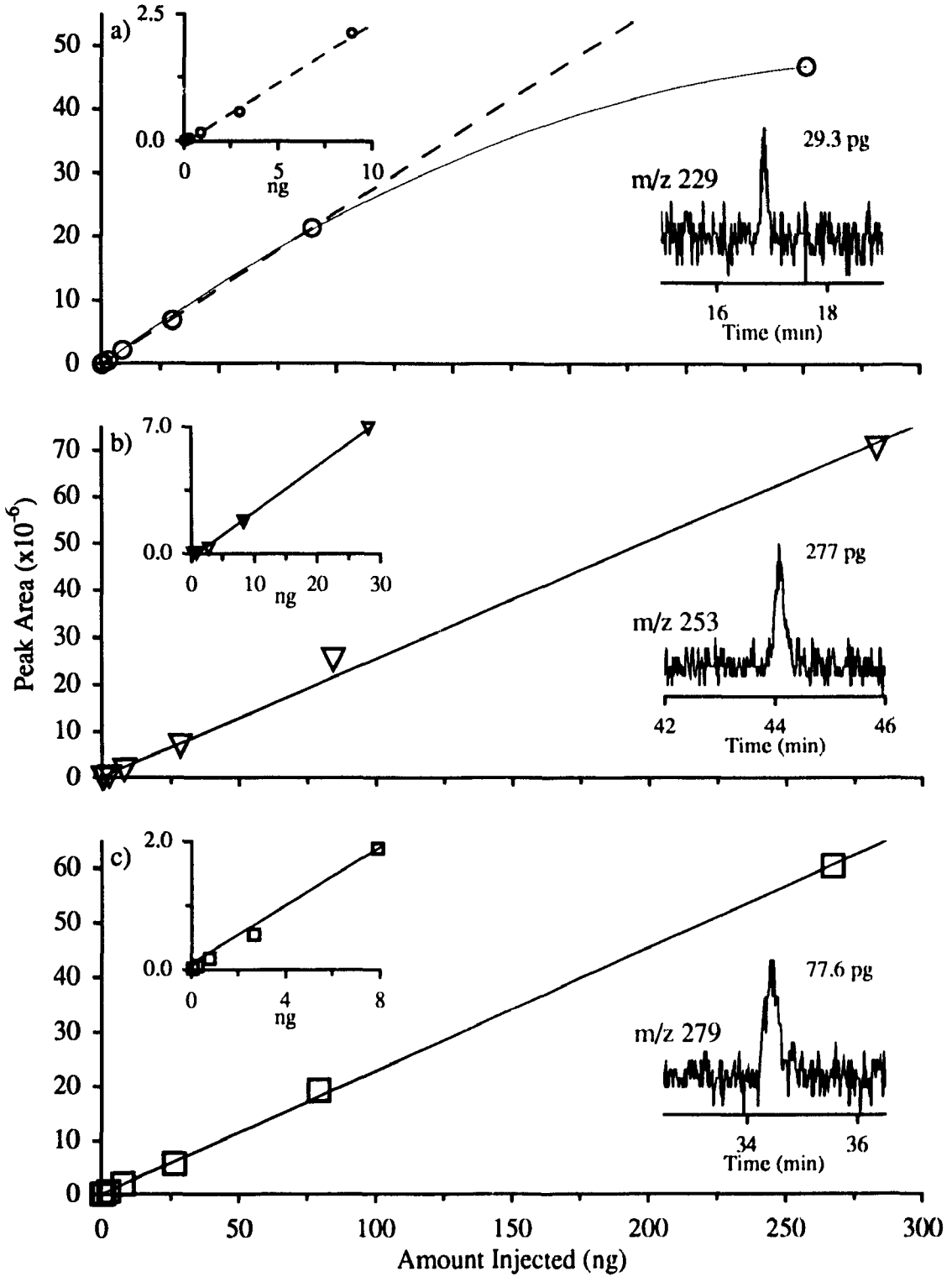

Figure VI-6: Heated nebulizer LC-MS calibration curves obtained for (a) benz[*a*]-anthracene, (b) benzo[*a*]pyrene and (c) dibenz[*a,h*]anthracene monitoring protonated molecules. Left insets show an expansion of the low ng region. Right insets show the low level LC-MS responses for each standard.

large amounts of analyte are present. It is most likely, however, that the pulse-counting detection system employed in the Sciex API III instrument is the limiting factor. Pulse counting is utilized in order to detect very low count rates; it will essentially allow the detection of a single ion event at the channel electron multiplier. However, the ion-counting circuitry can saturate and exhibit pulse pile-up phenomenon at higher count rates. This was observed to occur in the present experiment when injections of 900 ng resulted in a temporary cessation of the analyte ion current.

The low level responses for the three PAH standards, monitoring both the $M^{+\cdot}$ and MH^{+} ions, are shown in the second insets of Figure VI-5 and 6, respectively. The signal-to-noise ratios for these chromatograms varied between 2:1 and 7:1; extrapolation to 3:1 ratios produced the following approximate detection limits:

Compound	$M^{+\cdot}$ Detection Limit (pg)	MH^{+} Detection Limit (pg)
Benz[*a*]anthracene	88	44
Benzo[*a*]pyrene	356	275
Dibenz[*a,h*]anthracene	93	85

These detection limits were comparable to those of the belt interface (≈ 25 pg) and considerably better than those of the particle beam interface (between 1 and 4 ng). The variation in the values listed in the table above probably arise from the differences in the physical properties of the individual compounds. The proton affinities of the three standards could not be found in the literature, but based on the results listed above, the proton affinity of

benzo[*a*]pyrene must be lower than those of either benz[a]anthracene or dibenz[*a*,*h*]anthracene (the ionization energies of the three standards are similar). Since proton affinities increase and ionization energies decrease with increasing PAH size, this method of detection should be well suited for the detection of high molecular weight PAH (as will be demonstrated later).

VI.1.1 Benzene Charge-Transfer Ionization

One advantage of APCI (or chemical ionization) mass spectrometry is the potential to tailor the chemistry of the reagent gas system to ionize a sample in a particular manner. The choice of reactant ions can also provide further selectivity in the types of compounds which will or will not be ionized. For example, when benzene was added to an APCI source, the positive mode ionization process was interrupted and the molecular cation of benzene ($C_6H_6^{+\cdot}$) was the dominant reactant ion.[175] Trace compounds that have ionization energies lower than that of benzene (9.25 eV) will pick up a charge from the reagent cation (i.e., charge-transfer); those compounds that have ionization energies above that of benzene will not be seen. A previous APCI/MS study of gas-phase PAH with benzene charge-transfer conditions produced mass spectra that were dominated by molecular cations, but because of the rather high proton affinities of the PAH, the tendency to abstract a proton was not totally suppressed.[175]

The effect of adding increasing amounts of benzene to the ion source

on the mass spectra of three PAH standards is shown in Figures VI-7 to VI-9. The benzene was introduced into the source using a slight modification of the Sciex heated nebulizer (Figure VI-1); a capillary tube was fed through the make-up gas inlet line directly to the heated region of the interface. As the benzene is pumped into the interface it is instantly vaporized and carried by the coaxial make-up gas flow into the corona discharge plasma. Benz[a]anthracene produced a predominant MH^+ ion under normal source conditions (Figure VI-7a), although the $M^{+\cdot}$ ion had a relative intensity of approximately 50%. When a small amount of benzene was added to the source (5μL/min, Figure VI-7b) the $M^{+\cdot}$ ion became the most intense peak (since the ionization energy of benz[a]anthracene, 7.46 eV, is considerably lower than that of benzene). Proton-transfer ionization, however, was still very abundant because of the high proton affinity of benz[*a*]anthracene. Increasing the amount of benzene added to the source resulted in the increase of the $M^{+\cdot}$ ion intensity relative to the MH^+ ion (Figure VI-7c and d). In general, larger amounts of benzene added to the source produced a greater increase of the $M^{+\cdot}$ ion intensity relative to the MH^+ ion, but the proton-transfer chemistry could not be totally suppressed.

Similar effects were observed for the other two PAH standards (Figures VI-8 and 9); the MH^+ ion was dominant under normal source conditions while adding benzene to the source increased the relative intensity of the $M^{+\cdot}$ ion. Although the ionization energies of both benzo[*a*]pyrene and dibenz[*a,h*]anthracene (7.17 and 7.38 eV, respectively) are lower than that of benz[*a*]anthracene (since ionization energies decrease with increasing PAH size), the $M^{+\cdot}$ ion becomes the most intense peak only after the addition of

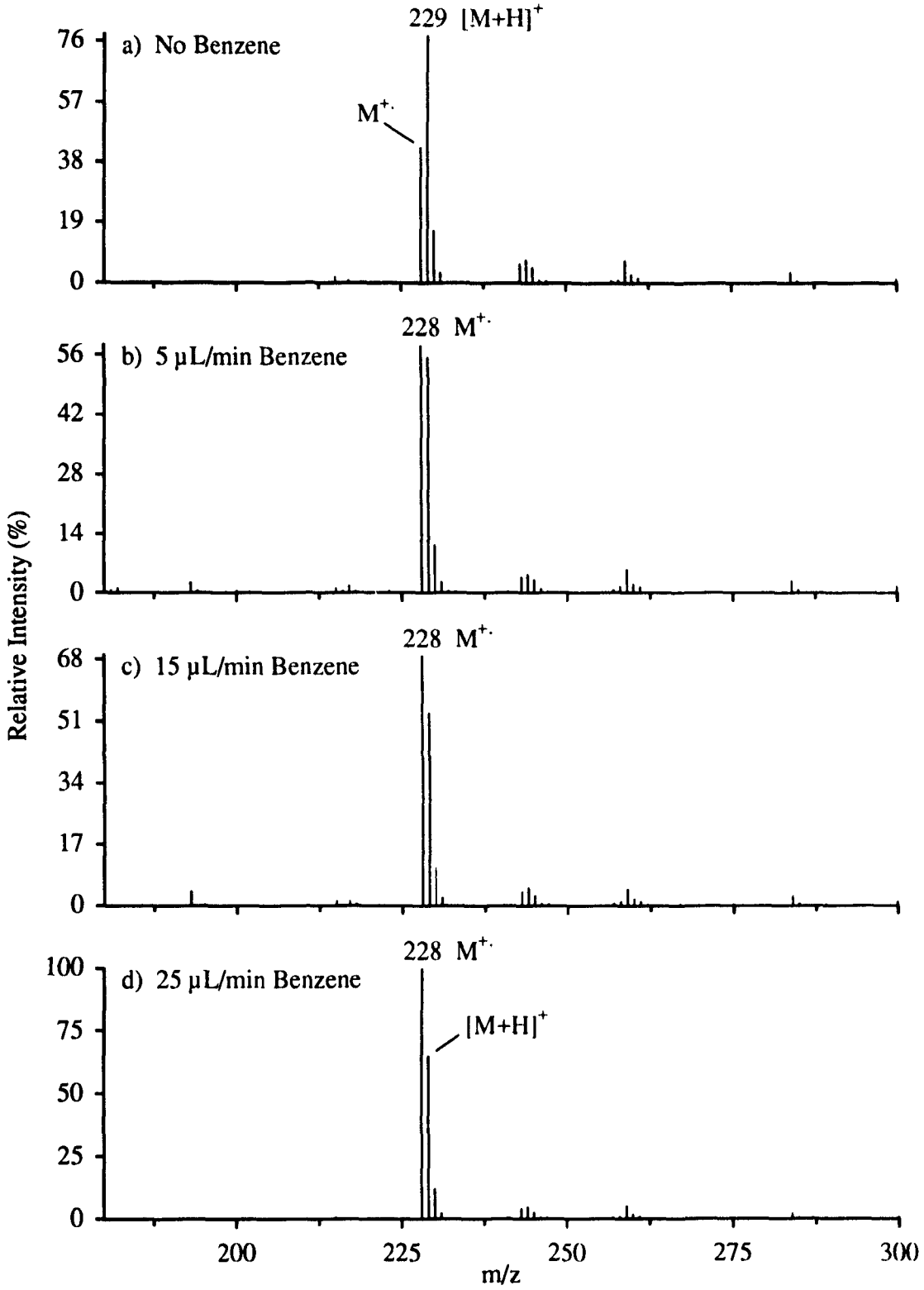

Figure VI-7: Background subtracted benzene charge-transfer APCI mass spectra of benz[*a*]anthracene using the heated nebulizer interface with increasing amounts of benzene added to the source.

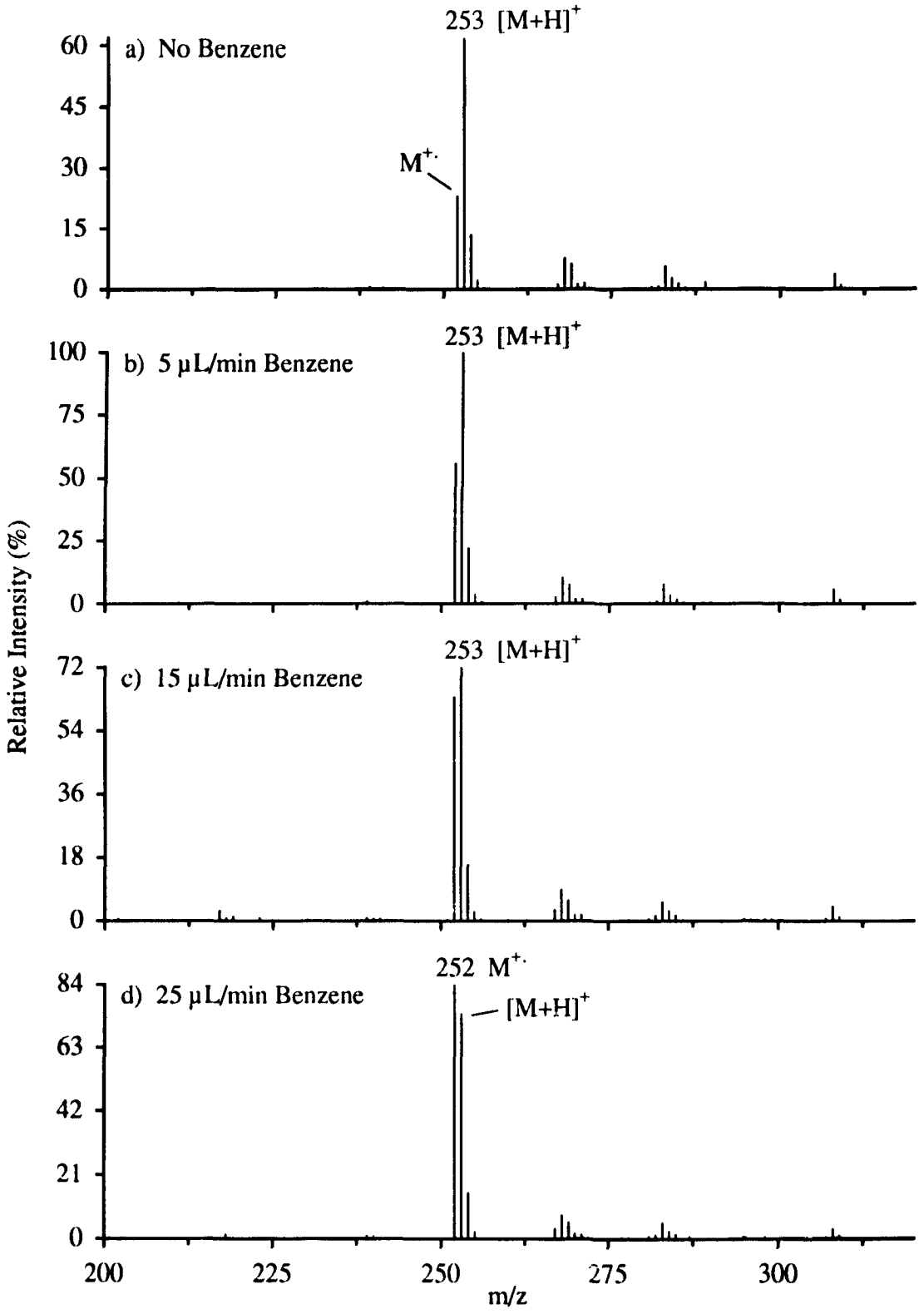

Figure VI-8: Background subtracted benzene charge-transfer APCI mass spectra of benzo[*a*]pyrene using the heated nebulizer interface with increasing amounts of benzene added to the source.

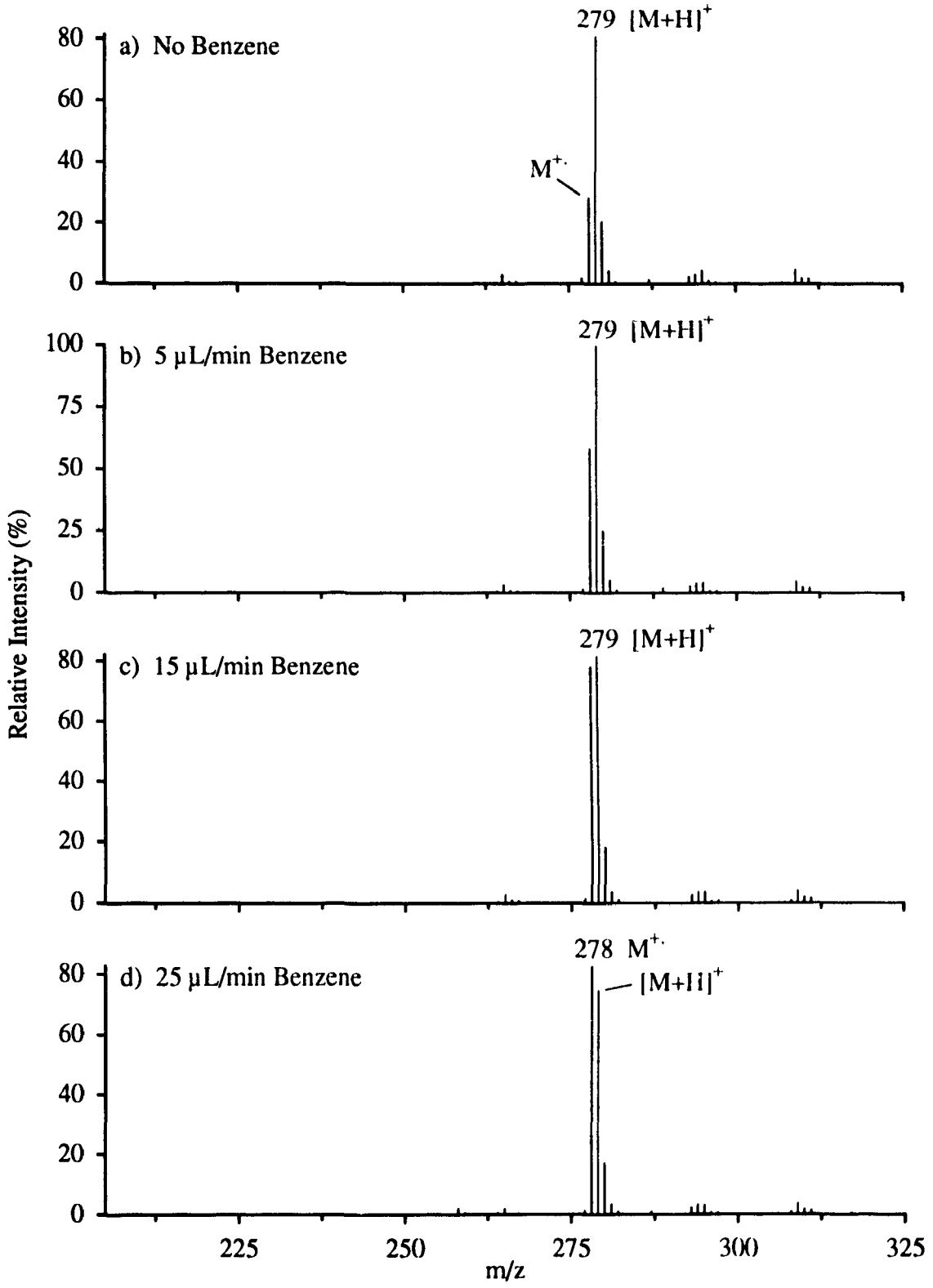

Figure VI-9: Background subtracted benzene charge-transfer APCI mass spectra of dibenz[*a*,*h*]anthracene using the heated nebulizer interface with increasing amounts of benzene added to the source.

much larger amounts of benzene (i.e., 25μL/min) to the source. Once again, this illustrates that the proton affinity of the PAH is the most dominant physical property influencing the resulting $M^{+\cdot}/MH^{+}$ ratios. Consequently, the $M^{+\cdot}/MH^{+}$ ion ratios produced under benzene charge-transfer conditions can still be used to discriminate between PAH isomers (that have different proton affinities). As mentioned earlier, experimental conditions and in particular, the amount of benzene added to the source will influence the resulting ion ratios such that care must be taken when comparing unknowns with standard compounds.

A significant limitation associated with benzene charge-transfer ionization is the subsequent increase in the background noise at low m/z ratios (e.g., below mass 250). Besides the extremely abundant $C_6H_6^{+\cdot}$ ion, intense background ions are produced from complex source reactions involving benzene, the mobile phases and ambient air. Other intense ions that have been tentatively identified include $C_6H_7^{+}$, $C_7H_7^{+}$ and $[(C_6H_6)_2]^{+\cdot}$. The intensity of these and many additional ions become much greater as the amount of benzene added to the source was increased. These background ions can be eliminated from acquired mass spectra, such as those in Figures VI-7 to VI-9, by using background subtraction routines. These routines cannot, however, eliminate the difficulties associated with the high background noise as discussed below.

The calibration curves obtained for three PAH standards under benzene charge-transfer conditions, monitoring both the $M^{+\cdot}$ and MH^{+} ions, are shown in Figures VI-10 and 11, respectively. The curves are very similar to those produced under normal source conditions (Figures VI-5 and 6);

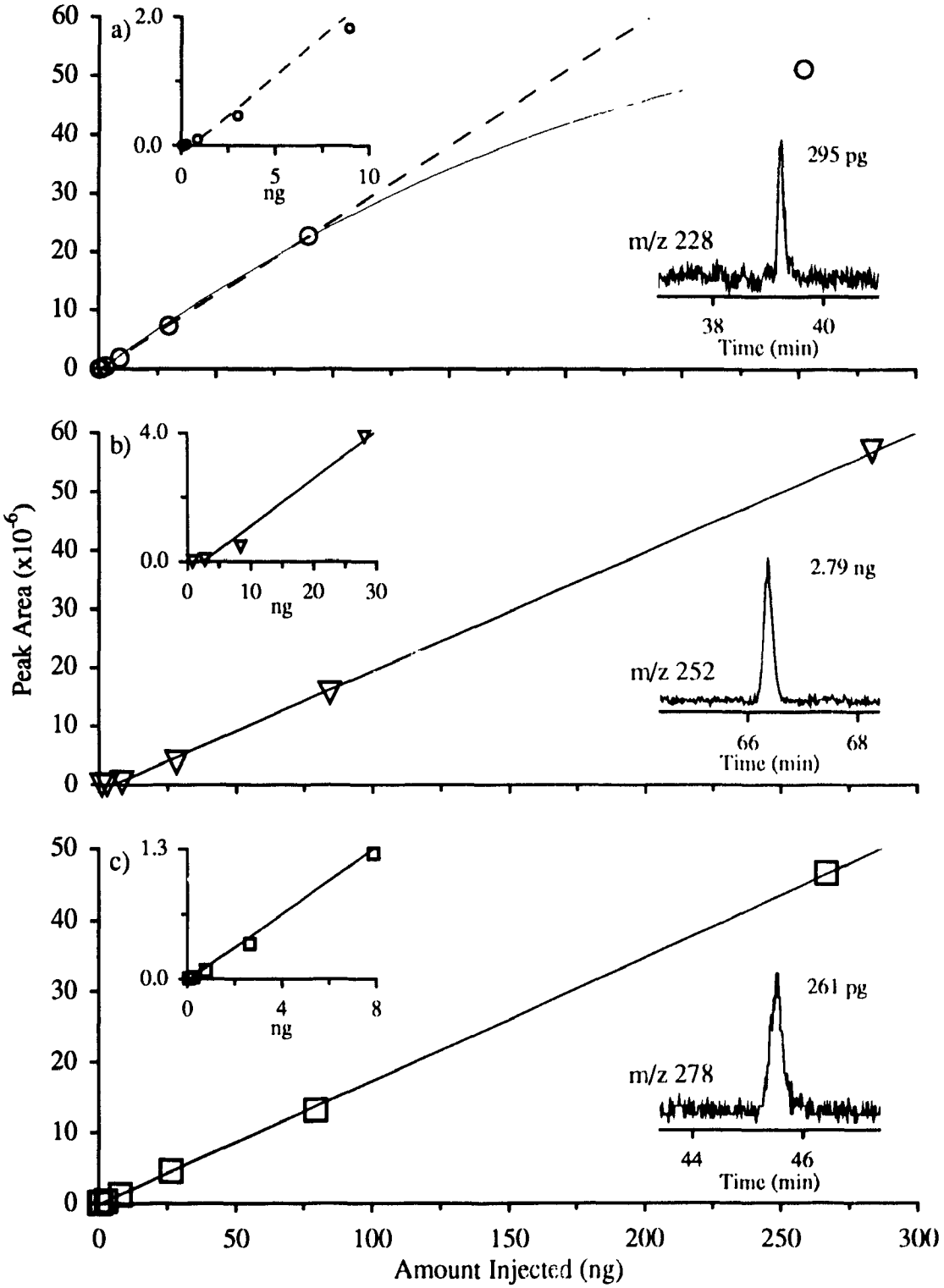

Figure VI-10: Heated nebulizer LC-MS calibration curves for (a) benz[*a*]anthracene, (b) benzo[*a*]pyrene and (c) dibenz[*a,h*]anthracene monitoring $M^{+\cdot}$ ions while adding 20 μL/min benzene to the source. Left insets show an expansion of the low ng region. Right insets show the low level LC-MS responses.

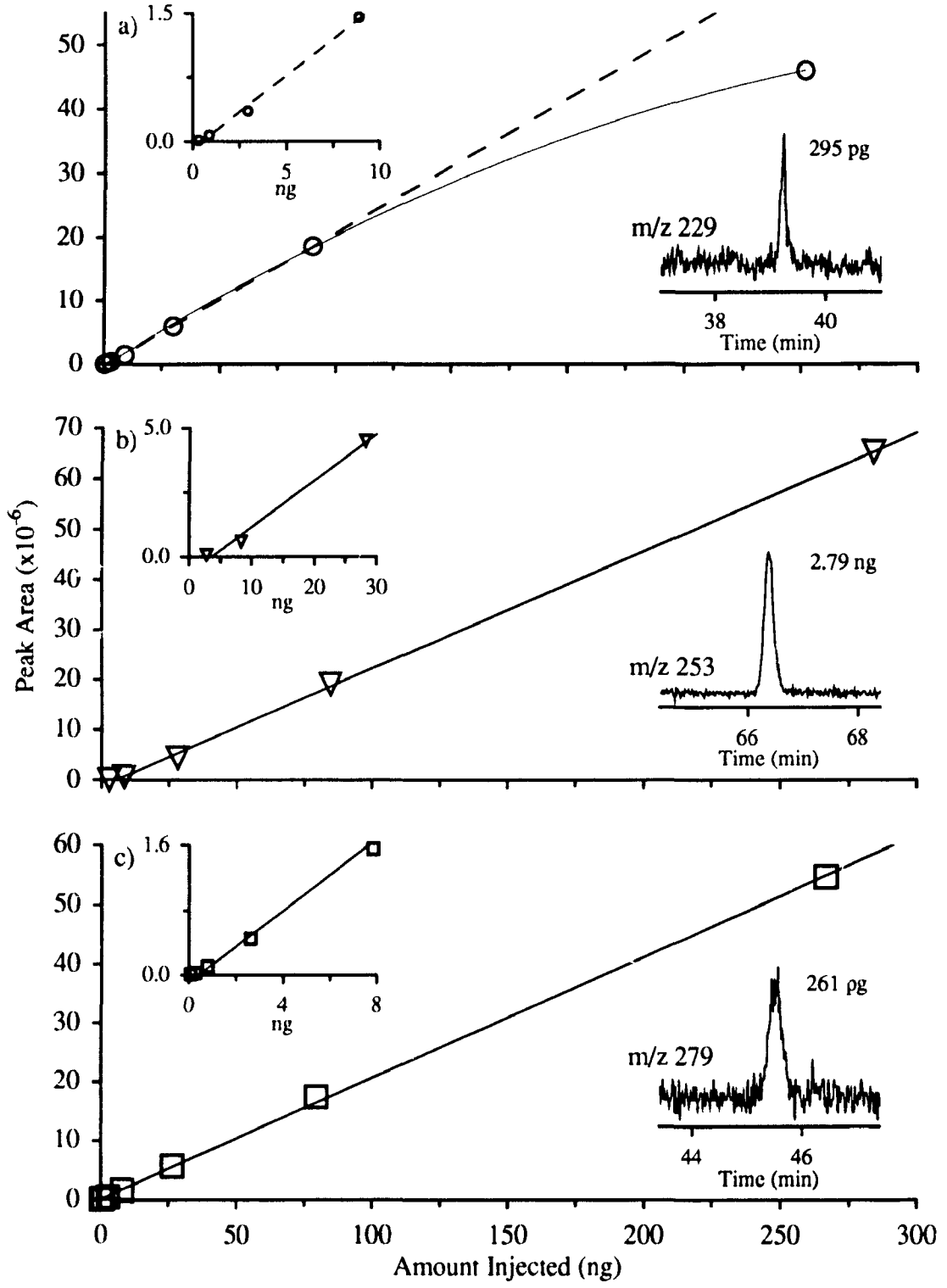

Figure VI-11: Heated nebulizer LC-MS calibration curves for (a) benz[*a*]anthracene, (b) benzo[*a*]pyrene and (c) dibenz[*a,h*]anthracene monitoring MH^+ ions while adding 20 μL/min benzene to the source. Left insets show an expansion of the low ng region. Right insets show the low level LC-MS responses.

benz[*a*]anthracene becomes non-linear above 100 ng while the other PAH produce linear responses from low (shown in the left insets) to high injection amounts. The linear dynamic ranges, however, are slightly narrower than those of Figures VI-5 and 6 primarily because of the higher background levels produced by benzene. The low level responses shown in the second insets of Figures VI-10 and 11 are also at higher concentrations than before. Extrapolating from these responses, the detection limits for a signal-to-noise ratio of 3:1 were approximately:

Compound	$M^{+\cdot}$ Detection Limit (pg)	MH^{+} Detection Limit (pg)
Benz[*a*]anthracene	161	211
Benzo[*a*]pyrene	728	558
Dibenz[*a,h*]anthracene	142	224

These detection limits were much higher than those obtained for the same PAH standards under normal source conditions. Although benzene enhances charge-transfer chemistry and ionization, any increase in analyte ion intensity is offset by the increase in background noise.

VI.1.2 Negative Ion APCI

Reactions between negative ions and neutral molecules have been studied much less extensively and systematically than positive ion/molecule

reactions.[181] Negative ion chemical ionization (NICI) mass spectrometry, however, has been shown to be an exceptionally selective and sensitive mode of detection for electronegative molecules.[182] Normally, methane is used as a reactant gas to form thermal electrons in a high vacuum ion source. Compounds with sufficient electron affinity and cross section can be ionized by various electron capture mechanisms.[181] Other reactant gases or gas mixtures such as CH_4/N_2O or CH_4/CH_3NO_2, which yield stable negative ions (such as OH^- or CH_3O^-, respectively), can also be used for NICI. In this case, both ionization by electron capture and by ion/molecule reactions occur. The most common reactions are deprotonation and formation of ion/molecule adducts. In addition, isomeric compounds that have different gas phase acidities or form different ion/molecule adducts can be distinguished.

The negative ion mass spectra of PAH have been studied with several different reagent gas mixtures: for example, methane CI produces $[M-H]^-$, $M^{-\cdot}$ or MH^- ions;[182,183,184] methane/nitrous oxide mixtures produce $[M-H]^-$, $M^{-\cdot}$, $[M+OH]^-$, $[M-H+NO]^-$ and $[M-H+N_2O]^-$ ions;[185] and oxygen CI will produce $M^{-\cdot}$ and $[M-H+O]^-$ ions.[186,187] These methods have been used successfully for the differentiation of isomeric PAH based on the appearance and ratios of characteristic ions.[185,183]

It is likely that in most instances negative ions observed under NICI and negative ion APCI conditions will be the same; this will certainly be true when stable negative reactant ions are produced. The reaction scheme for the formation of APCI reactant ions (in ambient air) in negative ion mode is shown in Figure VI-12. The initial ionization involves electron capture and dissociative electron capture by O_2. The mechanism then becomes more

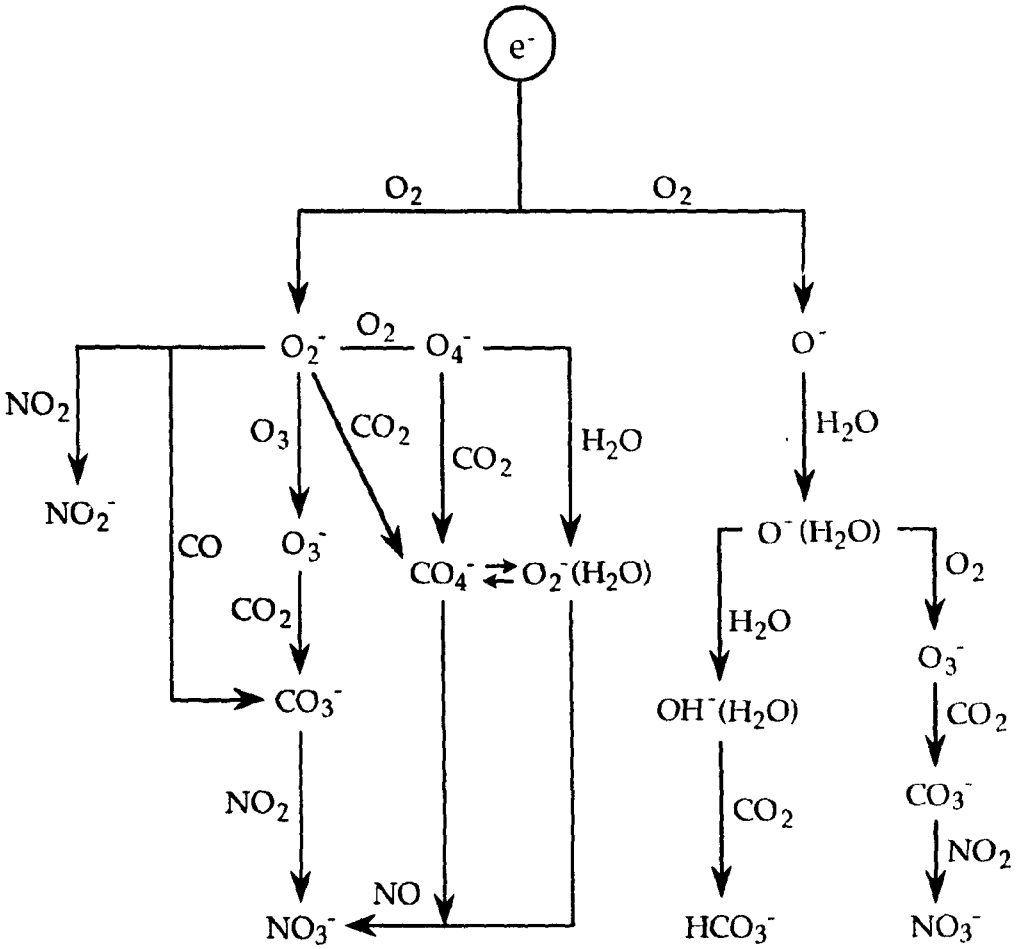

Figure VI-12: Negative ion atmospheric pressure chemical ionization reagent ion formation in ambient air.

complex due to the formation of a series of radicals and neutrals in the corona discharge region. These lead to the formation of a series of very stable ions: NO_2^-, O_3^-, CO_3^-, HCO_3^-, and NO_3^-. However, it is O_2^- and its clusters (O_4^- and $O_2^-(H_2O)_n$) that are the main reactant ions in trace analysis.

For an analyte to react, it must have either a higher electron affinity than O_2 to allow charge-transfer, or it must be more acidic than HO_2 (hydrogen superoxide) to allow proton-transfer. Fewer compounds meet these criteria than those imposed in positive ion mode APCI. Therefore, negative ion APCI can be much more selective and less prone to interference by impurities. For example, many pesticides, herbicides and fungicides, as well as many other types of compounds that are environmental hazards and are cytogenic or mutagenic, were shown to form stable negative ions under APCI conditions.[188] However, negative ions were not observed for benz[a]anthracene and other PAH standards.[188] In particular, the $M^{-\cdot}$ and $[M-H+O]^-$ ions previously observed during O_2 NICI of PAH were not observed under the APCI conditions.

The following experiments were performed to determine whether any negative ions could be observed for PAH under the LC conditions used in this study. The negative ion APCI mass spectra obtained from four PAH standards separated on a C_{18} column with an aqueous acetonitrile gradient are shown as Figure VI-13. In contrast to the previous report stating that PAH ions were not observed, the mass spectra of Figure VI-13 contain characteristic $[M+15]^-$ ions corresponding to each of the standards. Surprisingly, there were no $M^{-\cdot}$ or $[M-H]^-$ ions observed for any of the compounds. The electron affinities of most PAH are similar to or higher than that of oxygen (0.44 eV),

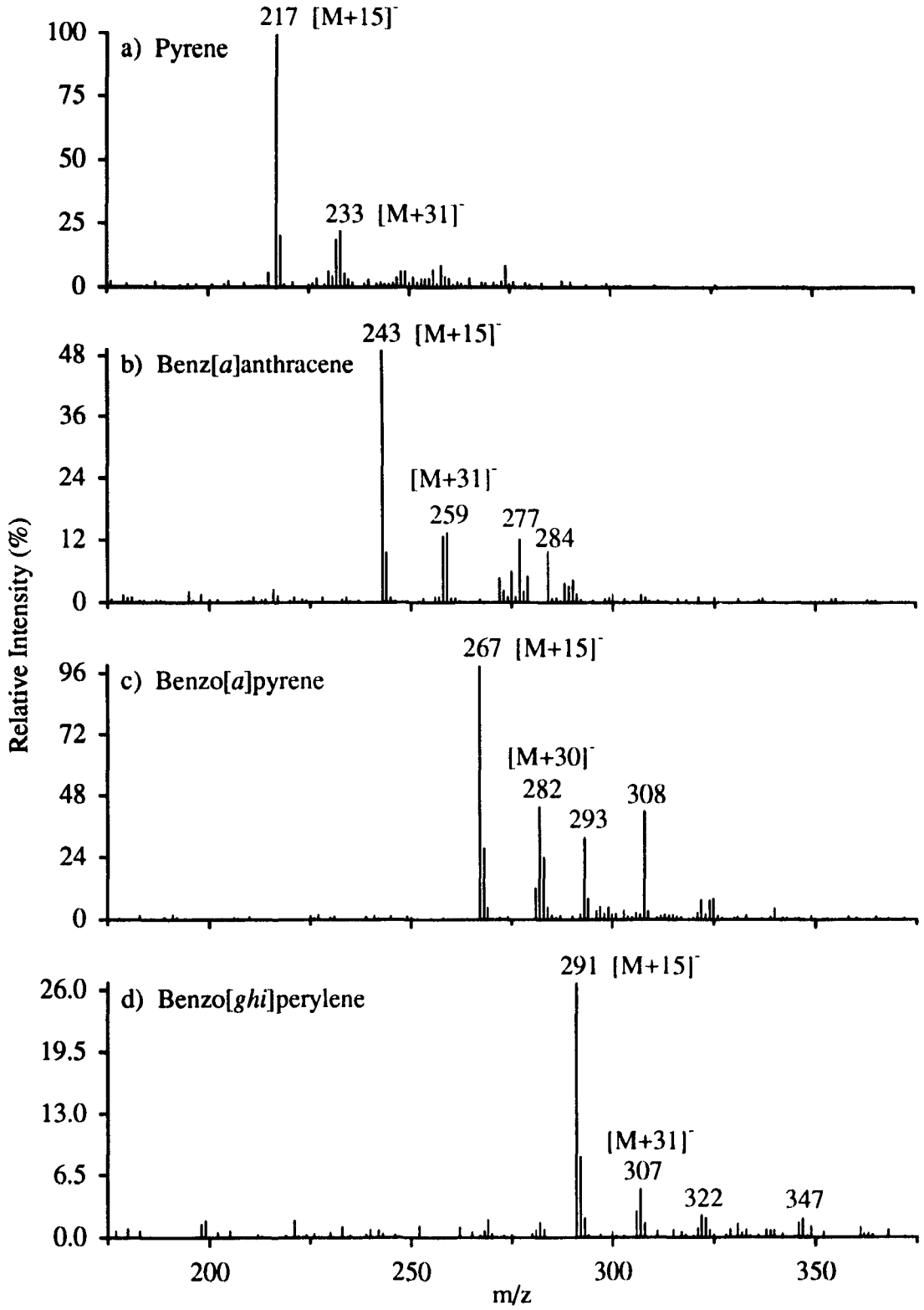

Figure VI-13: Background subtracted negative ion APCI mass spectra of PAH standards.

which would make charge-transfer ionization (producing the $M^{-\cdot}$ ions observed previously by O_2 NICI) thermodynamically favourable. The $O_2^{-\cdot}$ ion is also a Brønsted base and will react by proton abstraction with a wide range of substrates.[181] The proton affinity of the $O_2^{-\cdot}$ ion must be greater than the proton affinity of the $[M-H]^-$ ion for the reaction to be efficient; this probably does not hold for PAH since $[M-H]^-$ ions were not observed under O_2 NICI or negative ion APCI conditions.

Additional ions at $[M+30]^-$, $[M+31]^-$ and higher masses were observed in the spectra of Figure VI-13. Similar ions were observed during the NICI study of PAH using carbon dioxide (the reactant ions were assumed to be $O^{-\cdot}$, $O_2^{-\cdot}$ and $CO_3^{-\cdot}$).[189] These ions were assigned to the general type $[M-mH+nO]^-$. Similarly, the ions in Figure VI-13 can be assigned to the following nominal formulae:

Observed Ions	Nominal Formula
$[M+15]^-$	$[M-H+O]^-$
$[M+30]^-$	$[M-2H+2O]^-$
$[M+31]^-$	$[M-H+2O]^-$
$[M+45]^-$	$[M-3H+3O]^-$
$[M+46]^-$	$[M-2H+3O]^-$
$[M+47]^-$	$[M-H+3O]^-$

The spectra of Figure VI-13 also contain ions at higher masses that do not correspond to the general $[M-mH+nO]^-$ formula listed in the above table; these ions probably arise from various fragmentation reactions of larger [M-

$mH+nO]^-$ ions.

The formation of $[M+15]^-$ ions has also been observed for PAH during CH_4 negative ion CI experiments.[182] This ion was initially attributed to $[M+CH_3]^-$, formed by a fast radical addition reaction between the PAH molecules and CH_3 radicals present in the plasma of the hydrocarbon reactant gas. Subsequent methane CI experiments performed with deuterated-PAH standards produced $[M+14]^-$ ions that were rationalized as $[M-D+O]^-$ ions arising from reactions with traces of oxygen in the ion source.[182] The identity of the proposed $[M-mH+nO]^-$ ions produced in negative ion APCI (Figure VI-13) were also confirmed with deuterated-PAH standards. Figure VI-14 contains the mass spectra of the corresponding deuterated-PAH; the resulting ions were rationalized as follows:

Observed Ions	Nominal Formula
$[M+14]^-$	$[M-D+O]^-$
$[M+28]^-$	$[M-2D+2O]^-$
$[M+30]^-$	$[M-D+2O]^-$
$[M+42]^-$	$[M-3D+3O]^-$
$[M+44]^-$	$[M-2D+3O]^-$
$[M+46]^-$	$[M-D+3O]^-$

The $[M-mH+nO]^-$ adduct ions may be useful in the discrimination of PAH isomers. For example, Figure VI-15 contains the negative ion mass spectra of several mass 252 PAH isomers obtained under identical LC-MS conditions. Each isomer produced a unique spectrum that contained

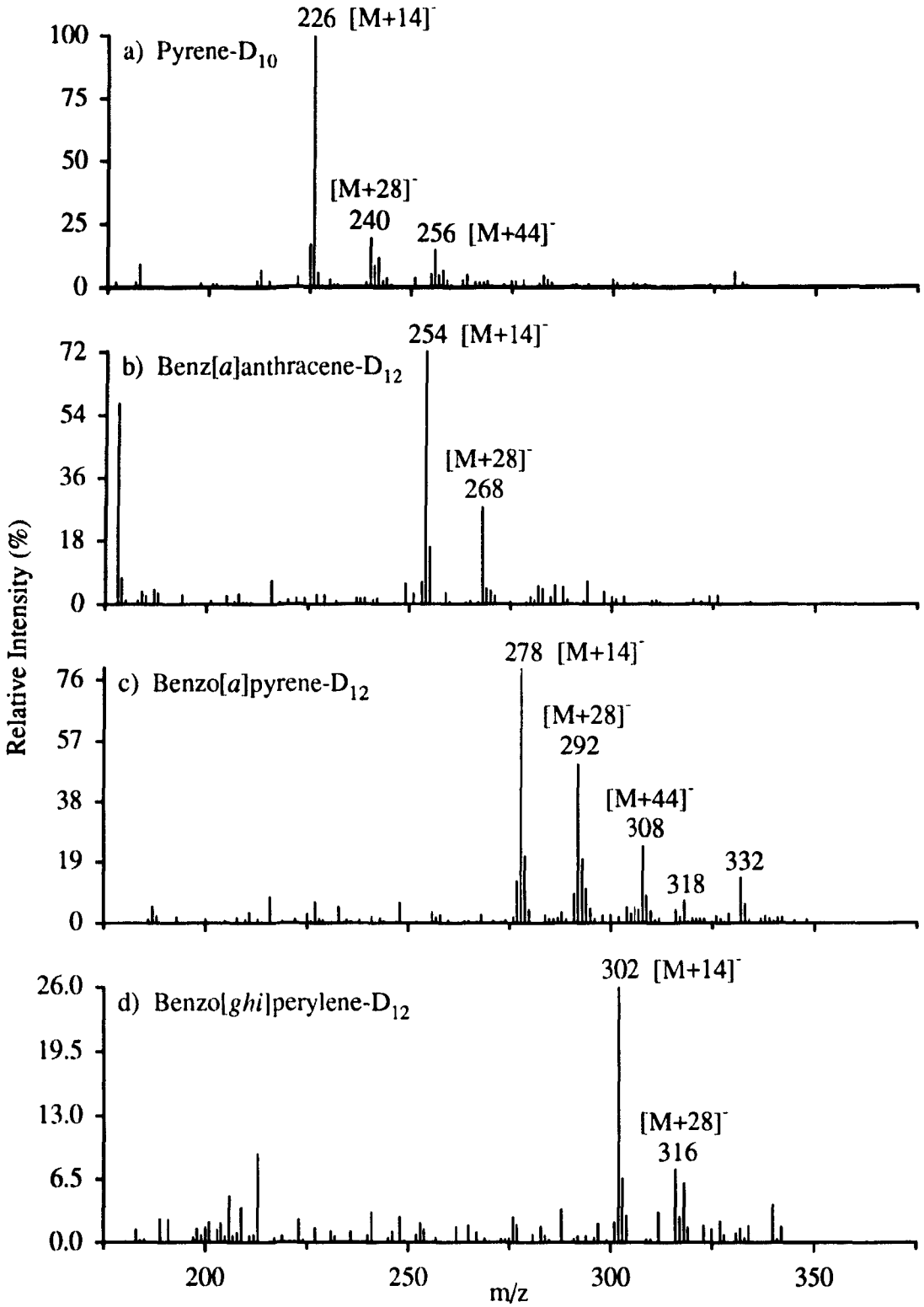

Figure VI-14: Background subtracted negative ion APCI mass spectra of perdeutero-PAH standards.

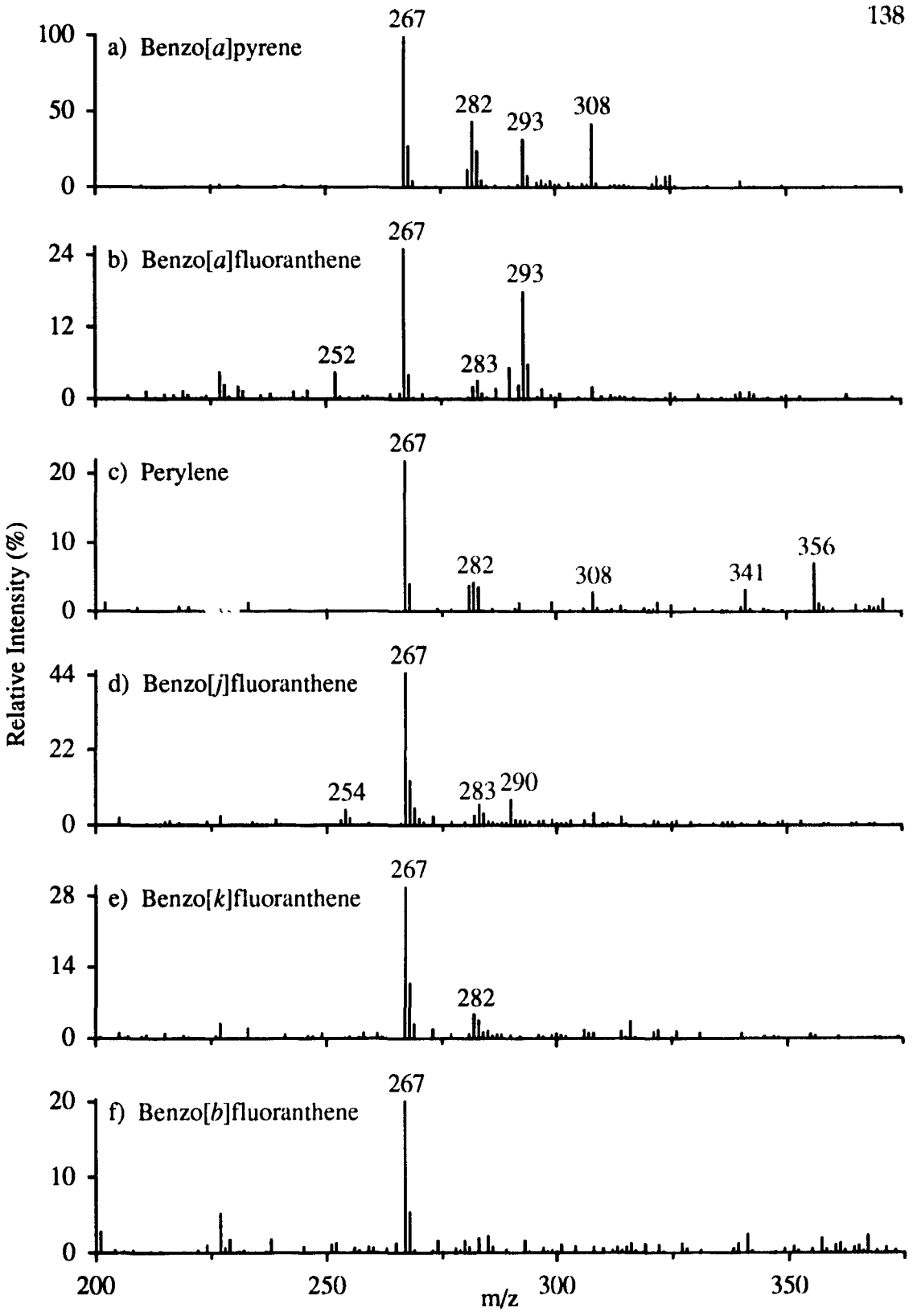

Figure VI-15: Background subtracted negative ion APCI mass spectra of mass 252 PAH isomers.

markedly different ions and intensities. Similar results were obtained for other sets of PAH isomers (e.g., mass 202, 228 and 276 PAH). Correlations between the observed adduct ions and the isomer structures have not been attempted, although the oxidative reactivity of individual isomers may be related to carcinogenic or mutagenic activity.[182,190]

The signal-to-noise ratios obtained under negative ion conditions for the PAH standards in Figures VI-13 and VI-15 were very poor (approximately 20 times less than that achieved under positive ion APCI). The reason for the low analyte ion intensities is probably related to the fundamental differences between the ion-formation processes in negative and positive ion MS. Positively charged ions can retain relatively large amounts of excess internal energy for a significantly longer time than their negative ion counterparts; other than abstraction of an electron from a nearby neutral, a positive ion can do little to neutralize its charge once it has been formed.[191] Negative ions, on the other hand, can merely eject an electron, and they do so readily if their internal energy exceeds the electron affinity of the neutral.

VI.1.3 Qualitative Analysis

All three modes of ionization described above, normal conditions (no modifier added to the source), benzene enhanced charge-transfer, and negative ion mode, could be used for the qualitative analysis of complex mixtures of PAC. The following experiments were, however, performed only

under normal conditions. These conditions rely on the mobile phase to produce primarily proton-transfer reagent ions, which are ideal for ionizing high molecular weight PAC (i.e., compounds with high proton affinities). The mobile phase required to elute these compounds from reversed-phase columns (acetonitrile/dichloromethane), however, is not capable of sustaining a reagent ion composition that is highly proton-transfer reactive. Therefore, it was found beneficial to maintain a constant post-column addition of water (10 μL/min) to the ion source using the same inlet described earlier for the addition of benzene to the source. This small amount of water (in comparison to the column flowrate of 200 μL/min) was sufficient to ensure that a suitable concentration of proton hydrates, the principal ions involved in proton-transfer, were present in the APCI plasma.

Although adding benzene to the source enhances charge-transfer chemistry, the resulting increase in background noise offsets any increase in analyte ion intensity. In addition, the higher molecular weight PAH are readily ionized by proton-transfer reactions; forcing these compounds to ionize by charge-transfer becomes increasingly difficult and much less beneficial.

Negative ion mode APCI produced mass spectra that were more complex and less intense than the corresponding positive ion techniques. This technique is clearly unacceptable for the analysis of complex mixtures that contain many unknowns and minor components.

NIST Complex Mixture of PAC from Coal Tar

The NIST Standard Reference Material 1597, complex mixture of PAC

from coal tar, is intended for use in the evaluation and validation of analytical methods, such as GC and LC, for the determination of PAC.[A374] Approximately 65 compounds have been identified in the coal tar based on molecular weight information obtained from GC-MS analyses and/or GC retention times.[172] It is an ideal test sample for GC analyses since it consists primarily of low molecular weight PAC (<300 Da) that are sufficiently volatile to pass through GC columns. However, this complex mixture does contain higher molecular weight components that are usually overlooked by GC analyses because they do not readily pass through the columns.

Figure VI-16 compares the chromatograms obtained from the LC-UV (top trace) and LC-APCI/MS analysis of the NIST coal tar mixture. The two chromatograms were not very similar in appearance; the UV chromatogram consisted of very intense peaks at the beginning of the analysis, while the APCI total ion chromatogram consisted of a series of peaks of nearly equal intensity. The wavelength used for detection (254 ± 2 nm) was the main reason for the difference; low molecular weight PAC are strong absorbers at this low wavelength, while the larger, late-eluting PAC absorb at higher wavelengths.

The tremendous ability to characterize complex PAC mixtures by LC-APCI/MS is illustrated by the selected ion chromatograms shown in Figures VI-17 to VI-19. These are only a selection of the many chromatograms that were generated from the full scan mass spectral data set. A variety of PAC components were readily detected and identified in these traces; for example, alkyl-PAH (m/z 142), oxygen (m/z 168), nitrogen (m/z 168) and sulphur (m/z 208 and 234) heterocycles, and many previously undetected high molecular

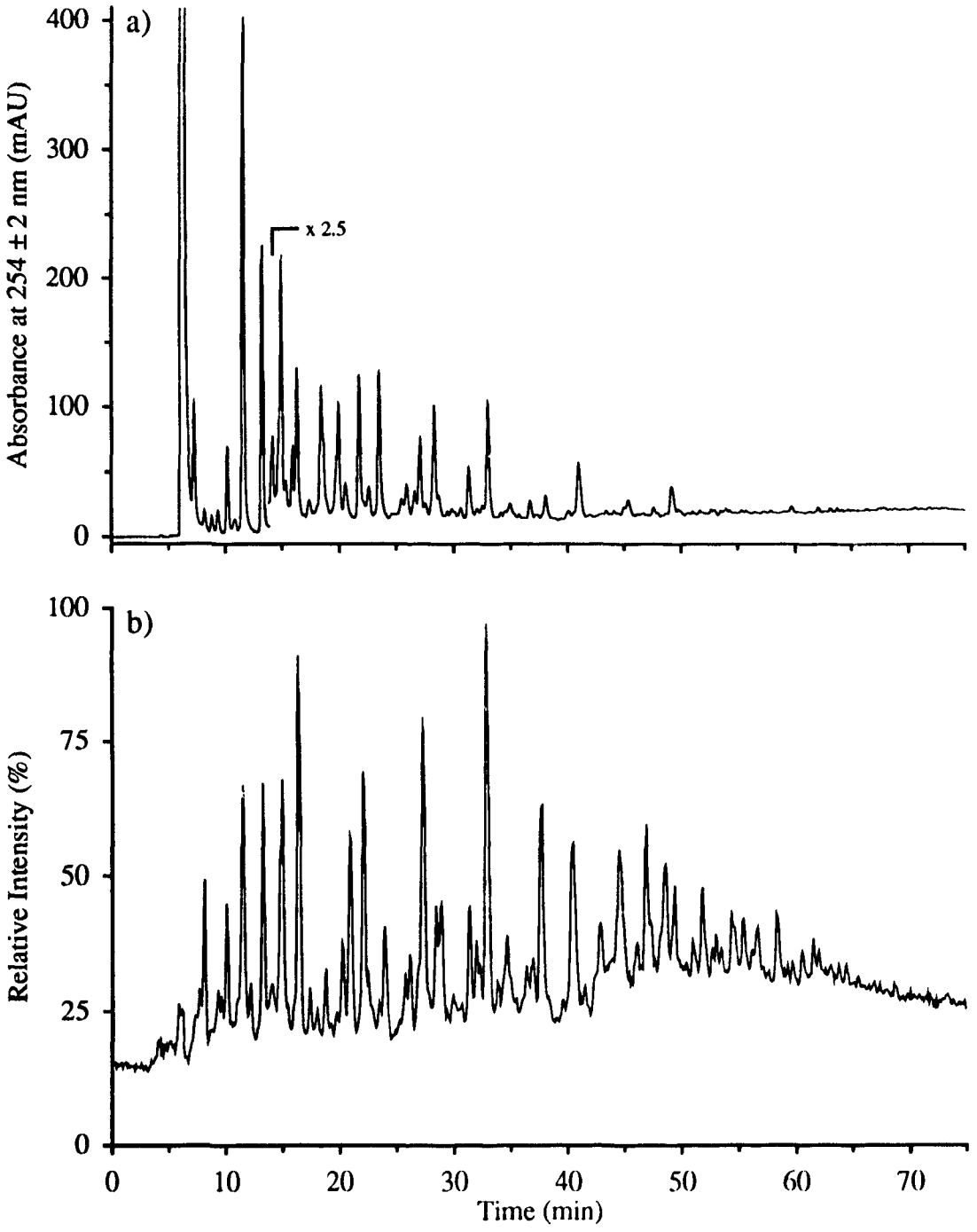

Figure VI-16: (a) LC-UV and (b) heated nebulizer LC-MS total ion chromatograms from the analysis of the NIST SRM 1597 coal tar mixture using a C_{18} column with an aqueous acetonitrile/dichloromethane gradient.

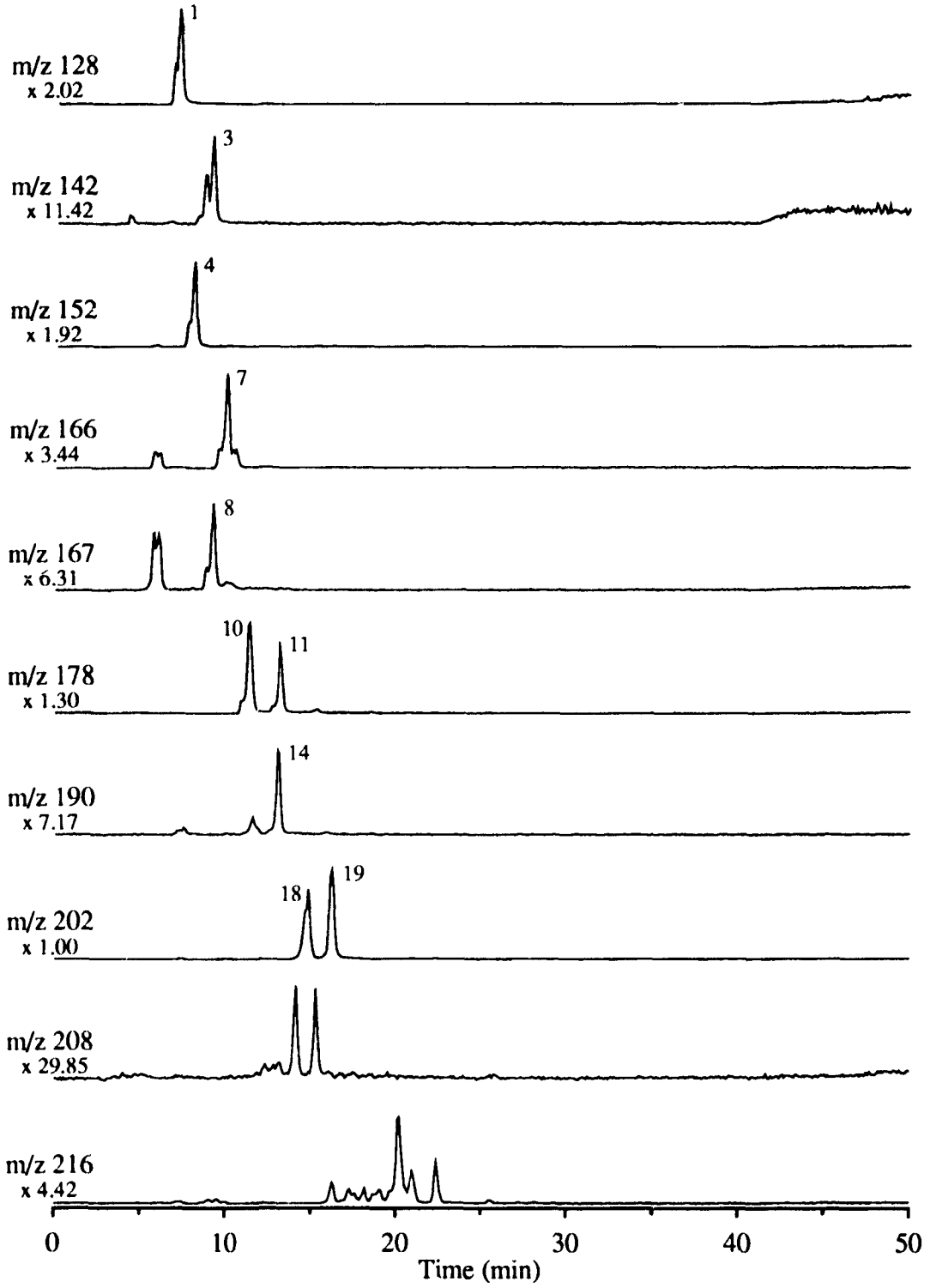

Figure VI-17: LC-MS selected ion chromatograms (sum of $M^{+\cdot}$ and MH^{+} ions) generated from the analysis of Figure VI-16b. See Appendix A for compound identities.

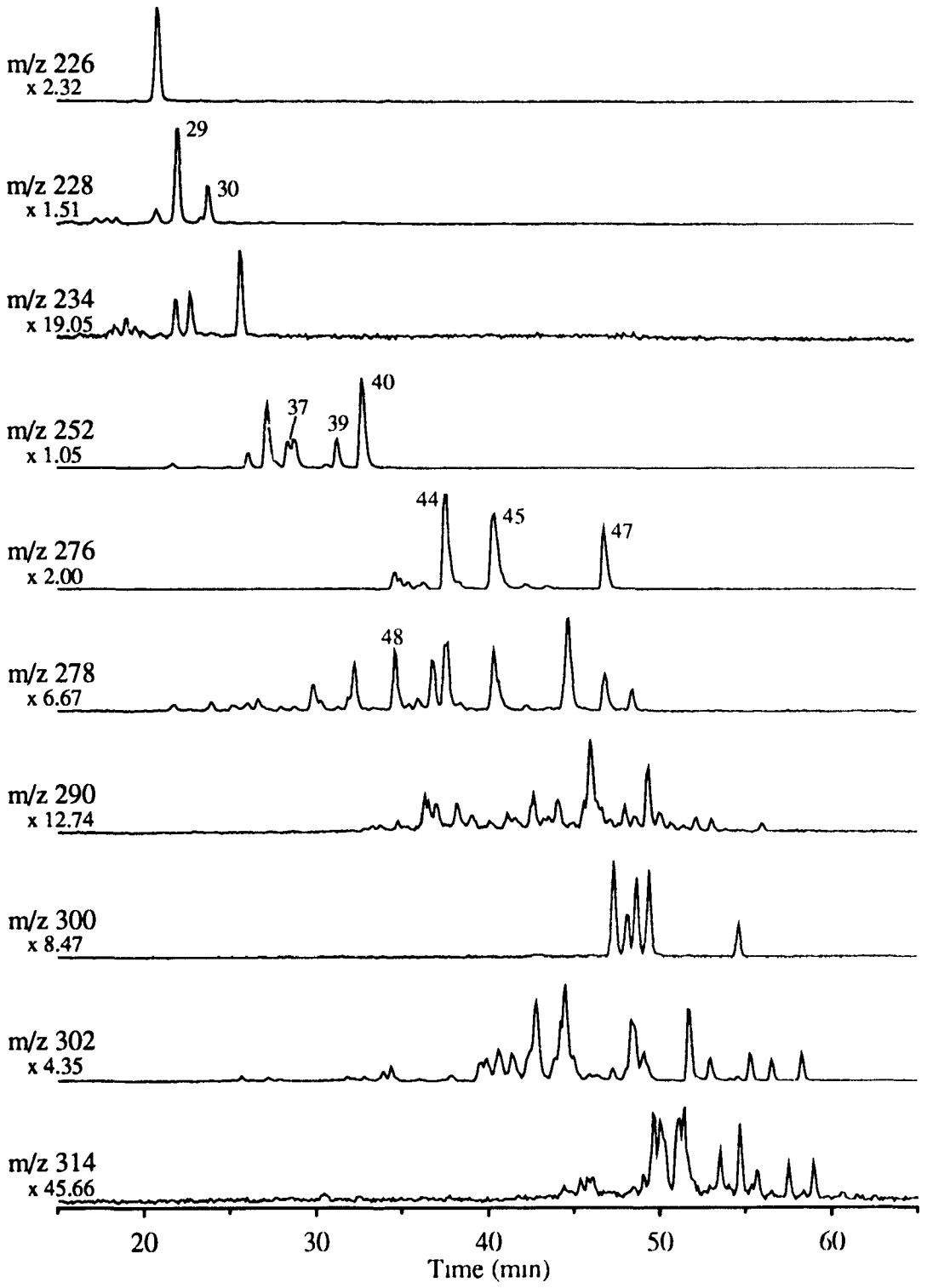

Figure VI-18: LC-MS selected ion chromatograms (sum of M^+ and MH^+ ions) generated from the analysis of Figure VI-16b. See Appendix A for compound identities.

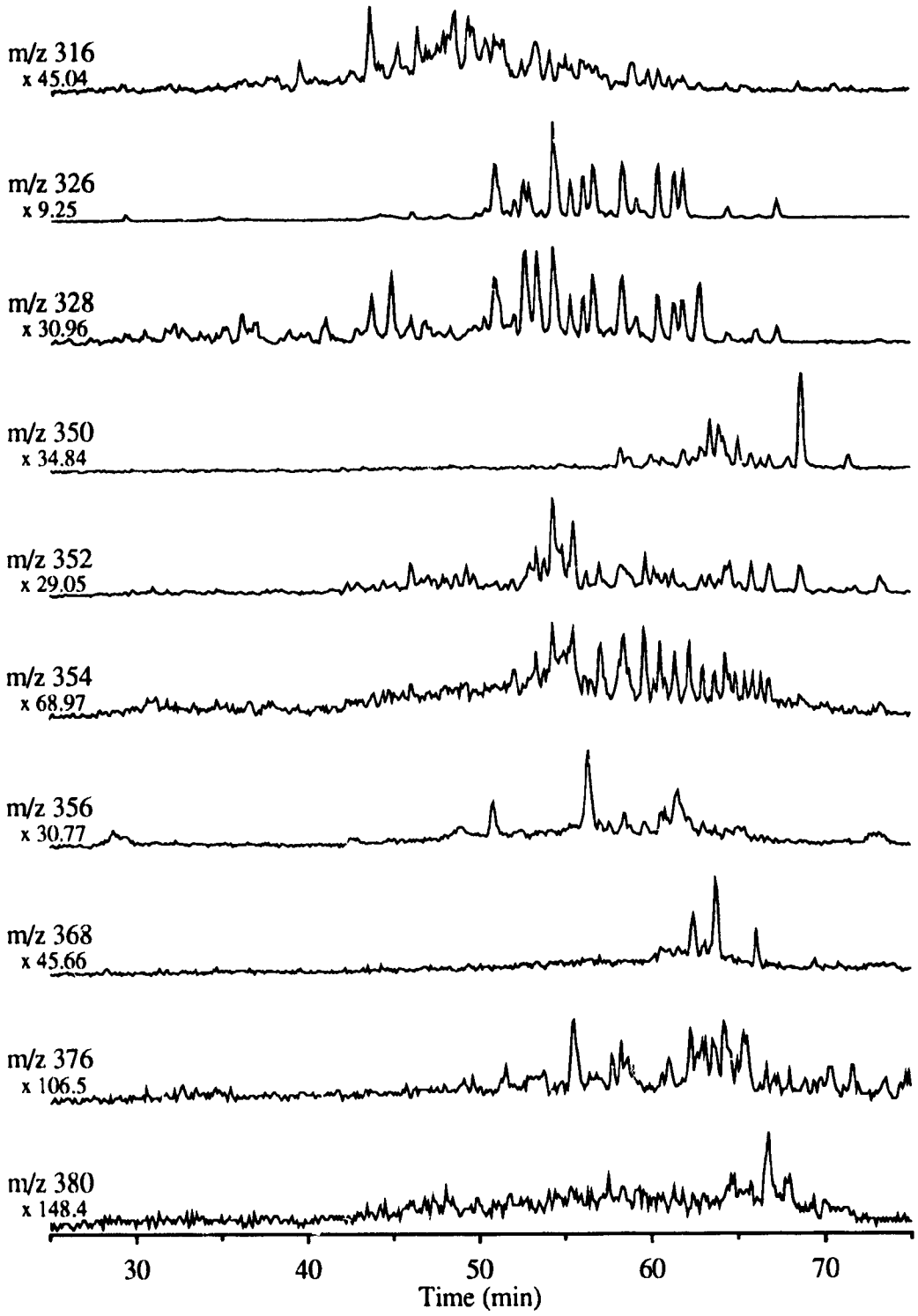

Figure VI-19: LC-MS selected ion chromatograms (sum of $M^{+\cdot}$ and MH^{+} ions) generated from the analysis of Figure VI-16b.

weight PAC (m/z 326 to 380).

In contrast to the moving belt and particle beam interfaces, the heated nebulizer was capable of easily detecting both the volatile, low molecular weight PAH (below mass 202) and the less volatile, high molecular weight PAC (above mass 302). Both the moving belt and particle beam interfaces were limited to a narrow range of analyte volatilities; compounds that were too volatile were lost to the interface vacuum, while the efficient vaporization of the analytes into the ion source became increasingly difficult with less volatile compounds. The extent to which the heated nebulizer interface can analyze compounds of low volatility will be discussed further in the following paragraphs.

Carbon Black Extract

The chromatograms obtained from the LC-UV and LC-APCI/MS analysis of the carbon black extract are compared in Figure VI-20. In contrast to the LC-UV and LC-APCI/MS coal tar chromatograms (Figure VI-16), these two traces were very similar. This was a result of the wavelength used for the LC-UV acquisition; in this instance, the detector was set to acquire the sum of the absorbances over the 236 - 500 nm wavelength interval. A more accurate representation of the true proportions of the low and high molecular weight PAC are produced with this wavelength range, as is reflected in the APCI/MS chromatogram.

Some of the selected ion chromatograms generated from the full scan mass spectral data set are shown as Figures VI-21 to 23. Unfortunately, most of the early eluting components (under 25 minutes) produced peaks that were

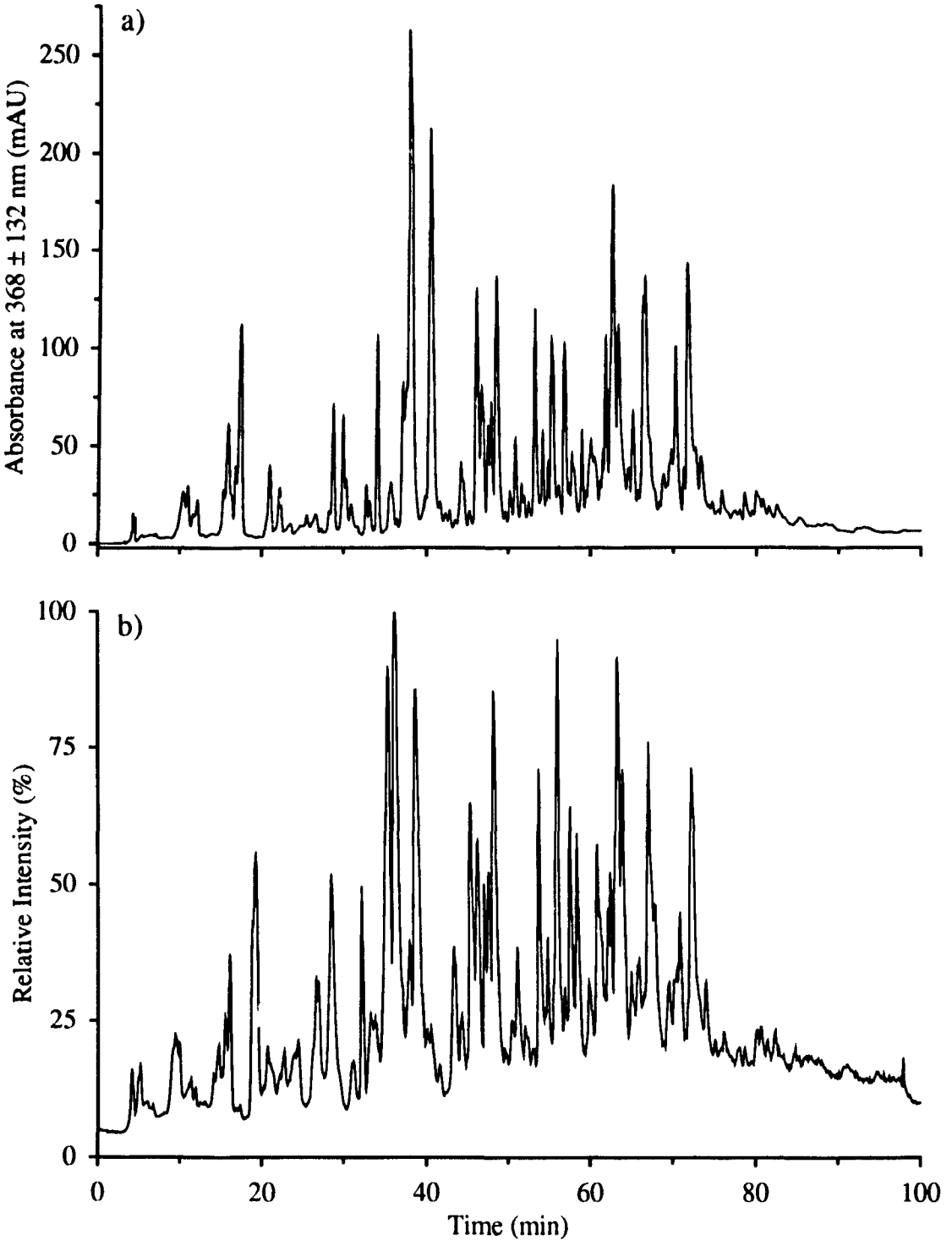

Figure VI-20: (a) LC-UV and (b) heated nebulizer LC-MS total ion chromatograms from the analysis of the carbon black extract using a C_{18} column with an aqueous acetonitrile/dichloromethane gradient.

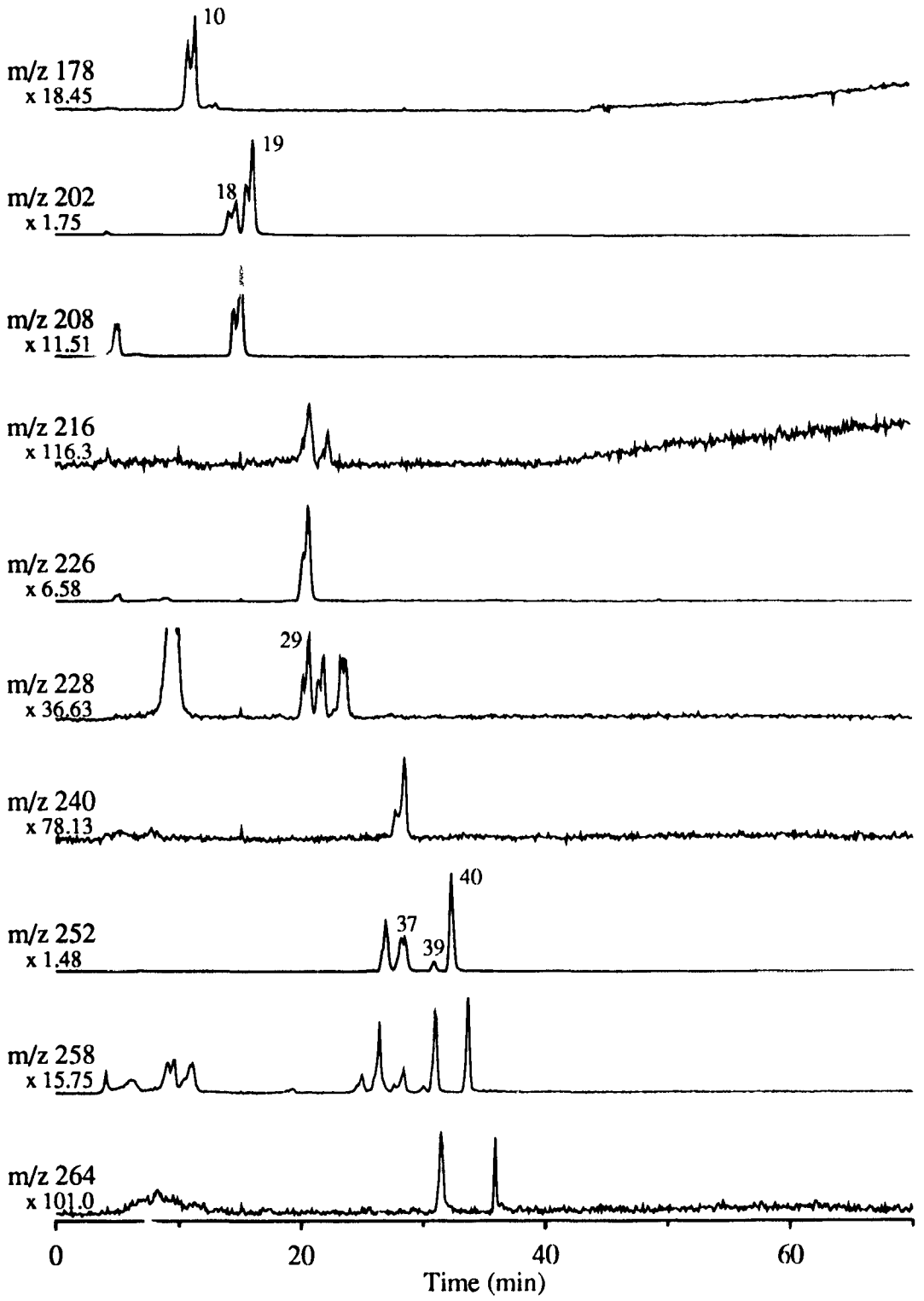

Figure VI-21: LC-MS selected ion chromatograms (sum of $M^{+\cdot}$ and MH^{+} ions) generated from the analysis of Figure VI-20b. See Appendix A for compound identities.

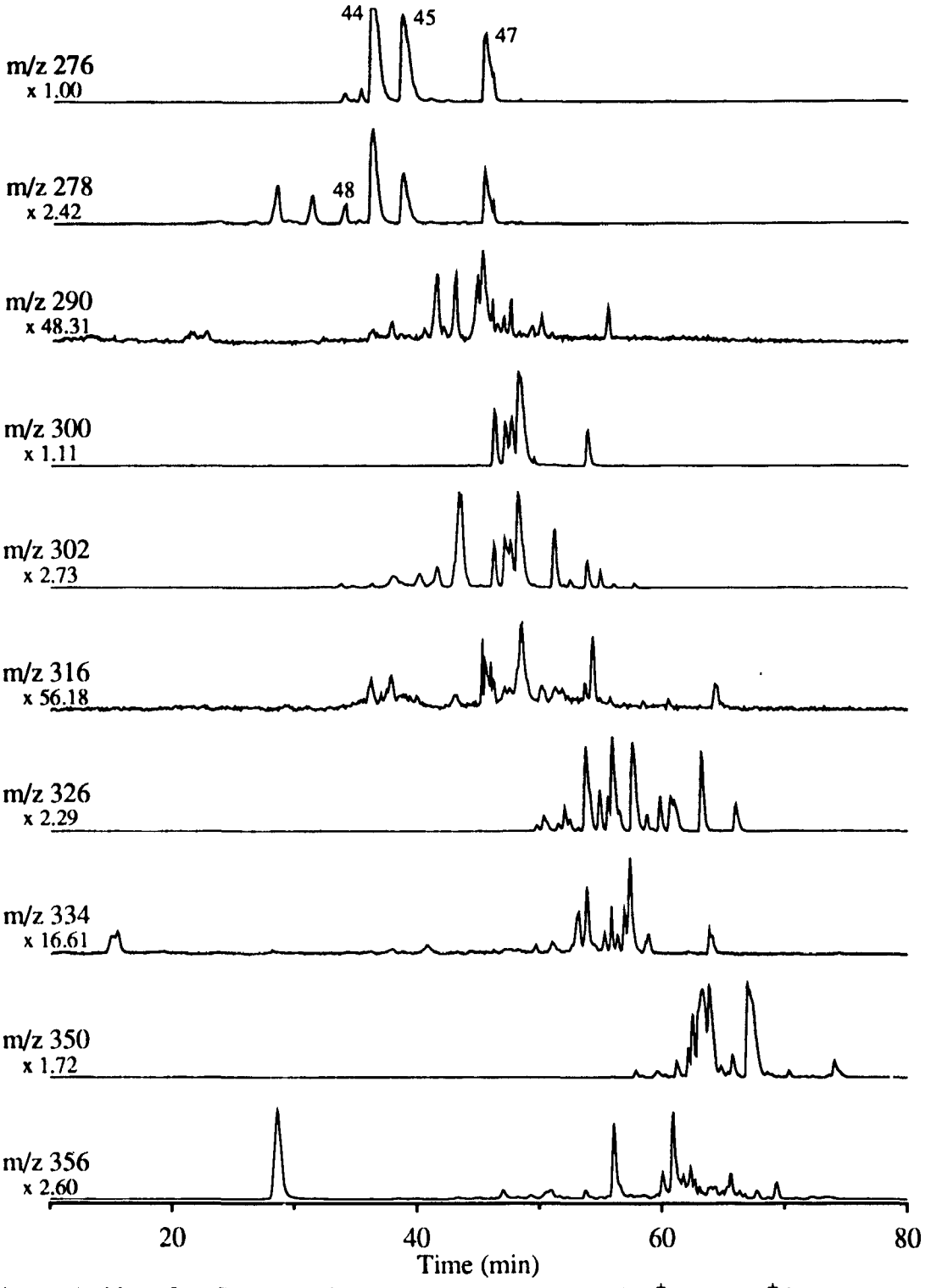

Figure VI-22: LC-MS selected ion chromatograms (sum of $M^{+\cdot}$ and MH^+ ions) generated from the analysis of Figure VI-20b. See Appendix A for compound identities.

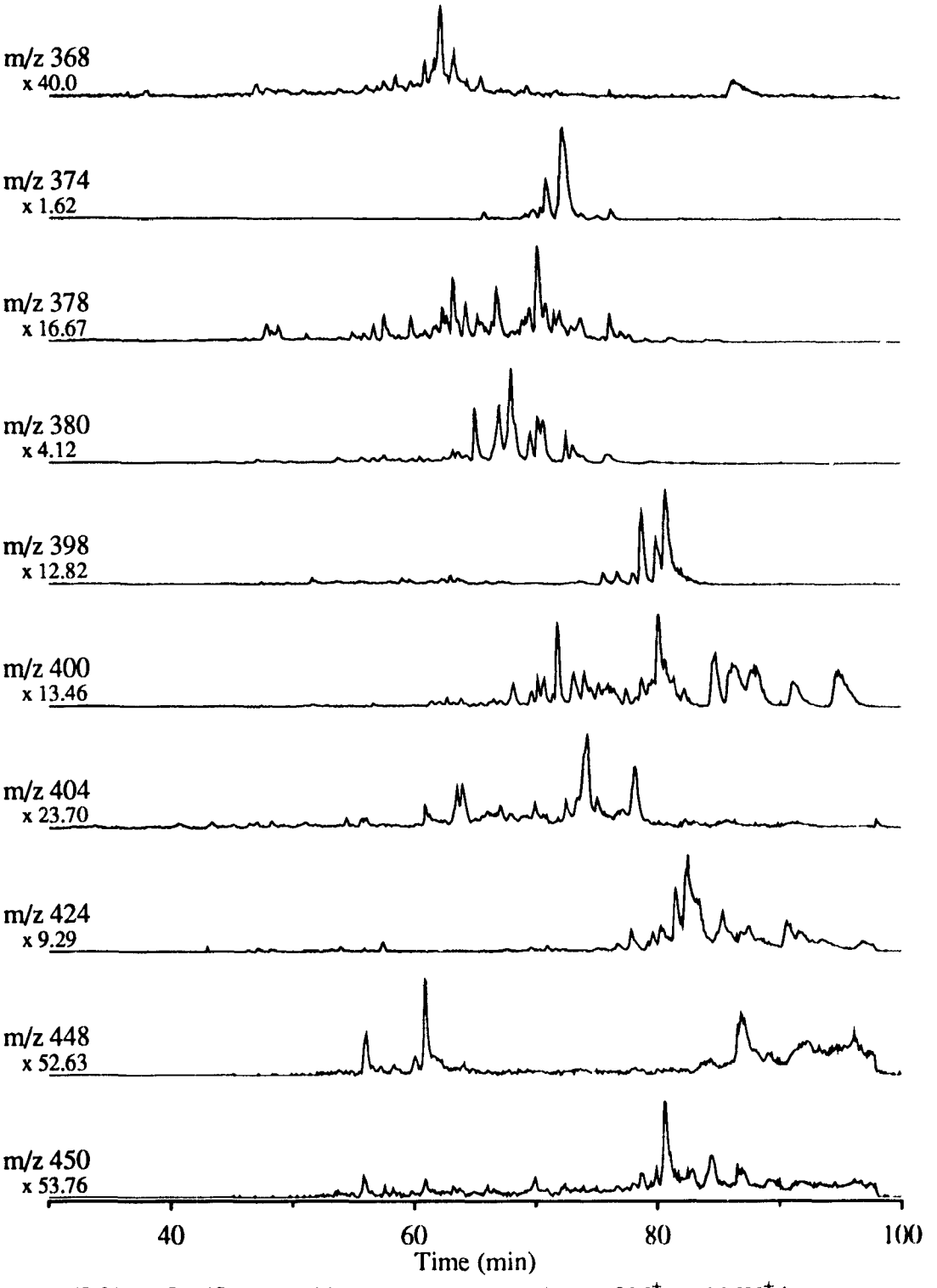

Figure VI-23: LC-MS selected ion chromatograms (sum of $M^{+\cdot}$ and MH^{+} ions) generated from the analysis of Figure VI-20b.

split. These were not partially resolved isomers; the peak splitting was the result of the strong solvent (in comparison to the mobile phase strength) in which the sample was dissolved. Ideally, the injected sample would be deposited at the top of the column while the sample solvent passes through the column as an unretained plug. In this case, the strong sample solvent has carried a portion of the most soluble components with it for a short distance causing the peaks to split. This could have been avoided by using a weaker sample solvent, but this would have caused the less soluble high molecular weight PAC to precipitate out of solution. The main goal in analyzing this sample was to examine the high molecular weight PAC.

Many selected ion chromatograms in Figures VI-21 to VI-23 were similar to those produced by the analysis of the NIST coal tar (Figures VI-17 to VI-19). The carbon black extract, however, contained a higher proportion of sulphur heterocycles (m/z 208, 258, 356 and 380), as well as a large number of high molecular weight PAH between mass 302 and 450. The high sensitivity that can be achieved for these compounds that have low volatilities is a result of the efficient vaporization and ionization processes of the interface. The highest PAH mass that can be analyzed by this technique is presently unknown because of the lack of commercially available standards. The carbon black extract, which has never been shown to contain PAH higher than mass 500,[142] was the only readily available high mass PAH sample. However, we have shown that LC-MS using a heated nebulizer interface is capable of analyzing complex mixtures of the all-carbon clusters (such as C_{60} and C_{70}) known as the fullerenes.[192-195] These molecules have physical properties that are similar to large PAH; i.e., low solubility in polar solvents,

high thermal stabilities and low volatilities that decrease with increasing cluster size. Remarkably, fullerenes as high as C_{120} (m/z 1440) have been detected by LC-APCI/MS techniques.[193]

Tar Sand Oil Fractions

The analysis of the tar sand oil fractions presents a different challenge than that encountered with the analysis of high molecular weight PAC; these mixtures are much more complex than most other real-world samples. In fact, conventional chromatographic techniques coupled to routine detectors (e.g., UV) usually produce very little information regarding the composition of the fractions. Detectors that can provide additional selectivity to the chromatographic separation are essential for this type of analysis. Mass spectrometric detection is the obvious choice

Figure VI-24 compares the LC-UV and LC-APCI/MS chromatograms obtained from the analysis of the neutral fraction of the tar sand oil. The two chromatograms were similar except that the UV trace showed an increased selectivity toward the early eluting compounds because of the wavelength monitored (254 ± 2 nm). The ability to generate selected ion chromatograms from the mass spectral data set, such as those in Figures VI-25 and VI-26, can provide detailed information about the sample. For example, the distribution of the alkylated homologues of mass 202 and 228 PAH is revealed in Figures VI-25 and VI-26, respectively. The most abundant species appear to occur in the C_3 to C_7 region for both series. The separation of individual isomers was achieved in the first few traces in Figures VI-25 (mass 202 and 216) and VI-26 (mass 228 only), but as the number of isomeric structures increased with

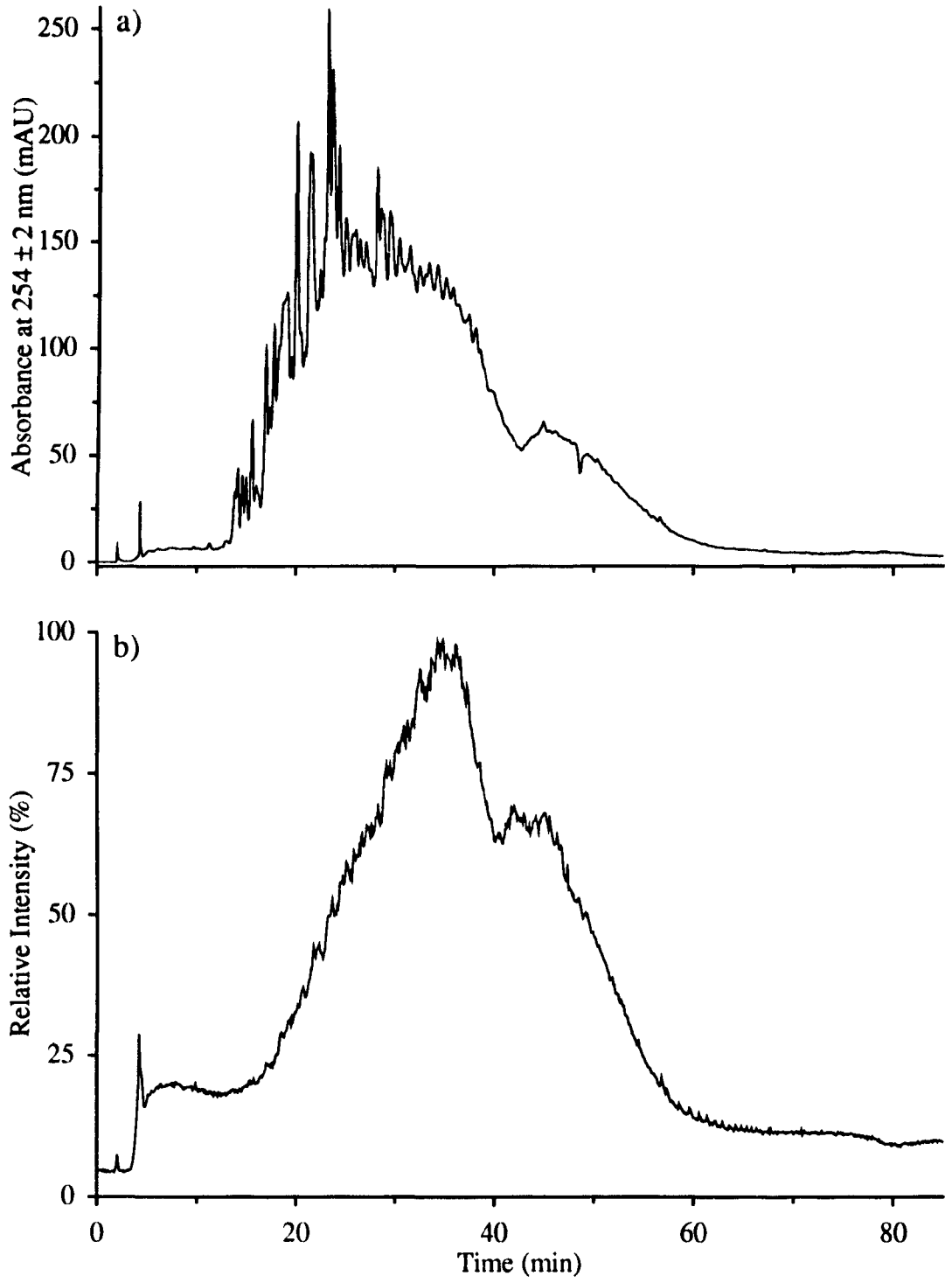

Figure VI-24: (a) LC-UV and (b) heated nebulizer LC-MS total ion chromatograms from the analysis of the tar sand oil neutral fraction using a C_{18} column with an aqueous acetonitrile/dichloromethane gradient.

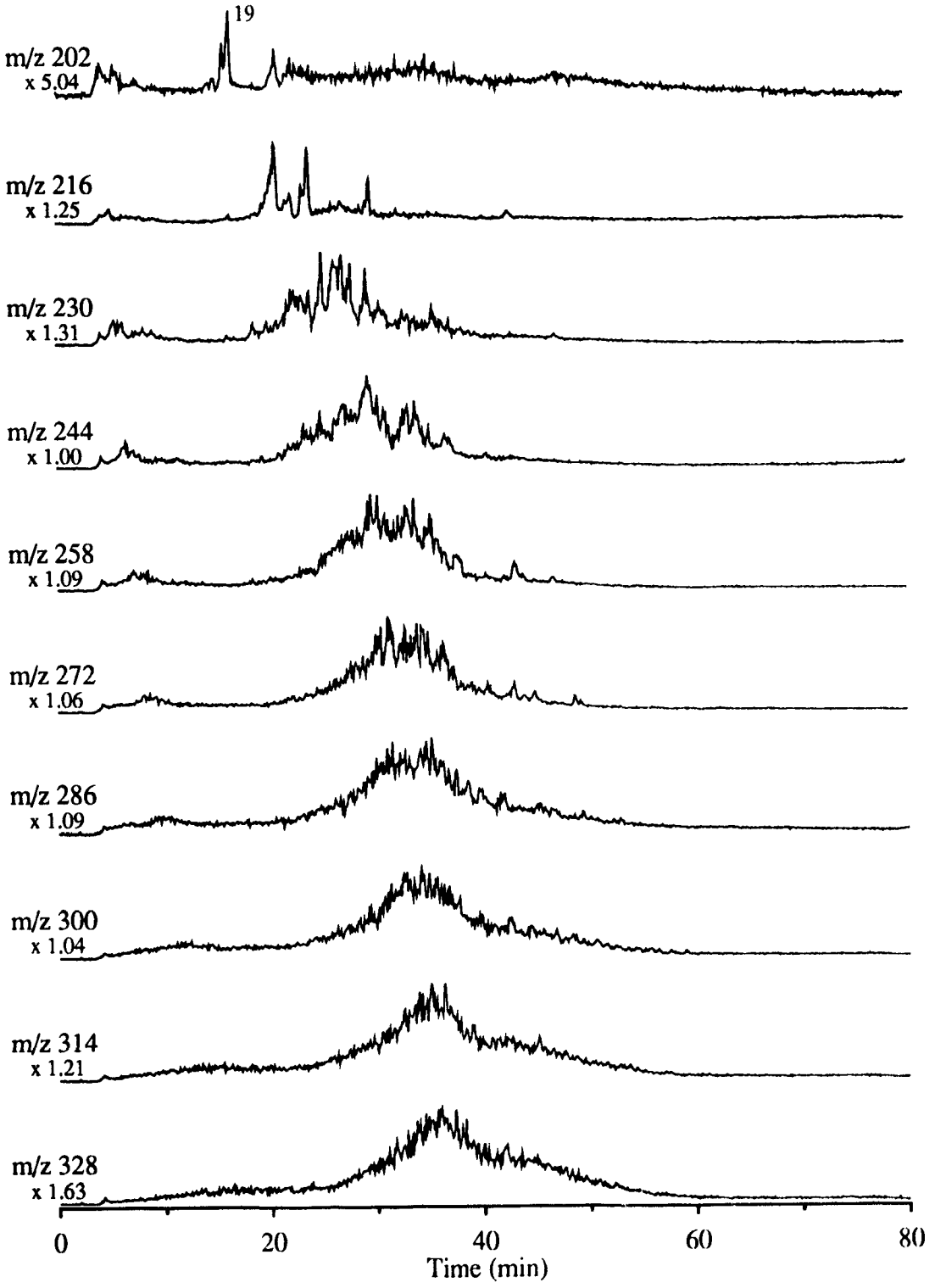

Figure VI-25: LC-MS selected ion chromatograms (sum of $M^{+\cdot}$ and MH^{+} ions) of mass 202 PAH and their alkylated homologues generated from the analysis of Figure VI-24b. See Appendix A for compound identities.

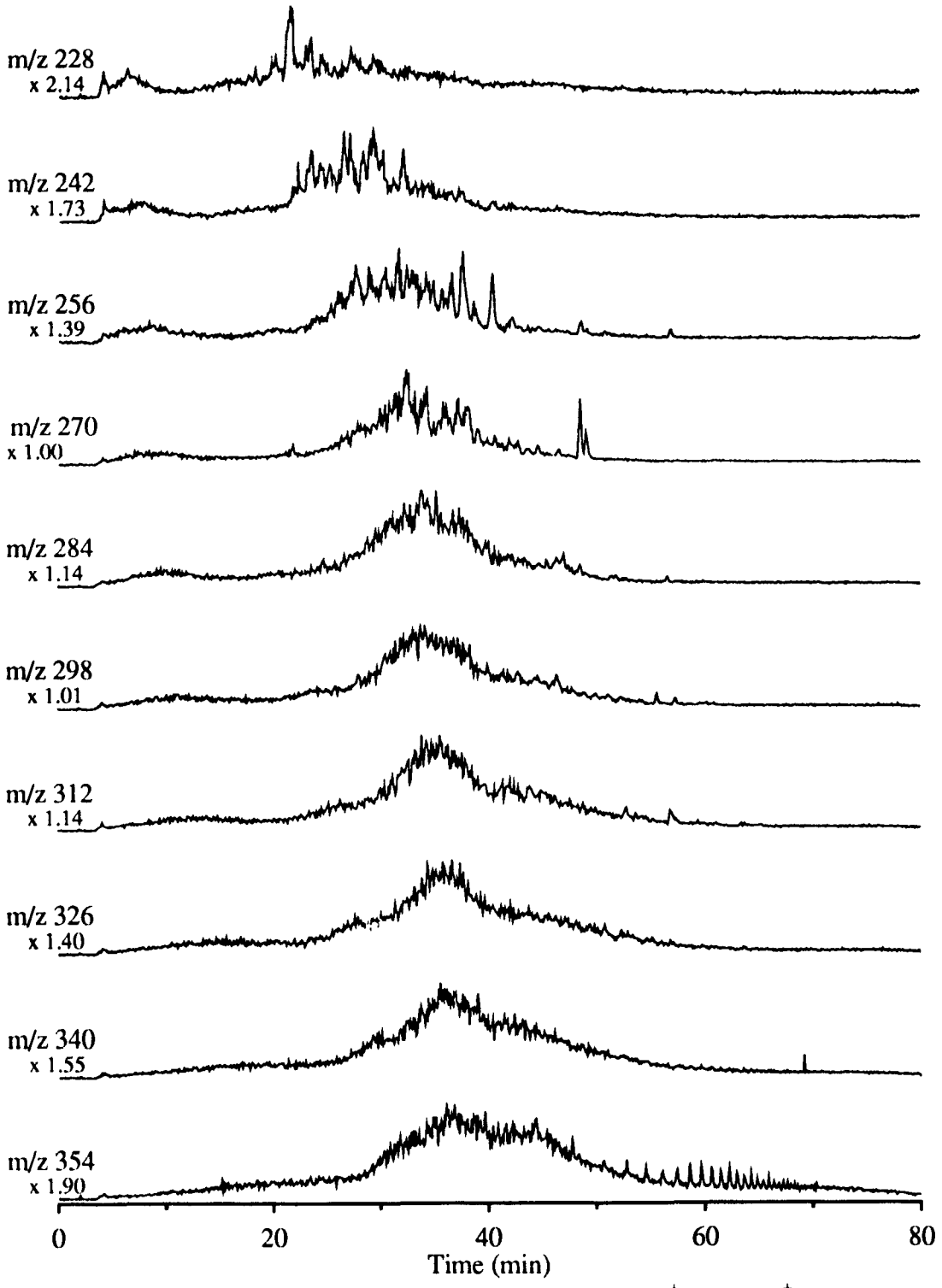

Figure VI-26: LC-MS selected ion chromatograms (sum of $M^{+\cdot}$ and MH^{+} ions) of mass mass 228 PAH and their alkylated homologues generated from the analysis of Figure VI-24b.

increasing alkylation, the resolution of individual components became nearly impossible. Alkylated PAH as high as mass 500 were detected.

Additional series of alkylated PAH starting at mass 178, 226 and 252 could be generated from the mass spectral data set. Alkylated PAH with varying degrees of unsaturation were also readily identified in this fraction. These probably result from the hydrogenation of larger ringed structures or perhaps even the formation of rings in the alkyl side chains (since this oil has been thermally cracked).

The chromatograms obtained from the LC-UV and LC-APCI/MS analysis of the nitrogen-containing PAC fraction are compared in Figure VI-27. Again, there was an excellent correspondence between the UV and TIC chromatograms. The selected ion chromatograms for carbazole and some of its alkylated homologues are shown as Figure VI-28. Alkylated compounds as high as mass 500 were also detected in this fraction, but the C_4 and C_5-alkyl carbazoles were the most abundant species. Underivatized carbazole (Figure VI-28, m/z 168) was not detected. The C_1-alkyl carbazole chromatogram (m/z 182) contains several intense peaks corresponding to a small amount of alkyl-PAH that were also present in this fraction.

Selected ion chromatograms corresponding to unsaturated alkyl or saturated cyclic derivatives of carbazole could also be produced. For example, Figure VI-29 shows a homologous series of alkylated hydroaromatic carbazole isomers. These components were very difficult to identify in the previous analysis of this fraction with the moving belt and particle beam interfaces because of the extensive fragmentation of the alkyl side chains. The APCI mass spectra of these compounds produced only abundant MH^+ ions.

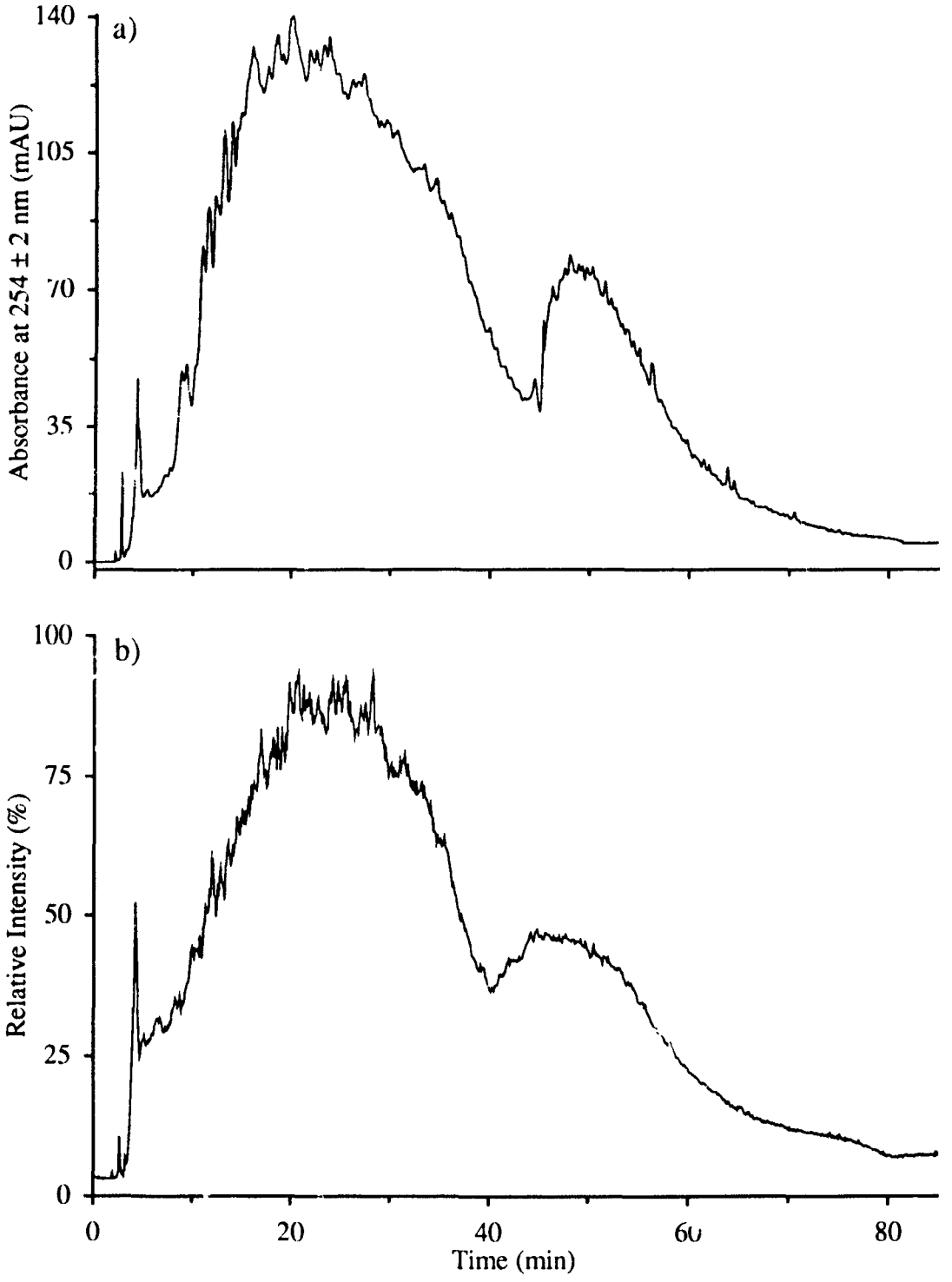

Figure VI-27: (a) LC-UV and (b) heated nebulizer LC-MS total ion chromatograms from the analysis of the tar sand oil nitrogen-containing PAC fraction using a C_{18} column with an aqueous acetonitrile/dichloromethane gradient.

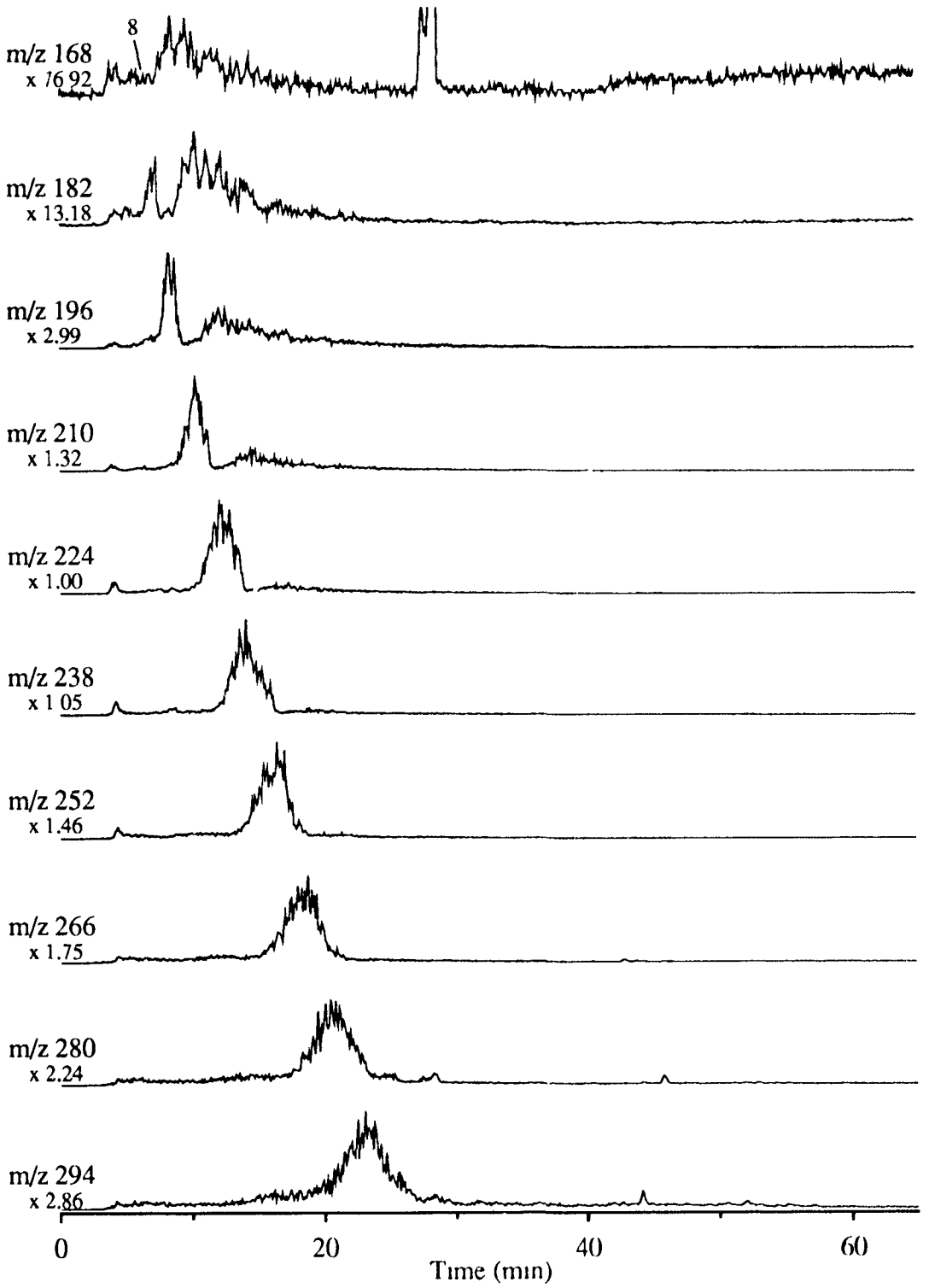

Figure VI-28: LC-MS selected ion chromatograms (MH^+ ions) of carbazole and its alkylated homologues generated from the analysis of Figure VI-27b See Appendix A for compound identities.

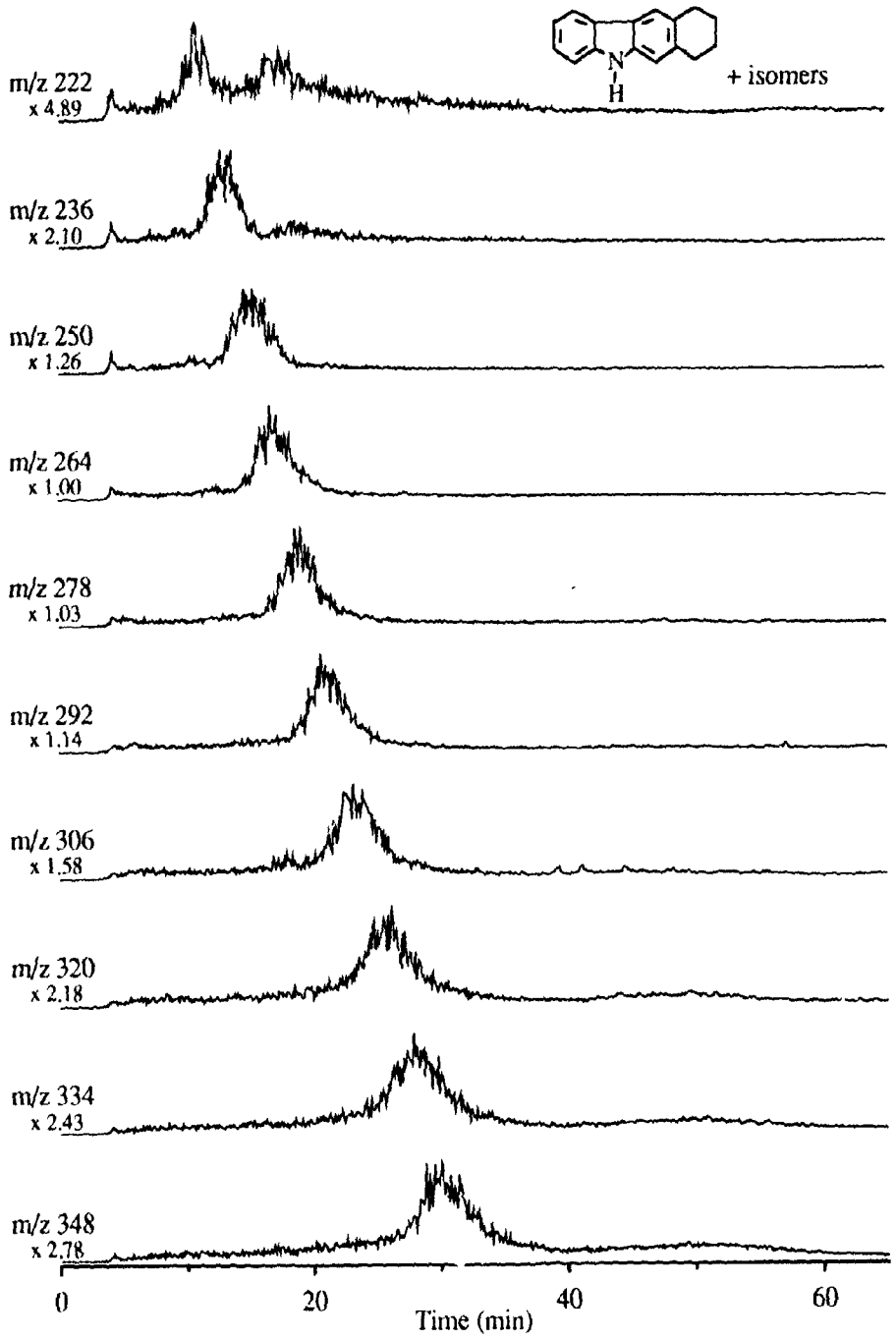

Figure VI-29: LC-MS selected ion chromatograms (MH^+ ions) of alkylated hydroaromatic benzocarbazole generated from the analysis of Figure VI-27b.

VI.1.4 Quantitative Analysis

The combination of LC with APCI/MS has been applied to the rapid and convenient quantification of several target compounds including pesticides and drugs in body fluids.[179,180] The following experiments were conducted to evaluate the ability of this technique, using both external calibration and internal standardization, to quantify PAH in complex mixtures. The calibration standards and procedure were identical with those described earlier in Chapter V for the quantification of PAH using the particle beam interface. A mixture of perdeutero-PAH standards (DPAC-1) was spiked at four different levels into both a certified NIST PAH standard mixture (SRM 1647) and a NIST complex mixture of PAH from coal tar (SRM 1597). These solutions were prepared primarily for internal standardization experiments, but since the volumes of both standard and internal standards were measured accurately, the same data sets could also be used for external calibration calculations. A total of 48 masses were monitored (both $M^{+\cdot}$ and MH^+ ions of 16 PAH and 16 perdeutero-PAH) in six acquisition periods (8 ions per period, 1 second total scan time). All the experiments were performed under both normal source conditions (i.e., no chemical modifiers added) and benzene charge-transfer enhanced ionization in order to determine if one method is superior to the other

An example of a typical analysis (under normal source conditions) of an SRM 1647/DPAC-1 solution (in a 10:1 volume spike ratio) is shown as Figure VI-30. In contrast to the previous results obtained with the particle beam interface, all of the PAH that were monitored were easily detected and

Figure VI-30: Analysis of a SRM 1647/DPAC-1 solution (10:1 volume ratio) using heated nebulizer LC-MS. A total of 48 ions monitored in six acquisition periods: (a) TIC (sum of all molecular ions and protonated molecules); Period 1, (b) m/z 128 + 129, (c) m/z 136 + 137, (d) m/z 152 + 153, (e) m/z 160 + 161; Period 2, (f) m/z 154 + 155, (g) m/z 164 + 165, (h) m/z 166 + 167, (i) m/z 176 + 177; Period 3, (j) m/z 178 + 179, (k) m/z 188 + 189, (l) m/z 202 + 203, (m) m/z 212 + 213; Period 4, (n) m/z 228 + 229, (o) m/z 240 + 241, (p) m/z 252 + 253, (q) m/z 264 + 265; Period 5, (r) m/z 276 + 277, (s) m/z 288 + 289, (t) m/z 278 + 279, (u) m/z 292 + 293; Period 6, (v) m/z 300 + 301, (w) m/z 312 + 313, (x) m/z 302 + 303, (y) m/z 316 + 317. See Appendix A for compound identities. Peak numbers with an asterisk represent the perdeutero-PAH internal standards.

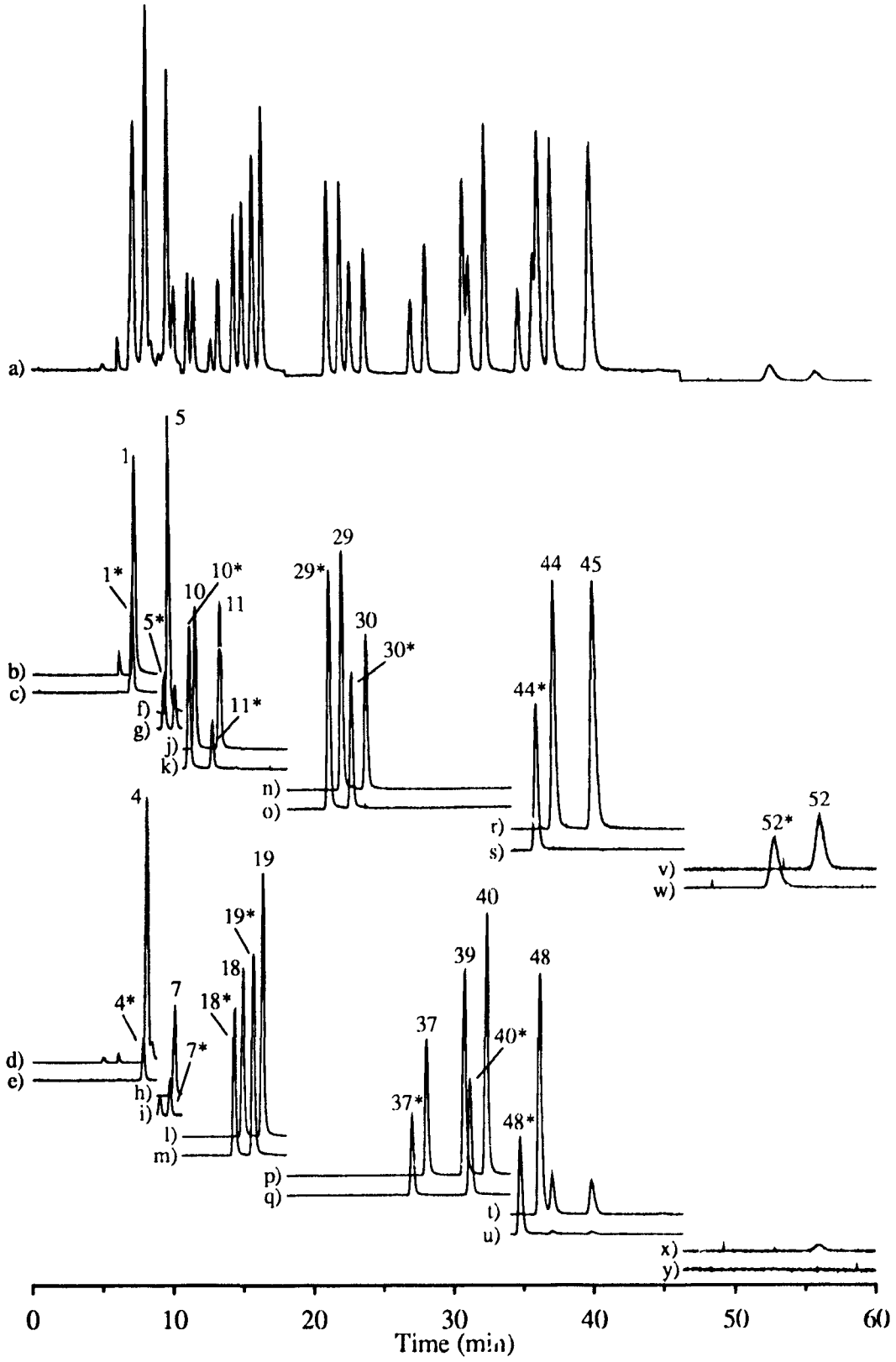

Figure VI-30: Figure caption on preceding page.

subsequently quantified. The addition of benzene to the source did not significantly alter the appearance of the chromatograms (data not shown), although there was a noticeable increase in background noise at lower masses.

Three examples of the external calibration curves that were obtained from the analyses of the NIST 1647/DPAC-1 solutions under normal source conditions are shown as Figure VI-31. The linear regression curves for these and all the other PAH monitored under normal and benzene charge-transfer conditions were not as satisfactory as those shown earlier in Figures VI-6 and VI-10 (possible reasons are given below). The regression coefficients varied between 0.68 - 0.94 and the curves did not pass through the origin; these results were an improvement in comparison to the external calibration curves obtained previously by the particle beam interface (Figure V-11).

The concentrations of the NIST coal tar PAH, calculated from the linear regression data using normal source conditions, are listed in Table VI-1 and compared to the values reported by NIST. The accuracy of the calculated values (expressed as a percent error from the NIST value) ranged from -6.4 to 94%; a slight improvement over the particle beam results, but still unacceptable. The extremely poor precision and the matrix effect were the reasons given for the low accuracy of the particle beam interface. These explanations, however, do not apply to the heated nebulizer interface; the precisions listed in Table VI-1 vary between 0.04 and 6.0% RSD, while matrix effects have not been previously reported for this interface. The calibration solutions used in these experiments, which were made for internal standardization experiments, were the most likely cause of the poor calibration curves and accuracy of measurements. The solutions were

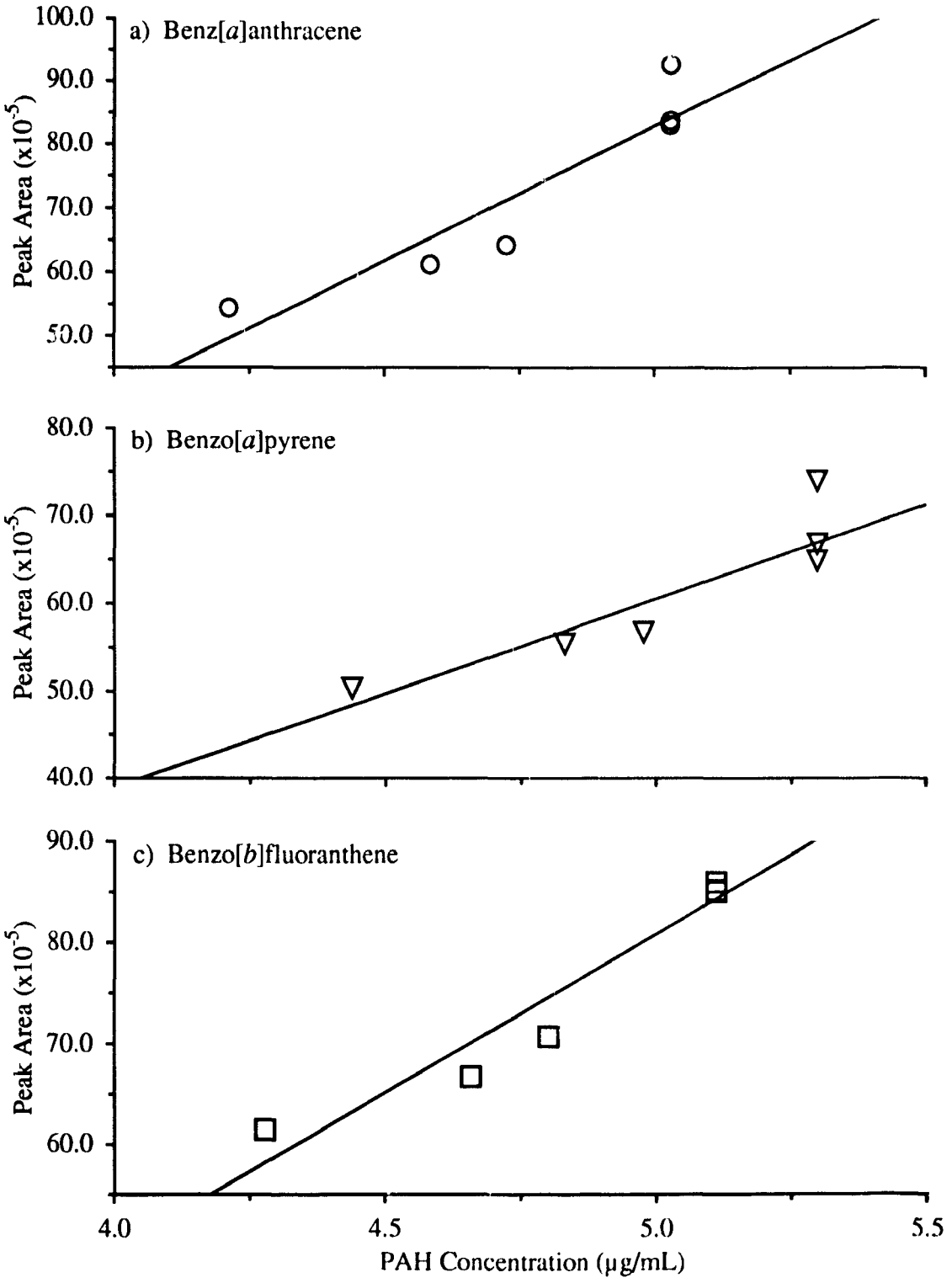

Figure VI-31: Heated nebulizer LC-MS external calibration curves obtained from the analysis of the SRM 1647/DPAC-1 solutions.

Table VI-1: APCI/MS quantitation results for the NIST coal tar SRM 1597 using external calibration and normal source conditions.

Compound	Certified Results* (μg/g)	Calculated Results (μg/g)	Stand. Dev. (n=3)	%RSD (n=3)	Relative Error (%)
Naphthalene	1160	747.1	26	3.5	-35
Acenaphthylene	250	430	6.8	1.6	72
Acenaphthene		431	0.17	0.04	
Fluorene	140	131	2.6	2.0	-6.4
Phenanthrene	462	226	14	6.0	-51
Anthracene	101	92.2	2.7	2.9	-8.7
Fluoranthene	322	304	16	5.1	-5.7
Pyrene	235	250	10	4.2	6.3
Benz[*a*]anthracene	98.6	123	3.1	2.6	24
Chrysene	71.7	102	2.7	2.7	42
Benzo[*b*]fluoranthene	66	99	2.2	2.2	50
Benzo[*k*]fluoranthene	43	83	1.1	1.3	94
Benzo[*a*]pyrene	95.8	115	2.6	2.3	20
Benzo[*ghi*]perylene	53.7	76.1	0.36	0.48	42
Dibenz[*a,h*]anthracene		26	0.07	0.26	
Indeno[123-*cd*]pyrene	60.2	80.8	0.52	0.65	34

* Reference 172.

prepared several days prior to the measurements, possibly resulting in small concentration changes from solvent evaporation. In addition, most of the NIST coal tar PAH concentrations were not within the very narrow range of the calibration solutions, probably leading to considerable errors from extrapolation. The concentrations calculated for the benzene charge-transfer external calibration experiments were also very poor and are not shown.

Three examples of the calibration curves that were obtained from the analyses of the NIST 1647/DPAC-1 solutions using the native/internal standard peak area ratios under normal source conditions are shown as Figure VI-32. The linear regression curves for these and all the other PAH monitored under normal and benzene charge-transfer conditions did pass through the origin (within experimental error) and produced regression coefficients between 0.94 and 0.998. Multi-point calibrations and 1:1 concentration ratios should be used to achieve the best possible accuracy and precision, but these highly linear calibration curves reduce this need.

The concentrations of the NIST coal tar PAH, calculated using the internal standards under normal source conditions, are listed in Table VI-2. Except for fluorene, fluoranthene and benzo[*a*]pyrene, the deviation of the calculated concentrations from the certified values ("relative errors") were less than 9.0%. The partial coelution of another mass 202 isomer (probably acephenanthrylene) with fluoranthene and a mass 166 isomer with fluorene in the coal tar solutions was the reason for their high calculated concentrations. The chromatographic peaks of both benzo[*a*]pyrene and its deutero analog were, however, completely resolved from any interferences. An explanation for its low measured concentration cannot be given.

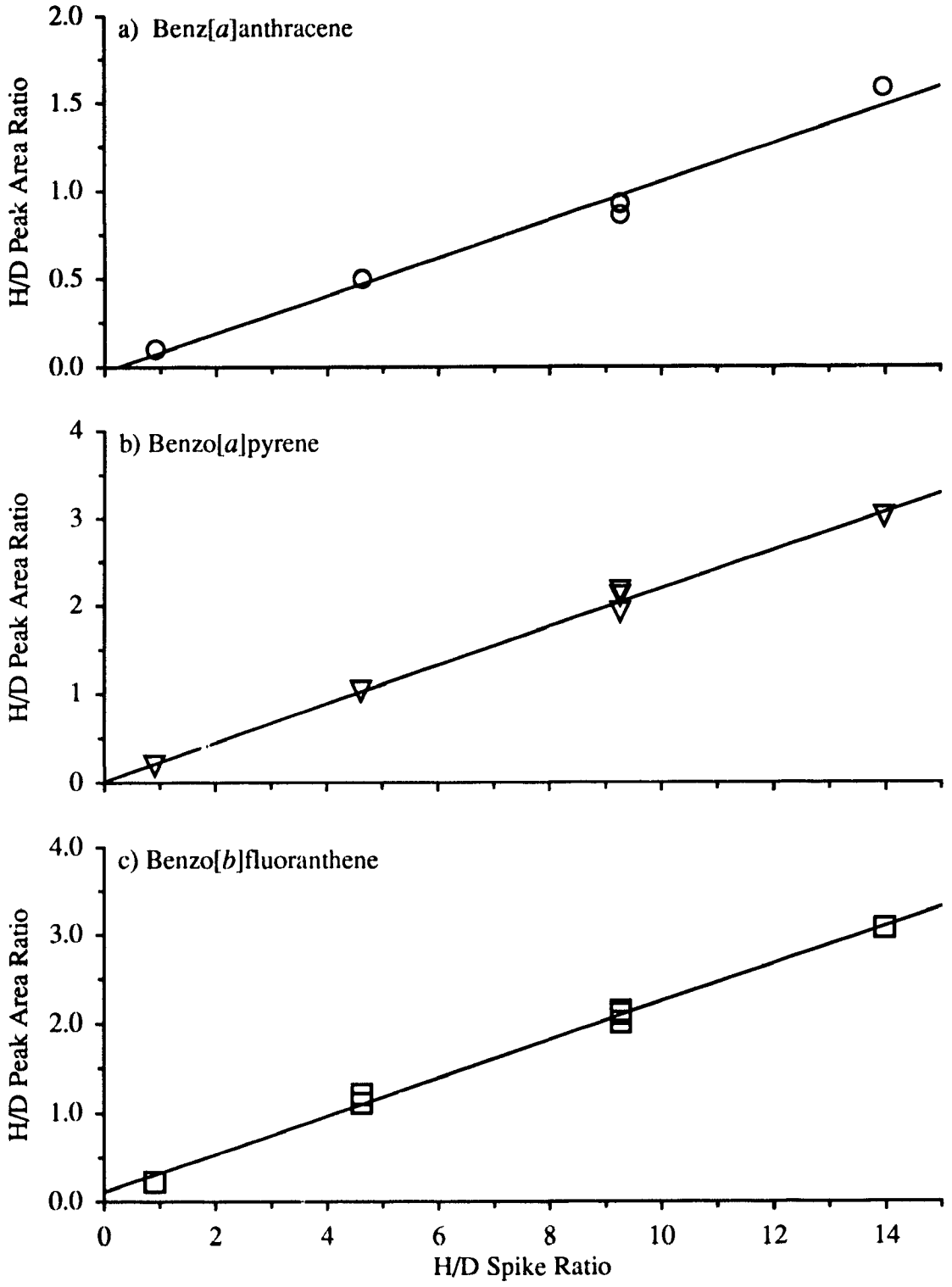

Figure VI-32: Plots of the proteo-/deutero-PAH peak areas vs the SRM 1647/DPAC-1 volume ratios using heated nebulizer LC-MS.

Table VI-2: APCI/MS quantitation results for the NIST coal tar SRM 1597 using internal standardization with perdeutero-PAH under normal source conditions.

Compound	Certified Results* (μg/g)	Calculated Results (μg/g)	Stand. Dev. (n=3)	%RSD (n=3)	Relative Error (%)
Naphthalene	1160	1149	33	2.9	-0.98
Acenaphthylene	250	247	9.0	3.6	-1.1
Acenaphthene		9.2	0.09	0.98	
Fluorene	140	161	7.4	4.6	15
Phenanthrene	462	461	15	3.2	-0.14
Anthracene	101	107	5.7	5.4	6.1
Fluoranthene	322	351	40	11	9.0
Pyrene	235	241	12	5.0	2.6
Benz[*a*]anthracene	98.6	105	4.8	4.6	6.8
Chrysene	71.7	70.4	5.3	7.5	-1.8
Benzo[*b*]fluoranthene	66	63	5.0	7.9	-4.6
Benzo[*k*]fluoranthene†	43	41	3.3	8.0	-4.9
Benzo[*a*]pyrene	95.8	84.8	1.0	1.1	-11
Benzo[*ghi*]perylene	53.7	57.0	1.9	3.3	6.2
Dibenz[*a,h*]anthracene		7.4	0.49	6.6	
Indeno[123-*cd*]pyrene††	60.2	59.9	15	25	-0.50

* Reference 172.

† Perdeutero-benzo[*b*]fluoranthene used as internal standard

†† Perdeutero-benzo[*ghi*]perylene used as internal standard.

The concentrations of the NIST coal tar PAH, calculated using the internal standards under benzene charge-transfer conditions, are listed in Table VI-3. The relative errors and precision of the measurements were very similar to those produced under normal source conditions (Table VI-2). Fluorene, fluoranthene and benzo[*a*]pyrene produced large relative errors for the same reasons as mentioned above, but naphthalene and phenanthrene also produced larger errors than before (Table VI-2). The latter was most likely a result of the much higher background noise (because of the benzene in the source), which hampered the ability to measure peak areas accurately. Clearly, there is no advantage in using benzene charge-transfer ionization over normal source conditions for quantitative analyses.

Table VI-3: APCI/MS quantitation results for the NIST coal tar SRM 1597 using internal standardization with perdeutero-PAH under benzene charge-transfer conditions.

Compound	Certified Results* (μg/g)	Calculated Results (μg/g)	Stand. Dev. (n=3)	%RSD (n=3)	Relative Error (%)
Naphthalene	1160	1072	52	4.9	-7.6
Acenaphthylene	250	254	2.8	1.1	1.6
Acenaphthene		9.0	0.32	3.6	
Fluorene	140	153	5.3	3.5	9.1
Phenanthrene	462	423	11	2.6	-8.3
Anthracene	101	108	3.6	3.3	7.1
Fluoranthene	322	378	9.0	2.4	17
Pyrene	235	239	7.3	3.1	1.7
Benz[*a*]anthracene	98.6	105	2.5	2.4	6.3
Chrysene	71.7	65.4	2.0	3.1	-8.9
Benzo[*b*]fluoranthene	66	64	2.2	3.4	-3.4
Benzo[*k*]fluoranthene†	43	40	1.0	2.5	-6.6
Benzo[*a*]pyrene	95.8	85.9	1.4	1.6	-10
Benzo[*ghi*]perylene	53.7	54.6	0.90	1.6	1.7
Dibenz[*a,h*]anthracene		6.5	0.29	4.4	
Indeno[123-*cd*]pyrene††	60.2	58.8	1.9	3.2	-2.4

* Reference 172.

† Perdeutero-benzo[*b*]fluoranthene used as internal standard.

†† Perdeutero-benzo[*ghi*]perylene used as internal standard.

VI.2 SFC Coupled to the Heated Nebulizer Interface

The most important requirement for any SFC-MS interface is that rapid decompression of the supercritical mobile phase to ambient pressures should occur immediately prior to ionization. For APCI/MS this requirement is not as critical as the decompression to the sub-atmospheric pressures encountered in conventional MS sources. However, if the phase transition does not occur in a controlled manner, the mobile phase and solute molecules will form liquid droplets and molecular clusters, causing detector instability. Overcoming these problems requires efficient heat transfer to the region of phase transition and a reduction in the distance over which the transition occurs.

Preliminary SFC-APCI/MS experiments were performed using a simple heated copper block in which a small hole was drilled to accommodate the SFC restrictor. The block was held on a clamp stand so that it could be moved freely in front of the orifice of the API source. Although mass spectra could be obtained using this approach, the sensitivities achieved for the PAH standards were poor and SFC-MS chromatograms were both noisy and irreproducible. Despite the high linear velocity of the emerging supercritical mobile phase, it was concluded that an additional make-up gas was required to focus and contain the expanding CO_2 jet and, more importantly, to improve the heat transfer to the adiabatically cooled jet.

A spray depositor from the moving-belt LC-MS interface, which allows the introduction of a concentric flow of nebulizing gas, was also tried as an SFC-APCI/MS interface. Although this approach greatly improved the

stability of the ion current and provided usable SFC-MS traces, the depositor was still supported by a clamp stand with essentially the entire laboratory acting as the API source. The quality and type of spectra obtained was therefore affected by the day-to-day condition of the ambient air in the laboratory.

The ideal SFC-APCI/MS interface for routine analytical use should retain the original airtight API flange on the source housing that, with the aid of a small extractor fan, can maintain a controlled APCI "atmosphere" within the housing. In addition, the flange has vernier controls for the precise positioning of the probe in relation to the discharge electrode and the orifice. Therefore, a heated nebulizer LC-MS probe was modified to act as an SFC-MS interface, shown schematically in Figure VI-33. The SFC column is connected to the combined fused silica transfer line and restrictor via a zero-dead-volume union mounted in the probe handle. High-purity air is introduced as a make-up gas (1-2 L/min) through a modified Swagelok union, and flows co-axially around the restrictor to the probe tip. The stainless steel probe tip (shown enlarged) was designed to provide good thermal contact at the end of the restrictor where the phase transition occurs. The probe tip is heated by a coil of resistance wire using a constant current power supply, and its temperature (typically 300°C) is monitored with a thermocouple. This design is capable of accommodating all the major commercial types of SFC restrictors, and allows for rapid replacement should a different flow rate be required or a restrictor become blocked.

Using the optimized interface described above, a microbore packed-column SFC system was coupled to the mass spectrometer and a test mixture

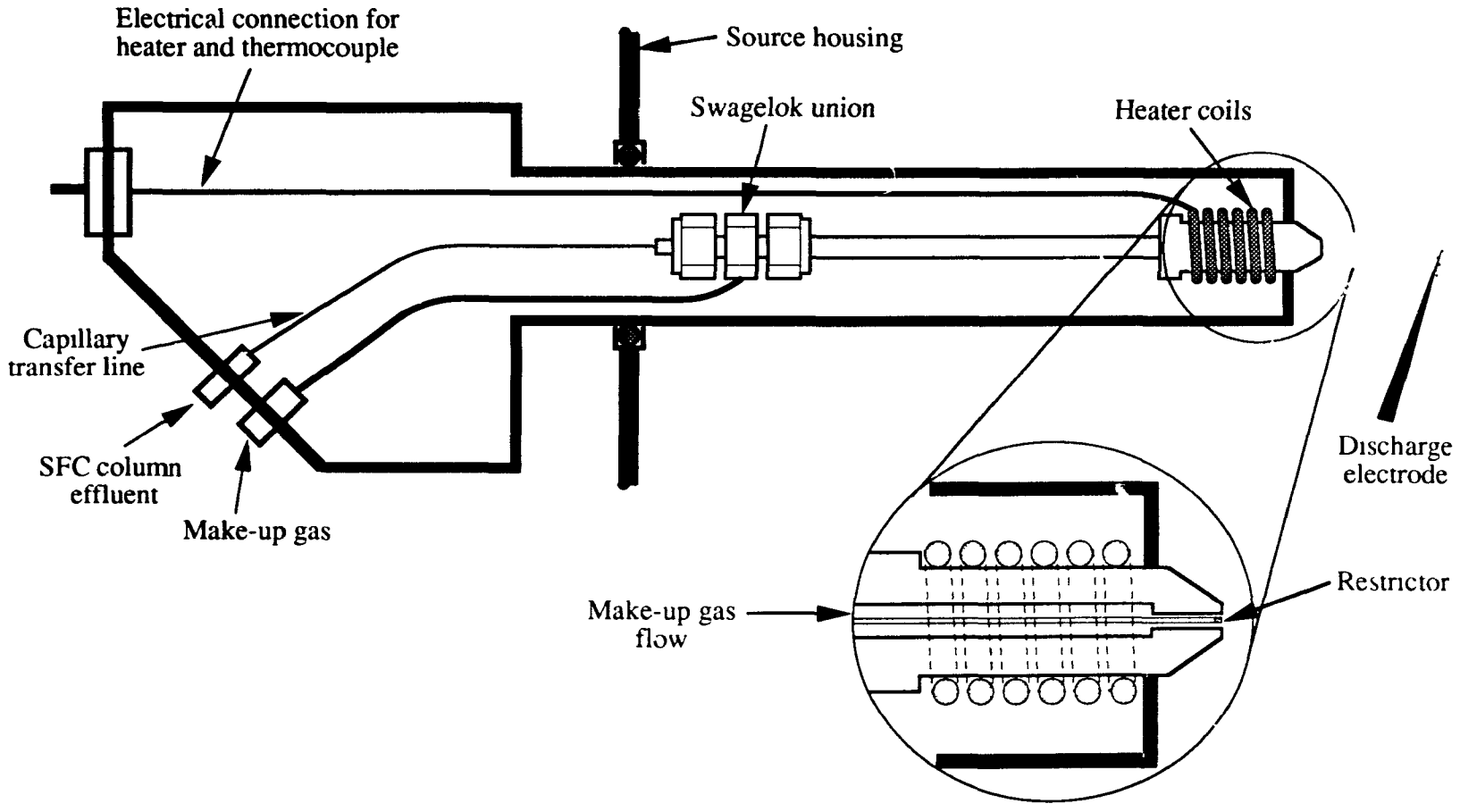

Figure VI-33· Schematic diagram of the SFC-APCI/MS interface.

of PAH analyzed under SFC conditions identical with those established using the PID (Chapter III); Figure VI-34 compares the SFC-PID chromatogram with the SFC-APCI/MS reconstructed ion chromatogram (the sum of $M^{+\cdot}$ and MH^+ ions of all the PAH standards). There was a good correspondence between the PID and APCI traces and no significant loss in chromatographic performance with the new interface was observed. The slight changes in retention time apparent in the SFC-APCI/MS trace, most notable for the late eluting components, was caused by the heat applied to the restrictor in the interface. A decrease in the restictor orifice diameter caused by the heat produced a corresponding reduction in the mobile phase linear velocity.

The APCI/MS response of the low molecular weight PAH (e.g., mass 128 and 178) was very poor because of their low proton affinities. These compounds were ionized primarily by charge-transfer reactions that are inherently less sensitive than proton-transfer under normal source conditions. The APCI response of the standards became greater as the proton affinities of the PAH increased with size.[157] This ionization enhancement, which is identical with that observed under LC-MS conditions, can be clearly seen in the individual SFC-APCI/MS mass spectra shown as Figure VI-35. The base peak in the spectrum of naphthalene and phenanthrene is the $M^{+\cdot}$ ion, while for perylene and benzo[*ghi*]perylene the dominant ion is the protonated molecule. These APCI spectra were almost identical with those acquired under LC-MS conditions shown earlier in Figure VI-3. Adduct ions at $[M+17]^+$ and $[M+33]^+$ were, however, observed in the mass spectra of Figure VI-35. Similar adduct ions were detected in LC-APCI/MS spectra, but their intensities were usually low enough to be hidden in the background noise. A

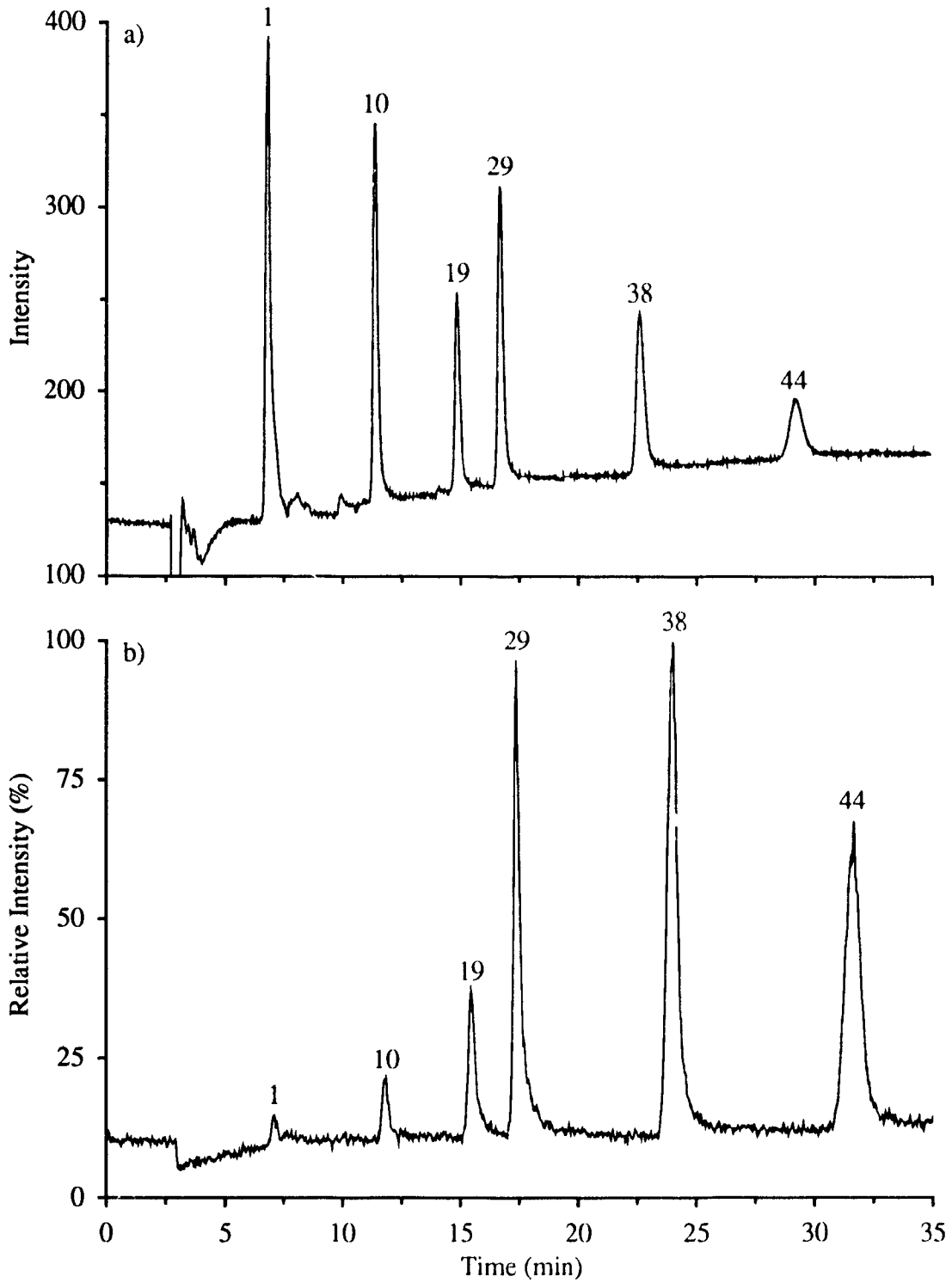

Figure VI-34: (a) SFC-PID and (b) SFC-APCI/MS reconstructed ion chromatograms (sum of $M^{+\cdot}$ and MH^+ ions) from the analysis of PAH standards using a C_{18} column. See Appendix A for compound identities.

discussion of the experiments used to identify these adducts will be continued further on in this chapter once a few more details about the SFC-APCI/MS ionization chemistry are presented.

The relative abundance of the $M^{+\cdot}$ and $[M+H]^+$ ions of the PAH standards in Figure VI-35 could be altered through variations of the source conditions. In particular, day-to-day variations in the $M^{+\cdot}/[M+H]^+$ ratios were observed to correlate with changes in the laboratory humidity. The high purity CO_2 mobile phase being continually sprayed over the discharge needle did not have a high enough moisture content to sustain a sufficient activity of reagent ions in the APCI plasma. Therefore, the ionization process was dependent on the humidity of the surroundings for the production of reactant ions (i.e., the hydrated protons).

In an attempt to control and enhance APCI proton-transfer chemistry, water vapour was added to the source by passing the make-up gas over a reservoir of water. Figure VI-36a shows the mass spectrum of benz[*a*]anthracene acquired with a high moisture content in the source. In comparison with the spectrum acquired previously under normal source conditions (Figure VI-35d), the addition of water had a negligible effect on the $M^{+\cdot}$ intensity while producing an absolute increase (approximately 3-fold) in the $[M+H]^+$ ion intensity. Similar effects were observed for other PAH standards (e.g., mass 252 276 and higher), although it was much less pronounced or even absent for the low molecular weight PAH (e.g., mass 128 and 178) because of their lower proton affinities.

As an alternative to proton-transfer ionization, charge-transfer chemistry in the source was also enhanced by using benzene as a chemical

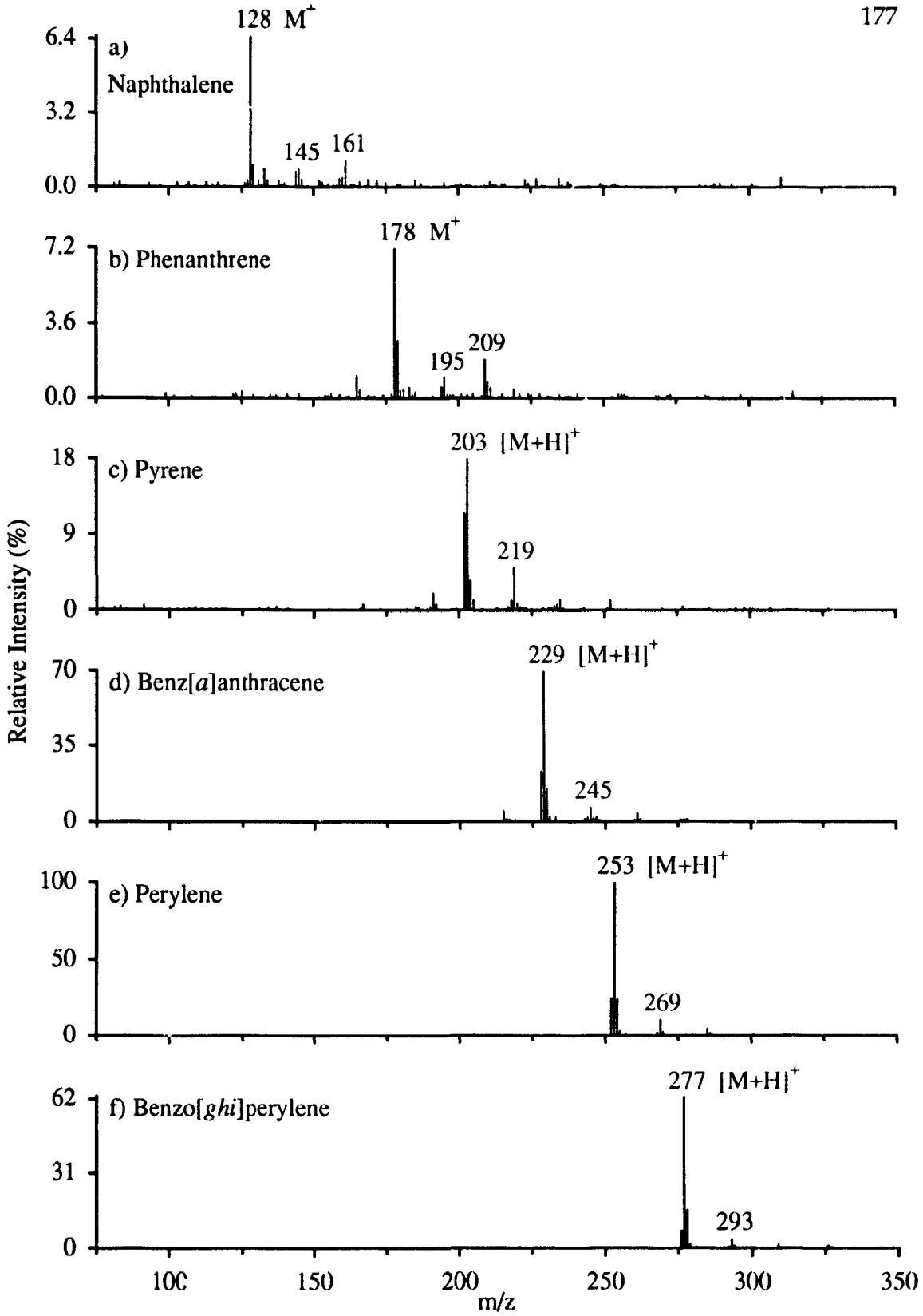

Figure VI-35: Background subtracted positive ion SFC-APCI mass spectra of PAH standards.

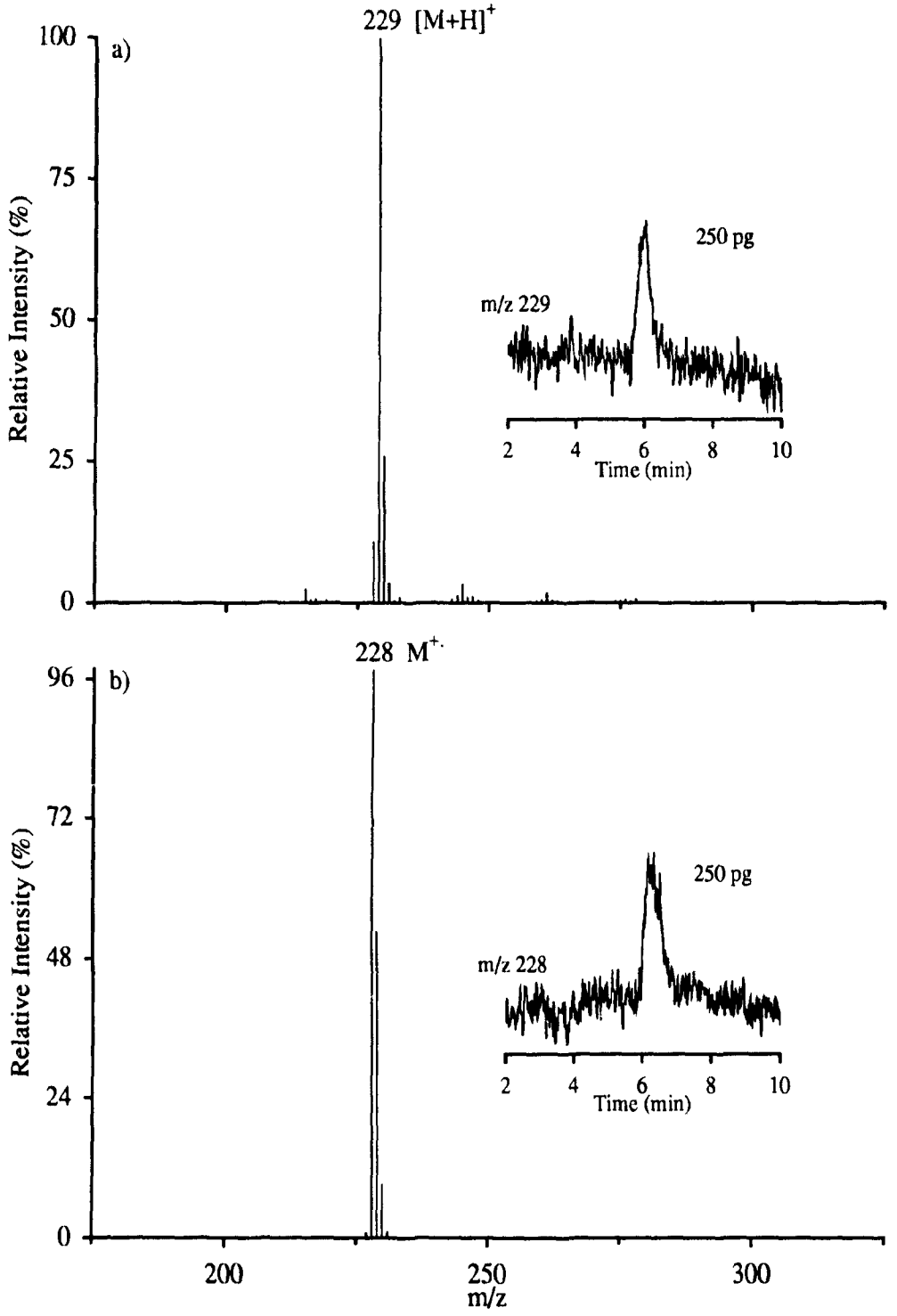

Figure VI-36: Background subtracted positive ion SFC-APCI mass spectra of benz[*a*]-anthracene using (a) water and (b) benzene vapour in the source. Insets show the single ion monitoring responses of the (a) protonated molecule and (b) molecular ion for 250 pg of benz[*a*]anthracene.

ionization modifier. Figure VI-36b shows the APCI mass spectrum obtained for benz[*a*]anthracene when the make-up gas was passed over a reservoir of benzene. A comparison of this spectrum with that in Figure VI-36a (which was acquired with a high moisture content in the source), illustrates that the predominant ionization process was charge-transfer with benzene cations. The relative intensity of the $[M+H]^+$ ion at m/z 229 is still significant because of the high proton affinity of benz[*a*]anthracene.

The sensitivities that can be achieved for PAH using SFC-APCI/MS will depend on the ionization energies and proton affinities of the individual compounds and the ionization conditions. In general, greater sensitivities can be achieved for low molecular weight PAH (e.g. naphthalene and phenanthrene) with benzene charge-transfer chemical ionization, while high molecular weight species are best analyzed under proton-transfer conditions. The insets in Figures VI-36a and VI-36b show the single ion monitoring SFC-APCI/MS responses obtained for the injection of 250 pg of benz[*a*]anthracene under proton-transfer and charge-transfer conditions, respectively. These results indicated that the detection limits for benz[a]anthracene were comparable at approximately 250 pg (signal/noise ratio of 3:1) for these two modes of ionization. Lower detection limits, approximately 45 and 160 pg, for benz[*a*]anthracene under normal and benzene charge-transfer conditions, respectively, were obtained previously by LC-APCI/MS. The broad chromatographic peaks produced by the SFC system (0.53 minutes wide at half height compared to 0.23 produced by LC) were responsible for the higher detection limits.

Although the experiments described above illustrate the tremendous

potential of using chemical ionization modifiers to control and enhance certain reactions in APCI, they were extremely difficult to perform. The make-up gas inlet was initially developed for improving the nebulization and heat transfer of the emerging SFC mobile phase. The gas flow required for this purpose was not necessarily the optimum flow rate for the introduction of the modifier; for example, too much benzene or too little water was added to the source under normal gas flows. In order to provide a practical analytical technique, a means of reproducibly controlling the composition of the APCI plasma in the source housing is needed. A modification of the current SFC probe tip to include an additional chemical ionization modifier inlet has been made. The evaluation of this new design is still in progress.

Isotopically labelled chemical ionization modifiers, introduced by passing the make-up gas over a solvent reservoir as described above, were used to probe the identity of the adduct ions seen in Figure VI-35. The number of hydrogens in each adduct was determined by adding D_2O to the source. Figure VI-37 compares the spectra of benz[*a*]anthracene acquired under (a) normal source conditions, and (b) under the same conditions as in (a) but with D_2O added to the make-up gas. An abundance of adduct ion signals were produced since the intensity of de-clustering reactions in the sampling orifice region of the MS was purposely reduced to a minimum. The addition of D_2O caused an increase in proton-transfer ionization (compare the relative intensity of the $M^{+\cdot}$ and MH^+ ions of Figure VI-37a), but the absolute ion intensities of the adducts remained similar.

Although adduct ions as high as m/z 327 were detected (Figure VI-37a),

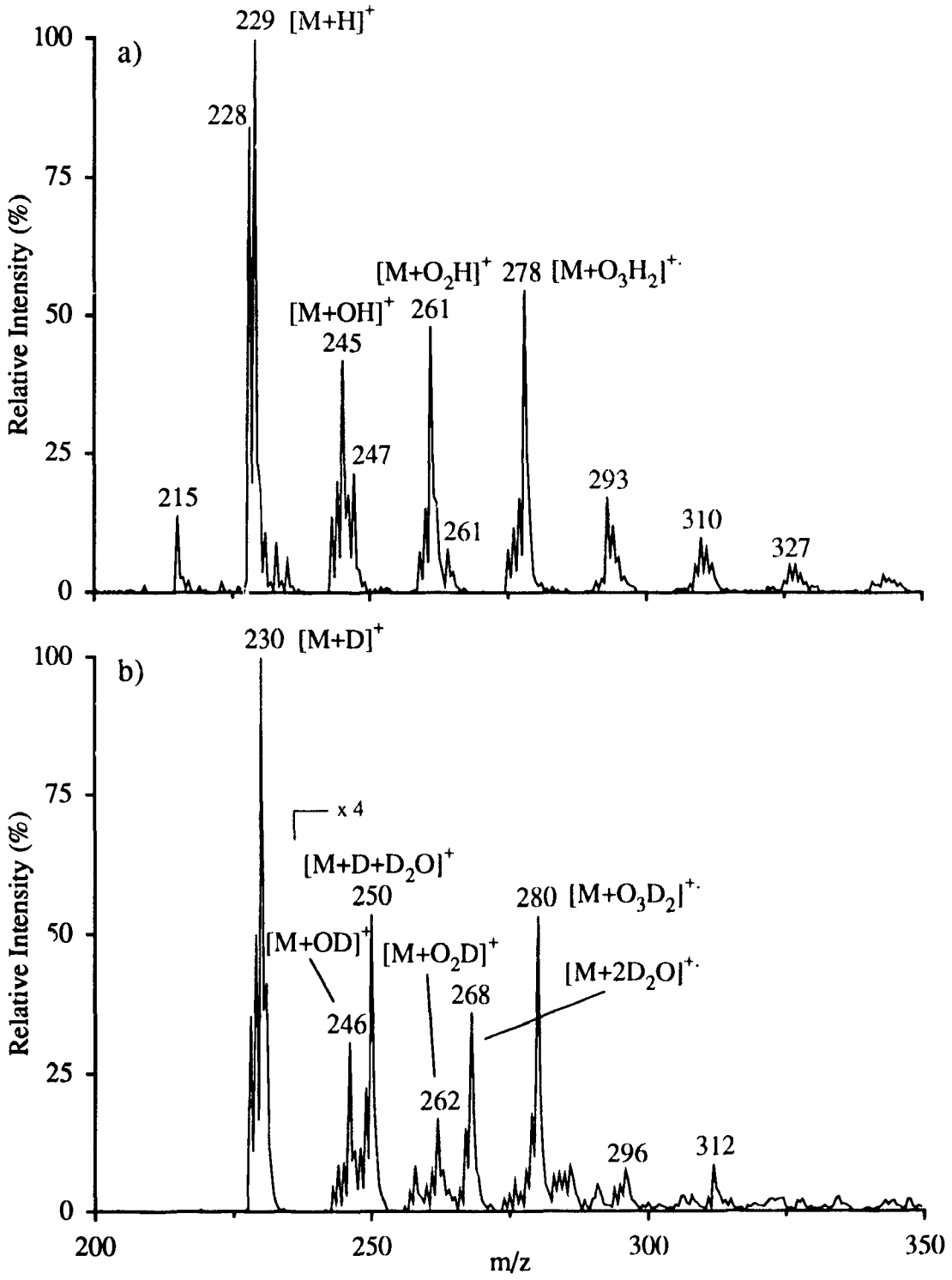

Figure VI-37: Background subtracted positive ion SFC-APCI mass spectra of benz[*a*]-anthracene using (a) normal source conditions and (b) D_2O vapour in in the source.

a detailed investigation was carried out on only the first three intense ions, m/z 245, 261, and 278. The tentative identification of these ions, based on the D_2O spectrum, are shown on the mass spectra of Figure VI-37. Water cluster ions at m/z 247 $(M+H+H_2O)^+$ and 264 $(M+2H_2O)^{+\cdot}$ in Figure VI-37a and at m/z 250 $(M+D+D_2O)^+$ and 268 $(M+2D_2O)^{+\cdot}$ in Figure VI-37b, were the result of inadequate de-clustering reactions in the MS orifice region and are not related to the adducts.

Tandem mass spectrometric experiments were used to investigate the fragmentation pathways of the adduct ions. Three modes of operation were used: 1) fragment ion spectra were acquired by selecting a single ion (precursor) in the first quadrupole (Q1), colliding the selected precursor with argon target gas in the second quadrupole (Q2) and scanning the spectrum of the fragment (product) ions with the third quadrupole (Q3); 2) spectra of the precursor ions that yield a common product ion (precursor ion scan) were obtained by mass selecting a single ion with Q3 while scanning Q1 and promoting dissociation of the precursor ions in the Q2 collision zone; and 3) spectra of precursor ions that lose common neutral fragments (constant neutral loss scan) were recorded by parallel scans of Q1 and Q3 with a constant mass difference while collisionally induced dissociation (CID) occurred in the collision zone of Q2.

The fragment ion spectra of the $[M+O_3H_2]^{+\cdot}$ and $[M+O_3D_2]^{+\cdot}$ adduct ions of benz[a]anthracene are shown as Figures VI-38a and VI-38b, respectively. Since the $[M+O_3H_2]^{+\cdot}$ adduct is an odd electron species, it first loses a hydroxyl radical followed by losses of H_2O and CO neutrals. These fragments were confirmed with the corresponding fragmentation of the

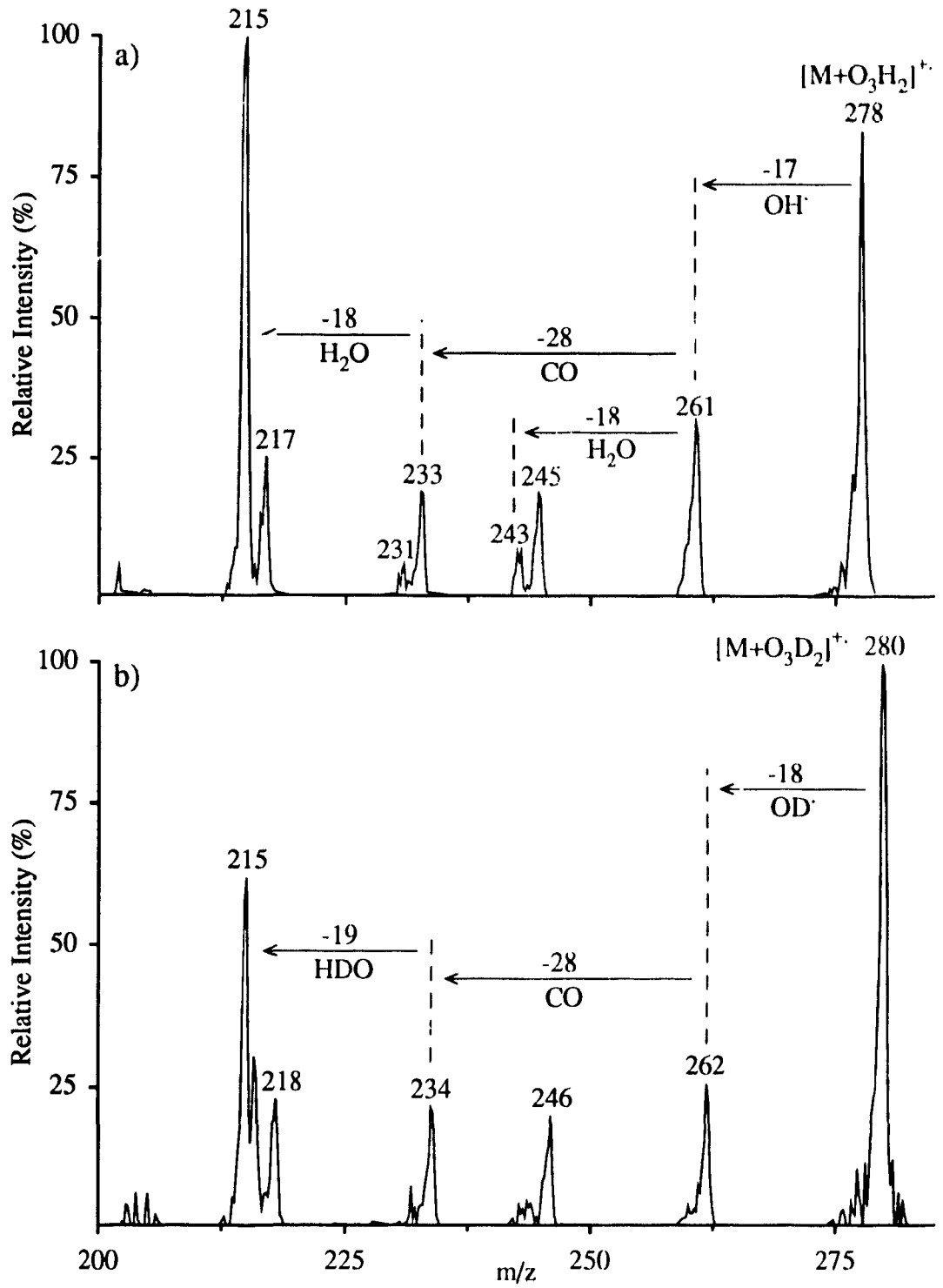

Figure VI-38: Fragment ion APCI mass spectra of (a) the m/z 278 adduct ion in Figure VI-37a, and (b) the m/z 280 adduct ion in Figure VI-37b.

$[M+O_3D_2]^{+\cdot}$ adduct. Similar experiments were performed on the other adduct ions (using fragment ion, parent ion and neutral loss scans), revealing a complex fragmentation pattern shown as Figure VI-39. Several experiments performed on the higher mass adducts (e.g., m/z 293, 310 and 327) have shown that they do not produce to the same fragment ions shown in Figure VI-39. These high mass adducts actually fragment to form ions that had a difference of few mass units from those of the m/z 278 adduct; for example, m/z 243, 244, 260, 276, 277 and 294 (which are evident in Figure VI-37a).

The formation mechanism of these adducts and the identity of the reactive species in the APCI source have not been confirmed. However, these adducts, their fragments, and the $M^{+\cdot}/[M+H]^+$ ratios of the PAH can be used as a means of distinguishing isomers. For example, the SFC-APCI/MS spectra of the five isomers of mass 228 PAH are shown as Figures VI-40. Although all the isomers produced the same adducts and fragments, their relative intensities were different:

Mass 228 Isomer	$M^{+\cdot}/[M+H]^+$	$[M-13]^+/M^{+\cdot}$	$[M+17]^+/M^{+\cdot}$
Benzo[*c*]phenanthrene	0.139	1.016	0.324
Benz[*a*]anthracene	0.106	0.192	0.281
Chrysene	0.137	0.913	0.581
Triphenylene	0.206	0.0281	0.204
Tetracene	0.142	0.0	--

Correlations between the ratios given in the table above and the physical properties of the isomers (i.e., ionization energies and proton affinities) could not be made. The chemistry occurring in the APCI plasma

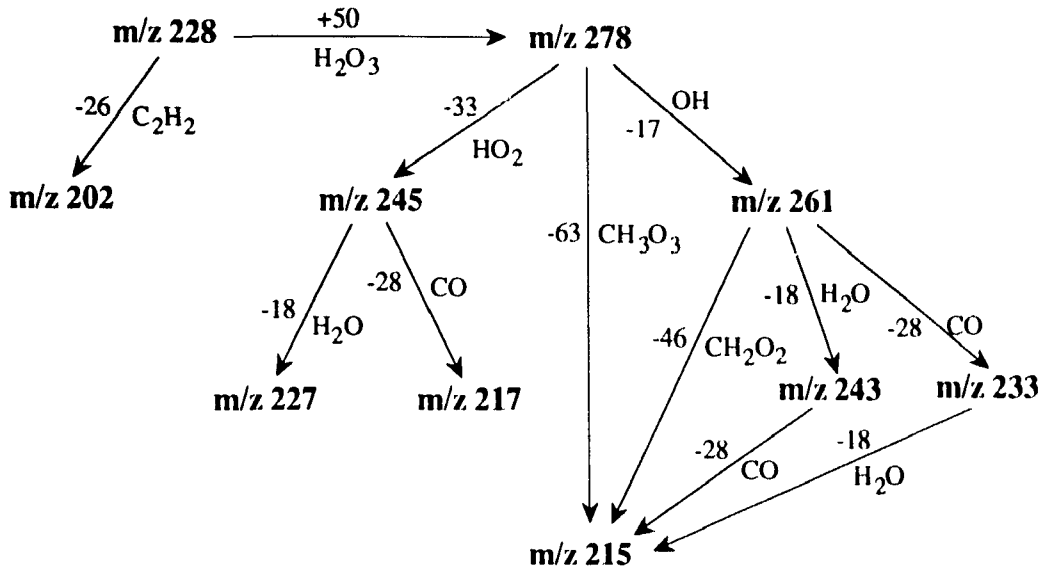

Figure VI-39: The m/z 278 adduct ion fragmentation pathway as deduced from MS/MS experiments.

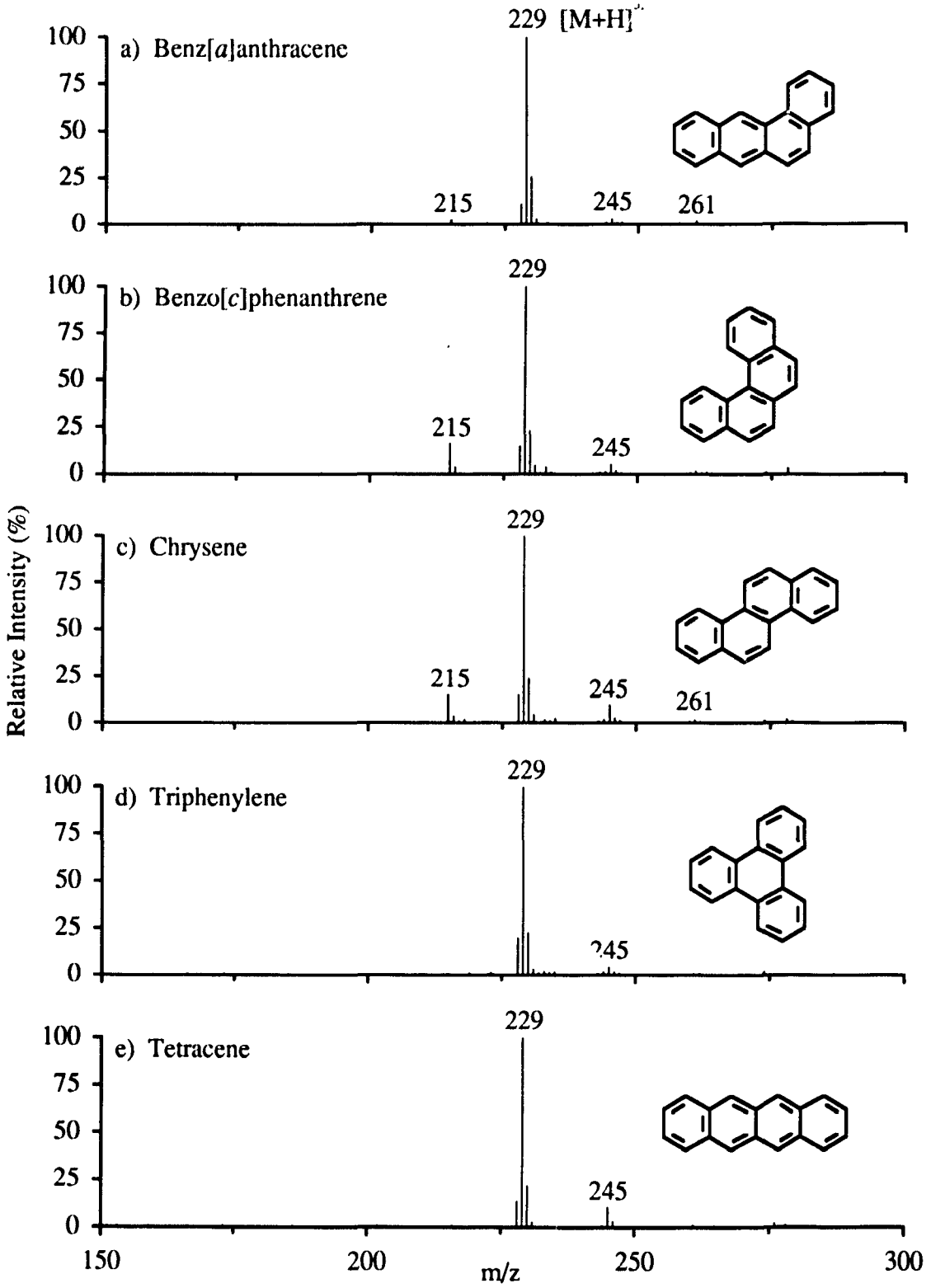

Figure VI-40: Background subtracted positive ion SFC-APCI mass spectra of five mass 228 PAH isomers.

and the subsequent de-clustering reactions in the gas curtain and orifice region of the MS are very complex. A better understanding of the APCI chemistry and, in particular, the adduct ion formation processes may, however, provide the basis of a reliable method of distinguishing PAH isomers.

SFC-APCI/MS of complex mixtures of PAC

The remainder of the SFC-APCI/MS experiments were performed using normal source conditions (i.e., ionization modifiers were not added to the source). Fluctuations in the laboratory humidity resulted in only minor changes in the PAH $M^{+\cdot}/[M+H]^+$ ratios observed in day-to-day experiments.

The SFC-PID trace and the SFC-APCI/MS total ion chromatogram of the NIST coal tar material separated on a C_{18} column are compared in Figure VI-41. As noted earlier, the shift in retention times apparent in the APCI trace (which is most pronounced for the late eluting components) was a result of heating the restrictor in the SFC-MS interface. The enhancement in the ionization of high molecular weight PAC (by proton-transfer reactions) is also clearly evident in the comparison of the two chromatograms.

The selected ion chromatograms for several components in the coal tar are shown as Figure VI-42. The chromatographic peaks of the early eluting compounds (m/z 128 to 178), which are the most concentrated components in this material, exhibit severe tailing from column overloading. Even though very small amounts of solution were injected, the sample capacity of the small diameter column being used (1 mm ID) is extremely low. The

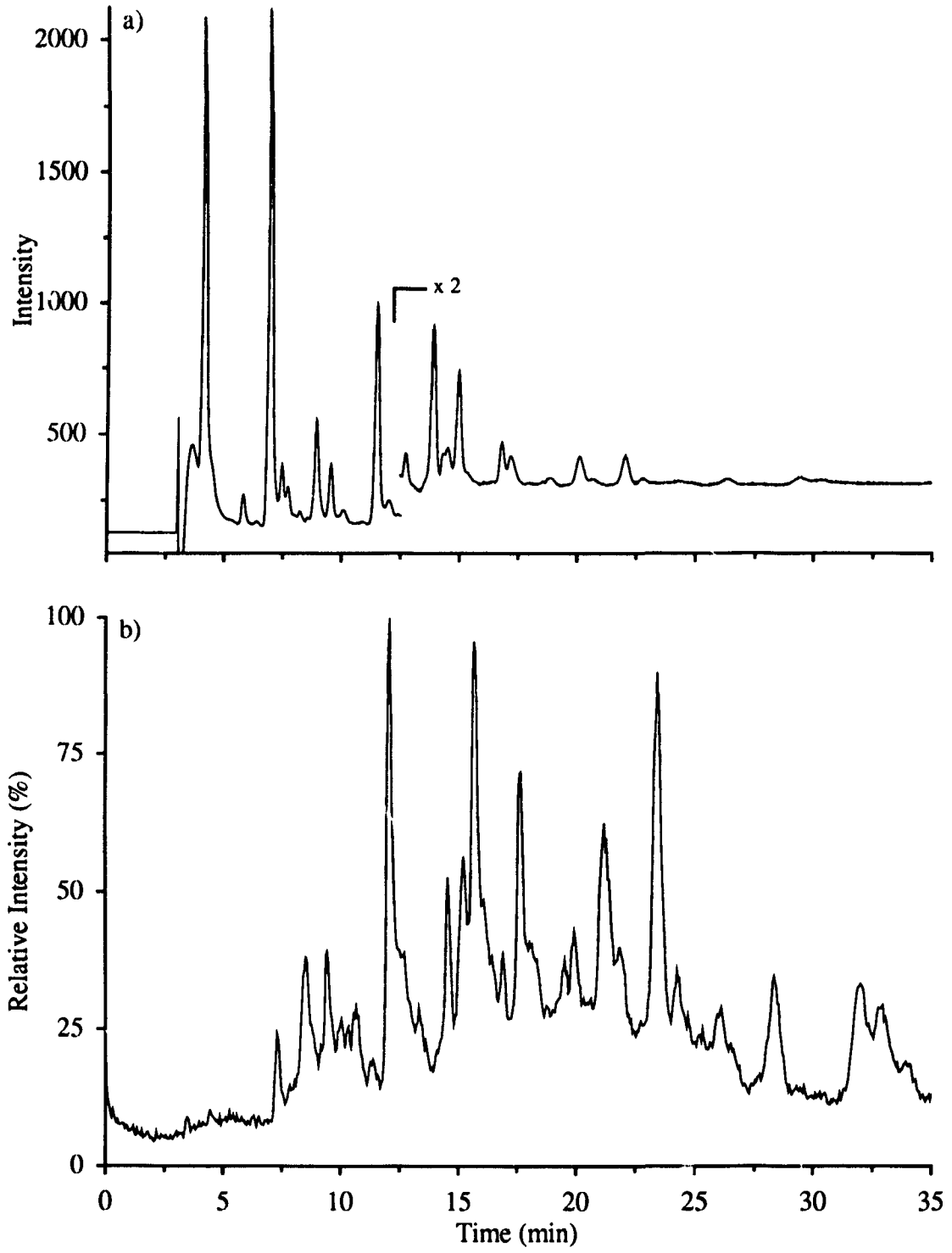

Figure VI-41: (a) SFC-PID and (b) SFC-APCI/MS total ion chromatograms from the analysis of the NIST SRM 1597 coal tar mixture using a C_{18} column.

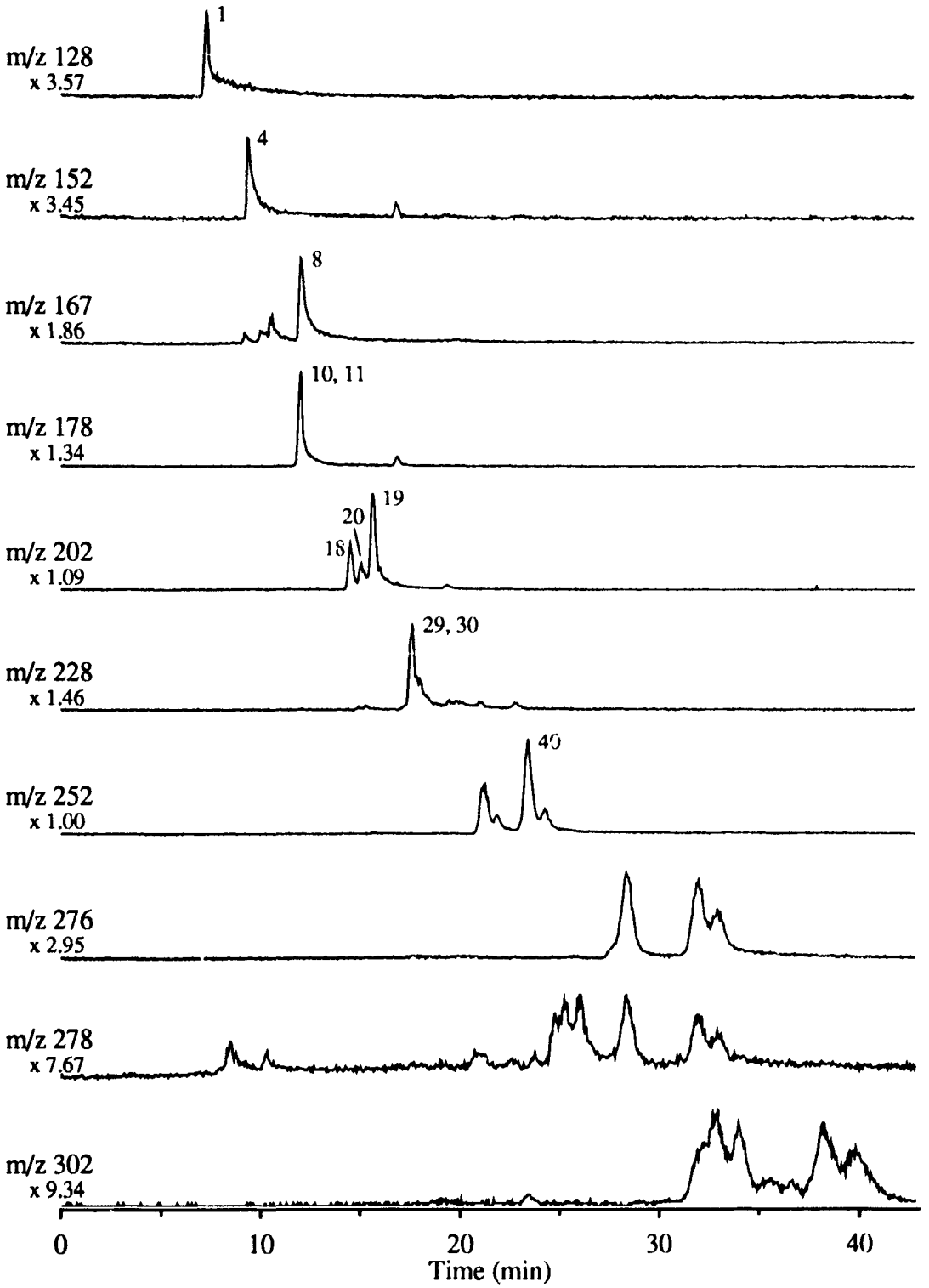

Figure VI-42: SFC-APCI/MS selected ion chromatograms (sum of $M^{+\cdot}$ and MH^{+} ions) generated from the analysis of Figure VI-41b. See Appendix A for compound identities.

chromatographic peaks of the later eluting components, which are present in much lower concentrations, do not exhibit this peak tailing.

The peak widths of the components shown in Figure VI-42 are, in general, twice as wide as those produced by an LC separation. Although a pressure gradient was used in the separation (which is similar to temperature programming in GC or gradient elution in LC), the chromatographic peak widths continue to increase with elution time (e.g., compare m/z 178 with m/z 276). In addition, the high molecular weight PAC detected previously by LC-APCI/MS (greater than mass 302, see Figure VI-19) were retained on the column. Clearly, the solvating strength of the supercritical CO_2 mobile phase was inadequate for the separation on the C_{18} column.

The addition of polar modifiers, such as methanol, has been used to improve peak shapes and reduce retention times of PAH on SFC columns.[196] For polar solutes, this effect is commonly attributed to competition between the modifier and the solute for active sites on the stationary phase.[101] However, other effects that can influence retention are the intermolecular attraction between methanol and solute molecules and the increased solvating power due to the presence of methanol.[99] For PAH, the reduced retention is probably caused principally by the latter effect.

Preliminary SFC experiments using 1 to 10% methanol in CO_2 as the mobile phase have shown significant decreases in PAC retention. However, the solvating power of the mixed mobile phase was strong enough to strip the stationary phase from the silica particles and subsequently block the restrictor after just a few analyses. Better columns with more stable chemically bonded phases will be required to overcome this problem.

The resolution of PAH isomers demonstrated in Figure VI-42 was poor in comparison to previous LC separations (e.g., Figures VI-17 to VI-19). For example, the NIST coal tar is known to contain 2 mass 178 isomers, at least 3 mass 228 isomers and up to 6 mass 252 isomers;[172] most of these were detected in the LC chromatograms (Figures VI-17 to VI-19), but not in the SFC chromatograms (Figure VI-42). The only exception to this statement is the SFC separation of the mass 202 PAH; three isomers, fluoranthene, acephenanthrylene and pyrene, are clearly visible in Figure VI-42. The Vydac 201TP reversed-phase LC column was unable to separate acephenanthrylene from fluoranthene (Figure VI-17).

The remaining two analyses of the tar sand oil fractions were performed with a 1 mm ID packed silica column instead of the C_{18} column used in the coal tar analysis. Lower PAC retention times and the ability to elute higher molecular PAC were the main reasons for using the silica phase.

The selected ion chromatograms for the mass 228 PAH and their alkylated homologues present in the tar sand oil's neutral PAC fraction are shown as Figure VI-43. In comparison to reversed-phase LC separations (e.g., Figure VI-26), the resolution of individual PAH isomers and the alkyl homologues was very poor (i.e., all the mass 228 PAH and alkyl derivatives elute at approximately 20 minutes). Reversed-phase materials separate PAC according to their solubility in the polar mobile phase (i.e., based on the number and length of alkyl substituents) while polar normal phase packings separate according to analyte polarity (i.e., PAC compound class). The position and length of an alkyl substituent on PAH does not affect the polarity of the molecule and consequently, the PAC isomers and alkyl homologues

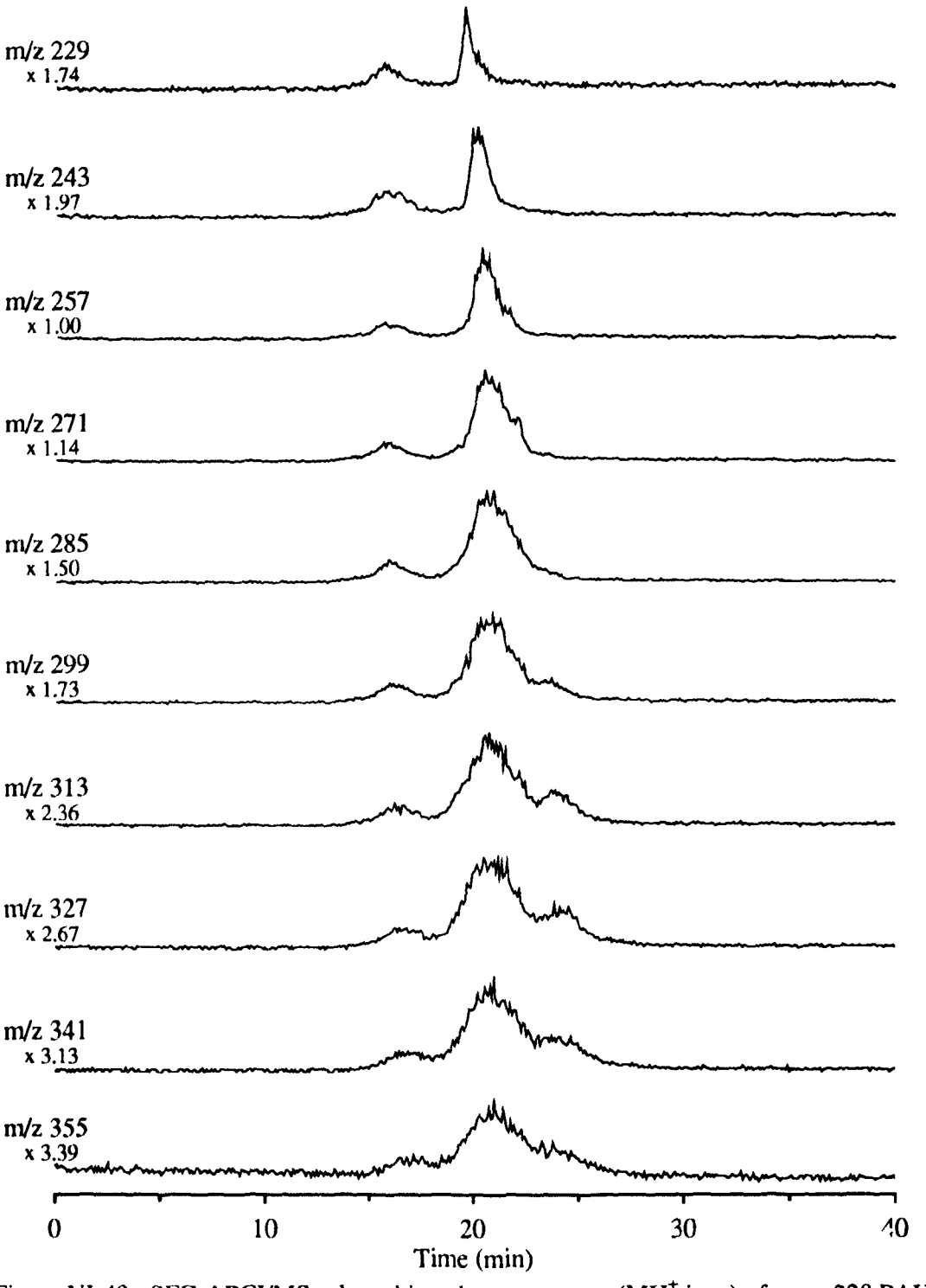

Figure VI-43: SFC-APCI/MS selected ion chromatograms (MH^+ ions) of mass 228 PAH and their alkylated homologues generated from the analysis of the tar sand oil neutral fraction using a silica column.

are not well resolved on the silica column.

The selected ion chromatograms for carbazole and several of its alkylated homologues identified in the tar sand oil's nitrogen-containing PAC fraction are shown as Figures VI-44. These chromatograms, like the previously acquired RPLC-APCI/MS traces (Figure VI-28), demonstrate that highly alkylated carbazoles are the predominant components of this fraction. The improved resolution of the isomers and poor separation of the alkyl homologue series observed in these traces was also a result of the silica stationary phase. Polar packing materials are capable of resolving isomers with respect to the location of the polar sites on the molecule; thus, the alkylated carbazole isomer resolution was probably a result of the varying position of the alkyl group(s) with respect to the polar site.

The retention of the high mass PAC (>350 Da) on the SFC column did not present a serious problem during the analysis of the tar sand oil fractions Although PAC as high as mass 500 have been detected in these samples, the aromatic portion of these molecules are between 128 and 252 Da. The remaining aliphatic portion (from 250 to 350 Da) does not significantly increase the retention over that of the unsubstituted aromatic. A representative mass spectrum taken from the SFC-APCI/MS analysis of the nitrogen-containing fraction presented in Figure VI-45a, shows that protonated molecules of alkylated carbazoles as high as m/z 490 could be detected. Similarly, the more complex spectrum from the neutral fraction, shown as Figure VI-45b, illustrates that many ions were also observed at high mass.

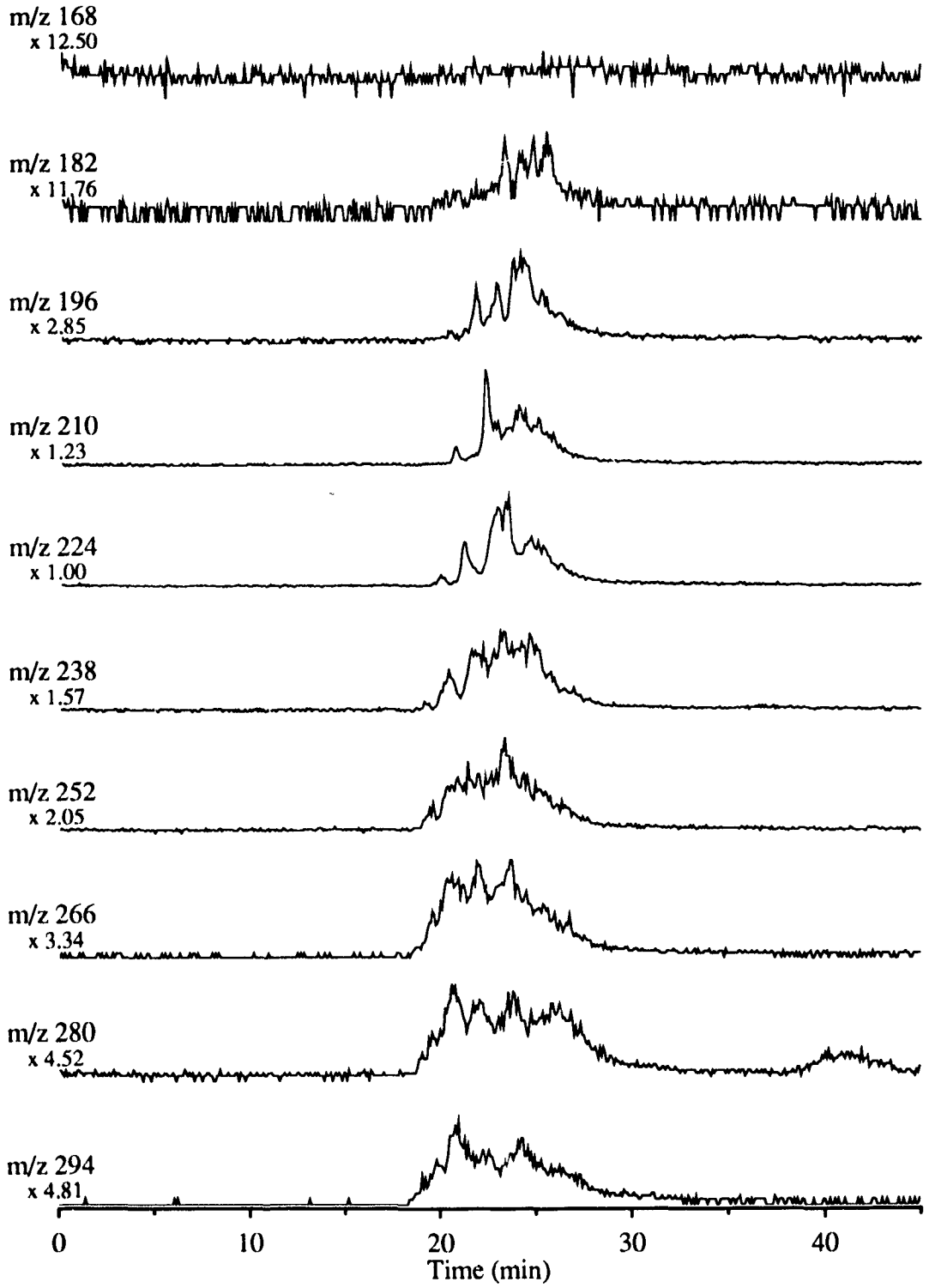

Figure VI-44: SFC-APCI/MS selected ion chromatograms (MH^+ ions) of carbazole and its alkylated homologues generated from the analysis of the tar sand oil nitrogen-containing PAC fraction using a silica column.

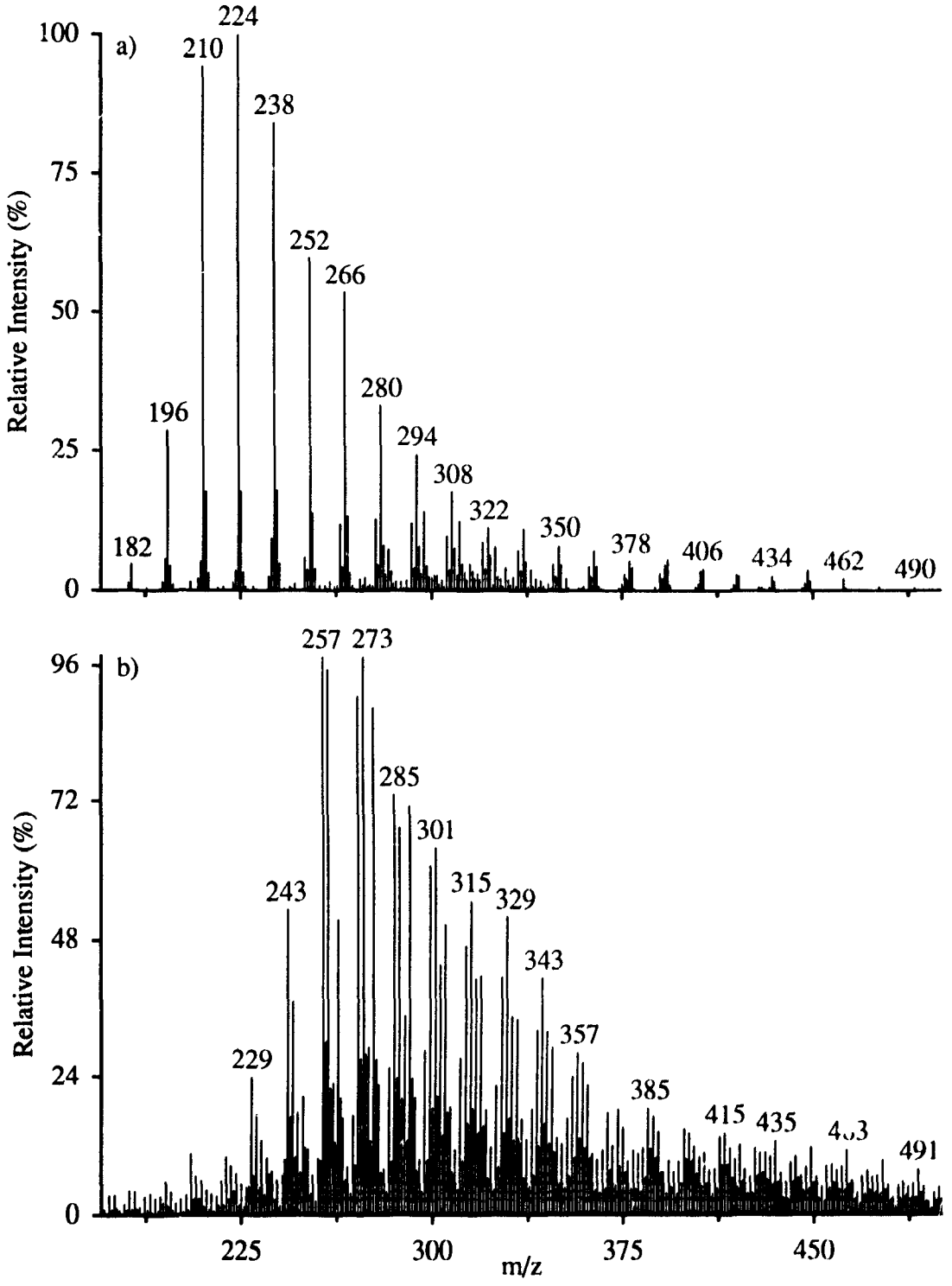

Figure VI-45: Background subtracted positive ion SFC-APCI mass spectra from the analyses shown in (a) Figure VI-44 and (b) Figure VI-43.

VII. THE IONSPRAY INTERFACE

Spray ionization techniques have revolutionized the direct coupling of liquid chromatography to mass spectrometry. The first such technique to gain widespread acceptance was the thermospray interface introduced by Blakley and Vestal.[197] More recently, techniques based upon ion evaporation from charged micro-droplets at atmospheric pressure (described below) have extended the range of analytes accessible to LC-MS to much larger and more labile molecules.[198,199] The electrospray technique[198,199] generates a charged aerosol at atmospheric pressure from a capillary held at an electric potential typically between 3 - 5 kV; the high voltage functions to both form and charge the micro-droplets. A significant limitation of electrospray is that it restricts LC flow rates to less than about 10 μL/minute. If higher voltages are used in an effort to nebulize increased liquid flows, a discharge at the electrospray capillary may occur producing a noticeable decrease in sensitivity for most analytes.

The introduction of ionspray (pneumatically assisted electrospray) by Henion and co-workers[200] has permitted the extension of the ion evaporation phenomenon to flow rates of up to 200 μL/minute. The ionspray interface facilitates the nebulization of liquid droplets by using a high flow of nitrogen or air coaxial to an electrospray capillary, Figure VII-1. The enhanced droplet formation associated with ionspray increases the stability, ruggedness and flexibility of the technique. For example, ionspray provides the flexibility required to permit interfacing with a variety of liquid separation techniques including those requiring gradient elution (e.g., 100% water to 100% methanol or acetonitrile) and modifiers or buffers.

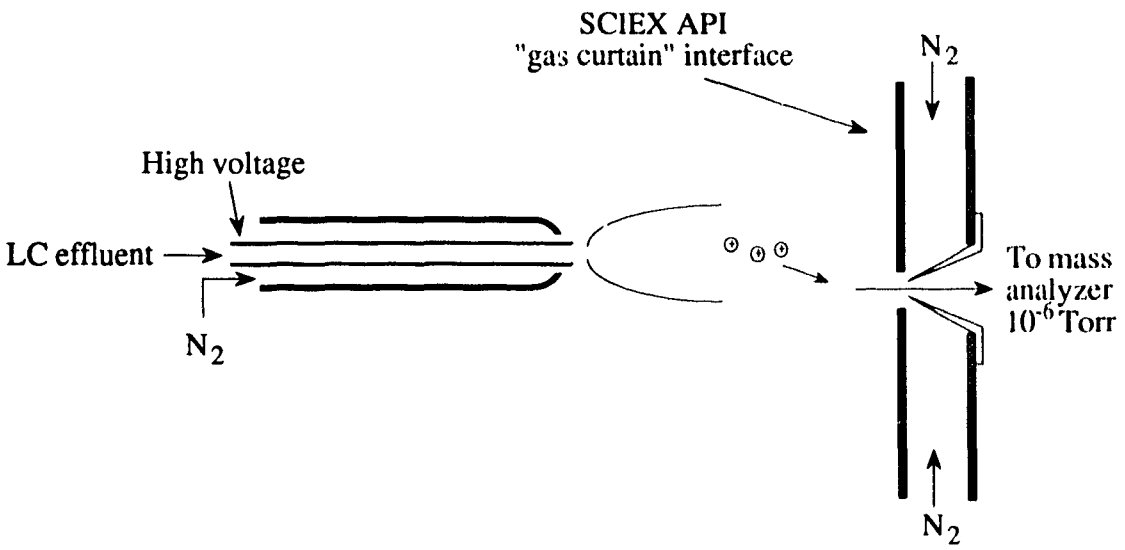

Figure VII-1: A schematic diagram of the ionspray LC-MS interface.

The ionization mechanism used by both electrospray and ionspray, called ion evaporation, is a process in which ions are emitted from charged droplets directly into the gas phase. The mechanism by which ions can be emitted from a liquid into the gas phase, which is currently at issue,[201,202] is independent of how the droplets are originally formed or charged. The theoretical treatment of Iribarne and Thomson[201] views this process as direct evaporation of solvated ions from small (< 1 μm) droplets (Figure VII-2) whose charge-to-volume ratio is almost large enough that electrohydrodynamic instability will result in droplet disintegration (the Rayleigh stability limit). At some point, all the solvent will have evaporated from the droplet, leaving a dry particle consisting of the involatile components of the solution. If this stage is reached before the critical ion evaporation limit, then the net charge will simply remain on the particle and no gas phase ions will be observed. This will happen if the initial droplet charge is too low, or if there is too much involatile material in the solution to allow a small enough final radius to be achieved.

This proposal has been criticized by Röllgen and co-workers[202] based on theoretical arguments to the effect that the field strength required for ion evaporation usually exceeds that for droplet break-up by the Rayleigh mechanism. Röllgen and co-workers[202] suggested that the gas-phase ions are produced predominantly by solvent evaporation from extremely small droplets (≈ 1 nm diameter), each of which contains just one excess ion, produced by a cascade of droplet divisions via Rayleigh instability. The model of Iribarne and Thomson[201] essentially proposes that the later stages of this cascade can be avoided by droplet disintegrations involving a highly

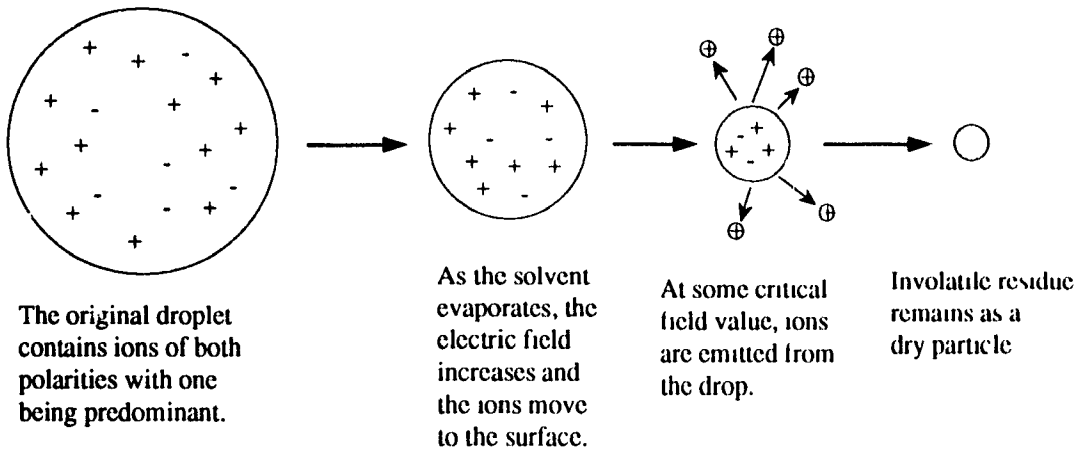

Figure VII-2: The ion evaporation process as proposed by Iribarne and Thomson (Reference A591).

asymmetric division such that one of the products is much smaller than the other and contains a single excess ion. The possibility that the two rival views might be mechanistically indistinguishable was raised previously by Smith *et al.*[203]

Despite the ion evaporation mechanism, it has become clear that the best results, in terms of both sensitivity and detection limits, are achieved for compounds that are already ions in solution (such as metallic and organic salts). Compounds with functionalities that can be ionized via solution-phase acid/base chemistry, such as carboxylic acids and amines, are also amenable to ionspray MS. In addition, some polar molecules are also ionized via attachment of ions other than a proton. For example, Na^+ or CH_3COO^- ions, which are either added to or already present in the analyte solution, are sometimes observed to attach to the analyte molecules.[204]

Since the applicability of ionspray ionization is limited to compounds that are ionic in solution or that can be ionized in solution by acid/base chemistry or by adduct formation, several important classes of compounds, such as PAH, cannot be analyzed with this technique. Certain heterocyclic and substituted PAC are, however, slightly basic and can be ionized in solution. For example, Figure VII-3a shows the ionspray mass spectrum acquired from the injection of 50 ng of aminopyrene in a 200 μL/min flow of 50% aqueous acetonitrile. Ionspray mass spectra of quinoline could also be obtained under these conditions, although other polar PAC (e.g., carbazole, cyano- and nitro-PAC) were not detected.

The addition of small amounts of organic acids to the mobile phase, which is often used to improve the chromatographic performance of polar

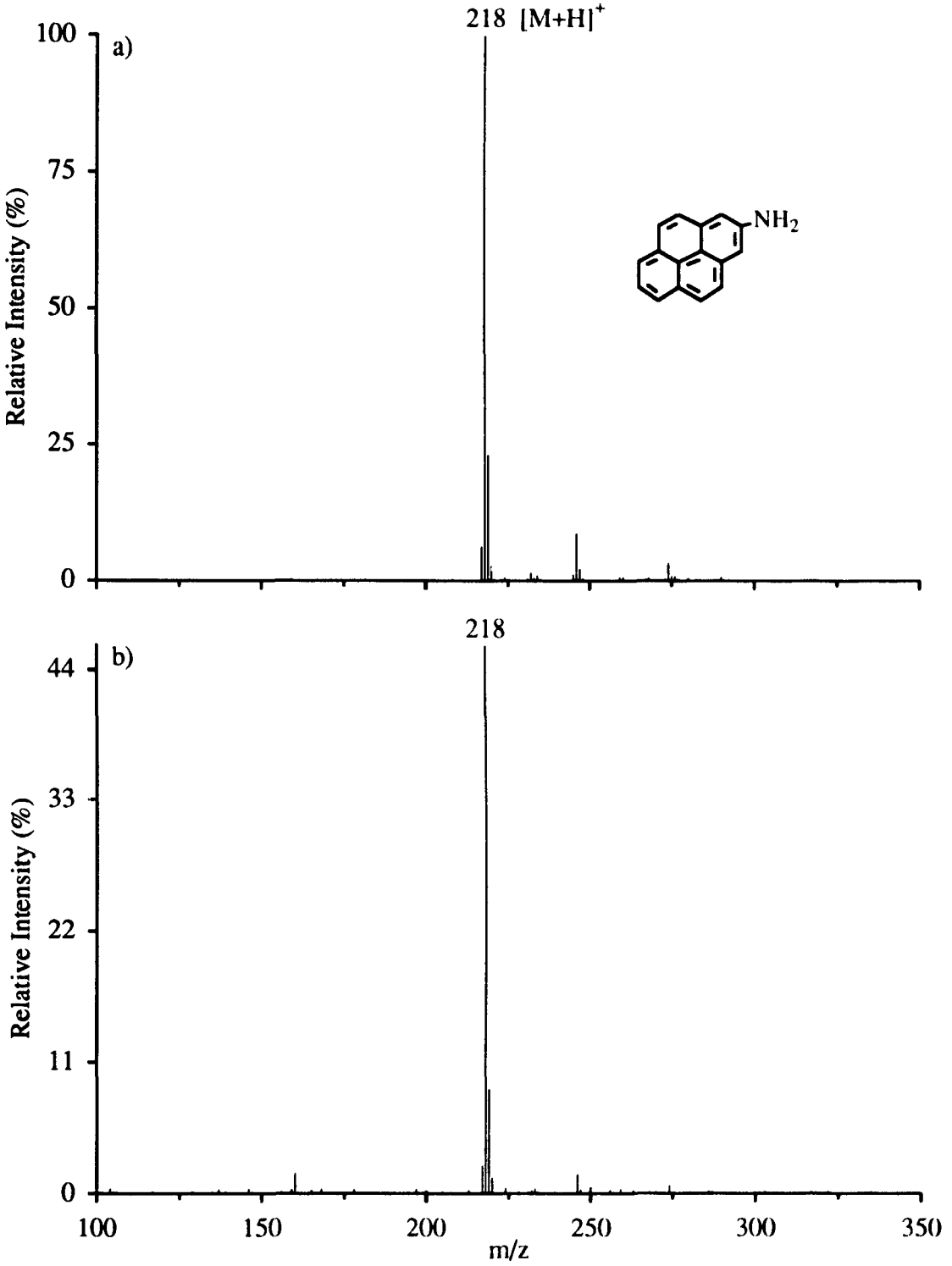

Figure VII-3: Background subtracted ionspray mass spectra of aminopyrene in a flow of (a) 1:1 aqueous acetonitrile (50 ng injection), and (b) 1:1 aqueous acetonitrile with 0.1% TFA (5 ng injection).

analytes, will assist in the formation of analyte ions in solution. The ionspray mass spectrum acquired from the injection of 5 ng of aminopyrene in a 200 μL/min flow of 50% aqueous acetonitrile containing 0.1% trifluoroacetic acid (TFA) is shown as Figure VII-3b. An increase in sensitivity of approximately 5-fold was produced with the use of the acid. Other polar compounds could also be ionized when using acid in the mobile phase; the ionspray mass spectra of carbazole, 9-cyanoanthracene and nitropyrene are shown as Figure VII-4.

Ionspray LC-MS may become useful for the selective detection of the polar compounds (that are ionizable in solution) in complex mixtures of PAC, but the inability to ionize and detect the large family of PAH greatly limits the applicability of this technique. However, ingenious methods by which neutral molecules are ionized in solution via charge-transfer complexation and electrochemical oxidation have been recently demonstrated.[205,206,207] These techniques are discussed in the following section.

VII.1 Charge-Transfer and Electrochemical Ionization

Recently, Van Berkel *et al.* reported the observation of molecular radical cations in the electrospray mass spectra of various alkyl-substituted metalloporphyrins.[208] This observation was significant because molecular ions, formed by loss or gain of an electron, are generally not observed in true

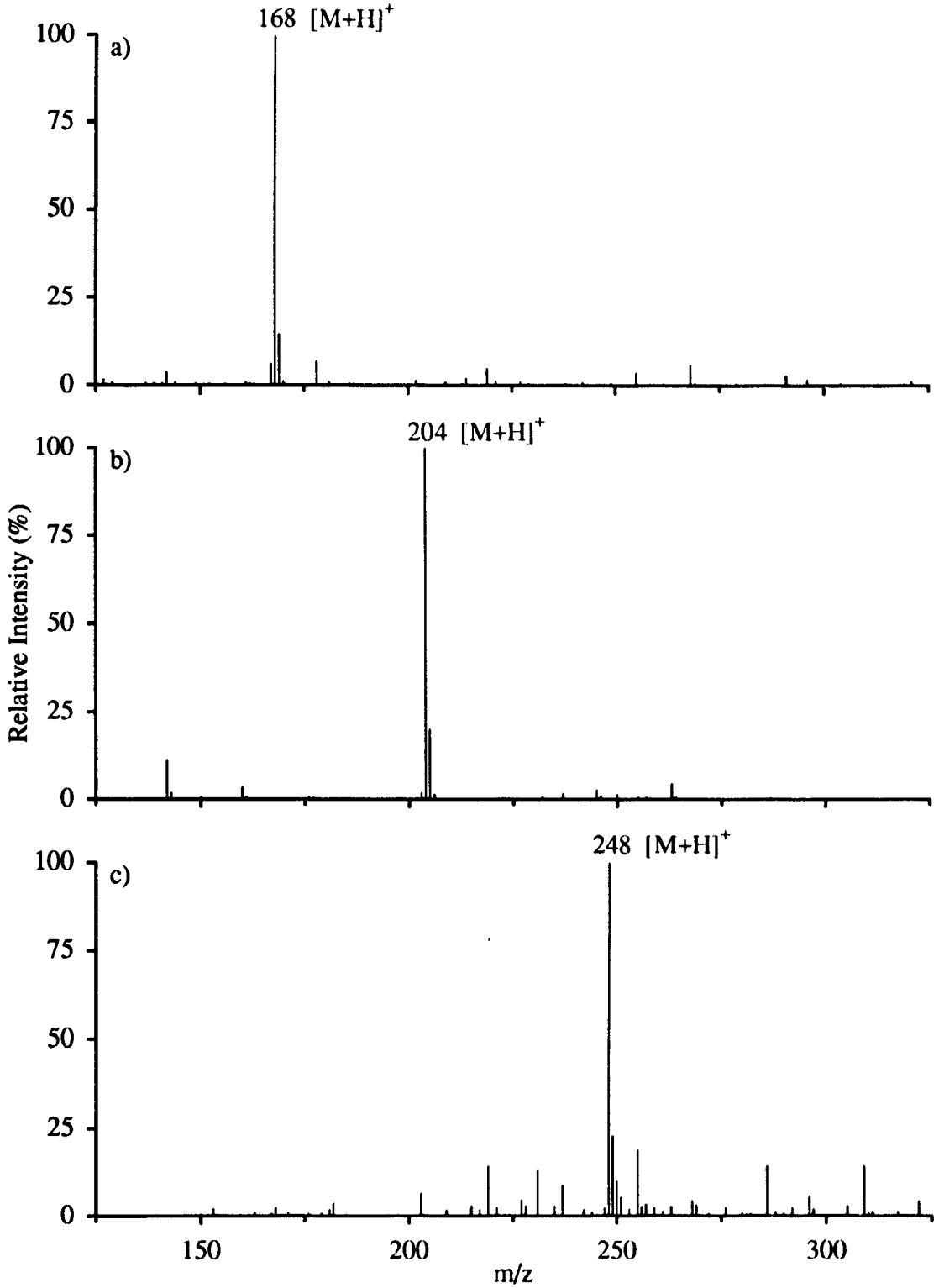

Figure VII-4: Background subtracted ionspray mass spectra of (a) carbazole, (b) 9-cyanoanthracene and (c) nitropyrene in a flow of 1:1 aqueous acetonitrile with 0.1% TFA.

electrospray ionization mass spectra (i.e., when no gas-phase ionization processes are at work). Tentatively, they interpreted their observations as an indication of either chemical oxidation of the porphyrins involving some species in the solvent system prior to or during the spraying process, or electrochemical oxidation in the electrospray needle. These preliminary explanations suggested that alternate types of solution chemistry, or a poorly understood phenomenon in the electrospray process, might be exploited to form ions in solution and successfully detect compounds not normally amenable to electrospray MS. This led to the use of charge-transfer complexation and electrochemical oxidation at the metal/solution interface of the electrospray needle to form radical cations in solution from neutral compounds.[205,206,207]

Charge-transfer complexes are formed by electron transfer between an electron donor (M) and electron acceptor (A), as shown in equation 1. In non-

$$M + A \rightarrow (M^{+} A^{-\cdot}) \rightarrow (M^{+\cdot})_{solvate} + (A^{-\cdot})_{solvate} \qquad (1)$$

polar solvents, charge-transfer complexes can exist as the neutral complex ($M^{+\cdot}A^{-}$). In polar solvents, such as methanol or acetonitrile, the complex can be dissociated, due to the solvation energy of the ions formed, into the respective cationic and anionic species.[207] Electron donors and acceptors are usually compounds of low ionization energy and compounds of high electron affinity, relative to one another, respectively.

Typical electron donors include PAH and other aromatic species that contain electron-donating groups, such as -OH, $-OCH_3$, $-N(CH_3)_2$ and $-CH_3$.

Common electron acceptors usually contain several electron-withdrawing groups, such as $-NO_2$, -CN, or halides. For example, Van Berkel *et al.* were able to acquire the electrospray mass spectrum of tetracene.[207] An abundant molecular ion at m/z 228 was observed when an equal molar amount of 2,3-dichloro-5,6-dicyano-1,4-benzoquinone (DDQ) was added to the sample. No ions were observed for the analyte when the DDQ was not present in the sample solution. A similar spectrum was also reported to be obtained from benzo[*ghi*]perylene when DDQ was used as the electron acceptor. However, no ions attributable to the analyte could be observed in attempting to analyze anthracene or phenanthrene in this manner.[207] The success or failure to ionize these PAH via charge-transfer complexation appeared to correlate with their ionization energies; i.e., radical cations were observed from the compounds of lowest ionization energy, tetracene (7.01 eV) and benzo[*ghi*]perylene (7.16 eV), but no ions were observed from the compounds of higher ionization energy, anthracene (7.42 eV) and phenanthrene (7.9 eV), when mixed with DDQ. This suggested that the degree of electron transfer was too small and/or solvation of the potential ionic species was too weak for discrete ions to be formed for these latter two compounds.

These observations were confirmed in the present study of over fifteen PAC standards. Charge-transfer ionspray mass spectra, using DDQ as the electron acceptor, were successfully acquired for the two compounds shown in Figure VII-5: tetracene and perylene. Perylene has low ionization energy (approximately 7.3 eV) similar to tetracene and benzo[*ghi*]perylene. Other ions besides the molecular cation were observed for benzo[*ghi*]perylene, but it is possible that they were due to impurities since the sample was slightly

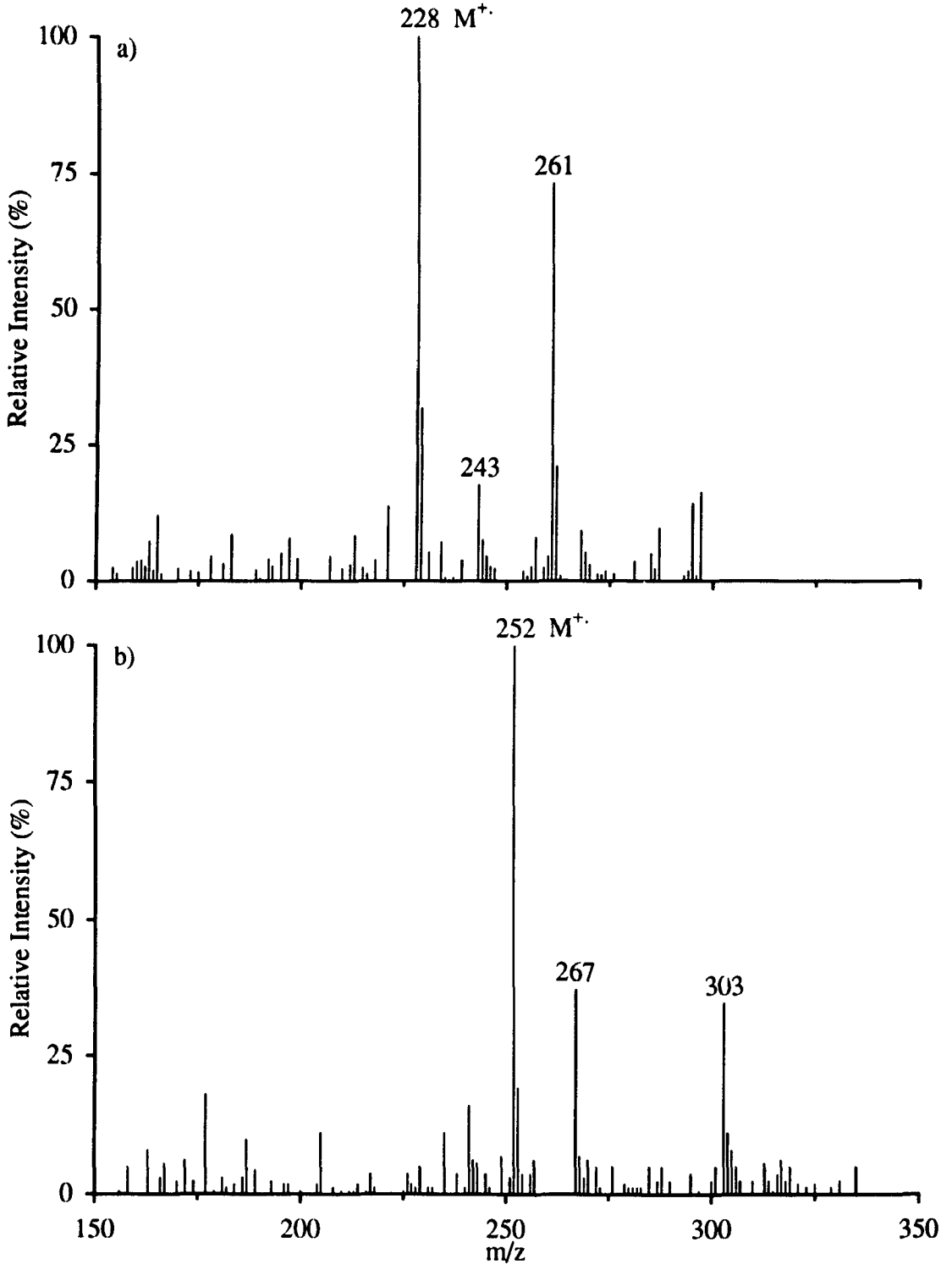

Figure VII-5: Background subtracted charge-transfer ionspray mass spectra of (a) tetracene and (b) perylene using DDQ as an electron acceptor.

contaminated with several other components. All the other PAC tested, which had ionization energies above 7.4 eV, did not produce any characteristic ions using this technique. The mass spectra of Figure VII-5 also contained ions from adduct formation (similar to those formed in the SFC-APCI/MS experiments discussed in Chapter VI). These adduct ions will be discussed in subsequent paragraphs.

Only three of the commonly detected low molecular weight PAH (below mass 276) possess ionization energies below 7.4 eV: tetracene, perylene and benzo[*a*]pyrene (which was not included in this experiment). Many PAH above and including mass 276 PAH have ionization energies below 7.4 eV. Therefore, ionspray charge-transfer complexation with DDQ could be used as a compound specific (i.e., PAH above mass 276) method of detection. By changing the solution chemistry (i.e., change the electron acceptor added to the solvent), one could alter the specificity of the ionization process.

Electrochemical oxidation at the metal/solution interface of the electrospray needle has also been used as a mechanism for the formation of molecular radical cations in electrospray ionization.[205,206] This technique has been shown to be consistent with the electrophoretic charge separation description of the electrospray process recently put forward by Kebarle and co-workers.[209] For this charge separation mechanism to be operational, charge balance requires that an oxidation reaction, ultimately resulting in electron flow to ground, must occur at the metal/solution interface within the electrospray needle to balance the positive-ion charge leaving in the spray. Van Berkel *et al.* were able to demonstrate that for some types of analytes, under appropriate conditions, a major oxidation product can be the molecular

radical cation of the analyte.[205] For example, the mass spectrum acquired for tetracene in a flow of dry dichloromethane/0.1% TFA exhibited only the radical cation.

The electrochemical oxidation ionspray mass spectra acquired for tetracene and perylene, simply using a flow of dichloromethane without DDQ or TFA, are shown as Figure VII-6. In contrast to the mass spectrum shown by Van Berkel *et al.*,[205] those of Figure VII-6 contained the adduct ions that were seen previously in Figure VII-5. Similar adduct ions were observed by Van Berkel *et al.* in the electrochemical oxidation spectrum of tetracene when a flow of methanol/dichloromethane (90/10 v/v) was used.[205] These ions were thought to arise from reactions of the radical cation with the solvents (methanol and/or water). These reactions did not occur when TFA was present in the solvent since it must have been able to stabilize or protect the radical cation. The adduct ions observed in both Figures VII-5 and VII-6 probably resulted from reactions with trace amounts of water in the solvent. The suppression of these reactions with TFA was not attempted in this study.

The specificity of this technique was similar to that of the DDQ charge-transfer method described above. The only PAH standards that produced characteristic ions (i.e., molecular cations or adduct ions) had ionization energies below 7.4 eV (e.g., tetracene, perylene and benzo[*ghi*]perylene). The similarity of the mass spectra and specificity of the two ionization techniques may imply that some, and perhaps, even all of the charge-transfer responses were a result of electrochemical oxidation. Further experiments to distinguish between the two processes have not been performed.

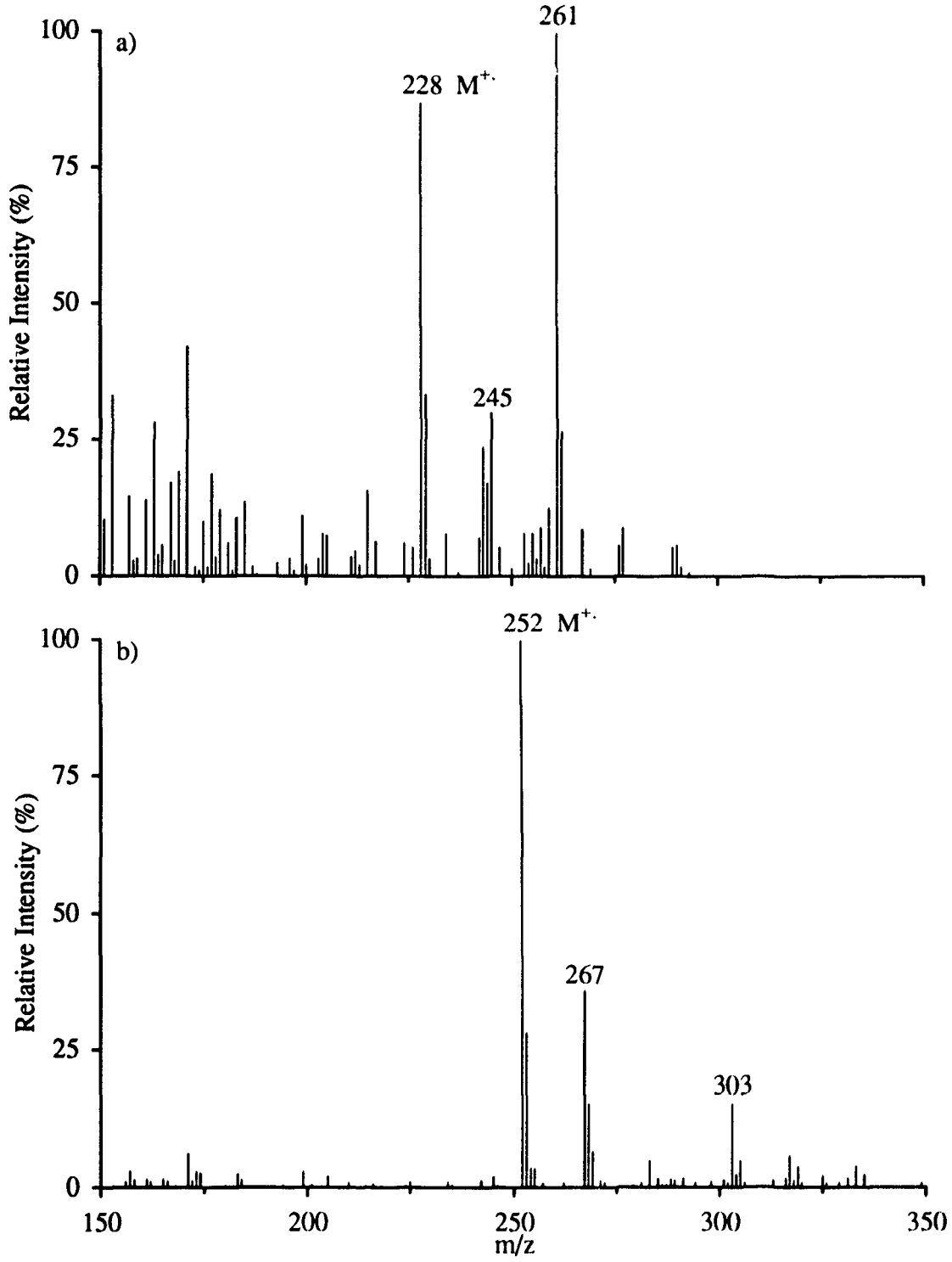

Figure VII-6: Background subtracted electrochemical oxidation ionspray mass spectra of (a) tetracene and (b) perylene.

VIII. CONCLUSIONS

The objectives of this research were to develop, implement and critically evaluate four different LC-MS interfaces for the analysis of complex mixtures of PAC. The moving belt interface, the first successful commercially available interface, relies on the removal of the LC mobile phase from the analyte prior to ionization in a high vacuum source. This is accomplished by depositing the LC effluent onto a moving polyimide belt, that passes through a series of vacuum locks, allowing the volatile mobile phase to evaporate. The analyte residue that remains on the belt surface is then vaporized directly into the ion source. A major advantage of this interface is its compatibility with more than one ionization mode (e.g., EI, CI and FAB), while the acquisition of conventional EI mass spectra facilitates the use of large spectral libraries for compound matching. Disadvantages include the loss of volatile compounds before ionization can occur and the difficulty in desorbing compounds of low volatility off the belt surface.

The working principle of the particle beam interface is the same as that of the moving belt, i.e., separating of the mobile phase from the analyte before ionization occurs. The LC effluent is nebulized with a high velocity jet of helium to form an aerosol of highly uniform sized droplets. A desolvation chamber is used to evaporate the solvent from the droplets leaving behind solid particles consisting of analyte and involatile mobile phase components. The high mass of the particles relative to the gas stream allows them to pass through a momentum separator (a series of skimming nozzle cones), thus producing a substantial enrichment of the analyte. Once entering the source, the particles are vaporized as they collide with the heated source wall. The

vaporized analyte molecules are then ionized by either EI or CI. A limited analyte volatility range, similar to that of the moving belt interface, is the particle beam's most significant limitation.

The heated pneumatic nebulizer interface uses an APCI source to couple LC to MS. The LC effluent is nebulized into a fine mist by a concentric jet of air or nitrogen in a heated quartz tube. The mobile phase is rapidly evaporated from the micron sized droplets via interactions with the heated gas, leaving extremely small particles each containing only a few analyte molecules. The heated gas and analyte mixture undergoes atmospheric pressure chemical ionization initiated by a corona discharge needle, usually producing MH^+ product ions in the positive mode. The large amounts of solvent and sample that are constantly sprayed into the source are drawn out of the chamber to either a condenser or a fume hood by an air pump.

The ionspray interface generates a charged aerosol at atmospheric pressure from a capillary held at a high voltage. Ions are emitted from charged droplets directly into the gas phase by a mechanism, which is currently at issue,[201,202] called ion evaporation. Optimum results, in terms of both sensitivity and detection limits, are achieved for compounds that are already ions in solution (such as metal and organic salts). Compounds with functionalities that can be ionized via solution-phase acid/base chemistry, such as carboxylic acids and amines, are also amenable to ionspray MS.

Chapters IV to VII provide a more detailed explanation of each of these interfaces while evaluating their ability to analyze PAC. The purpose of this study was to reveal the strengths and limitations of these techniques for complex PAC analyses. Table VIII-1 lists several criteria on which the

interfaces were evaluated and compared; the evaluation given for each interface was based on the results and experience gained during this study. A short summary and explanation of each qualifier is given in the following paragraphs.

Detection Limits

The LC-MS detection limits (signal-to-noise ratio of 3:1) for several PAH standards were obtained for the moving belt, particle beam and heated nebulizer interfaces. For example, the detection limit for coronene on the moving belt (i.e., 20 pg) was very good. PAH of similar volatility to that of coronene (e.g., mass 202 and higher) should produce similar responses. The lower molecular weight PAH are much more volatile and are susceptible to losses in the interface, while higher molecular weight PAC (e.g., >400) may not be volatile enough to be efficiently desorbed from the belt as it passes into the ion source. Therefore, these very low and very high molecular weight PAC will not have detection limits as good as that of coronene and the mid-range PAH.

The particle beam interface produced very poor detection limits (e.g., 3 ng for benzo[*a*]pyrene) because of its low transport efficiency. The detection limits become even worse for low and high molecular weight PAC for the same reasons mentioned above for the belt; the high volatility PAH are lost in the interface and the less volatile PAC are not vaporized in the source.

The heated nebulizer interface produced good detection limits (e.g., 275 pg for benzo[*a*]pyrene and 85 pg for dibenz[*a*,*h*]anthracene) for a much larger

Table VIII-1: A comparison of four LC-MS interfaces based primarily on their ability to analyze PAC.

+ - poor

++ - satisfactory

+++ - good

++++ - very good

Qualifier	Moving Belt	Particle Beam	Heated Nebulizer	Ionspray
Detection Limits	+++	+	+++	+
Dynamic Range	+++	++	++	+
Universality	++	+	++++	+
Stability/Reproducibility	+++	+	+++	+
Ease of Use	+	+++	++++	++
SFC Coupling	+++	+	++++	+
Qualitative Analysis	+++	++	+++	+
Quantitative Analysis	+++	+	+++	+
LC Constraints	++	++	+++	+
Commercial Availability	+	+++	+++	+++
Overall Rank	2	3	1	4

range of PAC than either the belt or particle beam interface. Compound volatility did not affect the performance of the heated nebulizer interface. The physical properties of the analytes (e.g., ionization energies and proton affinities), however, will ultimately dictate the sensitivity obtained. Low molecular weight PAH (e.g., < mass 202) have low proton affinities and are therefore ionized primarily by charge-transfer ionization, which is inherently less sensitive than proton-transfer in APCI. High molecular weight PAC, which have high proton affinities, are ideally suited for proton-transfer ionization. Therefore, it may be concluded that proton-transfer ionization is the preferred mode of operation since the main objective of LC-MS is the analysis of high molecular weight PAC.

A detailed investigation of the detection limits for ionspray was not performed. It is most likely that ionspray will be best suited for the detection of basic PAC (e.g., quinolines and amino-PAC) that can be protonated in solution. The charge-transfer complexation and electrochemical ionization ionspray modes, however, produced very poor signal-to-noise ratios for the limited number of amenable PAH studied.

Dynamic Ranges

Linear dynamic ranges of up to 4 orders of magnitude have been reported for PAH on the moving belt interface.[92] Particle beam dynamic ranges can be as high as 3 orders of magnitude, but the calibration curves are usually non-linear. This does not preclude their use in quantitative analyses, but it does increase the requirements for calibration and necessitates interpolation from multipoint curves.

The dynamic range of the heated nebulizer is usually much shorter (e.g., between 2 and 3 orders of magnitude) than those achieved with either the belt or particle beam interfaces. The high background noise associated with APCI and the pulse-counting detection system are the main reasons for the shorter ranges. The ionspray interface will most likely produce similarly short dynamic ranges since it is susceptible to the same limitations experienced by the heated nebulizer (i.e., high background noise and pulse-counting detection).

Universality

Both the moving belt and particle beam interfaces have a limited analyte volatility range in which they can operate effectively. The quantitative analysis of the NIST coal tar material by particle beam MS (Figure V-10) clearly showed the narrow range of analytes that could be analyzed. The heated nebulizer interface, on the other hand, does not appear to be limited by analyte volatility. In addition, both polar and non-polar analytes are readily ionized by APCI, albeit by different mechanisms (charge- or proton-transfer, respectively). Ionspray ionization is much more limited than all the other interfaces investigated; it is restricted to PAC that can be ionized in solution by either acid/base chemistry, charge-transfer complexation or electrochemical oxidation.

Stability/Reproducibility

The precision obtained from the belt interface for the determination of PAH in marine sediments, using both external and internal standardization,

were comparable to those of GC-MS (e.g., between 0.8 and 19% RSD).[4] The reproducibility of the particle beam interface, on the other hand, was extremely poor. Relative standard deviations as high as 50% were obtained for the quantitation of PAC in the NIST coal tar material. The particle beam interface is unusually susceptible to tremendous fluctuations in absolute response during intra- and inter-day runs.

The pneumatic spray of the heated nebulizer interface produces a steady pattern that is not prone to fluctuations, so that performance is stable and reproducible. Changes in the source conditions can, however, produce pronounced changes in the APCI ionization mechanisms. For example, adding benzene to the source greatly enhanced the amount of charge-transfer ionization. The source conditions must be controlled and reproducible from day-to-day in order to achieve long term stability. This can be accomplished by using the post-column addition of chemical ionization modifiers (such as water or benzene) to the source.

The stability and reproducibility of the ionspray interface will rely on the ability to control the solution chemistry (whether it is acid/base chemistry or charge-transfer complexation).

Ease of Use

The moving belt interface requires a significant amount of experience and constant attention to operate effectively. The deposition of the LC effluent onto the belt surface with the heated pneumatic probe is a very critical step; the effluent must be sprayed evenly onto the surface and excessive amounts of mobile phase must not enter the source and disrupt the

experiment. If the spray is too dry, however, a significant loss of the analyte may occur. Gradient elution complicates this deposition procedure even further since the temperature of the probe tip must be adjusted manually to accommodate the changing mobile phase composition. Changing the polyimide belt after it becomes too dirty or breaks is also a considerable chore. After the ion source has been cooled and vented, the interface must be taken apart for a new belt to be put in place (a procedure that can take at least two hours). The working lifetime of a belt can vary between weeks and hours.

In comparison to the belt interface, the particle beam interface is relatively straight forward to use. The LC column exit is connected to the nebulizer/desolvation chamber after the helium flow and momentum separator pumps have been turned on. Some adjustments of the helium flow and desolvation chamber temperature may be required, but these are usually minor and insignificant. Changing the capillary in the nebulizer chamber, if it becomes partially or completely blocked, is also easy; the nebulizer can be pulled off the desolvation chamber with the instrument still running, allowing easy access to the capillary. If the nozzle cones of the momentum separator become dirty, however, the interface must be shut down and completely taken apart to clean or replace them.

The heated nebulizer interface is also very easy to use. The column exit is connected directly to the probe after the heater and nebulizer gases are turned on. Control of the nebulizer temperature is not critical because a wide variety of analytes can be vaporized under the same conditions. Vernier controls are used to align the probe and corona discharge needle with the sampling orifice, although these are usually set near optimum and do not

require changing. The fact that the chromatographic system is decoupled from the high vacuum that is necessary for mass analysis makes this system very forgiving for the inexperienced or novice spectroscopist.

The ionspray interface is relatively simple to use only when acid/base chemistry is used to pre-form ions in solution. Small amounts of acid can be added directly to the mobile phase, although this may alter the chromatographic separations. The recently developed charge-transfer complexation and electrochemical ionization techniques are much more difficult to perform. Methods which allow the formation of ions in solution at the ionspray needle without affecting the chromatographic separations must be developed.

SFC Coupling

The ability to use an alternate chromatographic separation technique, such as SFC, can be advantageous if existing LC methods are not adequate for an analysis. The coupling of SFC to MS using the moving belt interface has already been demonstrated in our laboratory.[155] The SFC restrictor is easily accommodated into the belt spray deposition probe, which is then operated under normal conditions.

We have also demonstrated that the heated nebulizer interface can be modified to perform SFC-MS experiments. The design of the new interface is capable of accommodating all the major commercial types of SFC restrictors, and allows for rapid replacement should a different flow rate be required or a restrictor become blocked.

Both the particle beam and ionspray interfaces could be modified,

theoretically, to perform SFC-MS experiments. Major design changes would, however, be required since the rapid decompression of the supercritical mobile phase to ambient pressures will require a source of heat to control this phase transition.

Qualitative Analysis

Most PAC produce intense molecular ions under EI ionization that are ideal for compound identification. For example, the components of the carbon black extract were easily identified by using the belt interface with EI (Figure IV-5). Distinguishing between PAH isomers using EI mass spectra is, however, usually not possible; most PAH isomers produce identical EI mass spectra. Highly alkylated PAC undergo extensive fragmentation producing molecular ions that are usually very weak and difficult to distinguish from the fragment ions. The fragmentation pattern will suggest that the compound is alkylated, but the molecular weight may not be easily identified. The EI mass spectra of other substituted PAC (e.g., quinones or nitro-PAC) also consist of characteristic fragment ions that are very useful for compound identification.

APCI is a soft ionization technique that produces both molecular ions and protonated molecules for most PAC including highly alkylated compounds. Basic PAC (e.g., quinolines and amino-PAC) are easily identified since they only produce MH^+ ions, while PAH with high proton affinities produce intense MH^+ ions and $M^{+\cdot}$ ions of much less intensity. The $MH^+/M^{+\cdot}$ ion ratios can be used to distinguish between PAH isomers since the compounds usually have different ionization energies and proton

affinities. The lack of any characteristic fragment ions is a disadvantage of soft ionization techniques, but tandem MS experiments can provide additional structural information when it is required.

Ionspray is also a soft ionization technique but its present limited ability to ionize neutral molecules makes it unsuitable for routine qualitative analyses. Developing improved charge-transfer complexation systems and electrochemical ionization techniques may make it more applicable.

Quantitative Analysis

The ability to quantify PAH in complex mixtures by LC-MS with the moving belt interface has been previously demonstrated by our research group.[4] The precision obtained using both external and internal standardization methods were comparable to those of GC-MS analyses. The use of particle beam as a quantitative tool suffers from several important limitations, including: non-linear external calibration curves for most PAH; poor precision and reproducibility due to fluctuations in absolute response; and the matrix effect, which can cause unexpected signal enhancements when additional sample components co-elute with the analyte. The first two limitations can be overcome by using internal standards, although this does not solve the problems associated with the matrix effect. The only reliable means of preventing the matrix effect from influencing quantitation is through the use of co-eluting isotopically-labelled internal standards.[166] For PAH, the requirement of coelution would mean the use of di- or tri-deutero internal standards. Mass spectral overlap between the native analyte and the internal standard can, however, complicate the interpretation of the resulting

data.[168]

The heated nebulizer interface does not suffer from any inherent quantitation limitations; it produces linear calibration curves, good precision and reproducibility, and it does not suffer from any known matrix effects. The quantitation of the PAH in the NIST coal tar material using perdeutero internal standards was highly accurate and precise (see Tables VI-2 and VI-3).

LC Constraints

Both the particle beam and ionspray interfaces are restricted to low LC flow rates; below 0.4 and 0.2 mL/min, respectively. Ionspray also requires an ionization reagent (e.g., acid/base or complexation reagent) present in the mobile phase. A post-column addition of the reagent can be used, although this can introduce dead volumes that may degrade chromatographic performance

Severe limitations placed on the mobile phase composition and flow rates are also encountered when using the moving belt interface.[159] In general, solvent gradients are restricted to a low aqueous content and/or low flow rate to ensure that nearly all the mobile phase has evaporated before the belt enters the ion source.

The heated nebulizer interface does not have any LC flow or composition restrictions; it can accommodate flow rates as high as 1.5 mL/min of 100% water. The independent introduction of chemical ionization modifiers to the source (e.g., water or benzene) also eliminates the need to rely on the mobile phase to produce a suitable reagent ion composition in the APCI plasma.

Commercial Availability

Although the moving belt interface was the first successful commercially available interface, it is no longer advertised by manufacturers or widely available. The number of publications reporting the use of this interface and the actual number of belt interfaces in present use is low, especially in comparison to the other interfaces included in this study.

The particle beam interface is offered by most of the major MS manufacturers and is in general widely available. When particle beam was first introduced it caught the attention of many research groups resulting in numerous publications. With the arrival of new LC-MS interfaces, such as thermospray, electrospray and ionspray, interest in the particle beam interface has reduced dramatically.

Both ionspray (or electrospray) and the heated nebulizer interface are now being offered by most of the major MS manufacturers. The popularity of ionspray ionization has increased exponentially since its introduction, particularly in the bio-medical and pharmaceutical fields of research. The heated nebulizer is also gaining a significant amount of attention primarily because of its ability to handle higher LC flow rates and the large number of compound classes amenable to APCI.

Overall Rank

Given a choice of any of the four interfaces included in this study, which one should be recommended for PAC analyses by LC-MS? The first choice is clearly the heated nebulizer interface. It provides both accurate and reproducible mass spectral data, while being easy to use and maintain. It is

also the most suitable for the analysis of high molecular weight PAC, an area that GC-MS methods cannot perform well and for which LC-MS demand is greatest. The second choice is slightly more difficult to make, but based on the experiments performed in this study, the moving belt is preferred over the particle beam interface. Although the results obtained with the particle beam interface were disappointing, further improvements in interface design[210] and the use of high energy dynode electron multiplier detectors should provide the additional sensitivity required for routine analyses. However, the problems of non-linearity and the matrix effect still need to be addressed if it is to be used for quantitative analyses.

The use of charge-transfer complexation and electrochemical oxidation to pre-form ions in solution from neutral compounds that would not normally be amenable to ionspray is a novel idea that requires further investigation. Presently, the solution chemistry and experimental design have not been fully understood or optimized for peak performance. A considerable amount of additional research will be required before these ionization techniques become viable for routine LC-MS analyses.

IX. APPENDIX A

List of compounds tentatively identified in the complex mixtures of PAC.

Peak No.	Molecular Weight	Identification
1	128	Naphthalene
2	134	Benzothiophene
3	142	Methyl-naphthalenes
4	152	Acenaphthylene
5	154	Acenaphthene
6	154	Biphenyl
7	166	Fluorene
8	167	Carbazole
9	168	Dibenzofuran
10	178	Phenanthrene
11	178	Anthracene
12	180	Methyl-fluorenes
13	184	Dibenzothiophene
14	190	4*H*-Cyclopenta[*def*]phenanthrene
15	191	4*H*-Benzo[*def*]carbazole
16	192	Methyl-phenanthrenes
17	192	Methyl-anthracenes
18	202	Fluoranthene
19	202	Pyrene
20	202	Acephenanththrylene
21	208	Phenanthro[4,5-*bcd*]thiophene
22	216	Benzo[*a*]fluorene
23	216	Benzo[*b*]fluorene
24	216	Methyl-pyrenes
25	226	Benzo[*ghi*]fluoranthene
26	226	4*H*-Cyclopenta[*cd*]pyrene

Peak No.	Molecular Weight	Identification
27	228	Benzo[*c*]phenanthrene
28	228	Triphenylene
29	228	Benz[*a*]anthracene
30	223	Chrysene
31	228	Tetracene
32	234	Benzo[*b*]naphtho[1,2-*d*]thiophene
33	234	Benzo[*b*]naphtho[2,3-*d*]thiophene
34	240	4*H*-Cyclopenta[*def*]chrysene
35	252	Benzo[*j*]fluoranthene
36	252	Benzo[*e*]pyrene
37	252	Benzo[*b*]fluoranthene
38	252	Perylene
39	252	Benzo[*k*]fluoranthene
40	252	Benzo[*a*]pyrene
41	252	Benzo[*a*]fluoranthene
42	258	Chryseno[4,5-*bcd*]thiophene
43	264	11*H*-Cyclopenta[*ghi*]perylene
44	276	Benzo[*ghi*]perylene
45	276	Indeno[1,2,3-*cd*]pyrene
46	276	Indeno[7,1,2,3-*cdef*]chrysene
47	276	Anthanthrene
48	278	Dibenz[*a,h*]anthracene
49	278	Benzo[*b*]chrysene
50	278	Picene
51	290	7*H*-Indeno[1,2-*a*]pyrene
52	300	Coronene
53	302	Dibenzo[*b,e*]fluoranthene
54	302	Naphtho[1,2-*k*]fluoranthene
55	302	Dibenzo[*b,k*]fluoranthene
56	302	Dibenzo[*a,e*]pyrene

X. REFERENCES

1 M. L. Lee, M. V. Novotny and K. D. Bartle, *Analytical Chemistry of Polycyclic Aromatic Compounds* (Academic Press, New York, 1981).

2 J. R. Patel, I. R. Politzer, G. W. Griffen and J. L. Laseter, *Biomed. Mass Spectrom.* **5**, 664 (1978).

3 R. J. Schmitt, D. S. Ross and S. E. Buttrill, *J. Am. Chem. Soc.* **103**, 5265-5267 (1981).

4 P. G. Sim, R. K. Boyd, R. M. Gershey, R. Guevremont, W. D. Jamieson, M. A. Quilliam and R. J. Gergely, *Biomed. Environ. Mass Spectrom.* **14**, 375 (1987).

5 M. A. Quilliam and P. G. Sim, *J. Chromatogr. Sci.* **26**, 160-167 (1988).

6 J. Chrones and R. R. Germain, *Fuel Sci. Technol. Int.* **7**, 783-821 (1989).

7 C. E. Snape, *Proc. of The Fourth UNITAR/UNDP International Conference On Heavy Crude And Tar Sands, Volume 2*, Edmonton, Alberta, 457-466 (1988).

8 R. F. Sullivan, M. M. Boduszynski and J. C. Fetzer, *Energy and Fuels* **3**, 603-612 (1989).

9 W. Giger and M. Blumer, *Anal. Chem.* **46**, 1663-1671 (1974).

10 J. C. Lauer, D. H. Valles Hernandez and D. Cagniant, *Fuel* **67**, 1273-1282 (1988).

11 J. Chmielowiec, J. E. Beshai and A. E. George, *Fuel* **59**, 838-844 (1980).

12 J. F. McKay and D. R. Latham, *Anal. Chem.* **45**, 1050 (1973).

13 L. A. Blyshak, T. M. Rossi, G. Patonay and I. M. Warner, *Anal. Chem.* **60**, 2127-2131 (1988).

14 P. Burchill, A. A. Herod, J. P. Mahon and E. Pritchard, *J. Chromatogr.* **265**, 223-238 (1983).

15 P. Burchill, A. A. Herod and C. A. Mitchell, *Chromatographia* **21**, 67-76 (1986).

16 B. R. Clark, C. H. Ho and A. R. Jones, in *Analytical Chemistry of Liquid Fuel Sources. Tar sands, oil shale, coal, and petroleum*, P. C. Uden, S. Siggia and H. B. Jensen Eds., 283-294 (ACS, Washington, D.C., 1978).

17 H. S. Hertz, J. M. Brown, S. N. Chesler, F. R. Guenther, L. R. Hilpert,W. E. May, R. M. Parris and S. A. Wise, *Anal. Chem.* **52**, 1650-1657 (1980).

18 M. Novotny, M. L. Lee and K. D. Bartle, *J. Chromatogr. Sci.* **12**, 606 (1974).

19 C. E. Ostman and A. L. Colmsjo, *Fuel* **67**, 397 (1988).

20 C. E. Ostman and A. L. Colmsjo, *Chromatographia* **25**, 25 (1988).

21 M. M. Boduszynski, R. J. Hurtubise and H. F. Silver, *Anal. Chem.* **54**, 375-381 (1982).

22 M. M. Boduszynski, R. J. Hurtubise and H. F. Silver, *Anal. Chem.* **54**, 372-375 (1982).

23 L. Chan, J. Ellis and P. T. Crisp, *J. Chromatogr.* **292**, 355-368 (1984).

24 C. D. Ford, S. A. Holmes, L. F Thompson and D. R. Latham, *Anal. Chem.* **53**, 831-836 (1981).

25 D. W. Later, M. L. Lee, K. D. Bartle, R. C. Kong and D. L. Vassilaros, *Anal. Chem.* **53**, 1612-1620 (1981).

26 D. W. Later, B. W. Wilson and M. L. Lee, *Anal. Chem.* **57**, 2979-2984 (1985).

27 R. B. Lucke, D. W. Later, C. W. Wright, E. K. Chess and W. C. Weimer, *Anal. Chem.* **57**, 633 (1985).

28 M. Nishioka, R. M. Campbell, M. L. Lee, D. R. Muchiri, J. G. Stuart and R. N. Castle, *Anal. Chem.* **57**, 2211-2215 (1985).

29 J. E. Schiller and D. R. Mathiason, *Anal. Chem.* **49**, 1225 (1977).

30 R. S. Brown and L. T. Taylor, *Anal. Chem.* **55**, 723-730 (1983).

31 D. W. Later, T. G. Andros and M. L. Lee, *Anal. Chem.* **55**, 2126-2132 (1983).

32 D. W. Later, M. L. Lee and B. W. Wilson, *Anal. Chem.* **54**, 117-123 (1982).

33 C. E. Ostman and A. L. Colmsjo, *Fuel* **68**, 1249 (1989).

34 M. L. Selucky, Y. Chu, T. Ruo and O. P. Strausz, *Fuel* **56**, 369 (1977).

35 K. M. Semple, N. Cyr, P. M. Fedorak and W. S. Westlake, *Can. J. Chem.* **68**, 1092 (1990).

36 A. R. Jones, M. R. Guerin and B. R. Clark, *Anal. Chem.* **49**, 1766-1771 (1977).

37 C. E. Ostman and A. L. Colmsjo, *Chromatographia* **23**, 903 (1987).

38 L. S. Ramos and P. G. Prohaska, *J. Chromatogr.* **211**, 284 (1981).

39 F. Shue and T. F. Yen, *Anal. Chem.* **53**, 2081-2084 (1981).

40 D. A. Haugen, M. J. Peak, K. M. Suhrbier and V. C. Stamoudis, *Anal. Chem.* **54**, 32-37 (1982).

41 L. R. Snyder, B. E. Buell and H. E. Howard, *Anal. Chem.* **40**, 1303 (1968).

42 T. G. Harvey, T. W. Matheson and K. C. Pratt, *Anal. Chem.* **56**, 1277-1281 (1984).

43 P. Burchill, A. A. Herod, J. P. Mahon and E. Pritchard, *J. Chromatogr.* **281**, 109-124 (1983).

44 J. Chmielowiec and A. E. George, *Anal. Chem.* **52**, 1154-1157 (1980).

45 R. J. Crowley, S. Siggia and P. C. Uden, *Anal. Chem.* **52**, 1224-1228 (1980).

46 R. Miller, *Anal. Chem.* **54**, 1742-1746 (1982).

47 H. Zobel, M. Helms and S. Heidrich, *J. Chromatogr.* **509**, 27-32 (1990).

48 H. A. Cooper, R. J. Hurtubise and H. F. Silver, *Anal. Chem.* **58**, 3011-3016 (1986).

49 S. B. Hawthorne and D. J. Miller, *Anal. Chem.* **59**, 1705-1708 (1987).

50 G. F. Shilstone, M. W. Raynor, K. D. Bartle, A. A. Clifford, I. L. Davies and S. A. Jafar, *Polycyclic Aromatic Compounds* **1**, 99 (1990).

51 P. Burchill, A. A. Herod and E. Pritchard, *J. Chromatogr.* **246**, 271-295 (1982).

52 H. C. Dorn and D. L. Wooton, *Anal. Chem.* **48**, 2146 (1976).

53 T. G. Harvey, T. W. Matheson and K. C. Pratt, *J. Chromatogr.* **435**, 193-198 (1988).

54 L. R. Snyder and J. J. Kirkland, *Introduction to Modern Liquid Chromatography* (John Wiley & Sons, Inc., 1979).

55 A. Matsunaga, *Anal. Chem.* **55**, 1375 (1983).

56 J. M. Bayona, K. E. Markides and M. L. Lee, *Environ. Sci. Technol.* **22,** 1440-1447 (1988).

57 G. W. Mushrush, J. V. Cooney, E. J. Beal and J. M. Watkins, *Rapid Commun. Mass Spectrom.* **3**, 41 (1989).

58 M. Novotny, R. Kump, F. Merli and L. J. Todd, *Anal. Chem.* **52,** 401-406 (1980).

59 M. Novotny, D. Wiesler and F. Merli, *Chromatographia* **15,** 374 (1982).

60 P. Burchill, A. A. Herod and E. Pritchard, *J. Chromatogr.* **242,** 65-76 (1982).

61 J. Jacob, M. Alawi and G. Grimmer, *Polycyclic Aromatic Compounds* **2,** 13-17 (1991).

62 M. A. Poirier and B. S. Das, *Fuel* **63**, 361-367 (1984).

63 S. A. Wise, B. A. Benner, G. D. Byrd, S. N. Chesler, R. E. Rebbert and M. M. Schantz, *Anal. Chem.* **60**, 887-894 (1988).

64 D. K. Albert, *Anal. Chem.* **50**, 1822-1829 (1978).

65 P. Burchill, A. A. Herod and E. Pritchard, *J. Chromatogr.* **242,** 51-64 (1982).

66 I. Dzidic, M. D. Balicki, I. A. L. Rhodes and H. V. Hart, *J. Chromatogr. Sci.* **26,** 236-240 (1988).

67 R. J. Skelton, H. C. K. Chang, P. B. Farnsworth, K. E. Markides and M. L. Lee, *Anal. Chem.* **61**, 2292 (1989).

68 C. Willey, M. Iwao, R. N. Castle and M. L. Lee, *Anal. Chem.* **53,** 400 (1981).

69 R. Amos, *J. Chromatogr.* **204**, 469-478 (1981).

70 J. C. Fetzer and W. R. Biggs, *J. Chromatogr.* **386,** 87-101 (1987).

71 J. C. Fetzer and W. R. Biggs, *Chromatographia* **27**, 118-122 (1989).

72 K. Jinno, N. Anazawa, M. Okamoto, N. Tanaka, J. C. Fetzer and W. R. Biggs, *J. Chromatogr.* **402**, 173-178 (1987).

73 K. Jinno, T. Ibuki, N. Tanaka, M. Okamoto, J. C. Fetzer, W. R. Biggs, P. R. Griffiths and J. M. Olinger, *J. Chromatogr.* **461**, 209-227 (1989).

74 K. Jinno, S. Shimura, J. C. Fetzer and W. R. Biggs, *Polycyclic Aromatic Compounds* **1**, 151-159 (1990).

75 J. C. Fetzer and W. R. Biggs, *J. Chromatogr.* **346**, 81-92 (1985).

76 P. L. Grizzle and J. S. Thomson, *Anal. Chem.* **54**, 1071-1078 (1982).

77 S. D. Killops, *J. High Res. Chromatogr.* **9**, 302 (1986).

78 J. C. Fetzer and W. R. Biggs, *J. Chromatogr.* **295**, 161-169 (1984).

79 J. C. Fetzer, W. R. Biggs and K. Jinno, *Chromatographia* **21**, 439-442 (1986).

80 J. C. Fetzer and W. R. Biggs, *J. Chromatogr.* **322**, 275-286 (1985).

81 M. Novotny, M. Konishi, A. Hirose, J. Gluckman and D. Wiesler, *Fuel* **64**, 523-527 (1985).

82 S. A. Wise, W. J. Bonnett and W. E. May, in *PAH: Chemistry and Biological Effects*, A. Bjorseth and A. J. Dennis Eds., 791-806 (Battelle Press, Ohio, 1980).

83 C. Borra, D. Wiesler and M. Novotny, *Anal. Chem.* **59**, 339-343 (1987).

84 A. L. Colmsjo and C. E. Ostman, *Analytica Chimica Acta* **208**, 183-193 (1988).

85 P. Garrigues and M. Ewald, *Anal. Chem.* **55**, 2155-2159 (1983).

86 M. Novotny, A. Hirose and D. Wiesler, *Anal. Chem.* **56,** 1243-1248 (1984).

87 S. A. Wise, L. R. Hilpert, G. D. Byrd and W. E. May, *Polycyclic Aromatic Compounds* **1**, 81 (1990).

88 J. M. Bayona, D. Barcelo and J. Albaiges, *Biomed. Environ. Mass Spectrom.* **16**, 461-467 (1988).

89 D. I. Carroll, I. Dzidic, R. N. Stillwell, K. D. Haegele and E. C. Horning, *Anal. Chem.* **47**, 2369-2373 (1975).

90 W. A. Dark, W. H. McFadden and D. L. Bradford, *J. Chromatogr. Sci.* **15,** 454-460 (1977).

91 W. A. Dark and W. H. McFadden, *J. Chromatogr. Sci.* **16,** 289-293 (1978).

92 M. J. Hayes, E. P. Lankmayer, P. Vouros, B. L. Karger and J. M. McGuire, *Anal. Chem.* **55**, 1745-1752 (1983).

93 A. A. Herod, B. J. Stokes, H. J. Major and A. E. Fairbrother, *Analyst* **113,** 797-804 (1988).

94 P. G. Amateis and L. T. Taylor, *Anal. Chem.* **56,** 966-971 (1984).

95 W. L. Caudill, M. V. Novotny and R. M. Wrightman, *J. Chromatogr.* **261,** 415-418 (1983).

96 K. W. Sigvardson, J. M. Kennish and J. W. Birks, *Anal. Chem.* **56,** 1096-1102 (1984).

97 J. F. Anacleto, L. Ramaley, R. K. Boyd, S. Pleasance, M. A. Quilliam, P. G. Sim and F. M. Benoit, *Rapid Commun. Mass Spectrom.* **5,** 149-155 (1991).

98 A. L. Blilie and T. Greibrokk, *J. Chromatogr.* **349,** 317-322 (1985).

99 A. L. Blilie and T. Greibrokk, *Anal. Chem.* **57,** 2239-2242 (1985).

100 D. R. Gere, R. Board and D. McManigill, *Anal. Chem.* **54**, 736-740 (1982).

101 J. M. Levy and W. M. Ritchey, *J. Chromatogr. Sci.* **24**, 242 (1986).

102 P. G. Sim, C. M. Elson and M. A. Quilliam, *J. Chromatogr.* **445**, 239-243 (1988).

103 J. Cousin and P. J. Arpino, *J. Chromatogr.* **398**, 125-141 (1987).

104 S. M. Fields, K. E. Markides and M. L. Lee, *J. Chromatogr.* **406**, 223-235 (1987).

105 J. C. Fjeldsted, R. C. Kong and M. L. Lee, *J. Chromatogr.* **279**, 449-455 (1983).

106 J. C. Fjeldsted, B. E. Richter, W. P. Jackson and M. L. Lee, *J. Chromatogr.* **279**, 423-430 (1983).

107 B. J. Fuhr, L. R. Holloway and C. Reichert, *Fuel Sci. Tecnol. Int.* **7**, 643-657 (1989).

108 M. Novotny and S. R. Springston, *J. Chromatogr.* **279**, 417-422 (1983).

109 J. C. Fjeldsted and M. L. Lee, *Anal. Chem.* **56**, 619A-628A (1984).

110 M. Novotny, *J. High Res. Chromatogr.* **9**, 137 (1986).

111 K. Jinno, T. Hoshino, T. Hondo, M. Saito and M. Senda, *Anal. Chem.* **58**, 2696-2699 (1986).

112 S. B. Hawthorne and D. J. Miller, *J. Chromatogr.* **468**, 115-125 (1989).

113 E. Huang, J. Henion and T. R. Covey, *J. Chromatogr.* **511**, 257 (1990).

14 S. T. Musser and P. S. Callery, *Biomed. Environ. Mass Spectrom.* **19**, 348-352 (1990).

115 S. V. Olesik, *J. High Res. Chromatogr.* **14**, 5 (1991).

116 L. G. Randall and A. L. Wahrhaftig, *Anal. Chem.* **50**, 1703 (1978).

117 W. R. West and M. L. Lee, *J. High Res. Chromatogr.* **9**, 161 (1986).

118 G. Greenwood, in *Mass Spectrometric Characterization of Shale Oils*, T. Aczel Ed., 27-37 (ASTM, Philadelphia, 1986).

119 T. R. Henderson, J. D. Sun, R. E. Royer, C. R. Clark, A. P. Li, T. M. Harvey, D. F. Hunt, J. E. Fulford, A. M. Lovette and W. R. Davidson, *Environ. Sci. Technol.* **17**, 443-449 (1983).

120 L. Petrakis, D. T. Allen, G. R. Gavalas and B. C. Gates, *Anal. Chem.* **55**, 1557-1564 (1983).

121 M. V. Buchanan, *Anal. Chem.* **54**, 570-574 (1982).

122 M. V. Buchanan, *Anal. Chem.* **56**, 546-550 (1984).

123 L. R. Hilpert, *Biomed. Environ. Mass Spectrom.* **14**, 383-394 (1987).

124 C. S. Hsu, G. J. Dechert and K. D. Rose, *Proc. of The 38th ASMS Conference on Mass Spectrometry and Allied Topics*, Tucson, Arizona, 595-596 (1990).

125 W. A. Korfmacher, Z. Djuric, E. K. Fifer and F. A. Beland, *Spectros. Int. J.* **6**, 1-16 (1988).

126 M. L. Lee and R. A. Hites, *J. Am. Chem. Soc.* **99**, 2008 (1977).

127 K. Balasanmugam and J. M. Miller, *Org. Mass Spectrom.* **23**, 267-273 (1988).

128 C. Dass, *J. Am. Soc. Mass Spectrom.* **1**, 405 (1990).

129 G. Dube, *Org. Mass Spectrom.* **19**, 242-243 (1984).

130 R. D. Grigsby, S. E. Scheppele, Q. G. Grindstaff, G. P. Sturm, L. C. E. Taylor, H. Tudge, C. Wakefield and S. Evans, *Anal. Chem.* **54**, 1108-1113 (1982).

131 J. Visentini, Q. Zha and M. J. Bertrand, *Proc. of The 38th ASMS Conference on Mass Spectrometry and Allied Topics*, Tucson, Arizona, 182-183 (1990).

132 T. H. Wang, T. J. Thompson and R. B. Freas, *Proc. of The 38th ASMS Conference on Mass Spectrometry and Allied Topics*, Tucson, Arizona, 649-650 (1990).

133 T. W. Allen, R. J. Turtubise and H. F. Silver, *Anal. Chem.* **57**, 666-671 (1985).

134 S. J. DeCanio, V. P. Nero and D. A. Storm, *Proc. of The 38th ASMS Conference on Mass Spectrometry and Allied Topics*, Tucson, Arizona, 756-757 (1990).

135 J. E. Fulford, T. Sakuma and D. A. Lane, in *PAHS: Physical and Biological Chemistry*, M. Cooke, A. J. Dennis and G. L. Fisher Eds., 297-304 (Battelle Press, Ohio, 1982)

136 E. C. Horning, M. G. Horning, D. I. Carroll, I. Dzidic, R. N. Stillwell, *Anal. Chem.* **45**, 936-943 (1973).

137 D. A. Lane, *Environ. Sci. Technol.* **16**, 38A (1982).

138 P. J. Arpino and G. Guiochon, *Anal. Chem.* **51**, 682A (1979).

139 T. R. Covey, E. D. Lee, A. P. Bruins and J. D. Henion, *Anal. Chem.* **58**, 1451A-1465A (1986).

140 R. M. Smith, *Supercritical Fluid Chromatography* (The Royal Society of Chemistry, 1988).

141 C. M. White, *Modern Supercritical Fluid Chromatography* (Huthig, Heidelberg, 1988).

142 P. A. Peaden, M. L. Lee, Y. Hirata and M. Novotny, *Anal. Chem.* **52**, 2268-2271 (1980).

143 D. R. Clutter, L. Petrakis, R. L. Stenger and R. K. Jensen, *Anal. Chem.* **44**, 1395 (1972).

144 S. A. Wise and L. C. Sander, *J. High Res. Chromatogr.* **8**, 248 (1985).

145 S. A. Wise, W. J. Bonnett, F. R. Guenther and W. E. May, *J. Chromatogr. Sci.* **19**, 457 (1981).

146 S. A. Wise, L. C. Sander, R. Lapouyade and P. Garrigues, *J. Chromatogr.* **514**, 111 (1990).

147 S. A. Wise, L. C. Sander, H. C. K. Chang, K. E. Markides and M. L. Lee, *Chromatographia* **25**, 473 (1988).

148 S. A. Wise, in *Handbook of Polycyclic Aromatic Hydrocarbons*, A. Bjorseth Ed., 183-257 (Dekker, New York, 1983).

149 S. A. Wise, S. N. Chesler, H. S. Hertz, L. R. Hilpert and W. E. May, *Anal. Chem.* **49**, 2306 (1977).

150 K. G. Liphard, *Chromatographia* **13**, 603 (1980).

151 K. Qian and C. S. Hsu, *Anal. Chem.* **64**, 2327-2333 (1992).

152 E. P. Lankmayr and K. Muller, *J. Chromatogr.* **170**, 139-146 (1979).

153 P. L. Scolla and R. J. Hurtubise, *J. Chromatogr.* **357**, 127-138 (1986).

154 R. L. C. Fung, M.Sc. Thesis, Chemistry Department, McMaster University, Hamilton, Ontario, 1989.

155 H. Perreault, Ph.D. Thesis, Chemistry Department, Dalhousie University, Halifax, Nova Scotia, 1992.

156 P. R. Griffiths, *Anal. Chem.* **60**, 593A-597A (1988).

157 M. Meot-Ner, *J. Am. Chem. Soc.* **101**, 2396 (1979).

158 K. J. Krost, *Anal. Chem.* **57**, 763-765 (1985).

159 D. S. Millington, D. A. Yorke and P. Burns, *Adv. Mass Spectrom.* **8B**, 1819-1825 (1980).

160 C. S. Hsu, M. A. McLean, T. Aczel, S. C. Blum, W. N. Olmstead, L. H. Kaplan, W. K. Robbins and W. W. Schulz, *Proc. of the American Chemical Society, Division of Petroleum Chemistry, Symposium on MS in Fossil Fuels Research*, Washington, D.C., 649-652 (1990).

161 M. A. McLean and C. S. Hsu, *Proc. of The 38th ASMS Conference on Mass Spectrometry and Allied Topics*, Tucson, Arizona, 605-606 (1990).

162 R. C. Willoughby and R. F. Browner, *Anal. Chem.* **56**, 2626-2631 (1984).

163 P. C. Winkler, D. P. Perkins, W. K. Williams and R. F. Browner, *Anal. Chem.* **60**, 489-493 (1988).

164 I. S. Kim, F. I. Sasinos, R. D. Stephens, J. Wang and M. A. Brown, *Anal. Chem.* **63**, 819-823 (1991).

165 M. A. Brown, R. D. Stephens and I. S. Kim, *Trends in Anal. Chem.* **10**, 330 (1991).

166 F. R. Brown and W. M. Draper, *Biological Mass Spectrom.* **20**, 515-521

(1991).

167 J. S. Ho, T. D. Behymer, W. L. Budde and T. A. Bellar, *J. Am. Soc. Mass Spectrom.* **3**, 662-671 (1992).

168 D. R. Doerge, M. W. Burger and S. Bajic, *Anal. Chem.* **64**, 1212-1216 (1992).

169 R. F. Browner, P. C. Winkler, D. D. Perkins and L. E. Abbey, *Microchem. J.* **34**, 15 (1986).

170 T. A. Bellar, T. D. Behymer and W. L. Budde, *J. Am. Soc. Mass Spectrom.* **1**, 92-98 (1990).

171 M. R. Roby, C. M. Pace, L. D. Betowski and P. J. Marsden, *Proc. of The 38th ASMS Conference on Mass Spectrometry and Allied Topics,* Tucson, Arizona, 625-626 (1990).

172 National Institute of Standards and Technology, SRM 1597 Certificate of analysis (1987).

173 R. K. Boyd, *Rapid Commun. Mass Spectrom.* **7**, 257-271 (1993).

174 E. C. Huang, T. Wachs, J. J. Conboy and J. D. Henion, *Anal. Chem.* **62**, 713A (1990).

175 D. A. Lane, T. Sakuma and E. S. K. Quan, in *PAHS: Chemistry and Biological Effects*, A. Bjorseth and A. J. Dennis Eds., 199-214 (Battelle Press, Ohio, 1980).

176 E. C. Horning, D. I. Carroll, I. Dzidic, K. D. Haegele, M. G. Horning and R. N. Stillwell, *J. Chromatogr. Sci.* **12**, 725-729 (1974).

177 E. C. Horning, D. I. Carroll, I. Dzidic, K. D. Haegele, M. G. Horning and R. N. Stillwell, *J. Chromatogr.* **99**, 13-21 (1974).

178 T. Sakuma, W. R. Davidson, D. A. Lane, J. E. Fulford and E. S. K. Quan, in *Chemical Analysis and Biological Fate: PAH*, M. Cooke and A. J. Dennis Eds., 179-188 (Battelle Press, Ohio, 1981).

179 J. D. Gilbert, E. L. Hand, A. S. Yuan, T. V. Olah and T. R. Covey, *Biological Mass Spectrom.* **21**, 63-68 (1992).

180 H. Fouda, M. Nocerini, R. Schneider and C. Gedutis, *J. Am. Soc. Mass Spectrom.* **2**, 164-167 (1991).

181 A. G. Harrison, *Chemical ionization mass spectrometry* (CRC Press, Boca Raton, 1992).

182 G. K. Low, G. E. Batley, R. O. Lidgard and A. M. Duffield, *Biomedical and Environmental Mass Spectrom.* **13**, 95-104 (1986).

183 M. V. Buchanan and G. Olerich, *Organic Mass Spectrom.* **19**, 486 (1984).

184 S. Daishima, Y. Iida, A. Shibata and F. Kanda, *Organic Mass Spectrom.* **27**, 571-577 (1992).

185 M. Oehme, *Anal. Chem.* **55**, 2290-2295 (1983).

186 D. F. Hunt, C. N. McEwen and T. M. Harvey, *Anal. Chem.* **47**, 1730 (1975).

187 D. F. Hunt, G. C. Stafford, F. W. Crow and J. W. Russell, *Anal. Chem.* **48**, 2098 (1976).

188 E. C. Horning, D. I. Carroll, I. Dzidic, S. N. Lin, R. N. Stillwell and J. P. Thenot, *J. Chromatogr.* **142**, 481-495 (1977).

189 P. G. Sim and C. M. Elson, *Rapid Commun. Mass Spectrom.* **2**, 137 (1988).

190 J. E. Lovelock, A. Zlatkis and R. S. Bedar, *Nature* **193**, 540 (1962).

191 R. C. Dougherty, *Anal. Chem.* **53**, 625A (1981).

192 J. F. Anacleto, R. K. Boyd, S. Pleasance, M. A. Quilliam, J. B. Howard, A. L. Lafleur and Y. Makarovsky, *Can. J. Chem.* **70**, 2558 (1992).

193 J. F. Anacleto, R. K. Boyd and M. A. Quilliam, *J. High Res. Chromatogr.* **16**, 85 (1993).

194 J. F. Anacleto, H. Perrault, R. K. Boyd, S. Pleasance, M. A. Quilliam, J. B. Howard, Y. Makarovsky and A. L. Lafleur, *Rapid Commun. Mass Spectrom.* **6**, 214-220 (1992).

195 J. F. Anacleto, M. A. Quilliam and R. K. Boyd, *Anal. Chem.* in press.

196 I. K. Barker, J. P. Kithinji, K. D. Bartle, A. A. Clifford, M. W. Raynor, G. F. Shilstone and P. A. Halford-Maw, *Analyst* **114**, 41-45 (1989).

197 C. R. Blakely and M. L. Vestal, *Anal. Chem.* **55**, 750 (1983).

198 B. A. Thomson, J. V. Iribarne and P. Dziedic, *Anal. Chem.* **54**, 2219 (1982).

199 C. M. Whitehouse, R. M. Dreyer, M. Yamashita and J. B. Fenn, *Anal. Chem.* **57**, 675 (1985).

200 A. P. Bruins, T. R. Covey and J. D. Henion, *Anal. Chem.* **56**, 2642 (1987).

201 J. V. Iribarne and B. A. Thomson, *J. Chem. Phys.* **64**, 2287 (1976).

202 G. Schmelzeiser-Redeker, L. Butfering and F. W. Rollgen, *Int. J. Mass Spectrom. Ion Processes* **90**, 189 (1989).

203 R. D. Smith, J. A. Loo, C. G. Edmonds, C. J. Barinaga and H. R. Udseth, *Anal. Chem.* **62**, 882-899 (1990).

204 T. R. Covey, B. I. Shushan, B. A. Thomson and J. D. Henion, *Proc. of The 37th ASMS Conference on Mass Spectrometry and Allied Topics*, Miami Beach, Florida, 558-559 (1989).

205 G. J. Van Berkel, S. A. McLuckey and G. L. Glish, *Anal. Chem.* **64, 1586-**1593 (1992).

206 G. J. Van Berkel, S. A. McLuckey and G. L. Glish, *Proc. of The 39th ASMS Conference on Mass Spectrometry and Allied Topics,* Nashville, Tennesse, 1237-1382 (1991).

207 G. J. Van Berkel, S. A. McLuckey and G. L. Glish, *Anal. Chem.* **63, 2064-**2068 (1991).

208 G. J. Van Berkel, S. A. McLuckey and G. L. Glish, *Anal. Chem.* **63,** 1098 (1991).

209 A. T. Blades, M. G. Ikonomou and P. Kebarle, *Anal. Chem.* **63,** 2109 (1991).

210 S. Pleasance, J. F. Anacleto, M. R. Bailey and D. H. North, *J. Am. Soc. Mass Spectrom.* **3**, 378-397 (1992).